A CLOUD CHAMBER INVESTIGATION OF

PHOTONUCLEAR REACTIONS IN LIGHT NUCLEI

Ph.D. Thesis

submitted to

The University of Glasgow

I. F. Wright

March 1961

Page

4. The $C^{12}(\gamma,3\alpha)$ Reaction and the Isotopic Spin Selection Rules 36

4(a) Experimental Results on the $C^{12}(\gamma,3\alpha)$ Reaction 37

4(b) The Isotopic Spin Selection Rules and Their Application to the $C^{12}(\gamma,\alpha)$ Reaction 40

5. Choice of Cloud Chamber Experiments 45

5(a) The $He^{4}(\gamma,p)$ Reaction 45

5(b) The Photodisintegration of Nitrogen 46

5(c) $Ne^{20}(\gamma,\alpha)$, $Ne^{20}(\gamma,2\alpha)$ and $Ne^{20}(\gamma,\alpha p)$ Reactions 46

Chapter II

APPARATUS AND EXPERIMENTAL PROCEDURE 48

1. Expansion Chamber 52

1(a) Constructional Details 52

1(b) Illumination 55

1(c) Control Circuit 55

2. Operation of Synchrotron and Cloud Chamber 56

2(a) Collimation 56

2(b) 'Single Shot' Control for Synchrotron 57

2(c) Discussion of Operating Experience 60

3. Photography and Track Measurement 67

Chapter III

INVESTIGATION OF THE $He^{4}(\gamma,p)$ REACTION 71

1. Summary of Experimental Conditions 74

Page

2. Results 75

3. Discussion 79

Chapter IV

THE PHOTODISINTEGRATION OF NITROGEN 82

1. Additional Notes on Experimental Method 82

1(a) Apparatus and Analysis 82

1(b) Background Events 84

2. Energy Distribution of Low Energy Protons 85

3. Study of the (γ,p) and (γ,α) Reactions at Higher Energies 88

3(a) Accuracy of Recoil Measurements 89

3(b) Recoil Range Measurements 91

3(c) (γ,α) Events 92

4. The Relative Probabilities of the Various Reactions 93

5. Notes on the Identification of (γ,n) Disintegrations Leaving N^{13} in Particular States 95

6. Discussion 102

6(a) N^{14}(γ,p) Cross Section between 7.5 and 10.5 Mev 102

6(b) Photonuclear Reactions in N^{14} above 10.5 Mev 105

Page

Chapter V

THE (γ,α), ($\gamma,2\alpha$) AND ($\gamma,\alpha p$) REACTIONS IN Ne^{20} 110

1. Notes on the Experimental Method 115

1(a) Summary of the Cloud Chamber Conditions 115

1(b) Camera Arrangement for Microscope Measurement of Cloud Chamber Tracks 116

1(c) Analysis 121

2. Results 127

2(a) $Ne^{20}(\gamma,\alpha)$ Reaction 128

2(b) $Ne^{20}(\gamma,p)$ Reaction 130

2(c) $Ne^{20}(\gamma,2\alpha)$ and $Ne^{20}(\gamma,\alpha p)$ Reactions 131

3. Discussion 134

Chapter VI

SUMMARY AND CONCLUSION 143

Appendix I - Some Remarks on Recent Measurements of the $He^4(\gamma,p)$ and $He^4(\gamma,n)$ Cross Sections 154

Appendix II - Examination of the Nitrogen Photoproton Spectrum Reported by Spicer 159

Appendix III - Analysis of Cloud Chamber Tracks by Microscope Measurement of the Camera Films 164

PREFACE

The work described in this thesis was carried out in the University of Glasgow during the period October 1950 - May 1955 and consists of an investigation of a number of photonuclear reactions in elements of low atomic number using a Wilson cloud chamber as detector. This investigation was initiated by Mr. J. R. Atkinson and had, as underlying aims, the study of the potentialities of the cloud chamber as a tool in photonuclear investigations and the gaining of experience in the problems associated with the operation of a cloud chamber in conjunction with a high energy electron synchrotron. As a result this thesis discusses the results obtained both in terms of their intrinsic physical interest and in terms of the above aims.

In Chapter I the techniques and outstanding experimental results of low-energy photonuclear investigations* and the theories which have been advanced to account for these observations are reviewed critically. This review covers results published before the end of 1951 and includes some later results which were of importance in the planning of the last experiment described in this thesis. In keeping with the above aim Chapter I not only provides the background required for the discussion of the physical significance of the results obtained but also represents an examination of the potentialities of other techniques. This examination leads to the expectation that the

*i.e., investigations dealing with reactions initiated by quanta of energy up to 100 Mev.

cloud chamber will provide data not obtainable otherwise. The reasons for the choice of the three elements whose photo-disintegration has been studied in this investigation, namely Helium, Nitrogen and Neon, are given as a conclusion to this chapter. The remainder of the thesis follows the natural order in chapters dealing with the apparatus and experimental method, the $He^4(\gamma,p)$ reaction, the photodisintegration of Nitrogen and the (γ,α), $(\gamma,\alpha p)$ and $(\gamma,2\alpha)$ reactions in Neon. The discussion of these experiments includes a consideration of related results published subsequently. The final chapter summarizes the conclusions reached and lists possible future experiments. Examples of the cloud chamber tracks obtained are collected together in a separate atlas. These photographs are referred to as Plates to distinguish them from the other figures in the thesis.

The only earlier photonuclear investigations to make use of the cloud chamber technique are the pioneer and later work on the photo-disintegration of deuterium (Ch 37, Ph 50) and the work of Gaerttner and Yeater on the photodisintegration of various light nuclei. The results of these last workers were published during a period extending from a little before to some 12 months after the start of the work described here. As the technique used in this work was, in practically all respects, developed quite independently of the work of Gaerttner and Yeater the work described here is, in essence, completely original. In the region where the results of the

two investigations overlap the results of this work are more comprehensive than those obtained by Gaerttner and Yeater. The details are given in the appropriate parts of the text.

As is natural in an investigation of this type the whole of this work has been carried out in collaboration with other members of the department. The work on Helium follows a preliminary investigation by Mr. J. R. Atkinson and was carried out in collaboration with Mr. J. M. Reid. Mr. Reid was responsible for the synchrotron and for the circuits linking it to the cloud chamber while the author was responsible for the operation of the cloud chamber, for the design and construction of cameras and reprojection equipment and for the analysis. In November 1951, the author was joined by Mr. D. R. O. Morrison who assisted in the concluding stages of the work on Helium and shared equally in the experimental work on Nitrogen and Neon and in the analysis of the Nitrogen results. The author was responsible for the planning of both the Nitrogen and the Neon experiments. The analysis of the Neon results was carried out by Mr. G. I. Crawford and Miss M. B. McClements under the supervision of the author. This analysis made use of a technique developed by the author for the stereographic measurement of cloud chamber tracks 1 or 2 mm long.

In conclusion I should like to thank Professor P. I. Dee for affording me the facilities of his department and for his stimulus and encouragement, Mr. J. R. Atkinson under whose

immediate supervision this work has been carried out, all those named above who have shared this work with me and Dr. D. Greene, Dr. K. G. McNeil and Mr. J. C. W. Telfer who cheerfully assisted in running the synchrotron. I am indebted to the Australian National University of the award of a Research Scholarship during the period up to August 1953 and to the Nuffield Foundation for a Research Grant from September 1953 to September 1954.

Chapter I

SURVEY OF PHOTONUCLEAR INVESTIGATIONS

This chapter contains a review of the experimental and theoretical investigations of photonuclear reactions produced by quanta of energy less than 100 Mev. Its aim is to assess the possibilities of using the cloud chamber for photonuclear investigations. The field covered includes all photonuclear reactions except the photodisintegration of the deuteron and photofission. The photodisintegration of the deuteron was excluded because the existing experimental and theoretical results were in reasonable agreement and the cloud chamber is clearly not suited to providing the high statistical accuracy needed for improved results. Photofission was omitted because it is regarded as a reaction of very specialized interest. Since this is intended to provide the background for the investigations reported in this thesis it deals only with material published before the end of 1951. The general picture of photonuclear processes which is derived from this material was not altered in its essentials by material published during the course of these investigations.

This chapter also contains a discussion of some later results of particular interest and an outline of the reasons for choosing to study the $He^4(\gamma,p)$ reaction, the photonuclear reactions in N^{14} and the (γ,α), $(\gamma,2\alpha)$ and $(\gamma,\alpha p)$ reactions in Ne^{20}.

1. MEASUREMENT OF PHOTONUCLEAR CROSS SECTIONS AND YIELDS

The energy dependence of the cross section has been measured

for 17 (γ,n) reactions and 8 (γ,p) reactions for quantum energies up to 27 Mev. All these measurements have used X-rays from an electron accelerator as the source of high energy quanta. These X-rays provide the highest intensity source of such quanta and have the advantage that they are the only source for which the energy can be varied over a wide range. They have the disadvantage of a continuous energy distribution and this limits the accuracy of the cross section measurements. For this reason the method used is discussed in some detail in § 1 (a) and 1 (b). For a number of reactions for which a full cross section curve has not been measured there have been measurements of the reaction yield for X-rays of a single energy. This yield data is reported in cases where it provides additional information.

1 (a) <u>(γ,n) Cross Section Measurements</u>.

The (γ,n) cross section measurements have all used the β activity of the product nucleus as a measure of the number of disintegrations. This method has the advantage that the parent nucleus can be identified uniquely and also, since the disintegration is detected some time after the irradiation, there are no difficulties due to the background of neutrons and softer X-rays accompanying the main X-ray beam. While all (γ,n) cross sections cannot be measured in this way there are quite a large number of nuclei with suitable radioactive products so that a reasonable survey is possible.

All cross section curves measured to date have the same general shape; namely a fairly rapid rise to a maximum value followed by a decrease to a small value at some 12 Mev above the threshold. As a

general rule the curve is more or less symmetrical about the position of the maximum which shifts to lower energies as Z increases. The "half width" is substantially constant and independent of Z while the integrated cross section increases fairly rapidly with increasing Z.

(i) Yield Curve Method.

The method of determining photonuclear cross sections from measurements of the yield as a function of X-ray energy was introduced by Baldwin and Klaiber (Ba 48) and has been considerably developed by the workers at the University of Saskatchewan (Jo 50). Measurements by other workers have generally followed their technique which is described below.

The samples were irradiated in a cavity in the centre of a lucite block (8 cm. square section) and the resultant activities were measured for a series of X-ray energies. Statistical errors in the activity measurements were generally less than 2% and the X-ray energy was stabilised and measured to within 0.1 Mev. The X-ray monitor was calibrated against an r meter placed in the same cavity as the sample. Corrections to the measured activity for backscattering and self absorption were determined in separate experiments with samples of varying thickness.

The cross section was determined by solving the integral equation

$$Y(E) = \int^{E} \sigma(E')N(E',E)\,dE'$$

where $N(E',E)$ is the number of quanta between E' and $E' + dE'$ for a peak energy E. Since the values obtained for the cross section depend

essentially on the slope of the yield curve even small errors in this curve lead to large errors in the cross section. Johns et al (Jo 50) report that errors in the yield curve produced fluctuations in the calculated values of the cross section and they therefore smoothed their experimental values to obtain a smooth cross section curve. The method is therefore incapable of providing energy resolution of better than 1 - 2 Mev. Johns et al reported that, as a test, they tried to resolve two rectangular cross sections 1 Mev in width and separated by 2 Mev and found it impossible to do so.

In the yield curve analysis the following assumptions were made -

(1) The X-ray spectrum is given by the theoretical formulae derived by Schiff (Sc 51) for the thin target X-ray intensity in the forward direction.

(2) In calculating the response of the r meter it was assumed that the thickness of the lucite wall was such that the primary X-radiation was in equilibrium with the secondary electrons produced. This condition cannot be satisfied exactly for quanta whose energy is greater than 2 or 3 Mev. The wall thickness used (4 cm. lucite which is equal to the mean range of the electrons produced by 25 Mev betatron X-rays) was evidently chosen as the best compromise. Comparison with yield measurements using absolute methods of measuring the X-ray intensity (see p. 7) shows that the errors due to this assumption are not large.

Published spectrum measurements (Po 51, Ko 50) indicate that

Table 1.1

Summarized Results of (γ,n) Cross Section Curve Measurements

Parent Isotope	Threshold	Posn. of Max.	"Half Width"	σ_{max}	σ_{int}	Max. X-ray Energy Available	Ref.
	Mev	Mev	Mev	mb.	Mev-barn	Mev	
C^{12}	18.7	22.4	4.25	11.6	0.047	27	Ha51c
N^{14}	10.8	21.5	-	-	-	27	Ho51
Mg^{24}	16.8 (calc.)	19.4	5.1	11.1	0.064	27	Ka51a
Al^{27}	14	19.2	4.7	8.2	0.045	27	"
P^{31}	12.4	19.0	7.5	17 ±2	0.120	27	Ka51b
Fe^{54}	13.8	18.3	5.7	67 ±6	0.42	27	Ka51c
Ni^{58}	12.0	18.5	4.6	60 ±6	0.33	27	"
Cu^{63}	-	17.5	6	100	0.6	20.8	Di50
	10.9	17.5	6.0	100	0.63	27	Jo50
Cu^{65}	10.2	19.0 ?	6.0	160	1.26	27	"
Zn^{64}	11.6	18.5	7.1	120 ± 10	0.83	27	Ka51c
Mo^{92}	13.1	18.7	-	175	1.05	27	Mo51
Mo^{100}	~10 ?	~17	-	-	-	23	Du50a
Ag^{107}	~9.5	16.0	4	>160	>0.82	20.8	Di50
Ag^{109}	9.3	16.0	4	320	1.65	20.8	"
Sb^{121}	9.3	14.5	5.5	>210	>1.2	27	Jo50
Sb^{123}	9.3	14.5	5.5	340	2.0	27	"
Ta^{181}	7.7 ± 0.2	14.5	8	>130	>1.0	20	Mc49
	8.0	13.5	4.5	>78	>0.39	27	Jo50

5b

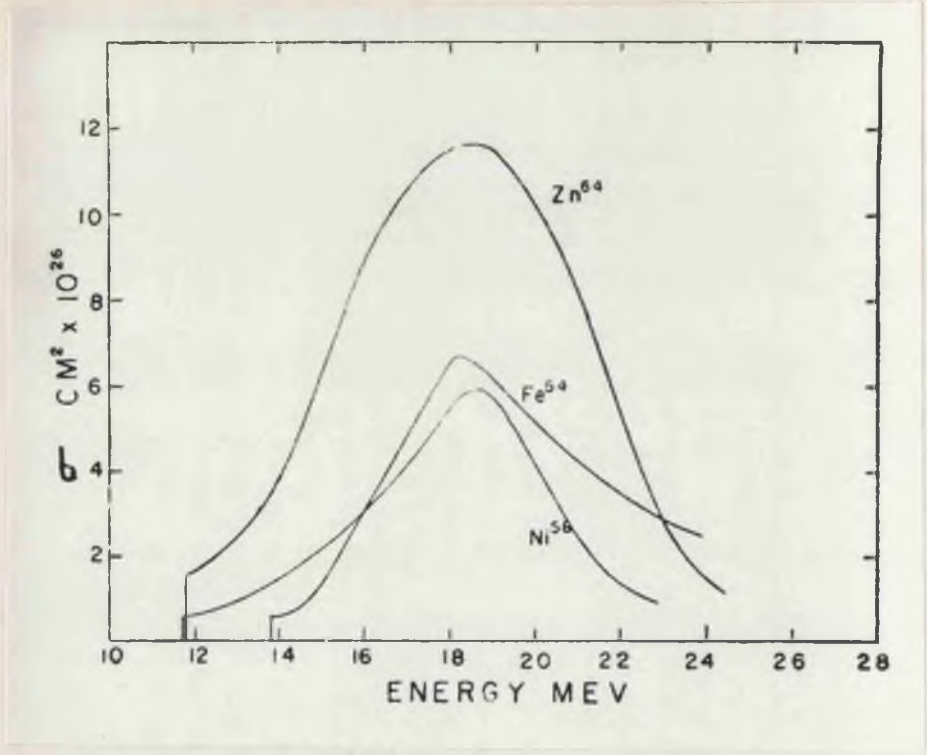

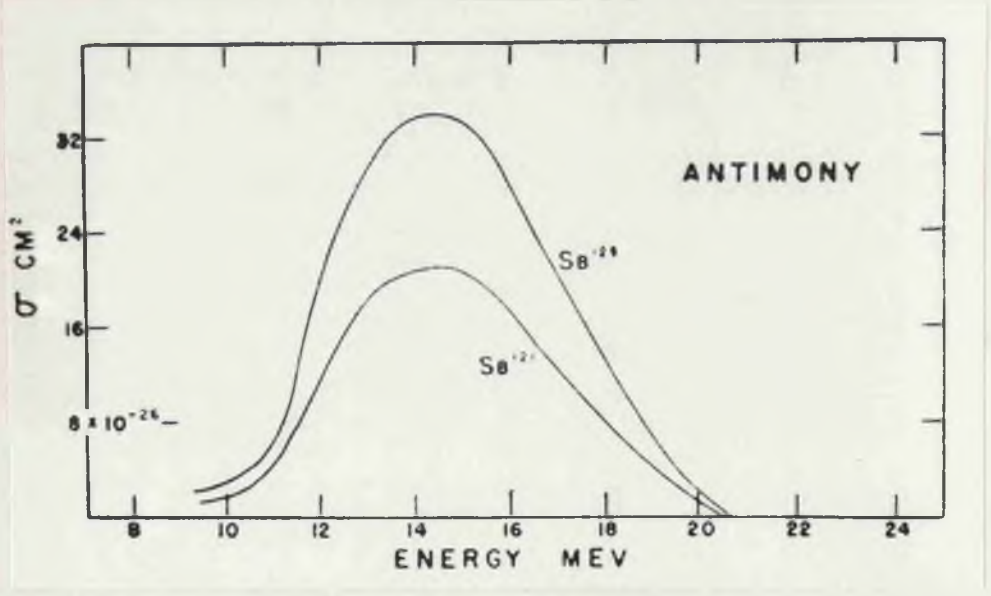

Fig. 1.1

Examples of (γ,n) cross sections measured by the yield curve method at the University of Saskatchewan.

provided the radiation is thin target radiation its spectrum is in accordance with the Schiff formula*. However since there is no published data on the type of target used and since, for these energies, it is very difficult to ensure that the electrons make only one traversal of the target the use of the Schiff formula can only be regarded as a reasonable approximation. By solving the $Cu^{63}(\gamma,n)$ yield curve using three different assumptions for the spectrum shape Johns et al showed that an error in the spectrum shape produced little change in the integrated cross section, a small error in the position of the maximum and an appreciable error in the half width.

(ii) <u>(γ,n) Cross Section Results.</u>

The characteristics of the cross section curves measured to date are summarized in Table 1.1. As has been mentioned all cross section curves have a single maximum** (for examples see Fig. 1.1). They show the following general features.

(a) Within experimental error the cross section curves are practically symmetrical about the position of the maximum. $C^{12}(\gamma,n)$ and $Fe^{54}(\gamma,n)$ are exceptions to this rule and both have a sharp rise

*Koch and Carter (Ko 50) find that their experimental spectrum contains slightly more quanta in the middle energy range than the theory predicts. This difference can be accounted for in terms of experimental inaccuracies since there appears to be nothing to stop the electrons making several traversals of the target, which would therefore be equivalent to a moderately thick target producing fewer high energy quanta than predicted by theory. The absence of the expected additional quanta below 10 Mev is attributed to the tendency to miss low energy electron pairs. An analysis of their data on the distribution of energy within the pairs indicates that this is quite probable.

**This maximum is usually referred to as the giant resonance.

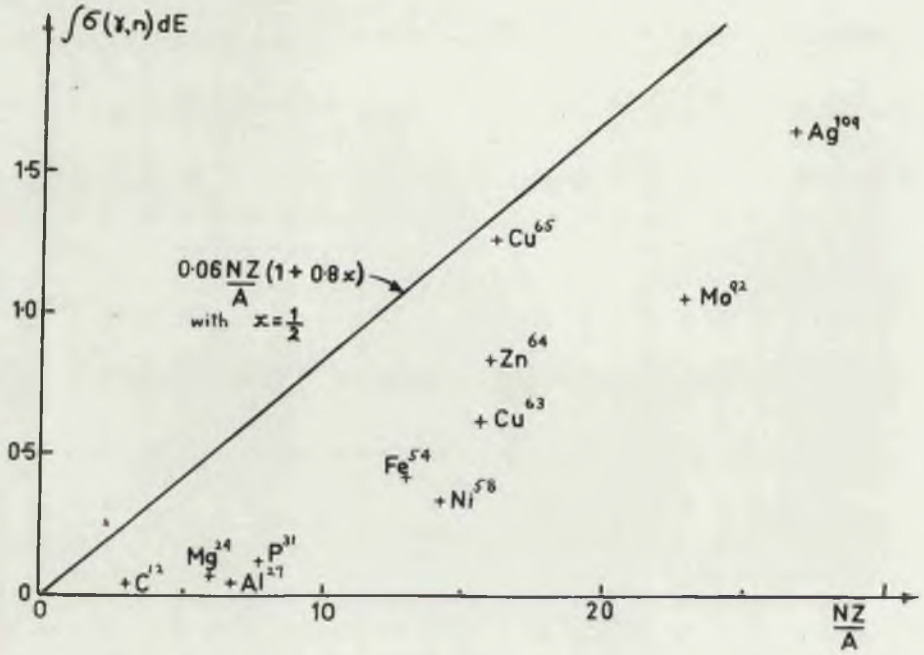

Fig. 1.2

Experimental values (as at November 1951) of the integrated cross sections for (γ,n) reactions plotted as a function of NZ/A. The straight line is the theoretical prediction of Levinger and Bethe (Le 50) for $\int_0^\infty \sigma_{E.D.} dE$, where $\sigma_{E.D.}$ is the cross section for electric dipole transitions summed over all photonuclear reactions.

and a longer tail. This behaviour is probably associated with the high (γ,n) thresholds in these two cases.

(b) The difference between the threshold and the position of the maximum is more or less constant and independent of Z, the average value being 6 Mev (extreme values 4 and 8 Mev).

(c) The half width is also more or less constant with an average value of 5.4 Mev.

(d) The integrated cross section is plotted as a function of NZ/A in Fig. 1.2. The straight line is the theoretical value for the integrated cross section for all nuclear photon absorption processes. The two sets of data are consistent with a picture in which, for light nuclei, the (γ,n) reaction is only one of a number of equally important processes while for heavy nuclei it is the dominant process.

1 (b) Comparison with Measurements of Related Quantities.

(i) Measurements of the Mean Photon Energy and Integrated Cross Section.

Several workers have measured the mean energy of quanta producing (γ,n) reactions by studying the absorption of betatron or synchrotron X-rays using the activity produced by some of the above (γ,n) reactions as the X-ray detector. The mean energy determined in this way is the mean value of a function involving the X-ray absorption coefficient and the product of the X-ray spectrum and reaction cross section. It is expected to be lower than the mean energy determined from the cross section curve but because the cross section is confined to a relatively narrow band of energies the difference will be small.

Table 1.2

"Mean" Energies of Photons Producing (γ,n) Disintegrations and Integrated Cross Sections deduced from them

Parent Isotope	Mean Photon Energy	Integrated Cross Section	Max. Energy of X-rays	Method (see note below)
	Mev	Mev-barn.	Mev	
C^{12}	22.1 ± 1.5	—	50	A
	28	0.086	50	B
	27	0.090	322	C
(C^{12}	23.5	0.047	27	D)
Cu^{63}	17.2 ± 0.4	—	50	A
	19	0.77 ± 0.15	46	B
	18	0.76	322	C
(Cu^{63}	17.5	0.63	27	D)
Cu^{65}	~19	~0.99	322	C
(Cu^{65}	19 ?	1.26	27	D)
Zn^{64}	18	0.77	~50	B
	19	~0.68	322	C
(Zn^{64}	18.5	0.83	27	D)
Ag^{107}	16	--	322	C
(Ag^{107}	16.5	--	20.8	D)

Methods used

A - measurement of absorption coefficients in two different elements.

B - measurement of absorption coefficients in a number of elements.

C - measurements of bremsstrahlung transition curves in lead.

D - results from the (γ,n) cross section curve measurements.

The following measurements have been made. Koch et al (Ko 51) measured, in good geometry, the absorption coefficient in lead and aluminium of the X-rays producing (γ,n) reactions in C^{12} and Cu^{63}. L. Marshall (Ma 51) made a similar measurement for $Cu^{63}(\gamma,n)$, $Zn^{63}(\gamma,n)$ and $C^{12}(\gamma.n)$ using a number of absorbers (Z ranged from 4 to 50). Strauch (St 51) obtained a number of mean energies by measuring transition curves in lead, for 320 Mev X-rays, using induced activities as detectors. It has been shown (Ey 51) that the mean energy can be obtained from the area under the transition curve.

Marshall et al (Ma 51a) and Strauch (St 51) have also obtained approximate values for the integrated cross sections by assuming that the photons producing these reactions are concentrated in a narrow band about the mean energy. The integrated cross section can then be deduced from the number of photons per unit energy interval at the mean energy, the measured activity and the X-ray intensity. These measurements provide a particularly useful check since the X-ray intensity measurements were made using a method (Bl 50, Ma 51a) which gives a reliable absolute determination of the X-ray intensity.

The mean energies and integrated cross sections are listed in Table 1.2. Comparison with the values deduced from the cross section curves (in brackets) shows good agreement in all cases except C^{12}. This disagreement may be due to experimental inaccuracies in the measurement of the $C^{12}(\gamma,n)$ cross section curve or alternatively it may indicate that this cross section has a much longer tail than those of other elements.

(ii) (γ,n) Yields for 50 and 100 Mev X-rays.

Perlman and Friedlander (Pe 48, Pe 49) used the radioactive product method and X-rays of 50 and 100 Mev to measure the yields of a number of (γ,n) reactions. These yields were corrected for absorption and backscattering and were expressed as yields relative to the yield for the $N^{14}(\gamma,n)$ reaction. These workers found that the relative yields are the same for both 50 and 100 Mev X-rays which indicates that either all (γ,n) cross sections have the same relative variation in the range 50 - 100 Mev or else the cross sections are vanishingly small above 50 Mev. Since the cross section measurements show that these cross sections have fallen to a small value by some 12 Mev above the threshold this suggests that these cross sections remain small at higher energies.

From this comparison it can be seen that the experimental data forms a consistent picture and indicates that the broad features of the cross section curves are fairly well established, i.e. practically all (γ,n) disintegrations occur within 12 Mev of the threshold; the cross section has a single maximum more or less symmetrically placed within this region and, in general, the integrated cross section increases fairly rapidly with increasing Z. The accuracy with which the absolute magnitude of the cross sections has been determined depends on the accuracy of the corrections for self absorption and backscattering. A comparison of the corrections used in the various cross section measurements and in the relative yield measurements of Perlman and Friedlander shows considerable variations

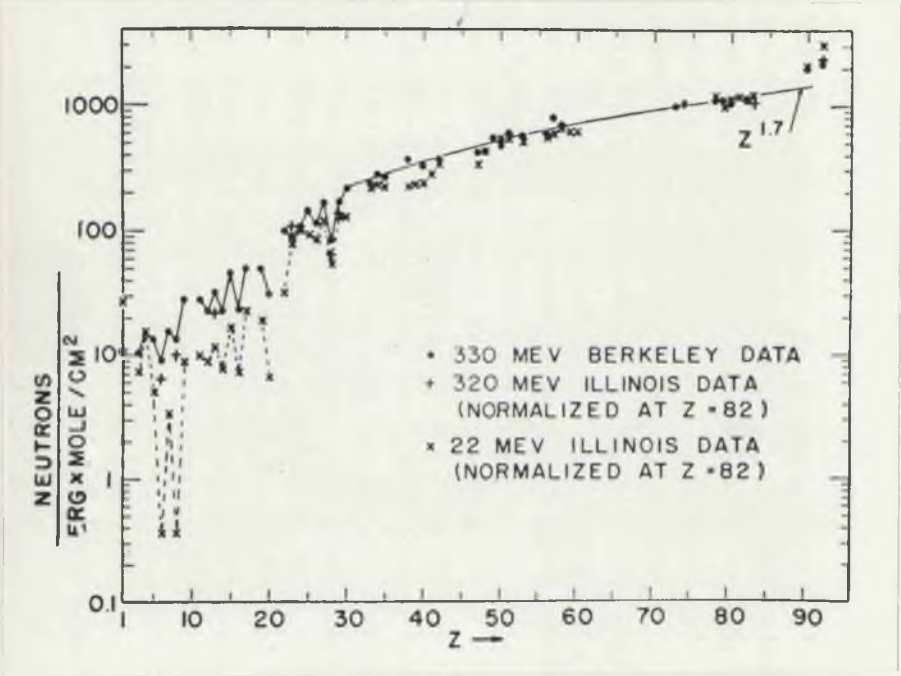

Fig. 1.3

Comparison of photoneutron yield measurements made by Terwilliger et al. (Te 51) (330 Mev Berkeley data) and Kerst and Price (320 and 22 Mev Illinois data, (Ke 51) and (Pr 50) respectively).

in these corrections and so indicates errors ~30%.

1 (c) Photoneutron Yield Measurements.

Price and Kerst have measured the neutron yields from a number of targets irradiated with X-rays of 18, 22 (Pr 50) and 320 Mev (Ke 51). Terwilliger et al (Te 51) have made similar measurements with 330 Mev X-rays. These yields are equal to the yield ($(\gamma,n) + (\gamma,pn) + 2(\gamma,2n) + \ldots$). For the heavier elements they provide a good indication of the behaviour of the total photonuclear cross section since, because of the coulomb barrier, the (γ,p) cross section will be small for these nuclei.

Both sets of workers use neutron counters that are similar to, but not quite identical with, the long counter of Hanson and McKibben (Ha 47) which is uniformly sensitive to neutrons of energy up to 5 Mev. The 330, 320 and 22 Mev yields are plotted in Fig. 1.3 where the results of Price and Kerst have been normalized to those of Terwilliger et al at Z = 82. The general agreement between the 320 and 330 Mev data is evidence for the reality of the trends shown. However it should be noted that there are systematic differences between the two sets of data which indicate that the neutron counters used have a somewhat different energy response*.

*For the normalized 320 and 330 Mev yields Price and Kerst's figures for light nuclei are consistently 30% lower than those of Terwilliger et al. The obvious explanation for this is in terms of the Z dependence of the mean neutron energy and a difference in the energy response of the two counters. Also, since both sets of workers make absolute measurements of the X-ray intensity, the factor of 1.27 required to normalize the 320 Mev data to the 330 Mev data implies a 27% discrepancy in the beam ~~energy~~ intensity and neutron counter calibrations.

Table 1.3

Summarized Results of (γ,p) Cross Section Measurements

Parent Isotope	Threshold	Position of Max.	"Half Width"	σ_{max}	σ_{int}	Max. X-ray Energy available	Ref.
	Mev	Mev	Mev	mb.	Mev-barn.	Mev	
O^{18}	16.0 ± 0.3	24	-	57 ± 19	0.15 ± 0.1	25.5	St 51b
Mg^{25}	10.6	20.5	4.5	13.7 ± 7	0.056 ± 0.028	24	To 51
Mg^{26}	14.2	22.6	3.3	21.8	0.096	27	Ka 51a

The following features of the results are of interest -

(1) For medium and heavy nuclei the yields vary quite smoothly from element to element. For 22 Mev X-rays Price and Kerst find that the yield is proportional to $Z^{2.1}$, while for 330 Mev X-rays Terwilliger et al find a $Z^{1.7}$ dependence. The yield from nickel is an exception; all workers find that the neutron yield from nickel is about half that for neighbouring elements.

(2) For light elements the yields are much smaller and also fluctuate considerably, the yields from elements of odd Z being greater than those for even Z. This result can be explained in terms of competition from the (γ,p) reaction (see He 51). The (γ,p) cross section should be significant for light nuclei and the ratio of the (γ,p) and (γ,n) cross sections is expected to depend on the relative (γ,p) and (γ,n) thresholds which fluctuate regularly with Z.

(3) Terwilliger et al measured the transition curve in lead for the quanta producing photoneutrons in lead. Their curve indicated a mean quantum energy of approximately 15 - 20 Mev.

1 (d) <u>(γ,p) Cross Section Measurements</u>.

Since most (γ,p) reactions lead to stable products the residual activity method is of limited usefulness in the measurement of these cross sections and only three (γ,p) cross sections have been measured using this technique. These results are summarized in Table 1.3. All three curves are similar to the (γ,n) cross section curves with a single maximum a few Mev above the threshold, but have a more gradual rise to this maximum which is also slightly further displaced

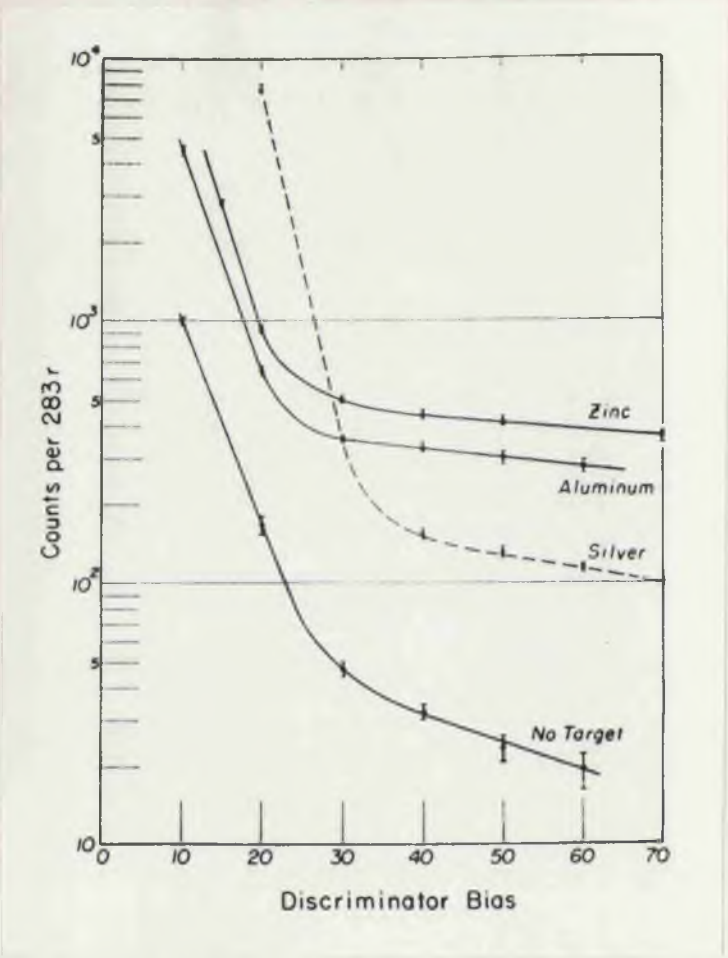

Fig. 1.4

Integral pulse height distributions obtained by Mann and Halpern (Ma 51c) in their photoproton yield measurements using scintillation counters. The tail of larger pulses is attributed to protons and the large number of smaller pulses to electron pile up. The integral pulse height distribution is the number of pulses larger than a given voltage V, plotted as a function of V.

from the threshold than in the case for the (γ,n) curves. Although this is just what would be expected if the (γ,p) cross section curve had inherently the same shape as the (γ,n) curve with the first 10 Mev or so reduced by the effect of the coulomb barrier there is clearly not sufficient evidence to conclude that this is generally true.

1 (e) Photoproton Yield Measurements.

(i) Photoproton Measurements with Counters.

Mann and Halpern (Ma 51c) have used a scintillation counter fitted with a ZnS screen to measure the proton yields from twenty elements irradiated with 23.5 Mev X-rays. Since ZnS gives much larger pulses for single protons than for single electrons it is, in principle, quite possible to separate the photoproton pulses from the background of electron pulses. However Mann and Halpern found that, even with elaborate shielding, the number of electron pulses is so large that they pile up within the resolving time of the counting system and may produce pulses comparable with or larger than the proton pulses. Since the half width of the X-ray pulse is only 0.5 μs these workers did not attempt to shorten the resolving time but operated the betatron at a reduced X-ray intensity in order to limit the amount of pile up. They separated this background by measuring the integral pulse height distributions which had the form shown by the examples in Fig. 1.4. The tail of larger pulses was attributed to protons since the particles producing them were not absorbed by 0.00035" Al (and therefore could not be α particles) but were absorbed by 0.0027" Al (and therefore were not electrons or neutrons). The large group of smaller pulses was attributed

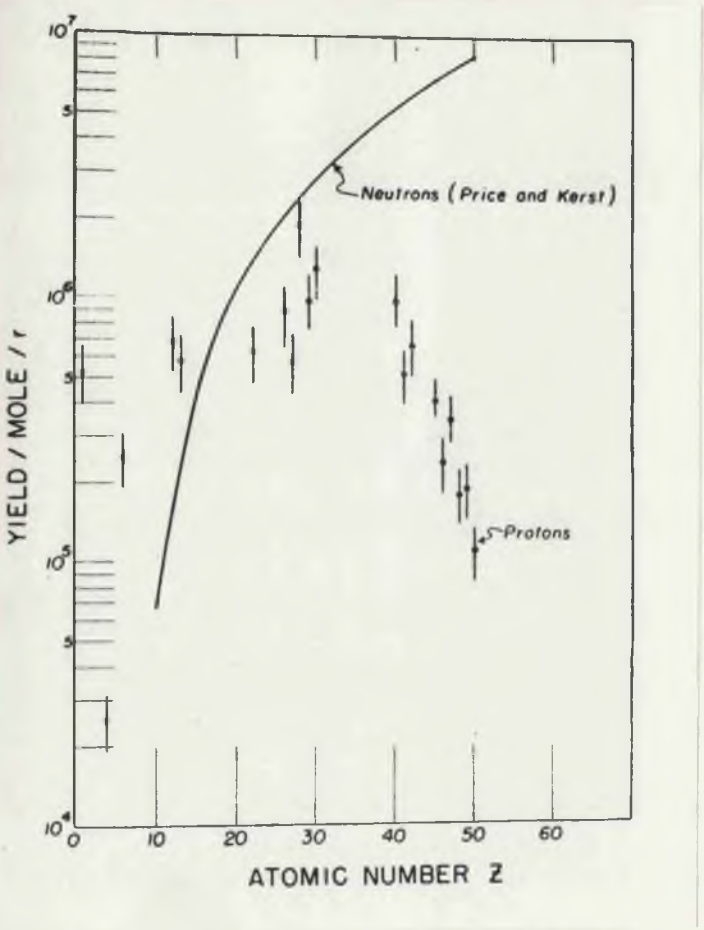

Fig. 1.5

Photoproton yields measured by Mann and Halpern (Ma 51c). These workers have since revised their corrections for absorption in the foil target and report (Ha 51) that the yields are 30% less than the values plotted. The ourve is a smoothed fit to the 22 Mev neutron yields measured by Price and Kerst (Pr 50).

to electron pile up. They estimated the proton yield by subtracting these background pulses (assuming an exponential fall off with pulse height) and extrapolating the difference back to zero bias. In calculating the yields Mann and Halpern had to make corrections of slightly more than a factor of 2 for the absorption of protons in the target (the targets used were approximately 5 Mev thick). They originally estimated these corrections using a proton spectrum of the form found by Byerly and Stephens (By 51) for copper but have since (Ha 51) reduced the yields corrected in this way by 30% in order to bring them into better agreement with measurements of the variation of yield with target thickness. These measurements were made for three thicknesses of aluminium and two of copper.

The measured yields are plotted in Fig. 1.5 and should be reduced by 30% to bring them into line with the revised absorption corrections. The fall off in yield for higher Z can be directly attributed to the effect of the coulomb barrier. Comparison with the neutron yield data of Price and Kerst for 22 Mev X-rays shows that a low neutron yield corresponds to a high proton yield and vice versa, which is further evidence for the smooth variation of the total photonuclear cross section. The outstanding example of this is nickel which had an exceptionally low neutron yield and has the highest proton yield. For light nuclei the proton yields are about twice the neutron yields but it is possible that this difference may be due to experimental errors.

Comparison of these results with those of workers who used

Table 1.4

Comparison of Photoproton Yield Measurements with Data from Nuclear Emulsion Experiments

Element	Mann and Halpern	Nuclear Emulsion Experiments		
	Yield* at 23.5 Mev	Yield*	X-ray Energy	Reference
Mg	4.8 ± 1.1	1.9 ± 1.4	22 Mev	To 51
Al		1.0	17.1 Mev	
		1.7	20.8 Mev	Di 50
		Hence	infer	
	5.8 ± 1.4	[~ 2.5	23.5 Mev]	
Cu	6.9 ± 1.4	10.7	24 Mev	By 51a
Ag	3.5 ± 0.7	1.2	20.8 Mev	Di 50

*Photoproton yield in units of 10^5 protons/mole/r.

Table 1.5

Photoproton Cross Section Measurements of Halpern and Mann

Element	Energy of Peak	σ_{max}	"Half-Width"	σ_{int}	$\sigma_{int(\gamma,n)}$
	Mev	mb.	Mev	Mev-barns	Mev-barns
C	21.5 ± 0.5	34 ± 8	1.7 ± 0.5	0.063 ± 0.016	0.047
Al	21.2 ± 0.5	22 ± 6	5.4 ± 0.5	0.12 ± 0.03	0.045
Ni	18.7 ± 0.5	58 ± 15	5.4 ± 0.5	0.32 ± 0.08	0.33
Co	21.5 ± 0.5	24 ± 6	5.7 ± 1.0	0.14 ± 0.04	-
Cb	21.3 ± 0.5	18 ± 5	6.6 ± 1.0	0.12 ± 0.03	-

Table 1.6

Relative (γ,p) Yields from the Activity

Measurements of Perlman and Friedlander

Parent Isotope	Rel. Yield ($N^{14}(\gamma,n) = 1.00$) 50 Mev	Rel. Yield ($N^{14}(\gamma,n) = 1.00$) 100 Mev
Si^{30}	6.6	5.8
Fe^{57}	7.6	7.6
Ni^{62}	5.0	5.4
Ge^{74}	-	2.5
Mo^{98}	3.1	5.0
Ru^{102}	3.6	3.7

nuclear emulsions to detect protons emitted from metal foils provides a check on their accuracy. The relevant data is given in Table 1.4. When allowance is made for the differences in X-ray energy the yields of Mann and Halpern are about a factor of two greater than the yields measured by nuclear emulsions for all cases except the measurements of Byerly and Stephens on copper.

Halpern and Mann (Ha 51) have used the above technique to measure five (γ,proton) cross sections by the yield curve method. The shapes of these cross section curves are similar to those found for the (γ,n) and other (γ,p) reactions and the relevant parameters are given in Table 1.5 together with the integrated cross section for the (γ,n) reaction where this has been measured. In view of the sources of error mentioned above and the fact that the quoted errors in the yield points are ± 5% it is felt that the errors quoted by Halpern and Mann are probably optomistic.

(ii) Measurements of Residual Activity.

During their relative yield measurements Perlman and Friedlander (Pe 48, Pe 49) measured the yields (relative to the yield for $N^{14}(\gamma,n)$) of six (γ,p) reactions. Their results are given in Table 1.6. The 50 Mev and 100 Mev yields are approximately equal suggesting that the cross sections are small above 50 Mev. The relative variation of the yields is in good agreement with the results of Mann and Halpern.

1 (f) <u>(γ,p) Cross Sections for p + Li^7 γ-rays</u>.

Hirzel and Wäffler (Hi 47) have measured the cross sections

Table 1.7

Measurements, by Hirzel and Waffler, of (γ,p) Cross Sections for p + Li^7, γ-Rays

Parent Isotope	Relative (γ,p) Cross Section	$\frac{\sigma(\gamma,p)}{\sigma(\gamma,n)}$ Exptl.	$\frac{\sigma(\gamma,p)}{\sigma(\gamma,n)}$ Theor.
Mg^{25}	2.83		
Mg^{26}	1.56		
Si^{29}	3.45		
Si^{30}	1.26		
Ti^{50}	1.62	0.054	0.012
Cr^{53}	8.1	0.324	0.047
Se^{77}	4.8	0.048	2.0×10^{-3}
Mo^{98}	3.5	0.028	1.4×10^{-3}
Pd^{105}	7.3	0.055	7.7×10^{-4}
Cd^{111}	4.4	0.034	2.9×10^{-4}
Cd^{112}	5.3	0.040	1.0×10^{-3}
Cd^{113}	6.0	0.046	5.4×10^{-4}
Sn^{117}	2.9	0.022	1.4×10^{-4}
Sn^{118}	1.5	0.011	1.8×10^{-4}

(relative to the $Cu^{63}(\gamma,n)$ cross section) of a number of (γ,p) and (γ,n) reactions produced by the $p + Li^7$ γ-rays. The results were analysed by a method which permitted the use of thick cylindrical samples with a consequent increase in activity. Three independent experimental methods were used to eliminate the disturbing effect of (n,p) reactions. Their results are listed in Table 1.7 and show a similar variation with Z to the measurements reported above. For the medium and heavy nuclei Hirzel and Wäffler compared their results with the predictions of the statistical theory by calculating the relative numbers of protons and neutrons emitted from the compound nucleus and comparing this with the experimentally measured ratio of $\sigma(\gamma,p)$ to $\sigma(\gamma,n)$ for a neighbouring nucleus. (In no case were they able to measure both for the same nucleus). In making the theoretical estimate it is necessary to know the binding energies quite accurately. For Ti^{50} and Cr^{53} Hirzel and Wäffler obtained the binding energies from the nuclear masses (Po 40). For other nuclei they calculated what they consider to be an upper limit to the proton-neutron ratio by putting the neutron binding energy equal to 7.5 Mev* and using the β-ray energy to give the difference in neutron and proton binding energies. These theoretical estimates are listed in Table 1.7 and are less than the experimental values by a factor of 10 - 100. Schiff (Sc 48), Courant (Co 51) and others have suggested explanations for this disagreement but none of these are compatible with all the relevant experimental results. These explanations are

*Hirzel and Wäffler regard this figure as a lower limit for the neutron binding energy.

Table 1.8

Mean Photon Energies, Relative Yields and Relative Cross Sections for Photon Reactions other than (γ,n) and (γ,p)

Reaction	Mean Photon Energy	Rel. Yield	Rel. σ_{int}	Ref.
	Mev			
($C^{12}(\gamma,n)$	27	7.4	12	St 51)
$C^{12}(\gamma,2n)$	-	< 0.0009	-	Pe 48
($F^{19}(\gamma,n)$	-	8.0	-	Pe 48)
$F^{19}(\gamma,2n)$	-	0.44 (50 Mev)	-	Pe 48
	-	0.65 (100 Mev)	-	
($Al^{27}(\gamma,n)$	-	6.8	-	Pe 48)
	-	-	7.1	Ka 51a)
$Al^{27}(\gamma,2p)$	-	0.41 (50 Mev)	-	Pe 48
	-	0.44 (100 Mev)	-	
($P^{31}(\gamma,n)$	-	21	-	Pe 48)
$P^{31}(\gamma,2n)$	-	< 0.3	-	Pe 48
$P^{31}(\gamma,2p)$	-	0.44 (50 Mev)	-	Pe 48
	-	0.49 (100 Mev)	-	
$S^{32}(\gamma,np)^{d}$	25	-	2.6	Ka51b
($Cu^{63}(\gamma,n)$	18	100 (standard)	100	St 51)
$Cu^{63}(\gamma,2n)$	-	7.4 (50 Mev)	-	Pe 48
	-	9.7 (100 Mev)	-	
$Cu^{63}(\gamma,2p)$	-	0.47	-	Pe 48
$Cu^{65}(\gamma,\alpha)$	-	-	$\sim 7 \times 10^{-3}$	Ha 51b
($Zn^{64}(\gamma,n)$	19	83	89	St 51)
	18.5	-	132	Ka 51c)
$Zn^{64}(\gamma,2n)$	29	3.9	6.7	St 51
$Zn^{64}(\gamma,pn)$	30	21	37	"

Table 1.8 Contd.

Reaction	Mean Photon Energy	Rel. Yield	Rel. σ_{int}	Ref.
	Mev			
$Zn^{64}(\gamma,p2n)$	~ 57	4.5	17	St 51
$Zn^{66}(\gamma,pn)$	~ 30	11	19	St 51
$Zn^{66}(\gamma,3n)$	-	2.9	-	"
$Zn^{66}(\gamma,p3n)$	-	3.3	-	"
$Zn^{66}(\gamma,p4n)$	-	1.4	-	"
$Zn^{67}(\gamma,4n)$	-	< 2	-	"
$Zn^{68}(\gamma,p)$	24	7.0	9.7	"
$Ge^{70}(\gamma,pn)$	-	9.9	—	Pe 49
$Rb^{87}(\gamma,\alpha)$	22	-	7×10^{-4}	Ha 51a
$Ta^{181}(\gamma,2p..)$ (Rare earth)	68	-	-	St 51

discussed in § 2 (c) on p.26 .

1 (g) Yields for Reactions other than (γ,p) and (γ,n).

A few investigations of more complex disintegrations have been made using the radioactive product method and, in addition, for very light nuclei ($Z \leq 8$) some measurements have been made by studying the stars formed in nuclear emulsions or in the gas of a cloud chamber (see next section). The results of the radioactive measurements are summarized in Table 1.8, which includes, for comparison, the corresponding data for the (γ,n) reactions in the same nuclei. The yields and integrated cross sections are given relative to Cu^{63}(γ,n) = 100. The experimental measurements were made by

(a) Perlman and Friedlander (Pe 48, Pe 49) who used the same technique as for the (γ,n) and (γ,p) relative yield measurements;

(b) Strauch (St 51) who measured relative yields and determined the mean photon energy from the transition curve in lead. He then used these results to estimate the integrated cross section;

(c) the group at the University of Saskatchewan (Ha 51a and b, Ka 51a, b and c) who used the yield curve technique to measure cross section curves.

Although there are not sufficient results to permit general conclusions the results do indicate that, for medium nuclei, the "complex" disintegrations are less likely than the ejection of a single nucleon, the integrated cross section apparently decreasing with the number of nucleons emitted. This suggests that the total photonuclear cross section has a maximum value near the maximum in the (γ,n) cross

section. There is some evidence that the total photonuclear cross section has a tail extending out to quite high energies.

A comparison of Strauch's results for $Zn^{64}(\gamma,pn)$ and $(\gamma,2n)$ with an experiment by Ghoshal (Gh 50) provides evidence that these photonuclear reactions proceed via a compound nucleus. Ghoshal bombarded Cu^{63} with protons and Ni^{60} with α particles and measured the cross section curves for the emission of a n, 2n or pn group. He found that

$$\sigma(p,n) : \sigma(p,2n) : \sigma(p,pn) = \sigma(\alpha,n) : \sigma(\alpha,2n) : \sigma(\alpha,pn)$$

just as would be expected if these reactions involved a Zn^{64} compound nucleus whose decay was independent of its mode of formation. The cross section curves for the corresponding photodisintegrations have not been measured so that a complete comparison is not possible but the following points of agreement are evident.

(a) The mean photon energies for the (γ,n), (γ,pn) and $(\gamma,2n)$ processes in Zn^{64} are 19, 29 and 30 Mev which is just less than the mean excitation energies found in the charged particle reactions (21, 32 and 33 Mev* respectively). As the particle absorption cross sections are rising and the photon absorption cross section is falling with increasing energy the second set of mean energies should be slightly higher than the first.

(b) $\dfrac{\sigma_{int}(\gamma,pn)}{\sigma_{int}(\gamma,2n)} \simeq 5.5$ which is in approximate agreement

*The binding energy of the α particle in Zn^{64} was taken as 1 Mev (De 48, Du 50).

with the value of 4 found for $\sigma_{max}(\gamma,pn) / \sigma_{max}(\gamma,2n)$. Although these two ratios are not strictly comparable approximate agreement can be expected since the cross section curves are only a few Mev wide.

1 (h) Photonuclear Reactions in Very Light Nuclei.

For the very light nuclei ($Z \leq 8$) quite a number of photonuclear reactions can be studied by observing the stars produced in nuclear emulsions or in cloud chambers. Because nuclear emulsions generally contain several light elements (C, N and O plus any loading present) the events of interest must be separated from those due to a large number of possible star producing reactions. Disintegrations involving only charged particles can usually be identified since their resultant momentum must equal that of the incident photon. Generally speaking disintegrations involving neutrons or those with fragments containing more than six nucleons cannot be identified. With the cloud chamber, identification is considerably easier since not only can unwanted nuclei be eliminated but also the stopping power can be adjusted within quite wide limits so that, even for heavy fragments, tracks of measurable length can be obtained.

(i) Disintegrations observed in Nuclear Emulsions.

The $C^{12}(\gamma,3\alpha)$ and $O^{16}(\gamma,4\alpha)$ reactions have been studied fairly extensively with this technique and the detection of a number of other reactions has been reported.

(a) $C^{12}(\gamma,3\alpha)$. This reaction has been observed with both the p + Li^7 γ-rays (Ha 48, Te 50) and with 25 Mev X-rays (Go 50, Wi 51a, Te 50). The stars measured by Wilkins and Goward (Wi 51a) are

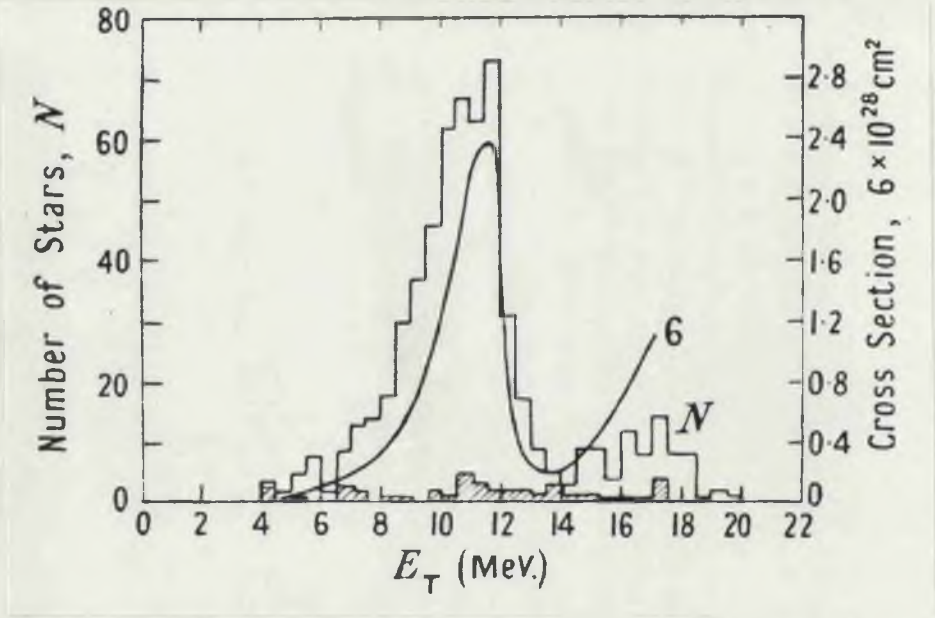

Fig. 1.6

Results of Wilkins and Goward (Wi 51a) for $C^{12}(\gamma,3\alpha)$ stars produced in nuclear emulsions irradiated with 25 Mev X-rays. The number of stars is plotted as a function of E_T, the total energy of the three α particles ($E_\gamma = E_T + 7.3$ Mev). The solid curve is the cross section obtained from this histogram.

plotted in Fig. 1.6 as a function of E_T, the total energy of the three α particles ($E_\gamma = E_T + 7.3$). The solid line is the cross section deduced using the theoretical X-ray spectrum. Wilkins and Goward estimate the maximum cross section to be 2.4×10^{-28} cm^2 and state that this may still be too low by up to 50%. From a study of the ranges of the α particles and the angles between them they show that in most cases the disintegration proceeds via the 3 Mev excited state in Be^8. There is not sufficient data to determine whether or not the re-increase of the cross section for quantum energies greater than 19 Mev is due to disintegrations involving a different set of levels. This reaction is discussed at some length in § 4 which deals with the measurements on the $C^{12}(\gamma,3\alpha)$ reaction since 1951 and their interpretation in terms of the isotopic spin selection rules.

(b) $O^{16}(\gamma,4\alpha)$. This reaction has been studied by Goward et al (Go 49, Go 50a, Go 51) using 25 Mev X-rays and some 200 stars have been measured. The threshold calculated from the masses is 14.5 Mev; the cross section curve starts at 20 Mev and increases steadily reaching a value of 2×10^{-28} cm^2 at the highest energy available (25 Mev).

The reported modes of disintegration are

(1) Somewhat over half the events proceed via either a 9.7 Mev or a 13.5 Mev level in C^{12} to the ground state of Be^8.

(2) Most of the remainder proceed via a level in C^{12} (at, very approximately, 11 Mev) to an excited Be^8 nucleus.

(3) In a few cases the O^{16} nucleus disintegrates

Table 1.9

Summarized Results for Photo-Disintegrations Reported in Nuclear Emulsions

(Excluding $C^{12}(\gamma,3\alpha)$ and $O^{16}(\gamma,4\alpha)$)

Reaction	No. of Events	Cross Section	Source of Quanta	Ref.
$Li^6(\gamma,n)Li^5$	7	$(5 \pm 2) \times 10^{-28}$ cm^2	$p + Li^7$	Ti 51
$Li^6(\gamma,d)He^4$	looked for but not found	$< 10^{-29}$	$p + Li^7$, $p + F^{19}$ (6.3 Mev) and Na^{24}(2.76 Mev)	Ti 50
$Li^7(\gamma,t)He^4$	27	$(1.2 \pm 0.6) \times 10^{-28}$	$p + Li^7$	Ti 50a
$B^{10}(\gamma,d)2\alpha$	11	$\sim 10^{-28}$	24 Mev X-rays	Go50b, Wi 50
$B^{11}(\gamma,t)2\alpha$	22 ($1/3$ doubtful)	"	"	
$N^{14}(\gamma,d)3\alpha$	13	$\sim 10^{-28}$	"	Go51a

directly into two Be^8 nuclei. In particular 6 of the 200 stars were found to involve two ground state Be^8 nuclei.

(c) Other disintegrations reported. The experimental results for these disintegrations are summarized in Table 1.9.

(ii) Disintegrations Observed in Cloud Chambers.

The only results of cloud chamber studies are those of Gaerttner and Yeater who have investigated the photodisintegration of N^{14} (Ga 50a, b,c), O^{16} (Ga 50b, c), C^{12} (Ga 51a) and He^4 (Ga 51b). These workers were concerned to reduce the time taken to collect and analyse data and achieved this by using a 5" diameter cloud chamber (Ga 49) incorporating overcompression immediately after the expansion* and by limiting their analysis to horizontal projections of the tracks.

Since Gaerttner and Yeater did not measure either ranges or magnetic rigidity their experimental measurements were limited to

(1) The number of charged particles involved in a particular disintegration.

(2) A visual estimate of the ionization density of the tracks. (This enables the recoiling nucleus to be separated from the lighter fragments but does not give any real indication of the nature of these fragments).

(3) The angle between the incident γ-ray and the horizontal projection of the tracks.

Their results are as follows

(a) C^{12}, N^{14}, O^{16}. In analysing their data Gaerttner

*The cycling time of this chamber was 5 - 6 seconds. The pressure of the gas filling was in the range $^1/_2$ - 1 atmosphere.

Table 1.10

Cloud Chamber Measurements on Flag Events by Gaerttner and Yeater

Target Nucleus	Fraction of Flags Involving a Neutron	σ_{int} Flags	Angular Distribution of Fragment
		Mev-barn.	
C^{12}	0.10	0.22 ± 0.09	$1 + 3 \sin^2\theta$
N^{14}	0.66	0.3	-
O^{16}	0.16	0.3	-

Table 1.11

Cloud Chamber Measurements on Star Events by Gaerttner and Yeater

Target Nucleus	X-ray Energy	R_{12}	R_{32}	R_{42}	$R_{3+4,2}$	N_{2+3+4}	N_5
C^{12}	100 Mev	-	0.178	0.032	0.21	1800	2
	50 Mev	-	0.092	0.017			
N^{14}	100 Mev	0.25	0.200	0.126	0.33	3111	17
	50 Mev	-	0.153	0.077		636	0
O^{16}	100 Mev	0.52	-	-	0.23	780	0

R_{12} -ratio of singles to flags.

R_{32} -ratio of 3 pronged stars to flags.

R_{42} and $R_{3+4,2}$ -defined similarly.

N_{2+3+4} -total number of flags, 3 and 4 pronged stars.

and Yeater divided the observed events into three groups - "singles" (single short tracks which are attributed to recoils from (γ,n) reactions), "flags" (pairs of tracks one of which is short and heavily ionizing) and "stars" (events with three or more tracks).

Their results for the flag events are as follows. For N^{14} they compared the number of flags for 50 and 100 Mev X-rays with the Cu^{62} activity produced by irradiation with corresponding amounts of X-rays. Putting number of flags/Cu^{62} activity = 1.00 at 50 Mev they find a value of 0.89 ± 0.14 for this ratio at 100 Mev. Although not very accurate this result indicates that all, or practically all, the quanta producing flags in N^{14} have energies less than 50 Mev.

Gaerttner and Yeater made the following estimate of the fraction of flags in which a neutron is emitted. Clearly a neutron has been emitted if both tracks of the flag are on the same side of the incident photon or if the resultant momentum has a component in the direction opposite to that of the incident photon. Assuming that the neutron is equally likely to be going "backwards" as "forwards" then the total number of flags in which a neutron is emitted is equal to $N_1 + 2N_2$ where N_1,N_2 respectively are the number of flags with the above characteristics. The results for the fraction of flags involving a neutron are given in Table 1.10 which shows that this fraction is small for C^{12} and O^{16} but very large for N^{14}. For the C^{12} flags the distribution of the projected angles of all fragment tracks was consistent with an angular distribution of the form $1 + 3\sin^2\theta$.

Gaerttner and Yeater obtained approximate integrated

cross sections for these flag events by running the betatron at a reduced X-ray intensity and comparing the number of flags (in air) with the number of ± electron pairs produced in the gas and having energies between 20 and 40 Mev (the assumed energy range for the flag producing quanta). These cross sections are also given in Table 1.10. They will be only approximate since they depend on a guess at the mean energy and since no check was made to see that the chamber was equally sensitive to both electrons and heavy particles. The results of Phillips et al (Ph 50) show that some care is necessary to avoid errors from this source.

The results for the star events are summarized in Table 1.11. The numbers of three and four pronged stars are both appreciable and less than the number of flags indicating that the cross sections for the more complex reactions are somewhat less than the cross sections for flag events, which are believed to be mainly (γ,p) and (γ,pn) events. For the two nuclei for which results are available the ratio of stars to flags increases between 50 and 100 Mev indicating that the star producing reactions have appreciable cross sections above 50 Mev. For N^{14}, Gaerttner and Yeater made additional runs for a series of peak energies between 20 and 100 Mev. The data from these runs has rather large statistical errors but it does indicate that the ratio of three pronged stars to flags is constant above 60 Mev and falls to almost zero as the X-ray energy is reduced from 60 Mev to 30 Mev. The ratio of four pronged stars to flags is also constant above 60 Mev and falls off slightly more rapidly than the above ratio below this energy. This

suggests that the cross sections for three and four pronged stars are peaks with mean energies between 40 and 50 Mev. Using these mean energies, the integrated cross sections for flags, three pronged stars and four pronged stars in N^{14} are approximately in the ratio of $1 : 1/3 : 1/4$.

(b) He^4. Gaerttner and Yeater's experiment on the photodisintegration of He^4 is described in more detail in Chapter III (see p. 80). Briefly they find that the only important reactions in He^4 are (γ,p) and (γ,n), that the mean energy of the quanta producing the (γ,p) disintegrations is approximately 27 Mev and that the angular distribution of the photoprotons is consistent with a $\sin^2\theta$ distribution. The 100 Mev yield for the (γ,n) reaction is 1.3 ± 0.3 times that for the (γ,p) reaction.

Thus the cloud chamber measurements provide a general picture of the photodisintegration of these nuclei. They indicate that for light nuclei the more complex reactions are probably more important than they are for heavier nuclei and the photon absorption cross section is appreciable at energies well above the giant resonance. Also it is clear, from the variation in the fraction of flags involving a neutron, that there are large fluctuations in the ratio of (γ,p) and (γ,pn) cross sections.

The nuclear emulsion measurements on the $C^{12}(\gamma,3\alpha)$ and $O^{16}(\gamma,4\alpha)$ stars give a considerable amount of information on the mechanism of the reaction in addition to the cross sections. These cross section measurements do not involve the analysis of a yield curve and therefore they are inherently more reliable than measurements by the

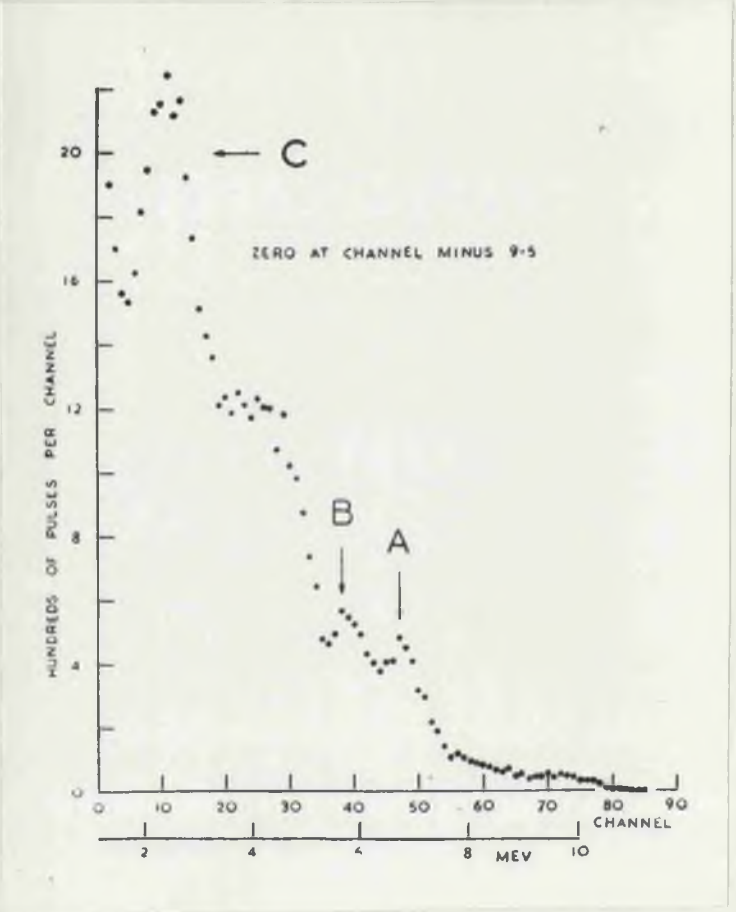

Fig. 1.7

Energy distribution of the photoprotons from argon irradiated with γ-rays from the p + Li^7 reaction (Wi 51c). Groups A and B are identified as photoprotons leaving Cl^{39} in the ground state and first excited state respectively. The tail extending from 7.5 to 10 Mev is attributed to the reaction $A^{40}(\gamma,\alpha)S^{36}$. These α particles should have little effect on the main distribution since the coulomb barrier will reduce the probability for their emission with lower energies.

yield curve method. Their energy resolution is determined by the accuracy of the range measurement of the total energy. For nuclear emulsions this is $\sim$ 1 Mev, for a cloud chamber it is $\sim$100 kev for stars in which all tracks can be measured. Since there are a number of star producing reactions that can be studied in nuclear emulsions and probably a considerable number that can be studied with a cloud chamber such measurements could be a fruitful source of information on the mechanism of photodisintegration.

2. ENERGY AND ANGULAR DISTRIBUTIONS OF THE EMITTED NUCLEONS

There have been only a few measurements of these distributions but these all indicate that, apart from a small percentage of nucleons which are emitted with all the available energy, the nucleons have the energy spectrum predicted by the statistical theory and an isotropic angular distribution.

2 (a) Measurements with Monoenergetic γ-Rays.

Wilkinson and Carver (Wi 51c) have measured the spectrum of photoprotons from argon irradiated with p + Li^7 γ-rays by measuring the pulse size distribution in an argon filled proportional counter which was lined with graphite in order to eliminate errors due to photoprotons from the wall ($C^{12}(\gamma,p)$ threshold = 16.0 Mev). The spectrum they obtained (see Fig. 1.7) contains a large number of protons whose energies are much less than the maximum available and has a shape very similar to that predicted by the statistical theory. Exact agreement cannot be expected for a light nucleus where individual level properties may influence the proton energy distribution quite markedly. The (γ,p)

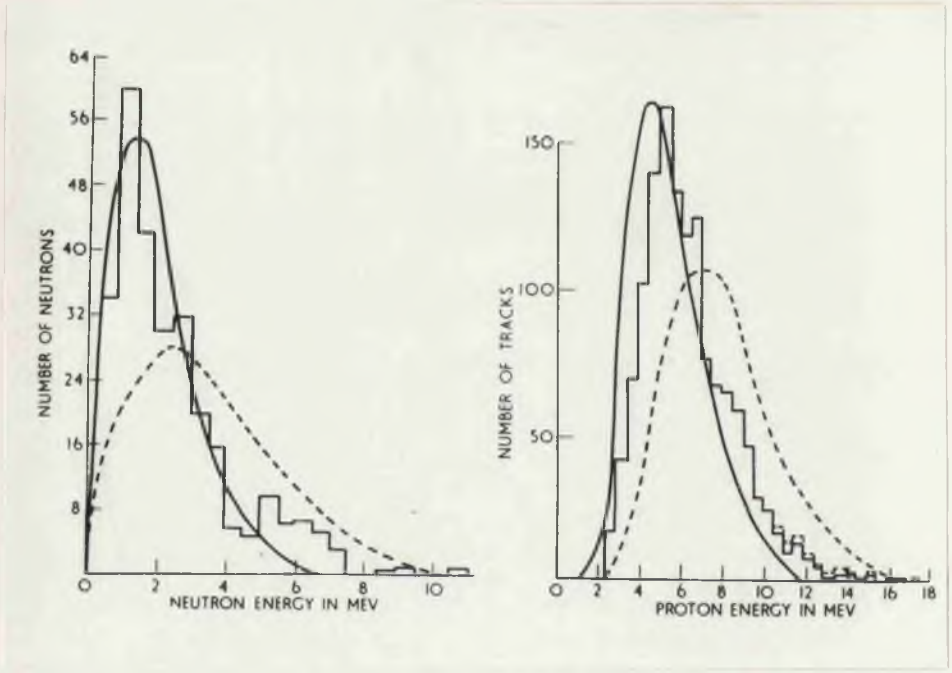

Fig. 1.8

Spectra of photoneutrons and photoprotons from copper irradiated with 24 Mev X-rays. These were measured by Byerly and Stephens (By 51a) using nuclear emulsions as detectors. The full curves are the spectra predicted by the evaporation model and the dotted curves are the spectra predicted by the Schiff model (Sc 48).

cross section found by Wilkinson and Carver is 5.4 millibarn which is several times that expected from the statistical theory.

2 (b) Experiments Using High Energy X-rays.

There have been several measurements of the energy and angular distribution of photoprotons ejected from thin metallic foil targets irradiated with 20 - 25 Mev X-rays using nuclear emulsions placed just outside a well collimated X-ray beam to detect the protons.

The elements whose spectra have been investigated are

Ag and Al - Diven and Almy (Di 50)

Cu - Byerly and Stephens* (By 51a)

Mg and Mg^{25} - Toms and Stephens (To 51)

Byerly and Stephens have also measured the energy spectrum of the photoprotons from copper by measuring proton recoils in nuclear emulsions placed near a copper target.

The energy distributions for copper (see Fig. 1.8) and that for silver are all in good agreement with the distributions predicted from the statistical theory and the theoretical X-ray spectrum** expect

*As one of their main claims Byerly and Stephens state that grain count measurements show that approximately 30% of the charged particles originating in the copper foil are deuterons and not protons. However Dr. Muirhead has pointed out to me that this result is unreliable because of the small length of track used for their grain counts and also because the observed results can be explained by additional shrinkage in the surface layer of the emulsion which is a fairly common occurrence. For these reasons this claim has been disregarded.

**If the "deuterons" reported by Byerly and Stephens are assumed to be protons and added to the proton distribution they will increase the height of this distribution below 6 Mev and thus bring it closer to the statistical prediction.

for high energies where there are more nucleons than are predicted by the statistical theory. The photoproton angular distribution measurements show that for both copper and silver the lower energy photoprotons have an isotropic angular distribution while the additional high energy photoprotons have an angular distribution which resembles a $\sin^2\theta$ distribution. Diven and Almy also show that the yield of the lower energy photoprotons is in reasonable accord with the yield predicted by the statistical theory. Although there are no corresponding angular distribution measurements for neutrons, some preliminary results indicate that it is probable that most of the neutrons emitted have an isotropic distribution. Price and Kerst (Pr 50) and Terwilliger et al (Te 51) have made rough measurements of the neutron angular distribution (averaged over all energies) and find that it is approximately isotropic for lead, iron and nickel. For the light nuclei sulphur and carbon the $(\text{yield})_{40°}/(\text{yield})_{90°} \simeq 0.95$ and 0.90 respectively suggesting that for these nuclei the neutron angular distribution is peaked at 90°.

For the light nuclei aluminium and magnesium the proton angular distributions are isotropic for all proton energies and the energy spectra are consistent with those to be expected from a slowly increasing level density.

The above results have a direct bearing on the suggested explanations for the large (γ,p) yields found by Wäffler and Hirzel and therefore it is convenient to consider these explanations before commenting on these results.

2 (c) Suggested Explanations of the Large (γ,p) Cross Sections Found by Wäffler and Hirzel.

(i) The Schiff Hypothesis

Schiff (Sc 48) assumed that the absorption of a photon produced a compound nucleus and suggested that, because the electromagnetic field of the quantum varies slowly across the nucleus, only certain "regular" energy levels could be produced by photon absorption. He showed that proton and neutron emission from these regular energy levels leaves the residual nucleus in a restricted set of levels whose density increases only slowly with energy. As a result the mean photoproton and photoneutron energies are greater than those predicted by the normal statistical theory and the (γ,p) yield is increased because of the greater probability that the protons will penetrate the coulomb barrier. The cross sections calculated by Schiff are in agreement with the results of Wäffler and Hirzel.

(ii) The Direct Ejection Hypothesis.

A number of workers (Co 51, Je 48, Le 50, Ma 51d) have suggested that, in at least a fraction of photon interactions, the photon energy is absorbed by an individual nucleon. If this is near the surface it may escape without further interaction. Because of their higher energy photoprotons of this type will have a greater probability of penetrating the coulomb barrier and hence this effect will lead to an increase in the (γ,p) cross section. Nucleons which do not escape are expected to share their energy and produce a compound nucleus.

Courant (Co 51) has calculated the cross section for this process using an independent particle model with a square well potential to describe the initial and final states. His (γ,p) cross sections are greater than those calculated from the statistical theory but are smaller ($\lesssim$10%) than the experimental values found by Wäffler and Hirzel. He predicts an angular distribution of the form $A + B \sin^2\theta$ for the directly ejected protons.

Thus on the Schiff hypothesis all photoproton and photoneutron spectra will have a higher mean energy than that predicted by the normal statistical theory. On the direct ejection hypothesis the spectrum will be that predicted by the normal statistical theory plus a contribution of higher energy with an angular distribution peaked at 90°. The relative proportion of these two parts will depend on Z and on the (γ,p) and (γ,n) thresholds. For the nuclei studied by Wäffler and Hirzel the spectrum is expected to consist almost entirely of directly ejected photoprotons since for these nuclei the (γ,p) threshold is greater than the (γ,n) threshold and hence the yield predicted by the statistical theory is very small. For copper and silver the (γ,p) threshold is less than the (γ,n) threshold. Hence the yield predicted by the statistical theory is much larger and may exceed the yield of directly ejected photoprotons.

The experimentally measured spectra (see Figs. 1.8 and 1.7) definitely exclude the Schiff hypothesis. It is not possible to make a complete test of the direct ejection hypothesis since there are no spectra for the elements studied by Wäffler and Hirzel, but the

observations on silver and copper are consistent with the above expectations both as regards spectrum shape and angular distribution. However this hypothesis meets with the following difficulties. The only calculation of the cross sections for directly ejected protons gives cross sections which are too small by an order of magnitude. Also the results of Wilkinson and Carver on A^{40} are in conflict with this hypothesis. These workers find a (γ,p) spectrum of the statistical shape with a cross section several times that predicted by the statistical theory and suggest that this result may be explained by a change in shape of the coulomb barrier. This last hypothesis is in conflict with the results of Diven and Almy who find that the statistical theory predicts the correct yield for silver, for which the coulomb barrier is greater. In view of these difficulties it is desirable that the measurement on A^{40} be repeated.

3. THEORETICAL INVESTIGATIONS AND DISCUSSION

The theoretical investigations of the photodisintegration of nuclei other than deuterium fall into three groups. Levinger and Bethe have calculated the integrated cross section for the sum of all photonuclear reactions. Since their result is not greatly affected by the validity of the nuclear model they assume, it is of great value in interpreting the experimental results. Several workers have proposed models which seek to explain the observed energy dependence of the (γ,n) cross sections, i.e. the giant resonance. The rather different models proposed in explanation of the large (γ,p) yields observed in middle weight nuclei have been discussed above.

3 (a) Sum Rule Calculations of Levinger and Bethe.

Levinger and Bethe (Le 50) noted that if the transition probability is summed over all excited states the result depends only on the properties of the nuclear ground state. In their calculations they assumed

(1) central forces, both ordinary and an ordinary exchange mixture, and

(2) a plane wave independent particle model for the nucleus.

For ordinary central forces they showed that

$$\int_0^\infty \sigma_{ED}\, dE = 0.06 \frac{NZ}{A} \text{ Mev-barn}$$

where σ_{ED} is the cross section for photon absorption by electric dipole transitions, i.e. the sum of these cross sections for all photonuclear reactions. This particular result is independent of the wave function for the nuclear ground state.

When exchange forces are present the value of this integral is increased and Levinger and Bethe found

$$\int_0^\infty \sigma_{ED}\, dE \simeq 0.06 \frac{NZ}{A} (1 + 0.8x) \text{ Mev-barn}$$

where x is the fraction of the force which is exchange in character. This integral is dependent on the ground state wave function but Levinger and Bethe claim that, since the main contribution to the additional term due to exchange forces comes from the short neutron-proton distances ($\sim 10^{-13}$ cm.), this result will be a fair approximation to that obtained from the α particle, or any other correlated nuclear

model.

They also calculated $\int_0^\infty \frac{\sigma_q}{E}\,dE$ where σ_q is the cross section for electric quadripole transitions. For medium and heavy nuclei the numerical value of this integral is only a few percent of the experimental value for $\int \frac{\sigma(\gamma,n)}{E}\,dE$ and therefore the bulk of the (γ,n) disintegrations cannot be due to quadripole transitions and must arise from electric dipole transitions.

For a sharply peaked cross section both the mean energy and the harmonic mean energy $(=\int \sigma\,dE / \int \frac{\sigma}{E}\,dE)$ will be approximately equal to each other and to the energy of the maximum. By calculating these quantities using the sum rules Levinger and Bethe showed that the existence of the giant resonance implied that there are strong correlations between the nucleons in the ground state and conversely that the presence of correlations between nucleons in the ground state could lead to a cross section of the giant resonance form.

3 (b) Suggested Explanation of the Giant Resonance.

Several workers have interpreted the peak in the cross section as a true resonance due to electric dipole absorption by a nuclear state which is described by classical models in which all protons move together against all neutrons. The first model of this kind was proposed by Goldhaber and Teller (Go 48) who assumed that both protons and neutrons stayed fixed on their respective spheres and that these two spheres oscillated with respect to one another. They found that the position of σ_{max} is proportional to $A^{-1/6}$ (26.5 Mev for C, 20 Mev for Cu and 16 Mev for U) and that $\int \sigma\,dE = 0.015A$

Mev-barn. (This is the same result as found by Levinger and Bethe for ordinary forces and N = Z = A/2).

Steinwedel, Jensen and Jensen (St 50, Je 50, St 50a) have made similar calculations using a hydrodynamic model. They interpreted the "resonance" as the lowest eigen frequency of interpenetrating proton and neutron fluids, contained within a fixed nuclear sphere and with a constant total density. They found that the position of the maximum is proportional to $A^{-1/3}$ and that the integrated cross section is just half that found by Goldhaber and Teller.

Since, as Levinger and Bethe have pointed out, the existence of a peak in the cross section is an expected consequence of the existence of correlations between nucleons in the ground state, this peak does not in itself provide significant evidence for the validity of either of these models. The A dependence of the peak position would be of value but the experimental results are not yet sufficiently accurate to provide evidence for or against either model. Both models imply that photonuclear reactions involve the formation of a compound nucleus.

3 (c) Summary and Discussion.

The scarcity of results on photodisintegration is illustrated by the fact that most of these results are from cross section and yield measurements and most cross section measurements are for the (γ,n) reaction. (γ,p) cross section measurements are experimentally more difficult and there have been only a few measurements of the more complex reactions.

The broad features of the (γ,n) cross sections are fairly well established but because of the limited experimental resolution (1 - 2 Mev) it is not known if these curves possess any finer structure. All (γ,n) cross sections have a well defined single maximum at an energy a few Mev above the threshold. The half width of this maximum is $\simeq$ 6 Mev and is approximately constant throughout the periodic table while the energy of the maximum decreases slowly with increasing Z. The cross section probably remains small above this maximum. (γ,p) cross sections have only been measured for light and medium nuclei and for these nuclei the (γ,p) cross section has a shape which is very similar to that of the (γ,n) cross section.

In discussing the implications of these and other results it is convenient to consider the results for medium and heavy nuclei before those for light nuclei.

(i) Photodisintegration of Medium and Heavy Nuclei.

For these nuclei the integrated (γ,n) cross section is very large and this implies that most of the disintegrations involved are the result of electric dipole transitions. This integrated cross section is about half the integrated cross section for all photonuclear processes as calculated by Levinger and Bethe. Since this calculation appears to be quite reliable this implies that the total photon absorption cross section has a maximum at an energy close to that in the (γ,n) cross section. This conclusion also follows from the experimental result that the cross sections for the more complex reactions are very much less than the (γ,n) cross sections and is

suggested by the neutron yield measurements for lead (see p. 10). This maximum in the total cross section is usually referred to as the giant resonance. The smooth increase of the neutron yields and the even smoother variation of neutron + proton yields imply that the total integrated cross section is a smoothly increasing function of Z, as is predicted by Levinger and Bethe.

There is only a little evidence relating to the mechanism of photonuclear reactions. The yield measurements for the $Zn^{64}(\gamma,n)$, (γ,pn) and $(\gamma,2n)$ reactions and the photoproton spectrum measurements indicate that for most disintegrations a compound nucleus is formed. However, it is clear that this is not always so since this picture does not explain the large (γ,p) cross sections found by Wäffler and Hirzel. Some experimental results suggest that these large cross sections are due to directly ejected photoprotons but this explanation presents difficulties which have still to be resolved. For those cases in which a compound nucleus is formed there is no evidence to determine whether the absorption of a photon leads directly to a compound nucleus or whether the photon interaction is confined to a single nucleon or small group of nucleons which transfer their energy to the nucleus as a whole by subsequent collisions.

There is not sufficient experimental information to decide for or against either of the models suggested as explanations for the giant resonance. Since these models require the formation of a compound nucleus they imply that the large (γ,p) cross sections discussed above are due to some separate process. The energy dependence of these cross

sections would therefore provide a test of the above models (and, more generally, of the mechanism of the photon interaction) since it is unlikely that any separate process would have the same energy dependence.

(ii) Photodisintegration of Light Nuclei.

For these nuclei the (γ,n) cross section has an energy dependence which is similar to that for heavier nuclei but the integrated cross section for the maximum is a much smaller fraction of the total integrated cross section predicted by Levinger and Bethe (see Fig. 1.2 on p. 6a). This is partly due to the fact that the (γ,p) cross section is relatively more important in these nuclei and may even be larger than the (γ,n) cross section. However it seems most likely that the combined integrated cross sections for the (γ,p) and (γ,n) reactions is still not a large fraction of the Levinger and Bethe prediction. This implies that either these reactions have a significant cross section at higher energies or other reactions are relatively more important for light nuclei. The results of the cloud chamber measurements of Gaerttner and Yeater indicate that other reactions are quite important and that their cross section is largest at an energy above the giant resonance. There is no experimental information about the mechanism of the photon interaction in light nuclei.

It is clear that there is a need for many more experimental results. For the reasons given below it seems likely that information on light nuclei would be of particular value in elucidating the

mechanism of photonuclear reactions. These reasons are

(1) The amount of information potentially available is greater since more photonuclear reactions have significant cross sections.

(2) Much more is known about the general nuclear properties of light nuclei.

(3) If some form of direct ejection mechanism is of importance it should show up more clearly in light nuclei where nucleons produced in this way are unlikely to form a compound nucleus by subsequent collisions.

For a study of photonuclear reactions in light nuclei the cloud chamber has the following advantages

(1) A reasonable choice of target nuclei since a number of light elements are gaseous or produce suitable gaseous compounds.

(2) Most photonuclear reactions produce visible events in a cloud chamber and events due to different reactions can generally be distinguished.

(3) There are no background difficulties since the charged particles of interest are clearly distinguished from the electron background and events due to neutrons are few and their number can be measured. The cloud chamber can therefore provide unambiguous information on (γ,p) reactions which are experimentally difficult to study and appear to be of particular interest.

(4) The energies of charged particles which stop in the

chamber* can be accurately determined from range measurements.

(5) Reactions involving the emission of several charged particles are easily studied. Except for a few reactions that can be observed in nuclear emulsions or lead to radioactive products, these reactions are virtually impossible to study by any other technique.

Hence the cloud chamber should provide a more complete picture of the photonuclear reactions in a particular nucleus than can be obtained from other methods. Because of the time required to collect and analyse data such an investigation will be a considerable undertaking but nevertheless it is clear from the need for more data that the potential of the cloud chamber method should be thoroughly investigated. The work described in this thesis was undertaken with this aim and a conscious effort was made to get the maximum amount of data by seeking good track quality and by careful analysis.

4. THE $C^{12}(\gamma,3\alpha)$ REACTION AND THE ISOTOPIC SPIN SELECTION RULES

The $C^{12}(\gamma,3\alpha)$ reaction is of particular interest since, as the most extensively studied star producing reaction, it provides a good picture of both the potentialities and difficulties of measurements on these reactions. In addition it provides a very clear confirmation of the validity of the isotopic spin selection rules for photonuclear reactions. These rules are expected to determine many of the features of the star producing reactions in neon which are the subject of one

*i.e. $E_p \lesssim 3$ Mev, $E_\alpha \lesssim 12$ Mev.

of the investigations described in this thesis.

4 (a) Experimental Results on the $C^{12}(\gamma,3\alpha)$ Reaction.

A number of workers have studied this reaction by measuring the stars produced in nuclear emulsions (see Go 55 for summary and references). The most extensive and thorough results are those of Goward and Wilkins (Go 53, Go 55 and earlier papers) who measured some 2500 stars in experiments lasting several years. For the irradiations they used γ-rays from the $Li^7(p,\gamma)$ reaction and 25, 33 and 70 Mev X-rays.

The $C^{12}(\gamma,3\alpha)$ stars were identified by calculating the momentum unbalance* and accepting all stars for which this was less than 40 $\frac{\text{Mev.}}{c}$. This excluded all events due to $C^{12}(\gamma,\alpha p)$ and $C^{13}(\gamma,3\alpha n)$ reactions but did not exclude events due to the $C^{12}(\gamma,3\alpha\gamma')$ reaction. However there was evidence to show that the number of these events was almost certainly small**. The energy of the γ-ray producing a disintegration is therefore equal to $(E_t + 7.3)$ Mev, and the cross section was obtained directly from this energy distribution and the X-ray spectrum. The energy resolution

*i.e. the difference between the momentum of the incoming photon and the resultant momentum calculated from the track measurements assuming the star to be due to the $C^{12}(\gamma,3\alpha)$ reaction.

**The most direct evidence was that, for 96% of the stars produced in the $Li^7(p,\gamma)$ irradiation, $E_t (= E_{\alpha_1} + E_{\alpha_2} + E_{\alpha_3})$ was just 7.3 Mev less than the energies of the known γ-ray lines, i.e. 17.6 Mev and 14.8 Mev. Other arguments based on agreement between the cross sections obtained for different X-ray energies and an analysis of the mean momentum unbalance in the direction of the X-ray beam showed that the proportion of $C^{12}(\gamma,3\alpha\gamma')$ events is most probably not significant at any energy.

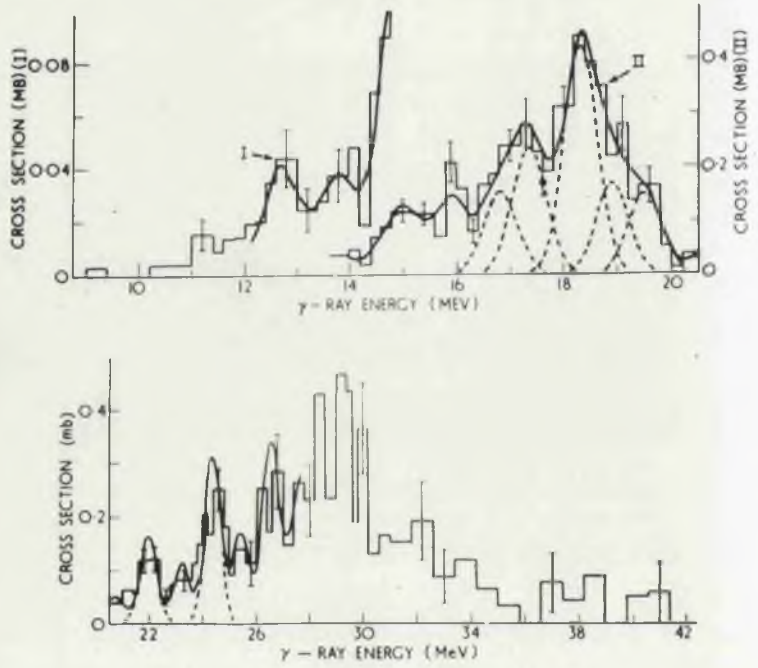

Fig. 1.9

Cross section for the $C^{12}(\gamma,3\alpha)$ reaction as measured by Goward and Wilkins (Go 53).

indicated by the width at half height of the peak from the sharp 17.6 Mev γ-ray line is 1 Mev. This cross section is given in Fig. 1.9 which shows that it rises to a maximum at 18.3 Mev, drops sharply to a small value at 20.5 Mev and then rises more slowly to a second maximum at 29.4 Mev. It seems likely that these broad maxima consist of a series of not fully resolved peaks which would imply the formation of a compound nucleus*.

The method used to study the mechanism of the reaction is as follows. It is provisionally assumed that the reaction is one of α emission to a level in Be^8 which then breaks up into two α particles, i.e. that the reaction can be written $C^{12}(\gamma,\alpha_1)Be^{8x}(\alpha_2,\alpha_3)$. If α_1 were known then E^x, the energy of the level could be calculated from the energies and directions of the three α particles. Since any of the three α particles could be α_1 each star gives three possible values of E^x, only one of which is significant. In the E^x distribution these significant values will give peaks superimposed on a continuum of spurious values. Since the direct disintegration of C^{12} into three α particles will lead to a smooth distribution of apparent E^x values, the occurrence of such peaks justifies the initial assumption and identifies the levels of Be^8 involved. Further, if the background of spurious values

*A cross section measurement by Goward, Jones and Lasich (Jo 55) provides further evidence for the suggested peaks. These workers measured the pulse height distribution due to $C^{12}(\gamma,3\alpha)$ events in a methane filled ionization chamber irradiated with 33 Mev X-rays. They achieved a resolution of about 0.4 Mev and found peaks (which were not well separated) at energies corresponding to the peaks suggested by the nuclear emulsion measurements.

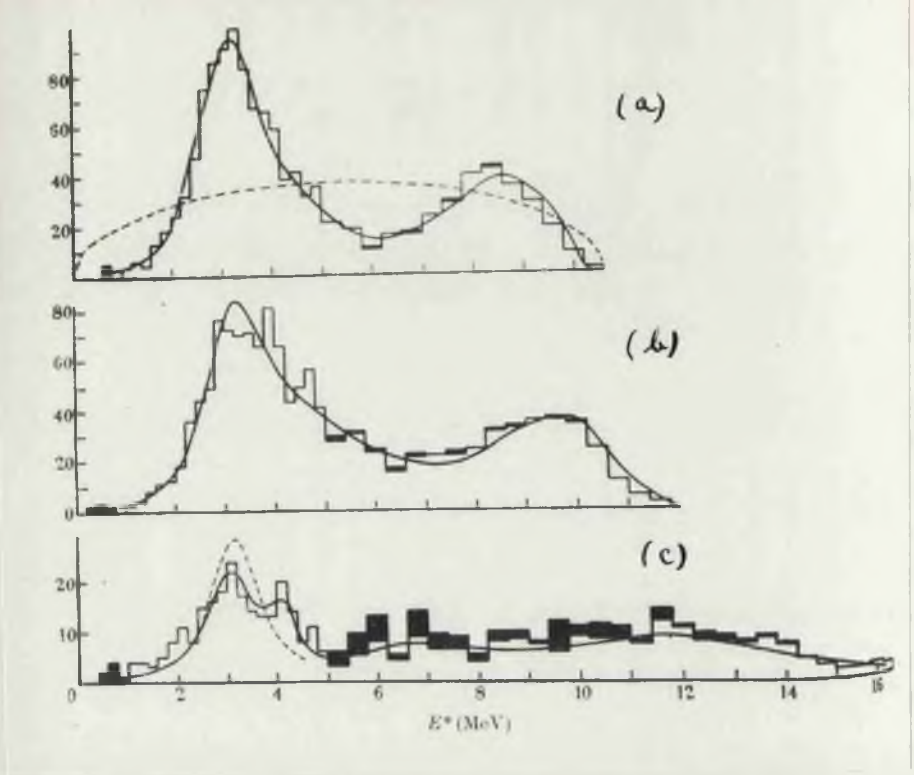

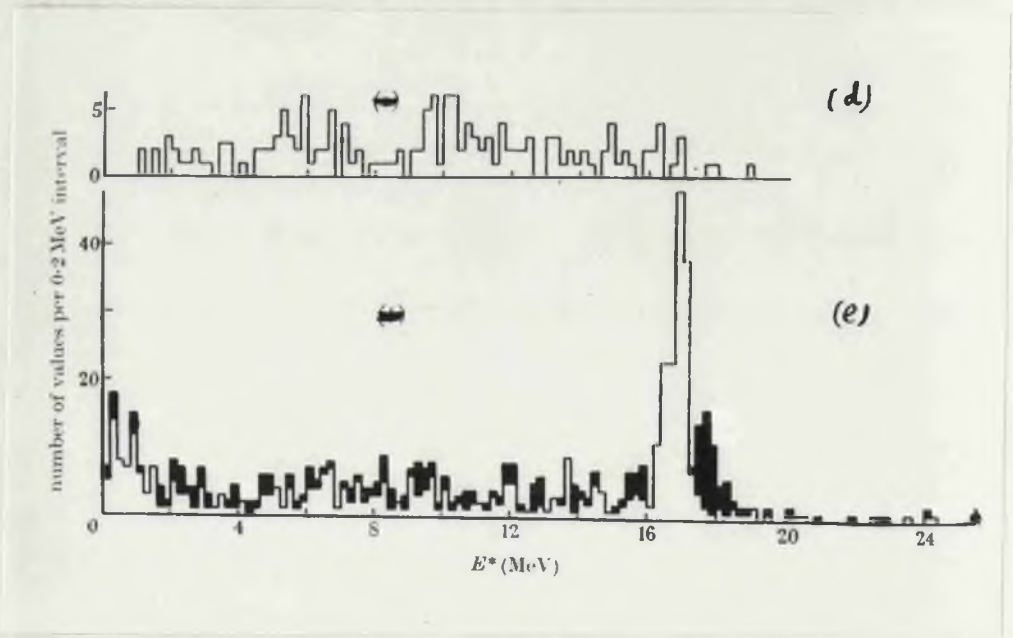

Fig. 1.10

Distribution of $E^*(Be^8)$ values (three values for each star) for $C^{12}(\gamma,3\alpha)$ stars produced by quanta in the following energy ranges: (a) 17.0 - 18.0 Mev; (b) 18.0 - 20.0 Mev; (c) 20.0 - 25.0 Mev; (d) 25.0 - 26.4 Mev; (e) above 26.4 Mev. Stars which give a value of $E^* < 0.3$ Mev have been excluded. The dotted curve in fig. (a) is the E^* distribution expected for three body disintegrations.

is much less than the number of events in a peak, only a few errors are made if this is identified as the significant value of E^x for the events concerned. This then identifies α_1 and so enables angular distributions to be obtained. Clearly this analysis will be less satisfactory if a number of Be^8 levels are involved or if these levels are broad.

Goward and Wilkins determined the E^x distributions for a number of ranges of photon energy. They found that at all energies the reaction is of the form $C^{12}(\gamma,\alpha_1)Be^{8x}(\alpha_2,\alpha_3)$ and that there is an abrupt change in the Be^8 levels involved when E_γ exceeds 26 Mev. This can be seen from the E^x distributions reproduced in Fig. 1.10. For E_γ greater than 26 Mev, 88% of the disintegrations leave Be^8 in narrow levels at 16.8 Mev, 17.6 Mev and possibly 16.4 Mev. For E_γ less than 25 Mev the fractions of disintegrations leaving Be^8 in various levels vary slightly about the following mean values - 83% for the broad 2.95 Mev level, 7% for the ground state and 10% for levels between 4 and 15 Mev. The angular distributions* for $E_\gamma > 26$ Mev and disintegrations to the 16.8 Mev level show that the initial photon absorption is by E1 (electric dipole) transitions and that the 16.8 Mev level has J (angular momentum) = 2. If E1 transitions are assumed the angular distributions for the 17.4 Mev level show that this level has J = 2 or possibly 0. For $E_\gamma < 25$ Mev the distributions of E^x values show that the 2.95 Mev level must have J = 2. The nature of the initial photon absorption for disintegrations leaving Be^8 in the 2.95 Mev

*i.e. the angular distribution of α_1, the angular correlation between α_1 and the direction of break up of the Be^8 nucleus and the angular correlation between this direction and the direction of the incoming photon.

level is less clear. Goward and Wilkins believe that the angular distributions show that this is due to a mixture of E1 and E2 transitions. However they note that the assumption of M1 + E2 transitions leads to angular distributions which are only slightly worse fits to the experimental distributions. These distributions may be somewhat in error because of ambiguities in choosing the correct E^x for a broad level. From an analysis of $C^{12}(\gamma,3\alpha)$ stars produced by $Li^7(p,\gamma)$ radiation Telegdi (Te 51a) concludes that the experimental data can be fitted by a mixture of M1 + E2 transitions and that a small admixture of E1 transitions would probably improve the fit. Consequently it seems best to regard the nature of these transitions as an open question. Since the ground states of both C^{12} and Be^8 are 0^+ the initial photon absorption for the small fraction of disintegrations leaving Be^8 in the ground state must be due to electric transitions. The angular distributions show unambiguously that these are predominantly E2 for 13 Mev $\leq E_\gamma <$ 15.6 Mev, E1 for 15.6 Mev $\leq E_\gamma <$ 20 Mev and E2 for 20 Mev $\leq E_\gamma <$ 26.4 Mev. For these three energy ranges the Be^8 nucleus is left in the ground state for 12%, 5% and 13% of disintegrations.

4 (b) <u>The Isotopic Spin Selection Rules and Their Application to the $C^{12}(\gamma,\alpha)$ Reaction.</u>

The assumption that nuclear forces are charge independent has important consequences for the photodisintegration of light nuclei. These consequences are usually expressed in terms of the concept of isotopic spin introduced by Wigner (Wi 37). Protons and neutrons are regarded as two possible states of a nucleon and this is expressed

formally by giving the nucleon an isotopic spin $\tau = \frac{1}{2}$ in charge space; the two possible orientations $\tau_z = +\frac{1}{2}$ and $-\frac{1}{2}$ corresponding to proton and neutron respectively. In describing a nuclear state the isotopic spins are combined in a way similar to angular momentum vectors to give a total isotopic spin $T = \Sigma\tau$ having a z component $T_z = \Sigma\tau_z = -\frac{(N - Z)}{2}$. For example, all states in C^{12} will have $T_z = 0$ but may have $T = 0$, if there are no corresponding states in B^{12} and N^{12}, $T = 1$ if there are corresponding states in B^{12} and N^{12} (with $T_z = +1$ and -1 respectively), and so on.

Radicati (Ra 52) has shown that for electromagnetic transitions the assumption that the nuclear forces are charge independent leads to the following selection rules.

For all multipolarities

$$\Delta T = 0, \pm 1 \qquad \text{when } T_z \neq 0$$

For E1 transitions

$$\Delta T = \pm 1 \qquad \text{when } T_z = 0^*$$

Because of the presence of coulomb forces and the neutron-proton mass difference these rules are not absolute but should be reasonable approximations for $Z \leq 10$. The departures from charge independence are usually allowed for by expressing real states as a mixture of a predominant state with one T value and an impurity state with the other

*Kroll and Foldy (Kr 52) have pointed out that these rules follow from the less restrictive assumption that nuclear forces are charge symmetrical (i.e. n - n and p - p forces are equal). However because of the considerable evidence that nuclear forces are charge independent it is usual to derive the above rules from this more restrictive hypothesis.

T value.

Gell-Mann and Telegdi (Ge 53) have pointed out that these selection rules are of particular importance for (γ,α) and (γ,d) reactions in self conjugate ($N = Z$, $T_z = 0$), even-even nuclei. For these nuclei the ground state is 0^+ and the lowest $T = 1$ state is at a rather high excitation energy W_1. Since the α particle and the deuteron have $T = 0$ their emission is subject to the selection rule $\Delta T = 0$. Hence, if nuclear forces are strictly charge independent, these reactions will obey the following rules*.

(1) For $E_\gamma < W_1$ all absorption proceeds either by M1 transitions through a state with $J = 1^+$, $T = 0$ or by E2 transitions through a state with $J = 2^+$, $T = 0$.

(2) For $E_\gamma > W_1$ absorption into $T = 1$ states is possible by E1, E2 or M1 but such absorption can result in deuteron or α particle emission only if there is sufficient energy for the residual nucleus to be left in a $T = 1$ state.

(3) At any energy (γ,d) and (γ,α) reactions leaving the residual nucleus in a $T = 0$ state can only proceed as in (1).

(4) In particular a (γ,α) transition to the ground state of the residual nucleus may proceed only by E2 absorption through a state with $T = 0$, $J = 2^+$.

(5) When corrected for differences in thresholds and barrier

*The wording of these rules and the subsequent discussion assume that a compound nucleus is formed. As will be seen the experimental results show that this is the case for the only (γ,α) reaction that has been fully investigated, namely $C^{12}(\gamma,3\alpha)$. The rules are still valid for direct interactions but are then of little interest since, for self conjugate nuclei, E1 transitions cannot lead to the direct ejection of an α particle.

penetrabilities (γ,n) and (γ,p) cross sections should, for each residual state, be identical with each other.

Since the selection rules are not absolute there will be a small probability of d or α emission to a T = 0 state following E1, E2 or M1 absorption into a T = 1 state. Re-emission of γ-rays would probably not compete strongly enough to suppress such a process but neutron or proton emission would be expected to do so. Thus, in the energy region between W_1 and the threshold for neutron or proton emission, whichever is the lower, α particles or deuterons may be emitted in violation of rules 2, 3 and 4.

For C^{12} the relevant thresholds are as follows - (γ,α) 7.4 Mev, (γ,p) 16.0 Mev, (γ,n) 18.7 Mev and (γ,d) 25.2 Mev. The lowest T = 1 state of C^{12} will be the analogue of the ground state of B^{12} and N^{12} and is therefore expected to be 1^+ and to have an energy of about 15.2 Mev. Similarly the lowest T = 1 state of Be^8 is expected to be 2^+ and to have an energy of approximately 16.8 Mev. The $C^{12}(\gamma,\alpha)$ reaction is therefore expected to have the following features. Below 17 Mev the cross section will be equal to the photon absorption cross section. This will be small below 15 Mev, where only E2 and M1 transitions are allowed. Its value between 15 and 17 Mev will depend on the number of 1^-, T = 1 states in this energy region. Between 17 Mev and 26 Mev the cross section will be small and due only to E2 and M1 transitions to T = 0 states. Above 26 Mev α emission to the T = 1 states of Be^8 is energetically possible and therefore the cross section is expected to rise and to be due to E1 transitions. Since, at these

energies, the total photon absorption cross section decreases with increasing energy the (γ,α) cross section should pass through a maximum at an energy a little above 26 Mev.

This picture is in very good agreement with the experimental results. The only feature of these results which is not specifically predicted by the isotopic spin selection rules is that the cross section does not drop at 17 Mev as is expected from the onset of competition due to the (γ,p) reaction. Instead there is a sharp drop at 19 Mev which is just above the (γ,n) threshold. However, as there is little definite information on the nature of the photon transitions between 17 and 19 Mev, it is quite possible that these are M1 and E2 transitions to T = 0 states. In this case the maximum at 18.3 Mev would simply be due to the presence of suitable energy levels in this energy region. Hence while this result does not follow from the isotopic spin selection rules it is not in conflict with them.

As has been mentioned, there is good evidence that the $C^{12}(\gamma,3\alpha)$ reaction involves the formation of a compound nucleus. The most direct evidence is that above 26 Mev the reaction is due to E1 transitions. Since the absorption of a quantum by an E1 transition requires the displacement of the centre of charge relative to the centre of mass it cannot lead to the direct ejection of an α particle. Between 26 and 30 Mev the ratio $\Gamma(\gamma,\alpha)/\Gamma((\gamma,n)+(\gamma,p))$ is ~ 0.1. As this is a reasonable value for the ratios of emission from a compound nucleus it suggests that in this energy region, at least, most photonuclear

disintegrations in C^{12} involve the formation of a compound nucleus. The fact that the cross section curve probably consists of a series of unresolved peaks also suggests that a compound nucleus is formed. In addition, while it is possible to imagine a mechanism that would lead to the direct emission of an α particle leaving Be^{8} in an excited state, it seems much more likely that a direct emission would result in a three-body break up.

5. CHOICE OF CLOUD CHAMBER EXPERIMENTS

As has been pointed out there are good reasons for believing that a program of photonuclear investigations using a cloud chamber would provide new and valuable information about (γ,p), (γ,pn) and the star producing reactions in light nuclei. The particular reactions studied in the present investigation were the He^{4}(γ,p) reaction, the photonuclear reactions in N^{14} and the (γ,α), (γ,2α) and (γ,αp) reactions in Ne^{20}. The reasons for this choice are outlined below and are discussed in more detail in the chapters concerned.

5 (a) The He^{4}(γ,p) Reaction.

It is clear that the photonuclear cross section of He^{4} will be an important test for any photonuclear theory. At the time this experiment was started (mid-1950) there were no other measurements of the He^{4}(γ,p) cross section. Since He^{4}(γ,p) events are quite distinctive and can be measured accurately, the cloud chamber method is a very suitable one for this measurement. Conversely this experiment is a very suitable one for developing the technique for photonuclear studies in a cloud chamber. Two further considerations were of importance in the

present case where the peak energy of the synchrotron available was only a few Mev above the reaction threshold. These were that the existing experimental and theoretical results indicated that, nevertheless, a large number of $He^4(\gamma,p)$ events could be obtained quite easily and that a cross section measurement in the energy region just above threshold was of particular importance.

5 (b) The Photodisintegration of Nitrogen.

The above review has shown that information on a number of photonuclear reactions in one particular nucleus is conspicuously absent. Since most photonuclear reactions produce visible events in a cloud chamber one important application of the cloud chamber method would be to study the various reactions in one nucleus. N^{14} appears to be a most suitable choice for such a survey, partly because of the number of reactions that can be studied without confusion and also because the (γ,p), (γ,n) and (γ,pn) reactions all have thresholds which are well below the energy of the giant resonance. Thus a study of these reactions might be expected to yield information about the change in the nature of the photonuclear process in going from energies below to energies in the vicinity of the giant resonance.

5 (c) $Ne^{20}(\gamma,\alpha)$, $Ne^{20}(\gamma,2\alpha)$ and $Ne^{20}(\gamma,\alpha p)$ Reactions.

The measurements on the $C^{12}(\gamma,3\alpha)$ stars show that a study of the star producing reactions can provide information on the mechanism of these reactions. This information is of particular value since it is not possible to get similar information for other reactions. A limitation on the $C^{12}(\gamma,3\alpha)$ results was that the cross section was

small in the region of the giant resonance which is of considerable interest. As is shown in Chapter V there are good reasons for believing that the $(\gamma,2\alpha)$ and $(\gamma,\alpha p)$ reactions in Ne^{20} will have appreciable cross sections in the region of the giant resonance and that in this respect they are probably unique among star producing reactions in light nuclei. A further reason for interest in these reactions is that the cross sections for the (γ,α), $(\gamma,2\alpha)$ and $(\gamma,\alpha p)$ reactions are subject to the same isotopic spin selection rules as was the $C^{12}(\gamma,3\alpha)$ cross section. Since the rules are known to be valid for C^{12} it would be of interest to see if they are equally valid for Ne^{20} where the effect of coulomb forces will be greater. The stars produced in Neon can only be measured in a cloud chamber.

Chapter II

APPARATUS AND EXPERIMENTAL PROCEDURE

When this investigation was started very little was known about the problem of operating a cloud chamber in the X-ray beam of an electron synchrotron or betatron. The only prior investigation, which used the General Electric 100 Mev betatron at Schenectady, was still in progress. In this work Gaerttner and Yeater had had as a primary aim the maximum possible reduction in the cloud chamber cycling time and for this purpose had developed an expansion chamber of novel design (Ga 49) (incorporating overcompression following the fast expansion) but, in their case, of small dimensions (5" diam. x 1-1/4" deep). One important conclusion from the work described in this thesis is that good results can be obtained with standard expansion chamber techniques. The quality of the tracks can be judged from the examples in the accompanying folder and, as an illustration, it might be noted that the tracks of recoil nuclei, 1/3rd - 3 mm long, were sharp and well defined and could be measured with reasonable accuracy. Although it is difficult to make a fair judgement on the basis of the photographs published in journals (Ga 49, Ga 51b), it seems probable that the tracks obtained by Gaerttner and Yeater are of lower quality than those obtained in Glasgow. The Glasgow tracks are sharper than the photo-nuclear events reproduced in 'An Atlas of Typical Expansion Chamber Photographs' (Ge 54). These events were photographed in some preliminary measurements at Schenectady with a 12" expansion chamber (Ba 48) and may have been chosen in preference to those obtained by Gaerttner and Yeater.

All the experiments described in this thesis were carried out with the 23 Mev synchrotron at the University of Glasgow. At peak energy this machine gave an X-ray yield of 1 r/min. at 1 metre and these X-rays were produced in a series of pulses each 40 μs long and separated by intervals of 1/50th sec. For operation with an expansion chamber the output from the synchrotron was restricted to a single pulse of X-rays and the start of the expansion was timed so that the X-rays were produced just when the chamber had reached maximum supersaturation. Because of this perfect shuttering (which is a common feature of most high energy accelerators) there was no need for the chamber to have any special characteristics such as, for example, a long sensitive time or a fast expansion rate. Accordingly these experiments were carried out with a conventional volume defined expansion chamber (of sensitive volume 12" diam. x 2-1/2" deep) which was already available in the laboratory and proved to be very suitable. In particular it was large enough to enable the energies of protons with energies up to 3-1/2 Mev and alpha particles with energies up to 12 Mev to be determined accurately from range measurements with a filling pressure such that the ranges of recoil nuclei with $Z \lesssim 10$ could be measured at the same time.

A major difficulty in almost all experiments with electron synchrotrons is the very large number of background electrons produced by the X-ray beam. Thus for the helium experiment, in which the X-ray beam passed through a 1/4" glass wall on entering the cloud chamber, the estimated number of relativistic electrons crossing the chamber per expansion is 10^5. This figure emphasizes the excellence of the

discrimination between protons and electrons provided by the cloud chamber but also indicates that there is a real problem in clearing residual nuclei from the chamber before the next expansion. It was found that this could be done quite simply by waiting for some 15 secs. after the fast expansion and then making the normal slow expansions at a sufficiently slow rate.

The value of overcompression in reducing the cycling time of a cloud chamber operating in an X-ray beam has been emphasized and clearly demonstrated by Gaerttner and Yeater (Ga 49, Ga 51b) who obtained a cycling time of 5 - 7 secs. and, more recently, by Goldwasser and Nicolai (Go 55a) who used a 12" diam. x 3" deep expansion chamber at a cycling time of 15 secs. No attempt was made to investigate the use of this technique in the experiments described here since, quite apart from the consideration that the good track quality may well be a consequence of the stability and reliability of the volume defined expansion chamber, the saving of time would have been of little value and much less than the probable development time (see Go 55a). For each of the experiments described here the taking of photographs was completed in a period of 3 or 4 weeks with machine time being shared with other experimenters. Both preparation for an experiment and analysis of the photographs taken always took considerably longer than this. The use of a fast cycling chamber would be of real value when machine running costs are high* or in an experiment with infrequently occurring events so that machine time is greater than analysis time.

*For our experiments the greatest running expense was the cost of the film for the cloud chamber cameras.

The diffusion chamber came into prominence during the course of this investigation when the expansion chamber was already in use and quite a lot had been learnt about the technique of operating it in the synchrotron X-ray beam. As a result its use for this investigation was never seriously considered, especially as there was no reason to expect any improvement in track quality and therefore its only possible advantage was a reduction in the cycling time. Experimental tests made subsequently in Glasgow by P. Swinbank (private communication from J.M. Reid) showed that, in fact, the diffusion chamber is rather less suitable for photonuclear experiments since it ceased to function satisfactorily with a density of background electron tracks which was well within the capabilities of the expansion chamber.

The remainder of this chapter contains a description of the expansion chamber and the arrangements made for operating it in conjunction with the synchrotron, together with comments on operating procedure and cloud chamber performance. It also contains a description of the cameras and the equipment used for track measurement by reprojection. This represents the apparatus and experimental procedures which were essentially common to the three experiments described later. The methods used to analyse the tracks of recoil nuclei (involving examination of the film under a low-powered microscope) are not described here since it is felt that they are best understood within the context of the nitrogen and neon experiments for which they were developed. The quality of the recoil tracks obtained in the nitrogen experiment was, in fact, a surprise and the technique of microscope measurement was introduced after the

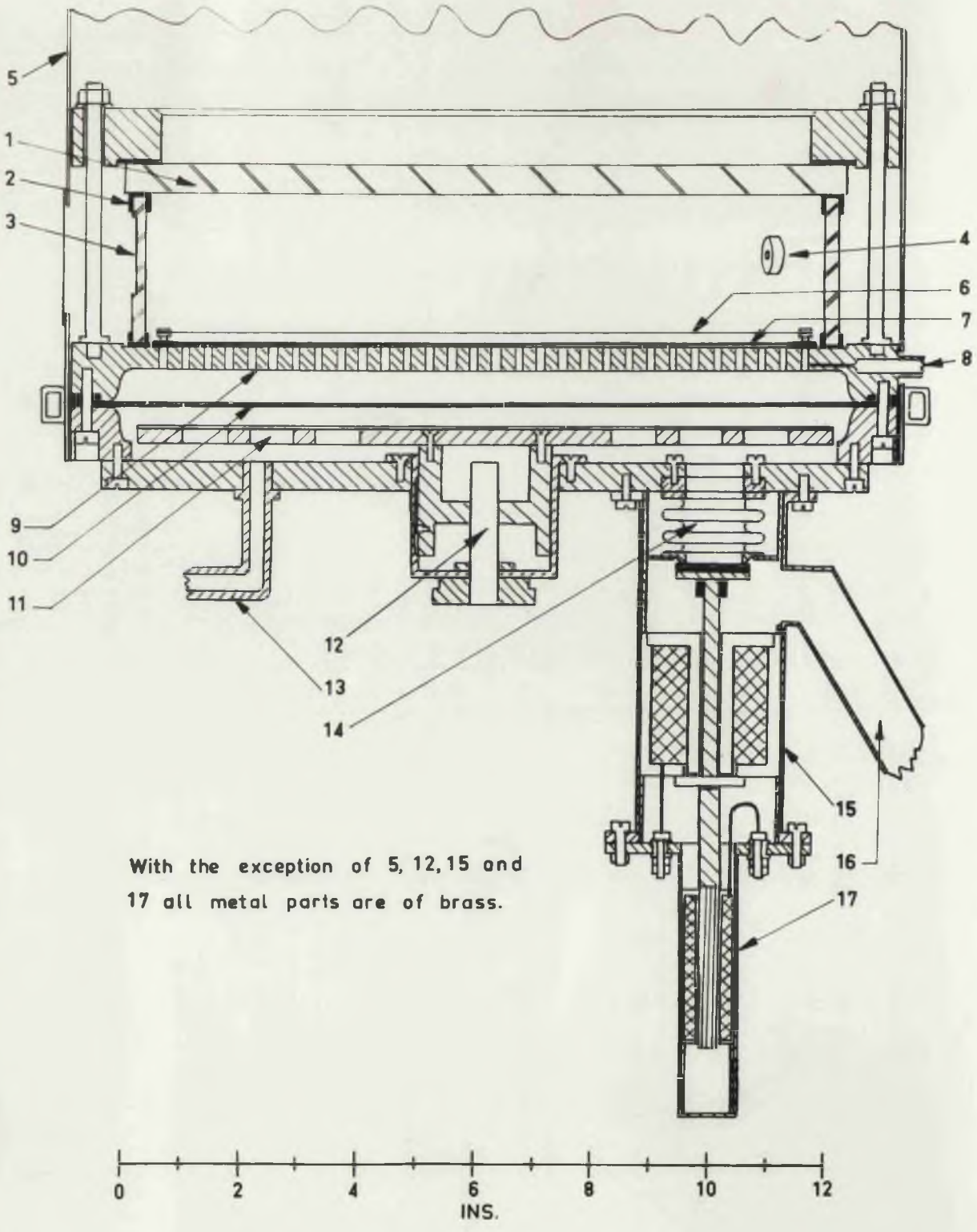
5
1
2
3
4
6
7
8
9
10
11
12
13
14
15
16
17
With the exception of 5, 12, 15 and 17 all metal parts are of brass.
0
2
4
6
8
10
12
INS.

Fig. 2.1

Fig. 2.1

1. Top glass plate.
2. U channel rubber gaskets.
3. Perspex cylinder with 0.090" thick window.
4. Unshuttered Po α source.
5. Thermal shield of aluminium sheet with water cooling tubes top and bottom.
6. Grid wires.
7. Black velvet cloth.
8. Gas inlet (0.020" dia.).
9. Perforated base plate.
10. Rubber diaphram.
11. Perforated stop plate.
12. Screw for setting expansion ratio.
13. Inlet to lower chamber.
14. Sylphon bellows.
15. Expansion valve.
16. Outlet to low pressure reservoir.
17. Reset solenoid and plunger.

For Fig. 2.1, see previous page.

photographs were taken in a form appropriate to this situation. The neon experiment used a modified camera arrangement and a method of analysis which were developed for film measurement by microscope.

1. EXPANSION CHAMBER

1 (a) Constructional Details.

The constructional details of the conventional volume defined expansion chamber used can be ascertained from the drawing in Fig. 2.1 and from the following notes which include comments on the modifications made during the course of these experiments. The paragraph numbers correspond to the item numbers of Fig. 2.1.

(1) Top Glass Plate and Provision of Electrostatic Clearing Field - the top glass plate was a "Triplex" sandwich in which a 1/2" thick piece of toughened plate glass was laminated to a piece of 1/4" plate glass. With this plate the chamber could be operated at pressures several times atmospheric, the makers stating that it will stand an excess pressure of three atmospheres with a safety factor of five. Because of the nature of the toughening process the surface of this plate could not be repolished after treatment but, nevertheless, it did not produce any detectable optical distortion. The electrostatic clearing field was applied between the base of the cloud chamber and a ring of aquadag painted on the underside of the top glass plate along the outside edge. The field used varied from 25 volts per cm. to 50 volts per cm. For the Nitrogen and Neon experiments provision was made for turning off the clearing field at the start of the expansion for a period of 2 seconds.

(3) Perspex Cylinder.

(i) For the Helium experiment the cloud chamber was

operated using the 12" dia. x 2-1/2" x 1/4" thick glass cylinder with which it was originally fitted. As can be seen from Plates 1 - 3 (see separate folder) there was a very considerable background of electrons produced in the wall by the X-ray beam though not sufficient to obscure proton tracks.

(ii) It was clearly very desirable to reduce the number of background electrons especially for work with other gases of higher stopping power and therefore greater ionization per electron track. For the Nitrogen and Neon experiments the glass cylinder was replaced by a perspex cylinder which was machined to provide an entrance window for the X-rays, 4" x 1-1/4" x 0.090" thick. With this window the electron background was reduced to a satisfactory level (see Plates 4 - 15). The reduction in electron background can be judged by comparing the background in Plates 1 - 3 with a background midway between that in Plates 4 - 5 and that in Plates 13 - 16. This comparison allows for the differences in X-ray yield and stopping power of the gases.

(5) Thermal Shield - for the Helium experiment the cloud chamber was fitted with a simple water cooling coil placed around the base plate (9), thus ensuring the desirable condition of non-convective stability in the gas of the cloud chamber (Wi 51, p55). However under these conditions the expansion ratio had to be increased at intervals during a run as the room temperature rose considerably because of the heat produced by the synchrotron magnet. For the Nitrogen and Neon experiments the cloud chamber was fitted with a simple thermal shield consisting of an aluminium cylinder extending from the base plate to 6" above the top

of the cloud chamber. This cylinder was cooled by water tubes at the top and bottom and had two large windows level with the perspex cylinder to allow for illumination. This arrangement proved quite effective in isolating the cloud chamber from the changes in room temperature and the optimum setting for the expansion ratio normally remained unchanged from start to finish of a seven hour run. Since the excess water in the chamber was never observed to condense on either the perspex wall or the top glass plate it follows that this arrangement also provided a suitable temperature distribution for non-convective stability of the gas.

(6) The rectangular grid of fine wires which provided fiducial markers for the Nitrogen and Neon experiments was 6 mm above the base plate (9). The wires parallel to and perpendicular to the direction of illumination were 0.005" and 0.002" dia, respectively.

(10) Rubber Diaphram - for the Neon experiment the 0.043" thick diaphram of natural rubber used in the Helium and Nitrogen experiments was replaced by a 0.048" thick diaphram of butyl rubber. This synthetic rubber is very much less permeable to gases than is natural rubber* and effectively solved the problems associated with the diffusion of gases through the diaphram. Its elasticity is considerably less than that of natural rubber but this did not produce any noticeable difference in the performance of the chamber.

*For the natural rubber diaphram the diffusion rate for air was 0.5 cm/day/atmos. pressure difference, the corresponding figure for butyl rubber being 0.05 cm/day. The large diffusion rate was not a problem in the Helium experiment since events in the gas which diffused in were easily distinguished from He(γ,p) disintegrations (see p.75ff), nor was it a problem in the nitrogen experiment since the lower chamber (13) was fed from a cylinder of compressed nitrogen and therefore diffusion had very little effect on the composition of the chamber gas.

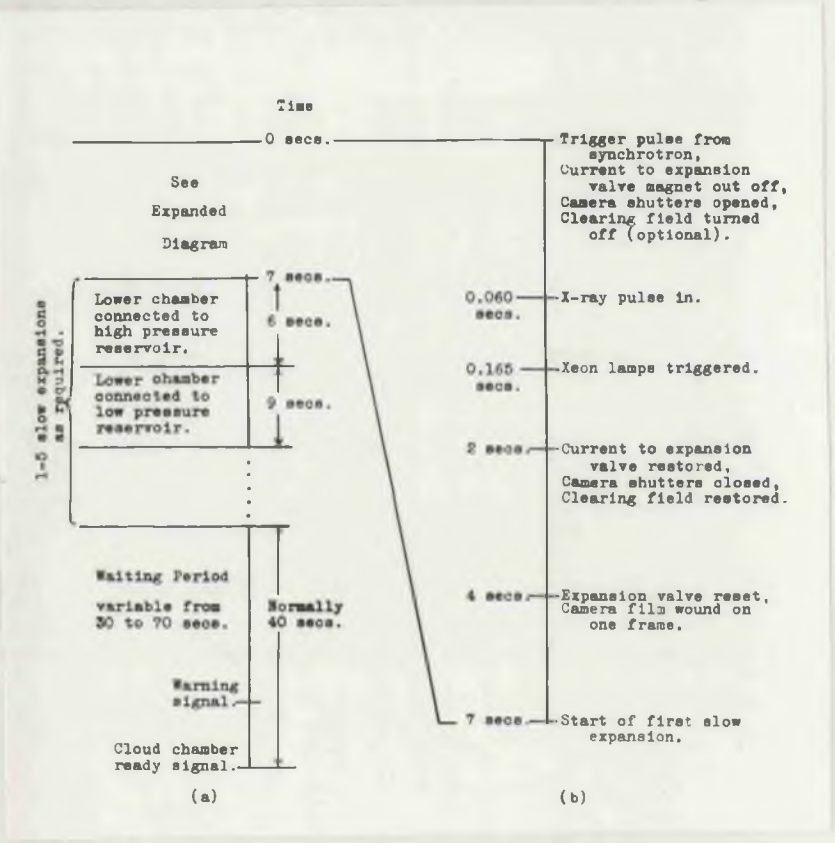

Fig. 2.2

Operations performed by cloud chamber control circuit. The times given in Fig. 2.2 (a) apply to the uniselector control unit used in the neon experiment. This cycle is based on experience gained when the slow expansions were controlled by hand (see discussion in § 2 (c) (iv) on p. 63).

(15) The expansion valve consisted of a rubber covered plate held against sylphon bellows by the keeper of a simple pot magnet and was controlled electronically by cutting off the heavy duty tetrode supplying current to this magnet. Although it was fairly slow in operation (the delay from the opening of the valve to maximum supersaturation was 1/20th sec.) this valve was quite satisfactory since this delay was constant to 2 or 3 millisec. or less (see §2 (c) (ii) p.60f).

1 (b) Illumination.

For photography the tracks were illuminated by a short flash of light from Xenon discharge lamps triggered some 110 millisec. after the X-rays had entered the chamber. For the Nitrogen and Neon experiments two lamps were used; these were placed on opposite sides of the chamber and dissipated 150 - 200 joules each. The light beam was defined by means of cylindrical lenses placed in front of the lamps and masks placed on the side of the chamber to give an illuminated depth of 4 cm. For the Helium experiment only one lamp was used and the height of the illuminated region was 4-1/2 cm. A lamp giving a flat beam of white light was used for visual observation of the tracks.

1 (c) Control Circuit.

The sequence of operations between expansions and the times at which they were performed are shown diagrammatically in Fig. 2.2. The sequence was initiated by a signal from the circuit linking the cloud chamber and synchrotron and, with the exception noted below, the remaining operations were then carried out automatically. The opening of the camera valve, the opening and closing of the camera shutters, the turning off of

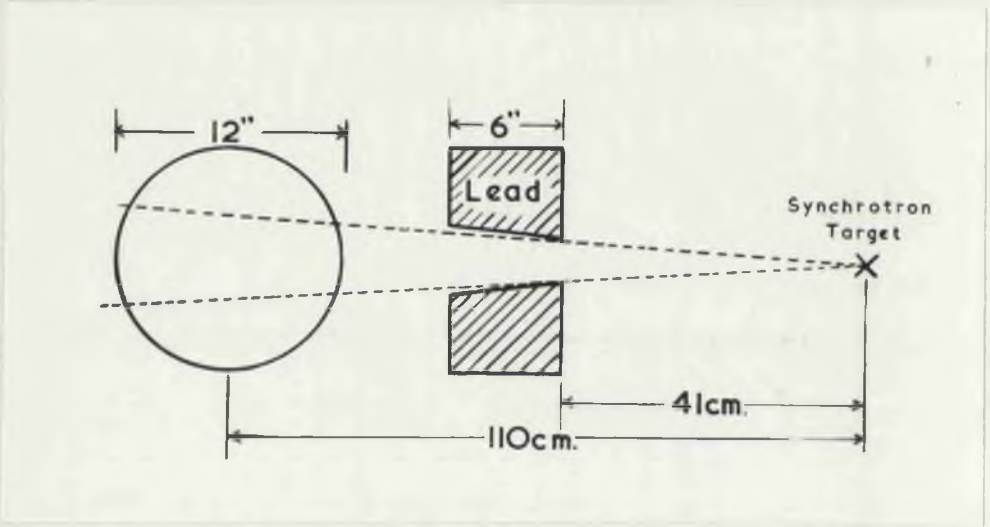

Fig. 2.3

Relative positions of synchrotron, collimator and cloud chamber. The dimensions of the beam at the centre of the cloud chamber were:-

Helium experiment	5.8 cm. wide x 4.6 cm. high,
Nitrogen and Neon experiments	10 cm. wide x 2.5 cm. high.

the electrostatic clearing field and the triggering of the lamps were controlled electronically while the remaining operations (whose timing was not critical) were controlled by switches operated by adjustable cams mounted on a shaft which was motor driven at a speed of about 1 r.p.m.

For the Helium and Nitrogen experiments hand control of the slow expansions was deliberately substituted for automatic control. Because of the large number of tracks formed in the chamber the cleaning of the chamber after each fast expansion was quite a problem and the flexibility of hand control was essential for the establishment of the most satisfactory slow expansion cycle.

For the Neon experiment completely automatic control was used and the mechanical part of the arrangement described above was replaced by a 25 step uniselector which controlled the reset solenoid, the winding on of the camera film, the slow expansions and the delay before the next expansion.

2. OPERATION OF SYNCHROTRON AND CLOUD CHAMBER

2 (a) Collimation.

The relative positions of the synchrotron, collimator and cloud chamber are shown in Fig. 2.3. The collimator was a 6" lead block pierced with a tapered rectangular hole, the angles of taper being slightly greater than the divergence of the beam. The cloud chamber was positioned so that the collimated X-ray beam was in the centre of the illuminated region, with an error of not more than ± 2 mm. Two collimators were used; that used during the Helium experiment defined a beam 5.8 cm. wide x 4.6 cm. high at the centre of the cloud chamber

while the collimator used for the Nitrogen and Neon experiments defined a beam 10 cm. wide x 2-1/2 cm. high at the same position.

2 (b) 'Single Shot' Control for Synchrotron.

In normal operation the synchrotron magnet was supplied with alternating current of mains frequency (50 cycles per sec.) and electrons were injected by a 20 kv., 5 μs pulse applied to the electron gun once each cycle when the magnetic field had a (small) value appropriate to the radius of the equilibrium orbit and the injection voltage. These electrons were accelerated while the magnetic field was increasing and directed onto a tungsten wire target close to the time when the magnetic field reached its peak value, i.e., 5 millisec. after electron injection. In common with all synchrotrons the X-ray yield was critically dependent on the timing of the electron injection pulse (a change of 1 μs producing an appreciable change in yield) and this control often required frequent adjustment during operation. The settings of the other synchrotron controls (time of r.f. turn on and turn off and controls for the r.f. oscillator) were not so critical and these controls were not normally altered after the initial adjustment when the machine was turned on.

For single shot operation all the synchrotron parameters (magnet excitation, r.f. excitation ...) were maintained as for normal operation with the exception that the injection voltage pulse was applied to the electron gun once only instead of 50 times per sec. As compared with the technique of exciting the magnet for one cycle only (Ko 46), this method is somewhat wasteful of electric power but has two great advantages.

(i) The synchrotron can be set up in normal operation and then switched to single shot operation with the knowledge that all the controls are correctly set.

(ii) The conversion of the synchrotron to single shot operation requires nothing more than a simple electronic gating circuit.

The circuit for controlling the joint operation of cloud chamber and synchrotron had three modes of operation.

(i) Single Shot - the circuit provided a single pulse which triggered the cloud chamber control circuit and then, after a fixed delay, a second single pulse which triggered the modulator providing the voltage pulse for the electron gun. Since the electrons must be injected at the correct magnetic field, these two pulses were derived from two peaking transformers supplying short pulses locked to the synchrotron magnet current, electronic gates being used to select the appropriate pulses. The time by which the cloud chamber pulse preceeded the electron gun trigger pulse could be varied between(- 10)millisec. and 110 millisec.

(ii) Single Shot Test - the cloud chamber control circuit was disconnected and a single gun trigger pulse was provided.

(iii) Continuous - the cloud chamber was disconnected and the gate controlling the electron gun trigger pulses was kept open so that all the timing pulses were fed to the electron gun modulator and the synchrotron operated at its normal repetition rate of 50 times per second. Passing the timing pulses through the gate in this way ensured that the trigger pulses to the gun modulator had exactly the same shape for both continuous and single shot operation and therefore that the timing of the

electron injection pulse was the same for both.

The normal operating procedure was as follows. Some 10 secs. before the end of the cloud chamber cycle a signal was sent to the synchrotron operator who checked the synchrotron on 'Single Shot Test'. If the output was satisfactory he then fired the cloud chamber and synchrotron on receiving the cloud chamber ready signal. A small drop in synchrotron output could generally be corrected by adjusting the gun timing on 'Single Shot Test' but a large drop could only be corrected by returning to continuous operation. When this was necessary it was usually also true that the single shot yield varied from one pulse to the next a few seconds later so that the average yield per photograph was low. In the early stages of these experiments the synchrotron performance in this respect was sometimes good and sometimes quite poor and it was found that this was correlated with the frequency stability of the mains supply. For one particularly good period in which the timing of the electron gun pulse was hardly touched during several hours the variation in the mains frequency was less than 0.1 cycle per sec. Consequently all runs from the latter part of the Helium experiment on were made during the period of the day when the mains frequency was most stable, i.e. from midnight to 6 a.m. It was found that under these conditions the synchrotron performance was consistently good.

The single shot X-ray output was measured with an ionization chamber by observing the height of the output pulse on the screen of a cathode ray oscillograph. This chamber was mounted behind a 3" lead wall and placed in the beam behind the cloud chamber.

2 (c) Discussion of Operating Experience.

(i) Condensable Vapour and Notes on Gases Used.

The condensable vapour for the cloud chamber was always provided by distilled water only. This had been the usual laboratory practice and was continued unaltered because it gave quite satisfactory results. In particular no comparison was made of the relative cloud chamber performance for a mixture of water + ethyl alcohol and water alone.

The helium used was of mineral origin and of the same quality as that supplied for medical purposes. The nitrogen was ordinary commercial compressed nitrogen. On the other hand the neon was spectroscopically pure, this being the only gas available. When the cloud chamber was first operated with neon it was found that the tracks of alpha particles from the polonium source were not as sharp as those obtained with helium and nitrogen. It was suspected that this was due to electrons produced in the primary ionization which were not forming negative ions immediately and therefore moved some distance under the influence of the electrostatic clearing field. Consequently a small amount of oxygen (1 cm. Hg pressure) was added to the cloud chamber and this produced a marked improvement in the sharpness of the tracks.

(ii) Effect of Varying the Cloud Chamber - Synchrotron Delay and the Lamp Delay.

The optimum delay between the triggering of the cloud chamber expansion valve and the production of the X-ray pulse was investigated for each of the three experiments. For these tests the electrostatic clearing field was left on during the expansion. The effect

of the changes in delay is shown by the sequence of photographs in Plate 12 which were taken during the Neon experiment. For delays of less than 55 millisec. the tracks are diffuse and the amount of diffusion increases rapidly with reduction of the delay time. For delays of 55 millisec. and greater the tracks are sharp and there is very little change in track quality with increasing delay time. For the longest delay (75 millisec.) there is a just detectable decrease in the sharpness of the tracks. These photographs were taken before the addition of the small quantity of oxygen referred to in the previous paragraph and therefore provide a sensitive measurement of the optimum delay time.

The cloud chamber could be operated for long periods at the minimum delay necessary for sharp tracks without any noticeable change in track quality showing that the time taken for the expansion was constant to at least 2 or 3 millisec. The cloud chamber was normally operated with a delay 5 milliseconds greater than the minimum delay required for sharp tracks.

No detailed investigation was made of the effect of varying the time between the X-ray pulse and the photographing of the tracks. The chamber was normally operated with this delay set to 110 millisec. which is slightly greater than the shortest delay for well developed tracks. This delay could be increased to several hundred milliseconds with little deterioration in track quality.

(iii) Effect of turning off the Electrostatic Clearing Field during the Expansion.

Turning off the clearing field during the expansion

led to an improvement in the sharpness of the tracks of recoil nuclei. Because of the large density of ions along these tracks some of the ions were dragged out by the clearing field. The tracks of protons and electrons were equally sharp no matter whether the field was left on or turned off.

This result can be seen by comparing Plates 10 and 11 which are two stereographic sets of photographs of (γ,p) events taken during the Nitrogen experiment. A comparison of the two side camera photographs of Plate 10 (field left on) with the top camera photograph shows that the track of the C^{13} recoil has been dragged out in a vertical direction. In contrast the track of the C^{13} recoil in Plate 11 (field turned off) is both much narrower and equally sharp in all three camera views. Plates 10 and 11 also show that turning off the clearing field leads to a reduction in the contrast between the proton and recoil tracks. Comparison of Plates 2 and 15 shows that there is a similar reduction in contrast for (γ,α) events. Thus it would be an advantage to keep the clearing field on when events such as low energy (γ,α) disintegrations in nuclei of low atomic number are of primary concern.

There is some evidence that the degree to which the tracks of recoil nuclei are dragged out is rather critically dependent on chamber conditions. Thus there is a considerable difference in the appearance of the recoil tracks in Figs. 4 and 5 although these photos were taken 30 minutes apart under identical conditions except that, for Plate 4, the photograph was taken 100 millisec. after the X-ray pulse while the corresponding delay for Plate 5 was approximately 150 millisec.

It is hard to see how this difference could account for all the observed change in the appearance of the recoil tracks. Hence this is probably due, in part, to some other cause such as a slight difference in super-saturation. Since the cloud chamber is known to be stable over long periods of time it is clear that any such difference will be small.

The clearing field was left on during the expansion for the whole of the Helium experiment. The provision for turning off the clearing field was introduced during the taking of photographs for the Nitrogen experiment and tried out in a limited way, the field being turned off at expansion for approximately one quarter of the photographs. In this experiment there were a large number of photoprotons with energies down to 0.5 Mev and it was desirable to see as many as possible of the associated recoil tracks (of length down to 1/6th mm.). The field was turned off at expansion for all the photographs taken during the Neon experiment with the exception of the test photographs of Plate 12.

(iv) Notes on Procedure Required to Clean Chamber after each Expansion.

For the Helium experiment there were some 10^5 relativistic electrons crossing the cloud chamber per X-ray pulse. The problem of removing the nuclei remaining after the fast expansion is illustrated by the result that if this was done by slow expansions in the usual way* then up to 20 slow expansions were required before the chamber was clean. However it was found that the number of slow expansions required could be

*i.e. the first slow expansion commenced immediately after the fast expansion and each slow expansion lasted a few seconds.

greatly reduced by suitable timing. The following comments are based on some, not very exhaustive, tests made at the start of the Helium experiment.

These tests showed that to reduce the number of slow expansions two things were necessary. Firstly a wait before commencing the first slow expansion and secondly the slow expansions must be made sufficiently slowly, an expansion lasting 10 secs. being suitable. The waiting time required varied from 15 - 20 secs. depending on the X-ray yield and this time was independent of whether the chamber was left in the expanded position or returned to the compressed condition immediately after the fast expansion. Under these conditions 5 or 6 slow expansions were sufficient to thoroughly clean the chamber, i.e., only a few large drops were formed during the last slow expansion. Increasing the waiting time from 15 - 20 secs. to 1 min. did not produce any change in the density of background drops produced in the first slow expansion nor any reduction in the number of slow expansions required.

In view of these results the following operating cycle was established and the times given were adhered to fairly closely.

0 secs.	fast expansion, chamber recompressed immediately
30 secs.	start of first slow expansion
40 secs.	end of first slow expansion, start recompression
45 secs.	end of recompression, start second slow expansion.

The slow expansions were continued until the chamber was observed to be thoroughly clean and were followed by a wait of 45 secs.

Total cycling time - approx. 2-1/2 mins.

Since the thousand or so photographs required for the Nitrogen experiment could be obtained in a few days running at the cycling rate already achieved no attempt was made to study in detail the conditions affecting the cleaning of the chamber in this experiment. However it was apparent that the chamber was considerably easier to clean than was the case for the Helium experiment. Thus the initial waiting period was reduced to 5 - 10 secs. and normally only 4 slow expansions were required to clean the chamber. The total cycling time was approximately 2 mins. This could be reduced to 90 secs. for the photographs taken at synchrotron energies of 21 Mev and 19 Mev. The synchrotron yields at these energies were approximately 2/3rds and 1/3rd respectively of the yield at 23 Mev.

For the Neon experiment the completely automatic control circuit described in § 1 (c) was used and the slow expansion cycle for this is given in Fig. 2.2. Normally three slow expansions were required.

A possible explanation for the above observations is that the difficulty in cleaning the chamber during the Helium experiment was due to strong convection currents set up following the fast expansion and persisting during the slow expansions so that the drops formed during the slow expansions did not all fall out in the normal way. 'Convection' currents were often observed in the slow expansions made during the preliminary stages of the Helium experiment and frequently appeared to carry up nuclei from the velvet base cloth. This explanation is suggested by the result that the initial waiting period required was the same no matter whether the chamber was left expanded or recompressed immediately

after the fast expansion and is in accordance with the observation that there was no change in the condition of the chamber when the waiting period was increased from 15 - 20 secs. to 1 min. Latent heat of condensation provides a possible mechanism for starting such convection currents. Because of the large amount of ionization and its wide distribution it is likely that a large fraction of the water vapour condensed. If half of the water vapour condensed then the temperature rise of the surrounding helium would approach 13°C. (This calculation assumes a pre-expansion temperature of 15°C and an expansion ratio of 1.2.). Thus the differences in ionization density within the chamber could have led to appreciable temperature gradients.

On this basis the greater ease with which the chamber was cleaned during the Nitrogen experiment is attributed to

(a) the reduction in electron background following the fitting of the perspex window. For the Nitrogen experiment the total ionization produced in the chamber per X-ray pulse is approximately one third of that for the Helium experiment;

and (b) the fact that this ionization covers a wider region of the chamber. The cross section of the X-ray beam was changed from 5.8 cm. wide x 4.6 cm. high to 10 cm. wide x 2.5 cm. high. Another factor which may have had some influence is the more uniform distribution of initial temperature which would be expected to follow the fitting of the thermal shield.

Since the convection currents discussed above would be set up as a result of the growth of the water drops and the tracks were

photographed while this growth was still in progress, significant distortion of the tracks would not be expected and was never observed.

(v) Additional Notes.

Adjustments to the expansion ratio were made by observing the tracks from the unshuttered polonium alpha source first in continuous white light and then in the short flash from the discharge lamps. For these tests the electrostatic clearing field was always left on during the expansion. The setting of the expansion ratio and the performance of the cloud chamber were always checked in this way before photographs were taken with the synchrotron. All fast expansions and slow expansions were observed and, in particular, the slow expansions were continued until the chamber was seen to be thoroughly clean.

3. PHOTOGRAPHY AND TRACK MEASUREMENT

The tracks were photographed with a stereographic set of two or three 60 mm. cameras. These cameras were fully automatic and were fitted with "Ental" enlarging lenses (focal length = 80 mm., aperture = f/4.5, manufactured by Taylor, Taylor and Hobson). The film used was Ilford recording film Type 5G91. The cameras were normally operated with the lenses set to f/11, except for the side camera looking into one of the lamps which was set to f/16.

For the Helium experiment two cameras were used. A top camera mounted centrally above the chamber and a side camera with its lens axis at an angle of 25-1/2° to the vertical. The plane of the film in this camera was tilted with respect to the lens axis and was at an angle of 30° to the horizontal. These films were analysed by the usual method of

stereographic analysis, i.e., the films were replaced in the cameras and the projected images of the tracks brought into coincidence on an adjustable table.

For the Nitrogen experiment a second side camera was added. The lens axis of this camera was also at an angle of 25-1/2° to the vertical and was separated from that of the other side camera by 90° in azimuth. The reason for using a third camera was that, for a pair of cameras, it is sometimes impossible to get a satisfactory coincidence on a track lying approximately parallel to the vertical plane joining them. This can be seen by considering the way in which the two images are brought into coincidence on a table free to tilt about a horizontal axis. If the table has been adjusted so that the origin of the track lies on this axis then, if the vertical plane joining the cameras is at a considerable angle to the track, the two images will, in general, be at an angle to one another and can be brought into complete coincidence by tilting the table. If the vertical plane joining the cameras is parallel to the track then the two images will always be on top of one another. In this case a coincidence is obtained by tilting the table until both images are of the same length. For a track passing out of the illuminated region the end point of the image is ill defined and often different for the two cameras. Hence the "coincidence" does not give the correct position for the track.

To analyse a track the images from the top camera and the appropriate side camera were used with the image from the third camera providing a very useful check. The films in the three cameras were

brought into register using the images of the grid wires which were built into the chamber. This automatically checked the accuracy of the reprojection system.

The reprojection table was constrained to tilt about a horizontal axis and could be locked in any position by means of a magnetic chuck. It was provided with the following additional degrees of freedom.

(a) The whole table could be rotated so that the horizontal axis pointed in any desired direction.

(b) The table moved horizontally and vertically so that the axis could be made to pass through any point within the cloud chamber volume.

In practice the axis was made to point either in the direction of the X-ray beam or at right angles to it. The direction chosen was that which gave the smaller angle of tilt when the two images were in coincidence. The position of the table was then adjusted so that the origins of the two images coincided on the axis and the table tilted to obtain a full coincidence. The coordinates of the origin were then obtained directly from the position of the table and the distance of the image along the axis. The direction of the track in space was given by the angle of tilt of the table and the angle between the image and the axis. The coordinates of the end point were measured by shifting the table so that this point was on the axis. The coordinates of the origin were used to check whether the event originated within the X-ray beam and those of the end point to check whether the track stopped within the illuminated region of the chamber.

Tests on artificial tracks showed that the length measurements were accurate to 1/2 mm. for all lengths and that the angles were accurate to 1° for tracks within 60° of the horizontal. For very steep tracks the measurement of coordinates provided the best method of determining their length and direction. From the measured coordinates of tracks whose lengths could be determined directly it was shown that the coordinate method was just as accurate for length measurements. Its accuracy for angular measurements is given by assuming an error of up to 1/2 mm. in the coordinate difference from which the angle is determined.

The cameras and reprojection table can be seen in Fig. 5.4 on p. 1196. It should be noted that the arrangement of the cameras shown in this photograph is that used for the Neon experiment and also that the protractor and pointer sitting on the reprojection table were only used during the analysis of the Neon experiment.

Chapter III

INVESTIGATION OF THE $He^4(\gamma,p)$ REACTION

As was pointed out in Chapter I (see p. 45) a number of considerations suggest a study of the $He^4(\gamma,p)$ reaction as a suitable first experiment in a program of photonuclear measurements using an expansion chamber in conjunction with an electron synchrotron. Further, at the time this experiment was started, there were good reasons for attempting a measurement with the Glasgow synchrotron whose peak energy (approximately 23 Mev) was only a few Mev above the threshold for this reaction (19.8 Mev). The experimental and theoretical results available then indicated that a large number of $He^4(\gamma,p)$ events could be obtained quite easily at this energy and that a cross section measurement in the energy region just above threshold was of particular importance. The relevant facts are given below.

Argo et al (Ar 50) had measured the cross section and angular distribution for the inverse reaction, $H^3(p,\gamma)$, for proton energies between 0.5 and 2.5 Mev. The $He^4(\gamma,p)$ cross section deduced from these measurements (by use of the principle of detailed balance) rose smoothly with increasing energy and had reached a value of 10^{-26} cm^2 at 21.6 Mev (the photon energy corresponding to an incident proton energy of 2.5 Mev). For this cross section and a peak X-ray energy of 23 Mev the Glasgow synchrotron and cloud chamber should give one $He^4(\gamma,p)$ disintegration per five expansions.

The importance of a measurement of the cross section in the

region just above threshold had been shown by the theoretical investigations of Flowers and Mandl (Fl 51) and, in particular, of Gunn and Irving (Gu 51) at Glasgow. The latter workers used approximate analytical calculations of the H^3, He^3 and He^4 photonuclear cross sections to determine the sensitivity of these cross sections to changes in the nuclear wave functions and nuclear size parameters. They found that all these cross sections are very dependent on both factors and hence measurement of these cross sections would be a good method of determining their values. In particular they found that the $He^4(\gamma,p)$ cross section should rise rapidly to a pronounced maximum a few Mev above threshold and that the position of this maximum (their calculated values vary between 4 Mev and 15 Mev above threshold) and the cross section at this maximum provide a sensitive test of the nuclear wave function and the nuclear size parameter. Gunn and Irving also compared their calculation with the available experimental data (the $H^3(p,\gamma)$ measurement mentioned above and a similar measurement of the $H^2(p,\gamma)$ reaction for proton energies up to 1.5 Mev by Fowler et al. (Fo 49)) and noted that both these experimental cross sections rise more rapidly than any of their theoretical calculations. On this basis the maximum of the $He^4(\gamma,p)$ cross section would be only some 3 Mev above the threshold and so probably within the range of the Glasgow synchrotron. Even if the cloud chamber experiment did not reach to the maximum it would be of value since it would certainly cover a greater energy range than that covered by the measurement of Argo et al*. and also

*It should be noted that the upper limit of 2.5 Mev in this measurement was set by the maximum energy of the Los Alamos Van der Graaf accelerator and as this was close to the maximum energy of any such accelerator at that time it was unlikely that the $H^3(p,\gamma)$ measurement would be extended to higher energies for some time.

provide quite independent evidence on the $He^4(\gamma,p)$ cross section. Such evidence was desirable since the absolute value of the $H^3(p,\gamma)$ cross section given by Argo et al. was established by a rather indirect process and was not independent of the value of the $H^2(p,\gamma)$ cross section given by Fowler et al. since both these measurements are referred back to a common geiger counter calibration (Fo 48). It is also worth noting that the validity of using the principle of detailed balance to predict reaction cross sections from the inverse reaction had never been confirmed experimentally for photonuclear reactions.

A study of the $He^4(\gamma,p)$ reaction is attractive from the point of view of technique since the energy range of particular interest (the first few Mev above the threshold) is also the region where the energy of the incoming photon can be obtained with greatest ease and accuracy (from the range of the recoil triton). This, combined with the fact that a $He^4(\gamma,p)$ disintegration is a very distinctive event, makes such a study a most suitable experiment with which to establish the technique of using the cloud chamber for photonuclear studies.

From the point of view of measuring the shape of the $He^4(\gamma,p)$ cross section this investigation proved to be a disappointment as only 12 $He^4(\gamma,p)$ events were found in 650 cloud chamber photographs indicating that the cross section is only approximately 1/10th of the value deduced from the measurement of Argo et al. (Ar 50). More recent measurements by other workers support the lower value reported here (see discussion later).

The experiment also established the technique of using the cloud chamber for photonuclear studies and in particular emphasized its

suitability for a study of the $He^4(\gamma,p)$ reaction with a higher energy synchrotron. Features of the experimental method which are of interest are discussed below.

1. SUMMARY OF EXPERIMENTAL CONDITIONS

Prior to the author's arrival in Glasgow Mr. J.R. Atkinson had taken some preliminary photographs with the uncollimated X-ray beam from the synchrotron. Although there was a very dense background of electron tracks some tracks with the characteristics expected for a $He^4(\gamma,p)$ event could be distinguished. However, as there were also a large number of single tracks (possibly recoils from fast neutrons) and a number of these showed scattering which gave them a similar appearance, it was not possible to be sure of this identification. Photographs taken with the chamber filled with hydrogen showed that there was a large neutron background.

This investigation was encouraging as it showed that proton tracks could be distinguished in spite of the electron background and that the yield of events of interest was probably reasonable. It was clearly desirable to reduce the number of "recoil" tracks and to use criteria which would identify $He^4(\gamma,p)$ events with certainty.

The experiment described here was made with a collimated X-ray beam 5.8 cm. wide by 4.6 cm. high at the centre of the cloud chamber. This beam passed through the 1/4" thick glass wall of the chamber but did not touch either the top glass plate or the chamber base. Ten to twenty centimetres of paraffin were placed between the collimator and cloud chamber to further reduce the neutron background. The chamber was filled with helium at a pressure of 140 cm. (chamber expanded) and in addition

contained up to 16 cm. of nitrogen + air. These latter gases diffused into the cloud chamber through the rubber diaphram during the experiment. The stopping power of the expanded gas mixture was obtained for each $He^4(\gamma,p)$ disintegration by measuring the length of the longest track from the unshuttered polonium source in the chamber.

As already described (see p. 67ff) the tracks were photographed with a pair of stereographic cameras* and analysed by replacing the films in the cameras and reprojecting the track images onto an adjustable table. All tracks of protons or heavier particles produced in the cloud chamber were measured to determine their origin, length and direction.

2. RESULTS

A $He^4(\gamma,p)$ disintegration will appear as a pair of tracks with a common origin, i.e., as a flag event. Because of the momentum of the incoming quantum the angle between these tracks in the forward direction will be slightly less than 180°. (See Plate 1). For the above experimental conditions the triton (maximum range** for 23 Mev X-rays = 3.7 cm.) will almost always stop in the chamber while the proton will generally pass out of the chamber.

Flag events were analysed with the axis of the adjustable table set in the direction of the X-ray beam. Hence events for which the two tracks were coplanar with the direction of the incoming quantum were

*The line joining these cameras was approx. parallel to the direction of the X-ray beam and therefore at a large angle to the $He^4(\gamma,p)$ tracks which were expected to have a $\sin^2\theta$ distribution (from the angular distribution found in the inverse reaction).

**All ranges quoted in this section are ranges in the expansion chamber.

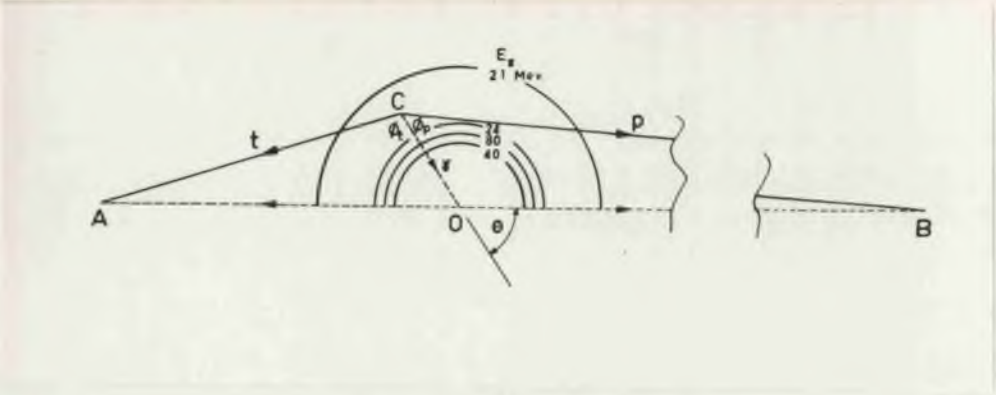

CA, CB velocity of triton and proton in the laboratory system

OA, OB velocity of triton and proton relative to the centre of mass

CO velocity of the centre of mass

$$= AB \times \frac{E_\gamma}{\sqrt{E_\gamma - \left(19.8 + \frac{E_\gamma^2}{2M}\right)}} \sqrt{\frac{M_p M_t}{2M^3}}$$

where E_γ energy of quantum in Mev

M_p, M_t masses of proton and triton in $\frac{\text{Mev}}{c^2}$

$M = M_p + M_t$

ϕ_t, ϕ_p observed angles between incoming quantum and triton and proton

θ angle of emission of proton in the centre of mass system

Fig. 3.1

Velocity diagram for the $He^4(\gamma,p)$ reaction. As indicated the locus of C is a circle whose radius is a function of E_γ. This radius is a rapidly decreasing function of E_γ just above threshold, reaches a minimum value at E_γ = 40 Mev and increases slowly with increasing E_γ at higher energies.

identified by the fact that, for both tracks, the two sets of images came into coincidence simultaneously. This test identified events due to the $He^4(\gamma,p)$ reaction or to the (γ,p), (γ,d) or (γ,α) reactions in one of the other nuclei present. Many of the $He^4(\gamma,p)$ events were then identified immediately by the fact that the triton range was greater than the maximum range of the recoil nucleus from any other two body reaction. The maximum recoil ranges for the (γ,p), (γ,d) and (γ,α) reactions in the other nuclei present were 7 mm., 9 mm. and 1.4 cm. respectively. $He^4(\gamma,p)$ events with short triton ranges (i.e., E_γ less than approx. 21.6 Mev) were identified from the fact that, for a given recoil range, the forward angle for the $He^4(\gamma,p)$ reaction is much less than the corresponding angle for any other reaction (compare the events in Plates 1 and 2).

For the energy range covered by this experiment the value of the forward angle is also a good measure of E_γ. Comparison of this E_γ with that determined from the triton range provided a further confirmation of the nature of the event. This analysis was considerably simplified by using a model based on the velocity diagram for the reaction (Fig. 3.1). In this model the lines CA, CO and CB were represented by three threads joined at C, passing through appropriate holes in a bakelite board and tensioned with weights. The position of C was adjusted until the angles between the threads corresponded to the measured angles and E_γ determined from the length CO. This model also simplified the other dynamical calculations since

$$E_p = \frac{M_p}{M_t}\left(\frac{CB}{CA}\right)^2 E_t$$

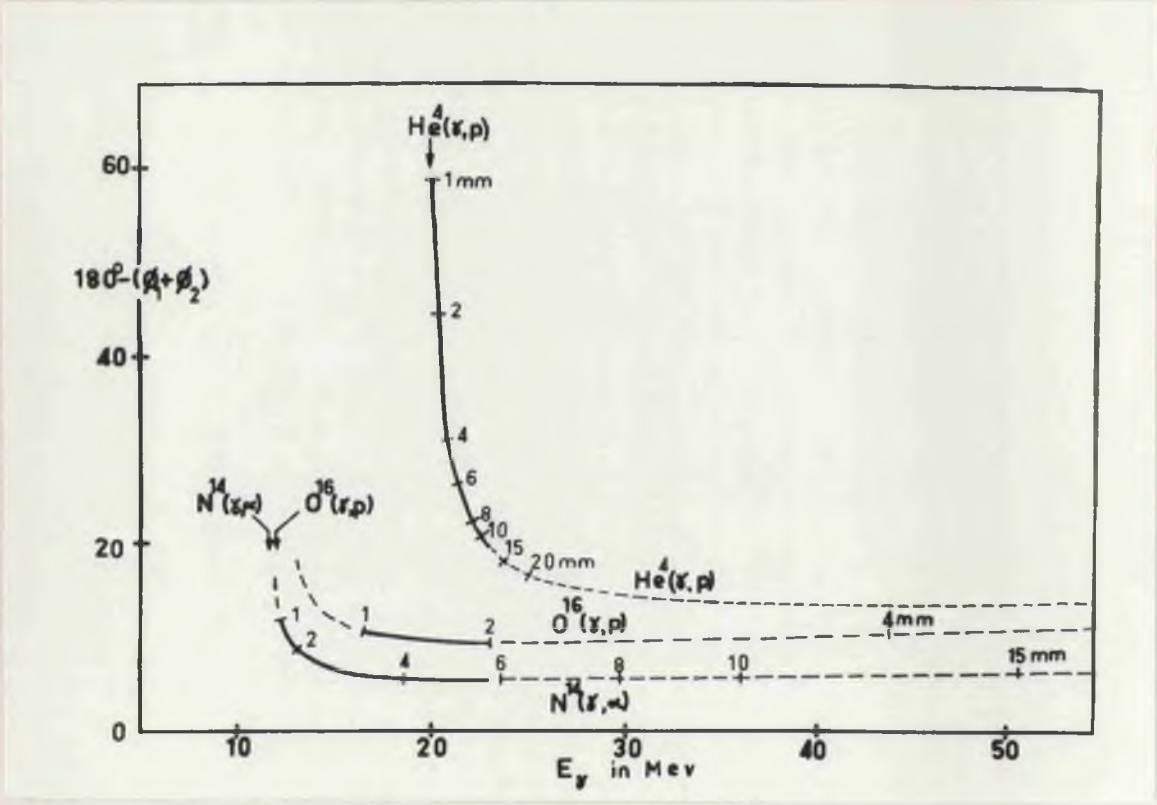

Fig. 3.2

Values of 180°- forward angle for the reactions marked and $\theta = 90°$. The arrows denote the thresholds for these reactions and the marked points the recoil range in mm. at S.T.P. The full curves indicate the region of interest in the present experiment.

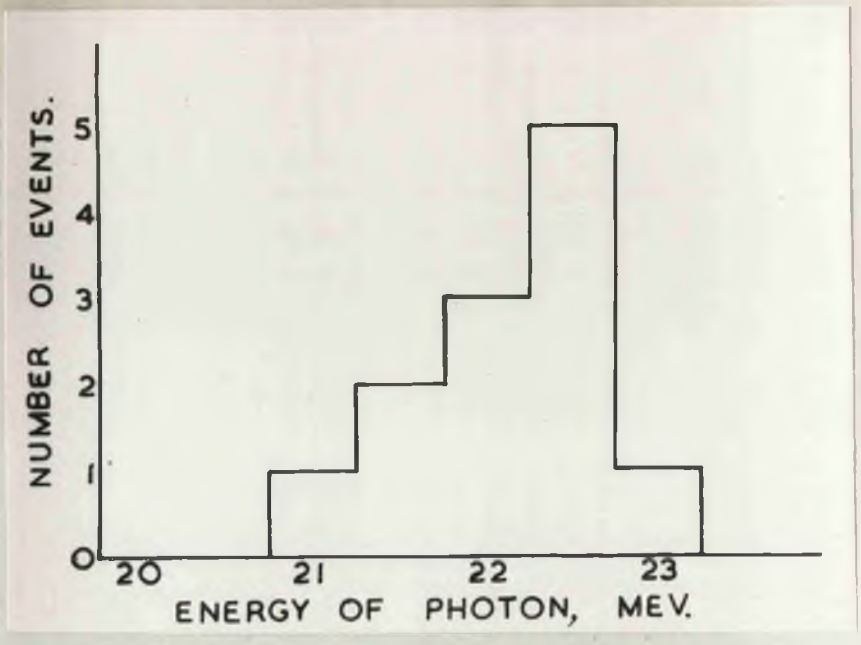

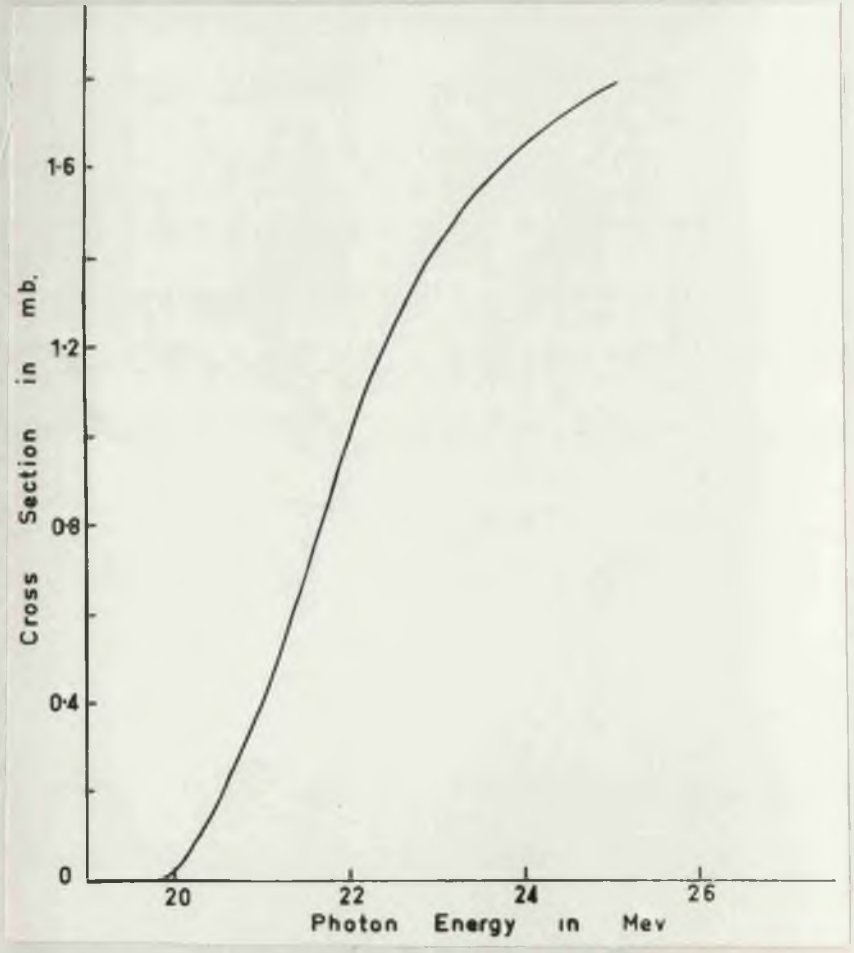

Fig. 3.3

(a) Energy distribution of the $He^4(\gamma,p)$ events found in the present experiment.

(b) $He^4(\gamma,p)$ mass section deduced from subsequent measurements on the $H^3(p,\gamma)$ reaction by Perry and Bame (Pe 55).

and $E_{\gamma(Mev)} = 19.80 + E_t + E_p$.

The accuracy of the angular analysis is illustrated by Fig. 3.2 which gives $180° - (\phi_p + \phi_t)$ for $\theta = 90°$ as a function of E_γ. An error of 1° in $(\phi_p + \phi_t)$ corresponds to an error of 0.1, 0.2 and 0.5 Mev in E_γ for E_γ = 21.0, 22.0 and 23.0 Mev respectively. Fig. 3.2 also shows the marked difference there is in the forward angle for a given recoil range as between $He^4(\gamma,p)$ and other reactions producing "coplanar" flags. The (γ,p) and (γ,α) reactions illustrated are those which give angles closest to the $He^4(\gamma,p)$ angle.

Twelve $He^4(\gamma,p)$ events were identified by the above criteria. For three of these both the proton and triton stopped in the illuminated region of the chamber and for a further seven the triton stopped in the chamber. The independent values of E_γ for each event always agreed within the expected errors* giving triple and double checks respectively on the nature of these events. The two events for which both proton and triton passed out of the illuminated region were identified from the minimum recoil range and the forward angle which also gave the value of E_γ for these events. The energy distribution of these twelve events is given in Fig. 3.3 (a) and indicates that the cross section increases rapidly with energy up to at least 23 Mev, the peak energy of the machine. The integrated cross section up to 23 Mev is 2.3 ± 1 Mev-mb. The values of $\theta_{\gamma p}$ for the 12 events are compatible with a $\sin^2\theta$ angular distribution as found by Argo et al. (Ar 50) for the $H^3(p,\gamma)$ reaction and therefore expected for the $He^4(\gamma,p)$ reaction.

*These are 0.15 and 0.05 Mev for E_γ determined from triton and proton ranges respectively.

The only other photonuclear reaction which can be produced in He^4 with 23 Mev X-rays is $He^4(\gamma,n)$ (threshold = 20.58 Mev)*. This reaction was not studied since the tracks produced (single tracks of the He^3 recoil nuclei with a maximum range, for 23 Mev X-rays, of 1.0 cm.) could not be distinguished from similar tracks produced by the recoil nuclei from $N^{14}(\gamma,n)$ and $O^{16}(\gamma,n)$, and He^4 recoils from the scattering of background neutrons.

All tracks of protons or heavier particles which originated in the gas of the cloud chamber and were not obviously $He(\gamma,p)$ events were carefully examined and readily identified as follows:**

(a) 20 (γ,p) or (γ,d) disintegrations in N^{14} or O^{16}.

(b) 25 $N^{14}(\gamma,pn)$ events. These were identified by the fact that the recoil and proton tracks were not coplanar with the X-ray beam direction and also the angle between these tracks was generally not close to 180° (for example see Plate 3).

(c) 2 (γ,α) disintegrations in N^{14} or O^{16}.

(d) 100 single tracks, i.e., tracks without a visible recoil track at the origin. Fifty were less than 1 cm. long, the remainder had ranges between 1 cm. and 9 cm. Fifteen of these single tracks were outside the X-ray beam. These must be events produced by background

*The thresholds for other reactions in He^4 are $He^4(\gamma,2d)$ 23.84 Mev, $He^4(\gamma,pn)$ 26.07 Mev and $He^4(\gamma,2p2n)$ 28.30 Mev.

**These figures are estimates from data on half the photographs. The results of the measurements on other tracks for the remaining photographs are not available to the author at present.

neutrons; with the correction for the volume of the X-ray beam the total of such events was approximately 25*.

Since all other tracks are quite distinct in appearance from the $He^4(\gamma,p)$ events the identification of these is quite certain. With a collimated X-ray beam the background of events produced by neutrons is quite small and this background can be readily estimated from the number of events outside the X-ray beam.

3. DISCUSSION

The $He^4(\gamma,p)$ cross section reported here is approx. 1/10th of the cross section deduced from the measurements of Argo et al. (Ar 50) on the $H^3(p,\gamma)$ reaction which was the only other value for the $He^4(\gamma,p)$ cross section in this energy range at the time of the experiment discussed here. Subsequent experiments by other workers are in agreement with this lower value. In particular, the $He^4(\gamma,p)$ cross section deduced from a careful measurement of the $H^3(p,\gamma)$ cross section by Perry and Bame (Pe 55) has a similar energy dependence (see Fig. 3.3 (b)) and gives a value of 2.17 ± 0.15 Mev-mb for the integrated cross section up to 23 Mev. The direct measurements of the $He^4(\gamma,p)$ cross section (Fu 54, Go 57), which are slightly less accurate in this energy region, confirm the results of Perry and Bame.

*75 of the singles were therefore photonuclear tracks. The short tracks were clearly recoil nuclei from the $He^4(\gamma,n)$, $N^{14}(\gamma,n)$ and $O^{16}(\gamma,n)$ reactions. The longer tracks were probably $N^{14}(\gamma,p)$ events in which the recoil tracks were not seen. The nitrogen experiment (see Chapter IV) showed that, for 23 Mev X-rays, there are a large number of photoprotons of energy less than 1-1/2 Mev (the proton energy corresponding to a range of 9 cm.). The ranges of the associated recoils are less than 1 mm. and these tracks would have been difficult to see in the dense background of electron tracks.

While this investigation was in progress Gaerttner and Yeater (Ga 51b) published the results of a cloud chamber investigation of the $He^4(\gamma,p)$ reaction using 100 Mev X-rays. For this work they used a 5" diameter cloud chamber, with an illuminated depth of 1/2", which was filled with helium plus alcohol and water vapour at a total pressure of 1 atmosphere. From the results of previous experiments with the cloud chamber filled with methane and oxygen they found that the maximum recoil ranges for carbon and oxygen flags would be 2.0 and 1.4 cm. respectively. They therefore identified as $He^4(\gamma,p)$ events all flags with a visible recoil length greater than 2 cm. (a total of 119). Gaerttner and Yeater note that for all these flags there was a marked difference in density between the two tracks and the resultant momentum was in the direction of the X-ray beam. From these observations they eliminate the possibility that some of these flags may be due to the $He^4(\gamma,d)$ reaction, or to the $He^4(\gamma,pn)$ and $He^4(\gamma,2p2n)$ reactions. The correction for the helium flags not identified (i.e., flags orientated so that the visible recoil length was less than 2 cm.) was calculated from the illuminated depth. The values of E_γ for the $He^4(\gamma,p)$ events were determined from the values of the forward angle. The average value of E_γ was 27 Mev. (This value is only approximate since this method is inaccurate above 25 Mev). The integrated cross section determined from this mean energy and the total number of events was 0.034 ± 0.012 Mev-barn. The angular distribution of the protons (and tritons) in the centre of mass coordinate system was approximately $\sin^2\theta$. The results of the experiment described in this chapter cannot be directly compared with these figures but the rise in

the cross section and the value of the integrated cross section up to 23 Mev (2.3 ± 1 Mev-mb) are clearly compatible with the above mean energy and total integrated cross section.*

The experiment described in this chapter was carried out independently of the work of Gaerttner and Yeater. Within its limited energy range it provided a more accurate value for the $He^4(\gamma,p)$ cross section and a more positive identification of the $He^4(\gamma,p)$ events. In particular it showed very clearly that they can always be separated from events due to (γ,p) and (γ,α) reactions in other nuclei and hence that it is practicable to mix a heavier gas with helium to increase the stopping power. A total stopping power of four times air at N.T.P. would enable triton range measurements (which give the most accurate values of E_γ) to be extended up to an energy corresponding to an E_γ of 45 Mev. Measurements of the range of the He^3 recoil nuclei under similar conditions would give the $He^4(\gamma,n)$ cross section up to 70 Mev. An experiment using this method would be of value at the present time since there is considerable disagreement between existing experimental values for the $He^4(\gamma,p)$ and $He^4(\gamma,n)$ cross sections above 30 Mev. These experimental values and their theoretical implications are summarized and discussed in Appendix I.

*In addition to the (γ,p) measurements Gaerttner and Yeater identified as $He(\gamma,n)$ events all single tracks of length greater than 4 cm. The expected maximum length of the single tracks from $C^{12}(\gamma,n)$ and $O^{16}(\gamma,n)$ is 2 cm and measurements with a hydrogen filled cloud chamber showed that there were no long tracks due to neutron recoils. They identified 57 (γ,n) events in a portion of the data containing 45 flags with recoil lengths greater than 4 cm. The ratio of (γ,n) and (γ,p) yields is therefore about 1.3.

Chapter IV

THE PHOTODISINTEGRATION OF NITROGEN

The considerations that led to the conclusion that N^{14} would be a particularly favourable choice for a comprehensive survey of photonuclear reactions over a wide range of energies are as follows. For this nucleus the (γ,p), (γ,d), (γ,pn), (γ,α), $(\gamma,2\alpha)$ and $(\gamma,\alpha p)$ reactions can all be studied in a cloud chamber and, with the exception of events from the first two reactions, events of different kinds are easily distinguished from one another. Of the reactions that cannot be studied in a cloud chamber, namely - (γ,n), $(\gamma,2n)$ and (γ,γ), the cross section for the (γ,n) reaction has already been measured (Ho 52), the $(\gamma,2n)$ reaction is energetically impossible with 23 Mev X-rays (threshold = 30.7 Mev) and the cross section for the (γ,γ) reaction is expected to be small. Further, the thresholds for the (γ,p), (γ,n) and (γ,pn) reactions are all well below the energy of the giant resonance found in the (γ,n) reaction (23 Mev) and thus a study of these reactions might be expected to yield information about the change in the nature of the photonuclear process in going from energies below to energies in the vicinity of the giant resonance.

1. ADDITIONAL NOTES ON EXPERIMENTAL METHOD

1 (a) Apparatus and Analysis.

In order to estimate the energy of the photons responsible for the photonuclear events observed in the cloud chamber, irradiations were made at three different values of the peak X-ray energy, these energies

being approximately 19, 21 and 23 Mev. The X-ray dose for each of these three irradiations was measured using an ionization chamber (see p. 59) and these measurements were expressed in terms of the conventional 'r-unit' by the following procedure. For each peak energy the ionization chamber response was compared with the activity induced in a copper disc irradiated in a standard position in front of the cloud chamber and counted in a standard geometry. The relative number of r-units for the 19, 21 and 23 Mev runs were then calculated from the peak energies using the Cu^{62} activation curve as measured at Saskatchewan (Ka 51). Absolute values were obtained by subsequently comparing (at a peak energy of 23 Mev) the activity induced in the copper disc with the response of a Victoreen thimble mounted at the centre of a perspex cylinder 8 cm. in outside diameter. The estimated accuracy of this comparison is 20%.

The photographs obtained with the stereographic set of three cameras were analysed by each of the following techniques. Measurements were made on the images of all tracks of length greater than 3 mm.

(i) The events were viewed under a low powered microscope, the final image being approximately seven times the original track size. (The microscope magnification was 40 and the chamber - film reduction 1/6). Each recoil length was measured with the eyepiece scale.

(ii) The length, direction in space and coordinates of the origin and end points of each track were measured by replacing the films in the cameras and projecting the images onto an adjustable table as described in Chapter II, p.67ff. These lengths were converted to ranges in air at

Table 4.1

Reaction Thresholds and Classifications

Photonuclear Reactions		Threshold Mev
$N^{14} + \gamma \rightarrow n + N^{13}$		10.54
$p + C^{13}$		7.54
$d + C^{12}$	Collinear Flags	10.26
$\alpha + B^{10}$		11.62
$p + n + C^{12}$	Non-collinear Flags	12.49
$\alpha + n + B^{9}$		19.96
$\alpha + \alpha + Li^{6}$	Stars	16.07
$p + \alpha + Be^{9}$		18.20

Neutron Reactions		
$N^{14} + n \rightarrow p + C^{14}$	Non-collinear Flags (except for slow neutrons)	- 0.63
$\alpha + B^{11}$		0.15

S.T.P.* using the stopping power of the gas (nitrogen saturated with water vapour) as calculated from its composition and the expanded pressure (1.4 atmospheres) which was measured during each 6 hour run.

The events were classified as -

(1) Collinear Flags - events in which the recoil and fragment were very nearly in a straight line for all three films. This group is intended to consist of events in which the recoil and fragment are the only two products of the reaction. For these events the momentum of the incident photon and the scattering of the recoil may both cause a small departure from exact collinearity. The criterion used was that events in which the recoil was within $\pm$ 10° of its expected direction were counted as collinear.

(2) Non-Collinear Flags.

(3) Unclassified Flags - events with a visible recoil of uncertain direction (e.g. because of its short length).

(4) Singles - events without a visible recoil.

(5) Stars - events with three or more prongs.

(6) Tracks coming from the chamber wall.

The thresholds for the photonuclear reactions possible in N^{14} are given in Table 4.1 together with the expected classification of the events produced.

1 (b) Background Events.

Reactions initiated by the neutrons which accompany the X-ray beam will give rise to a background of unwanted tracks. In particular,

*i.e., 15°C and 760 mm of mercury.

since the $N^{14}(n,p)C^{14}$ reaction is exothermic there may be a relatively large number of proton tracks initiated by slow neutrons. These proton tracks have a characteristic length of 7-1/2 mm. (the range in the chamber of a proton of 0.58 Mev) and should occur uniformly throughout the chamber. The energy distribution of tracks stopping in the chamber shows that they form a distinctive group which is easily identified and eliminated (see Figure 4.1 on p. 84a and discussion in § 2).

Fast neutrons produce both (n,p) and (n,α) events which appear as non-collinear flags of length greater than 1 cm. The number of these background events was estimated from the number occurring outside the beam and also from the number of tracks coming from the perspex wall. Both estimates indicate that the correction required is small, the number (15) of tracks longer than 1 cm. with origins outside the X-ray beam being only 2% of the number (660) of tracks within the beam, whereas the two volumes are equal.

The number and distribution of recoil protons ejected from the perspex wall by fast neutrons* confirms this estimate of the background and shows further that the fast neutron flux within the X-ray beam is not significantly greater than the fast neutron flux elsewhere in the chamber.

2. ENERGY DISTRIBUTION OF LOW ENERGY PROTONS

If it is assumed that the collinear flags (with (γ,α) events

*This estimate was obtained from the data for the 19 and 21 Mev runs for which the number of tracks of photoprotons from the C^{12} and O^{16} in the perspex wall is small and therefore easily allowed for.

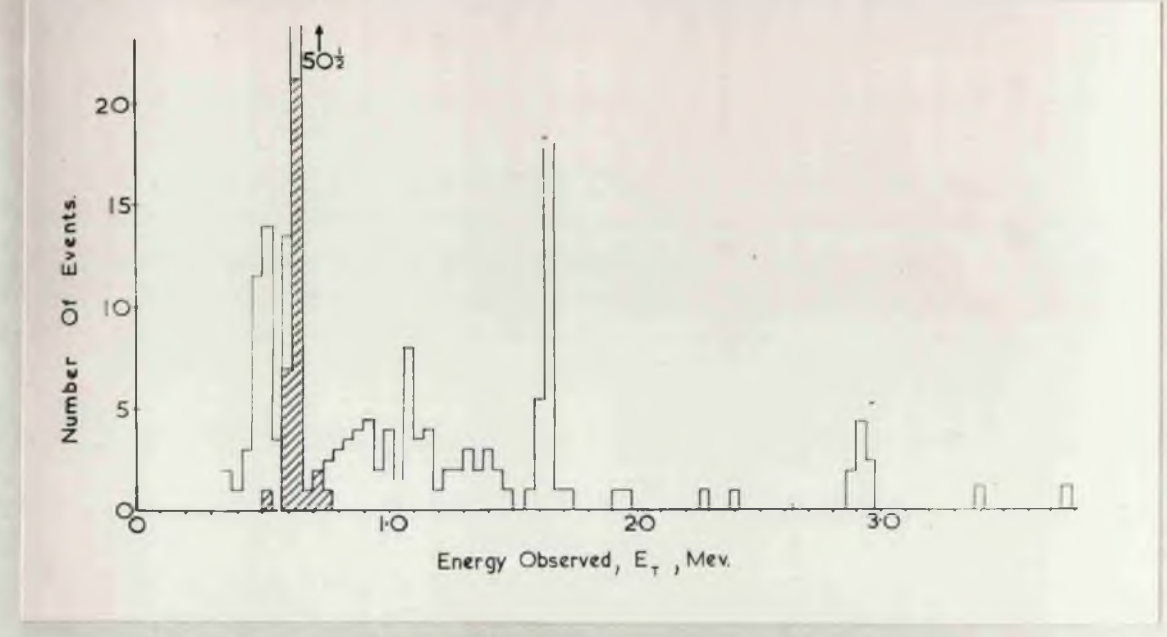

Fig. 4.1

Distribution of the total energy (i.e. $E_p + E_\gamma$) of collinear flags, unclassified flags and singles stopping in the chamber, assuming these to be (γ,p) events. (See § 1 (a) for description of the classification). Events occurring outside the X-ray beam have been shaded.

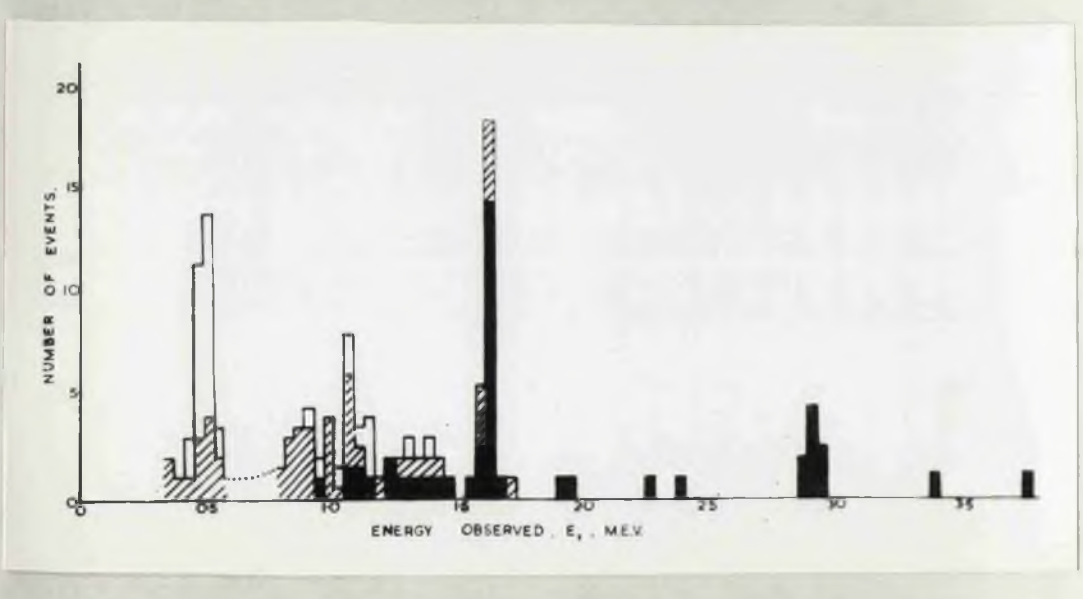

Fig. 4.2

The energy distribution of Fig. 4.1 after subtraction of events due to the $N^{14}(n,p)C^{14}$ reaction. Collinear flags are shown as solid rectangles, unclassified flags as shaded rectangles and singles as open rectangles.

excluded), unclassified flags and singles stopping in the chamber are (γ,p) events, then the distribution of E_t, the total kinetic energy of the proton and recoil, is as given in Fig. 4.1. The proton kinetic energy was obtained directly from the measured track length and the recoil energy was then calculated using momentum conservation. Events occurring outside the X-ray beam are shaded and it can be seen that they are all due to (slow n,p) reactions. In Fig. 4.2 the (slow n,p) events have been subtracted and the classification of events is indicated. It can be seen that unclassified flags and singles only occur at proton energies for which recoils would be very short. (For a 1 Mev proton the recoil length is approximately 1/3 mm.).

Distinct groups are observed at 0.51 ± 0.02, 1.63 ± 0.02 and 2.92 ± 0.03 Mev, the latter group being small in number as most of the protons leave the chamber, and a broad group centred at about 1.15 ± 0.05 Mev.

The occurrence of definite groups implies that these photoprotons arise from the resonance absorption of quanta into excited states of the N^{14} nucleus. It is therefore of interest to compare these results with the information about the excited states of N^{14} derived from other reactions and, in particular, to make a comparison with the measurements made on the $C^{13}(p,\gamma)N^{14}$ reaction. This reaction has been studied by Seagrave (Se 52) and by Woodbury et al (Wo 53) using protons of energy up to 2.6 Mev and by Willard et al (Wi 57) who used protons of energy between 2.5 and 3.2 Mev. These workers find that the $C^{13}(p,\gamma)N^{14}$ (ground state) reaction has resonances at centre of mass energies of 0.52, 1.64 and

Table 4.2

Comparison of the Observed Proton Groups with the Predictions from the $C^{13}(p,\gamma)N^{14}$ Reaction

N^{14} E	$E_t = E_p + E_r$		$\sigma_{int.}$		Fraction of events stopping	No. of tracks	
	calc.	obs.	(p,γ)	(γ,p)		calc.	obs.
Mev	Mev	Mev	Mev-mb.	Mev-mb.			
8.06	0.52	0.51	0.065	0.603	0.99	34	32
9.18	1.64	1.63	0.044	0.813	0.62	24	26
10.43	2.89	2.92	0.033	1.05	0.20	10	9

2.89 Mev as well as a broad resonance at 1.16 Mev. These energies correspond closely to the energies of the groups observed in this experiment and indicate that these proton groups come from the reaction $N^{14}(\gamma,p)C^{13}$(ground state).

The comparison of the two reactions can be extended to cover the cross sections by using the principle of detailed balancing. The integrated (γ,p) cross sections for the resonances at 0.5, 1.6 and 2.9 Mev were calculated from the (p,γ) cross sections using this principle. The $C^{13}(p,\gamma)N^{14}$(ground state) cross sections for the 0.5 and 1.6 Mev resonances were obtained by combining the results of Seagrave (Se 52) and Woodbury et al (Wo 53). The expected number of tracks in each of the narrow groups was then calculated from the (γ,p) cross sections, the measured X-ray doses and an allowance for the percentage of tracks which do not stop in the chamber. In Table 4.2 this estimate is compared with the number actually found. The agreement is very satisfactory and confirms the validity of applying the principle of detailed balancing to photonuclear reactions.

A nuclear emulsion measurement by Spicer (Sp 53) of the energy distribution of photoprotons from nitrogen irradiated with 11.5 Mev X-rays is in conflict with the present results. In this work a narrow beam of X-rays passed through a gas target chamber and the photoproton energy distribution was deduced from ranges measured in nuclear emulsions placed out of the beam, allowance being made for the energy lost by the proton before it reached the emulsion. The energy distribution found is

reproduced in Fig. A 2.1 on p.160a. It can be seen that there is no sign of a peak at 2.7 Mev (the proton energy corresponding to $E_p + E_R$ = 2.9 Mev) but instead the number of protons increases rapidly with decreasing energy from 3.6 Mev to 2.2 Mev, the experimental lower limit since protons of energy less than this may fail to reach the emulsion. It is difficult to see how this result can be reconciled with the absence of tracks between 2.0 and 2.8 Mev which is such a striking feature of the distribution obtained in the present investigation and which is believed to be very reliable since, not only is the method inherently cleaner (e.g. (n,p) reactions are automatically eliminated since they either produce non-collinear flags or form a distinctive group), but also the results agree very well with all the data available from the inverse reaction.

Spicer's results are examined in detail in Appendix II on p.159. It is found that there are good reasons for believing that the tracks measured by Spicer are a background of short range tracks not detected in the background measurements. This background is also present in a measurement made by Spicer of the spectrum of photoprotons from O^{16} and possibly in similar measurements by other workers. It is concluded from this that nuclear emulsion measurements of photoproton spectra with moderate or low yields ($\lesssim 10^5$ protons/mol/r) are liable to be in error at the low energy end ($E_p \lesssim 3$ Mev).

3. STUDY OF THE (γ,p) AND (γ,α) REACTIONS AT HIGHER ENERGIES

For proton energies greater than 3 Mev the probability of a

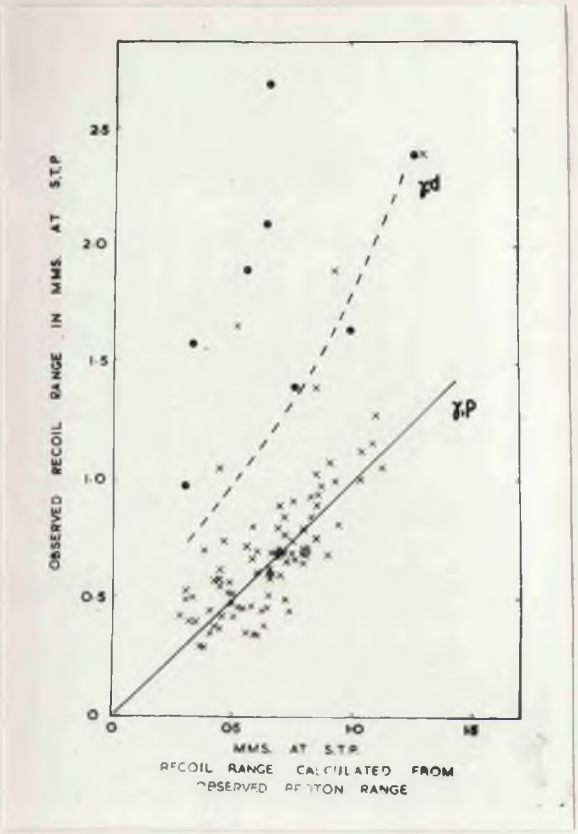

Fig. 4.3

Comparison of the observed recoil ranges for collinear and unclassified flags stopping in the chamber with the ranges calculated from the range of the associated fragment track assuming this to be a proton. The dotted curve gives the expected ranges of the recoils from (γ,d) events. The circles give the recoil ranges of non-collinear (γ,pn) events which fall just outside the criterion for collinear flags (see text § 3 (a)).

proton stopping in the chamber is very small and consequently the photo-proton energy distribution cannot be determined from proton range measurements. However, since the proton momentum is directly related to the momentum of the recoiling C^{13} nucleus, this distribution can be determined from the range distribution of these recoils, which are from 1 - 4 mm. long. These lengths can be determined quite readily from microscope measurements.

3 (a) Accuracy of Recoil Measurements.

The accuracy of these measurements was investigated by measuring the lengths of the recoils associated with the protons which stop in the chamber. These measurements were made for recoils of collinear and unclassified flags of length greater than 1 cm. Since these tracks are either known or believed to be collinear, the recoil length was obtained from the lengths of the recoil and fragment images on the film and the fragment length measured by reprojection. Measurements were made on all three films and a mean taken, this being weighted according to the quality of the recoil track. The measurements on the film from the top camera generally had more weight than those from the side cameras.

These results are shown in Fig. 4.3 where these lengths are plotted as crosses. The abscissa in this plot is the recoil range calculated from the fragment range assuming this to be a proton. The necessary range-energy relationship for C^{13} was taken from a review of experimental range-velocity relations made by Mr. D.R.O. Morrison (Ph.D. Thesis - University of Glasgow). Practically all of the points group closely about

the (γ,p) line and the accuracy of the recoil range measurements can be estimated from their spread. For the 1.64 and 2.89 Mev groups the root mean square deviations are 26% and 16% respectively. Since the expected range straggling is about 15% the error introduced by the cloud chamber is less than 0.2 mm., which is comparable with or less than the unavoidable limitation imposed by straggling.

Since the range of a collinear flag recoil leads to a value of the fragment momentum this technique provides the same information as is obtained from measurements of magnetic curvature but has the advantage that a measurement can be made on practically all tracks whereas curvature measurements can only be made on long tracks. The error in momentum due to range straggling of the recoil is comparable with the error in the curvature measurements arising from multiple scattering. (For a magnetic field of 5,000 gauss and a chamber filled with one atmosphere of nitrogen, the error in curvature for a 5 Mev proton - measured over a track length of 10 cm. - is approximately 15%).

In Fig. 4.3 a few (five) points are observed well off the expected (γ,p) line. These can only be (γ,d) events or (γ,pn) events where the neutron has been emitted in approximately the same direction as the proton. For comparison, the recoil ranges of some non-collinear (γ,pn) events which fall just outside the criterion for collinear flags are shown on the figure as circles. Since the distribution of these ranges completely overlaps the distribution of the five collinear recoils in question, it is clear that these latter cannot be definitely identified

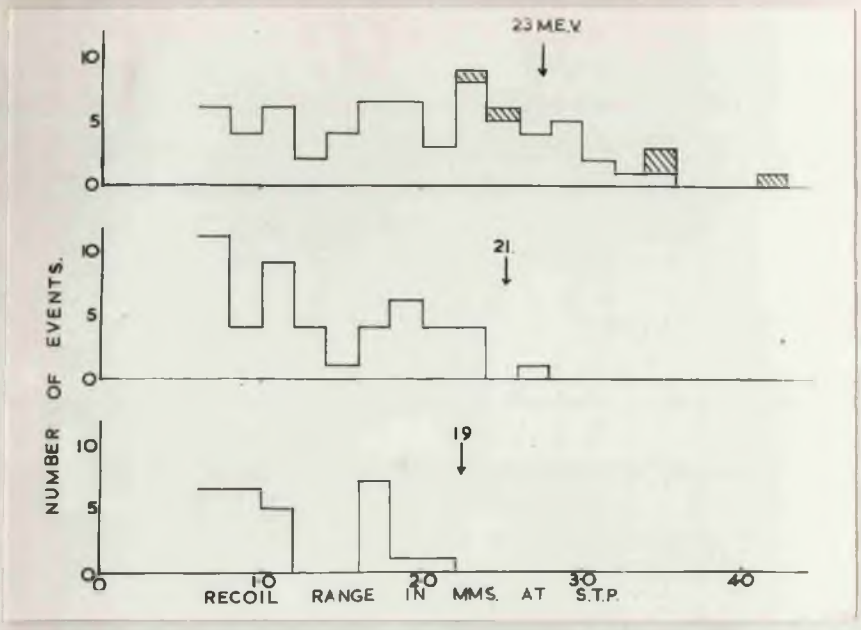

Fig. 4.4

The range distribution of collinear flag recoils for the 19, 21 and 23 Mev runs. The shaded events are (γ,α) disintegrations.

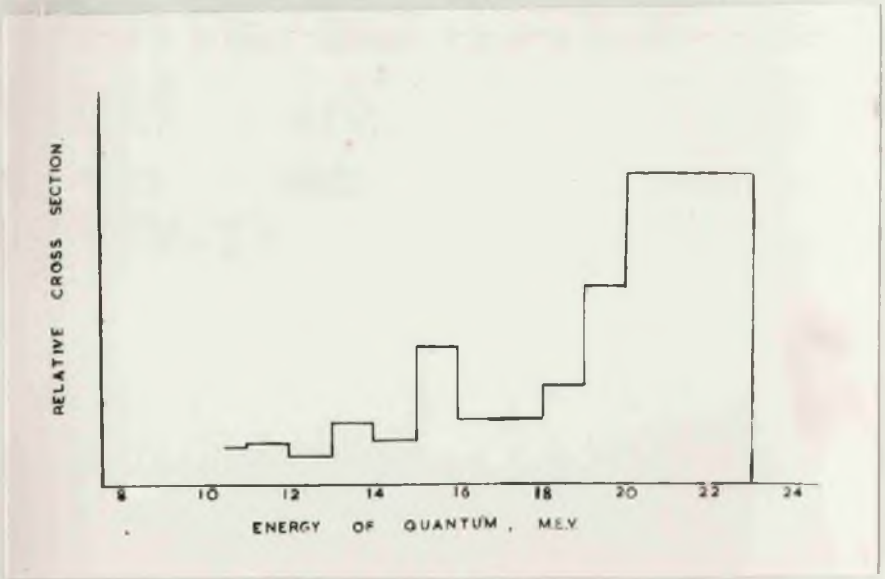

Fig. 4.5

The (γ,p) "cross section" calculated from the 23 Mev recoil range distribution assuming that all the protons leave the residual C^{13} nucleus in its ground state. The true (γ,p) cross section is expected to rise as steeply as or more steeply than this "cross section". (See text § 3 (b)).

and that the comparison of recoil and fragment ranges is an unsatisfactory method of identifying (γ,d) events when (γ,pn) events are also present.

3 (b) Recoil Range Measurements.

The accuracy of recoil range measurements and of the range-velocity data has been demonstrated for tracks which stop in the chamber. These events were of low energy and had short recoils. Recoils from protons of energy greater than 3 Mev will be longer and therefore the measurements will be more accurate.

For collinear flags in which the fragment leaves the illuminated region the fragment direction can be measured by reprojection and this gives the recoil direction. The recoil range can then be calculated from the microscope measurement of the projected recoil image. These measurements were only made on the film from the top camera as the geometrical calculations are extremely lengthy for the other films. The data for $(E_\gamma)_{max}$ = 23 Mev were obtained from half the films since the fragment directions were not measured for the remainder. In order to avoid the errors inherent in measuring steeply inclined tracks only those within 45° of the horizontal were considered - this excluded 29% of the tracks (assuming an isotropic distribution). If unclassified flags are assumed to be collinear their recoil ranges correspond to protons of energy less than 3 Mev so that only collinear flags need be considered here.

The recoil range distribution for the three peak synchrotron energies is shown in Fig. 4.4. For the purposes of comparison the recoil ranges have been corrected to the values they would have if emitted at

90° to the Y-ray direction. The ranges of recoils from (Y,α) events have been shaded. It can be seen that approximately equal numbers of events occur in all range intervals. For a synchrotron spectrum the number of quanta decreases with increasing energy. Hence the (Y,p) cross section must rise as the energy increases.

In order to deduce the (Y,p) cross section from the above measurements it is necessary to know the number of protons leaving C^{13} in an excited state and this information is not at present available. If it is assumed that in all cases the C^{13} nucleus is left in the ground state, then the 'cross section', deduced from the data for the 23 Mev run, is shown in Fig. 4.5. If the residual C^{13} nucleus is left in an excited state, the apparent value of E_Y calculated from the recoil range will be too low. The true E_Y will be higher by between 3 Mev (the lowest excited state of C^{13}) and 6 Mev (above which neutron emission produces non-collinear flags). It follows that the true (Y,p) cross section rises as steeply as or more steeply than the 'cross section' shown in Fig. 4.5.

A possible source of error is the presence of (Y,d) events which would tend to have longer recoils than (Y,p) events and therefore produce an artificial rise in the (Y,p) cross section near the peak energy. No experimental evidence is available for or against the presence of (Y,d) events, but, on theoretical grounds (Ge 53), their number is expected to be very small.

3 (c) (Y,α) Events.

(Y,α) events which stop in the chamber can be identified since

Table 4.3

Relative Numbers of Events for the Various Reactions at the Three Peak Synchrotron Energies

Reaction	19 Mev	21 Mev	23 Mev
(γ,p)	13	32	127
(These totals include only those (γ,p) events with E_γ greater than the (γ,n) threshold)			
(γ,pn) Probable	4	22	132
Upper Limit (see text)	(13)	(27)	(147)
(γ,α)	0	0	5 + ?3
$(\gamma,star)$	0	0	8
(γ,n) (Calc.)*	8 ± 2	23 ± 5	75
No. of r at 1 metre	0.014	0.024	0.050
No. of photos	304	265	333

*Note. The errors indicated in the number of (γ,n) disintegrations for the 19 and 21 Mev runs represent only the errors in the relative numbers at the 3 energies and arise from uncertainties in the synchrotron energy scale and in the monitoring arrangements. The absolute number of (γ,n) disintegrations may differ from these figs. by a further ± 20%.

for a given fragment range the recoil from a (γ,α) reaction will be at least three times as long as those from other reactions producing collinear flags. Suspected (γ,α) events were analysed by comparing the measured recoil length with that calculated from the range, the maximum difference being 15% of the calculated range, which is consistent with range straggling. The 'appearance' of each of these tracks (i.e. ionization, multiple scattering and ionization change at the origin) was consistent with the fragment being an alpha. This gave five (γ,α) events. (γ,α) events in which the fragment leaves the chamber or in which the density change is too small to be detected visually will not have been included above. From the recoil range distribution (Fig. 4.4 on p. 91a) it can be seen that there are no collinear events with longer recoils than the highest energy (γ,α) event, which has a fragment length of 2-1/2 cm. The probability of a track of this length leaving the chamber is less than 20% so that it is very unlikely that any (γ,α) event will have been missed because its fragment does not stop in the chamber. Since the difference in density between the alpha and the B^{10} recoil track was not always very marked the 16 singles of appropriate range were carefully re-examined. The majority of these singles looked like protons (from track density and multiple scattering), there being only three of them which resemble alphas, so that we may take eight as an upper limit to the number of (γ,α) events.

4. THE RELATIVE PROBABILITIES OF THE VARIOUS REACTIONS

The relative numbers of events from the different reactions are listed in Table 4.3. In order to facilitate comparison with the (γ,n)

reaction only (γ,p) events which occur at energies above the (γ,n) threshold (10.54 Mev) have been included. The number of such events was obtained from the measured recoil lengths of collinear flags. It was assumed that the number of (γ,d) events is negligible.

The numbers of (γ,pn) events have been taken as equal to the numbers of non-collinear flags. Since they do not include any allowance for the possibility that some of the unclassified flags may be (γ,pn) events these numbers represent lower limits to the numbers of such events. However it is believed that they are also the best estimates available since it is thought that the unclassified flags are all (γ,p) events with short recoils. All the unclassified flags had recoil lengths less than that corresponding to a 3 Mev proton and this enabled the reasonableness of the above assumption to be tested in the following way. The expected number of protons of energy less than 3 Mev which leave the chamber before stopping was calculated from the known proton spectrum up to 3 Mev and the probability that a proton of a particular energy will leave the chamber. This estimate was then compared with the total of unclassified flags and collinear flags with short recoils which leave the chamber. The estimated number was 58 $\pm$ 15 and the observed number 73. Thus the assumption is perfectly reasonable but the possibility that some of the unclassified flags may be (γ,pn) events cannot be ruled out. These considerations show that an upper limit of 30 may be given to the total number of such events for the three X-ray energies. The upper limits derived on this basis are given in brackets in Table 4.3. It should be noted that the number of

unclassified flags added to the 19 Mev total is probably abnormally high due to one of the films being of somewhat poorer quality.

The number of (γ,n) events was calculated from the induced activity measurements of the Saskatchewan group (Ho 52).

It can be seen that the number of (γ,p) events increases with increasing X-ray energy as rapidly as the number of (γ,n) events and that the number of (γ,pn) events increases rather more rapidly. Thus both the (γ,p) and (γ,pn) cross sections must have an energy dependence which is similar to that of the (γ,n) cross section (Ho 52), i.e. they will be small at low energies and rise rapidly about 20 Mev. The (γ,α) and (γ,star) cross sections are an order of magnitude lower but have a similar energy dependence. Using the usual techniques of momentum balance four of the eight star events were identified as (γ,αp) events and three as (γ,$\alpha\alpha$) events, while one was too steeply inclined to permit accurate measurements. Thus the (γ,α), (γ,αp) and (γ,$\alpha\alpha$) cross sections are all about $1 - 2 \times 10^{-28} cm^2$.

5. NOTES ON THE IDENTIFICATION OF (γ,n) DISINTEGRATIONS LEAVING N^{13} IN PARTICULAR STATES

The purpose of this section is to point out that an analysis of the (γ,pn) events should provide a measurement of the numbers of (γ,n) disintegrations leaving N^{13} in a number of its low lying levels and to report upper limits deduced from the present experiment for the numbers of (γ,n) disintegrations leaving N^{13} in the 2.36,(3.51 and 3.56) and 6.91 Mev levels.

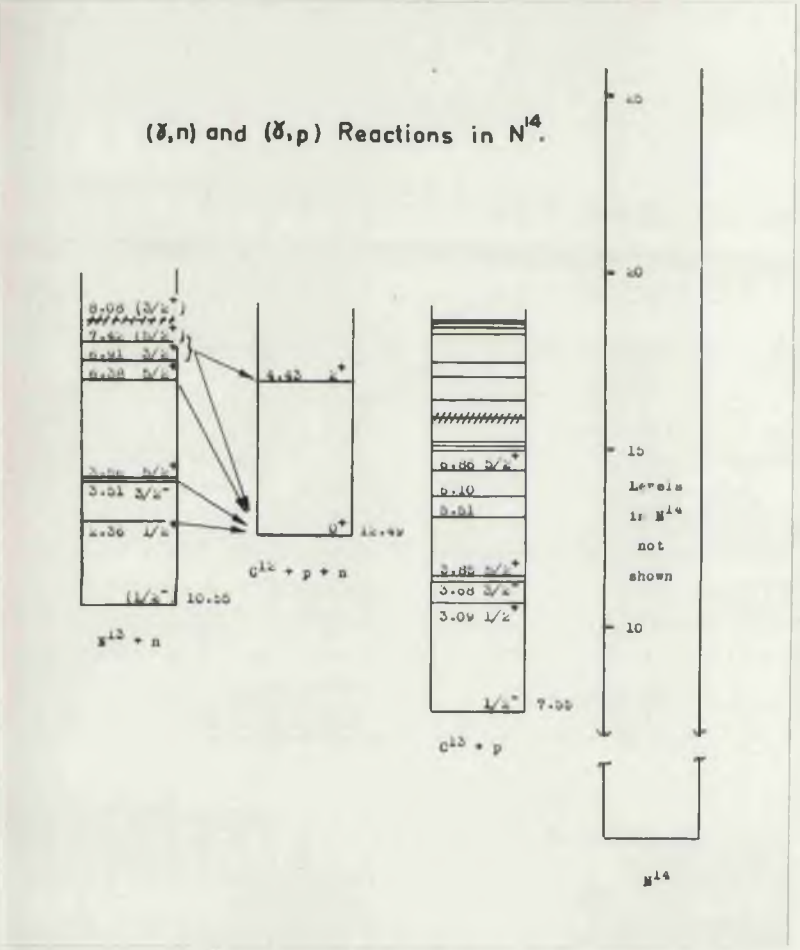

Fig. 4.6

Energy level diagram for the (γ,p) and (γ,n) reactions in N^{14}. The level data is taken from Ajzenberg-Selove and Lauritsen (Aj 59).

Table 4.4

Properties of N^{13} Excited States

Energy of N^{13} Level	E_p(c.m.)[1]		$\frac{\Gamma_{p_1}}{\Gamma_{p_0}+\Gamma_{p_1}}$	Level Width	Expected Width of Proton Peak
	C^{12} gnd. state	C^{12} 4.43 Mev			
Mev	Mev	Mev		kev	kev
2.36	0.37	-	-	32	90
3.51	1.45	-	-	63	110
3.56	1.50	-	-	61	110
6.38	4.10	(0.01)	-	-	-
6.91	4.59	0.50	0.55[2]	115	140
7.42	5.06	0.97	Prob.[3] appreciable	$\simeq$ 85	$\simeq$ 120
(8.08)[4]	(5.66)	(1.58)	Prob.[5] small	($\sim$ 350)	

Notes

(1) i.e. proton energy in the N^{13} coordinate system.

(2) See (Re 56a).

(3) Since the $C^{12}(p,p'\gamma)$ cross section has a large resonance at the energy corresponding to the 7.42 Mev level, (Br 56) and others.

(4) Unconfirmed level.

(5) Since the $C^{12}(p,p'\gamma)$ cross section shows no indication of a resonance at the energy corresponding to 8.08 Mev excitation (Br 56).

The number of (γ,n) disintegrations leaving N^{13} in the ground state is given by the (γ,n) yield calculated from the measured N^{13} activity. This follows directly from the fact that the energy of the first excited state of N^{13} is greater than the energy required for dissociation into $C^{12} + p$ (see Fig. 4.6) so that in practically all cases in which N^{13} is left in an excited state the final product nucleus will be C^{12} and not N^{13}. The protons from excited states of N^{13} will have definite energies in the coordinate system of the N^{13} recoil. For (γ,pn) events in which the proton stops in the chamber the proton energy can be accurately determined from range measurements. Thus the (γ,pn) events arising from (γ,n) transitions to excited states in N^{13} will be identified as events giving sharp peaks in the distribution of proton energies corrected to the coordinate systems of the corresponding N^{13} recoils*. The expected energies of the proton peaks from all the known low lying levels of N^{13} are given in Table 4.4 (columns 2 and 3) for protons leaving C^{12} in the ground state and, where energetically possible, in the 4.43 Mev state. Range measurements under the conditions of the present experiment give the proton energy distribution up to 3 Mev and therefore it is expected that the following disintegrations could be identified - (γ,n) events leaving N^{13} in the 2.36, 3.51 and 3.56 Mev levels and those (γ,n) events leaving N^{13} in the 6.91, 7.42 and (8.08) Mev levels for which the N^{13} nucleus decays to the first excited state

*For convenience this distribution will be called the corrected proton energy distribution and is to be distinguished from the observed proton energy distribution, which is the distribution in the laboratory system.

Table 4.5

Energies and Ranges of Protons of Interest in Analysis of $N^{14}(\gamma,np)$ Events

Energy of N^{13} Level	E_p(c.m.)[1] of Interest	In Laboratory Coordinate System				
		E_p(min)	E_p(max)	L_p(min)	L_p(c.m.)[2]	L_p(max)
Mev	Mev	Mev	Mev	cm.	cm. (for 1.4 atmos. N_2)	cm. (for 1.4 atmos. N_2)
2.36	0.37	0.16	0.8	0.16	0.39	1.11
3.51) 3.56)	1.47	1.02	2.0	1.64	3.0	5.3
6.38	(4.10)	-	-	-	-	-
6.91	0.50	0.28	0.79	0.29	0.56	1.09
7.42	0.97	0.50	1.34	0.56	1.51	2.55

Notes

(1) i.e. proton energy in the N^{13} coordinate system.

(2) i.e. L_p for $E_p = E_p$(c.m.)

of C^{12}. The probability for decay to the first excited state of C^{12} is known to be appreciable for the 6.91 and 7.42 levels and is probably small for the broad unconfirmed level at 8.08 Mev (see values of $\Gamma_{p_1}/(\Gamma_{p_0}+\Gamma_{p_1})$ in Table 4.4). The 8.08 Mev level is therefore not included in the subsequent discussion especially as the modifications required if it proves to be important are self evident.

It should be noted that because of the large momenta of the N^{13} recoils there are no significant peaks in the observed energy distribution (i.e., in the laboratory coordinate system) of protons from (γ,np) events. The expected spread of proton energy and range for the peaks of interest is given in Table 4.5.

The expected widths of the peaks in the corrected proton energy distribution can be calculated using the results of the present experiments. The factors contributing to the width of the peaks are

(a) the width of the level in N^{13}

(b) the error in the range measurement of proton energy

(c) the error in the correction to the coordinate system of the N^{13} recoil due to errors in the measurement of the C^{12} recoil.

The expected errors in E_p (widths of peak at half height) due to (b) and (c) are 30 kev and 80 kev* respectively. The N^{13} level widths and the expected widths of the corresponding peaks in the

*This figure is derived from the observed momentum unbalance for stars in Neon (see Chapter V, §1(c) on p.124). This is a more appropriate estimate of the errors in measuring longer recoils than the data from collinear flags in nitrogen.

corrected proton energy distribution are given in Table 4.4. These figures show that the proton groups corresponding to the following three sets of levels should be easily separated - 2.36, 6.91 Mev; 7.42 Mev and 3.51, 3.56 Mev. The last two levels are clearly too close to allow the corresponding events to be distinguished. However the proton groups corresponding to the 2.36 and 6.91 Mev levels will probably appear as two incompletely resolved peaks and it may be possible to make a satisfactory separation using the value of E_T $(= E_p + E_h + E_{C^{12}})$ to provide an additional criterion. Because of the giant resonance the mean values of the E_γ distributions are probably nearly the same for (γ,n) events leaving N^{13} in the 2.36 and 6.91 Mev levels and therefore the mean values of E_T should differ by approximately 4 Mev.

Of the 132 non collinear flags obtained in the 23 Mev run of the present experiment, 37 were events in which the proton stopped in the chamber. These events were not analysed in the manner indicated above since the camera arrangement used was not suitable for the determination of recoil lengths and directions*. However it was possible to obtain some useful preliminary results from a study of the proton ranges and the appearance of the tracks. Since this study was made at a time when the only excited states of N^{13} known were the 2.36, 3.51 and 3.56 Mev levels the initial discussion will be confined to these three levels.

*In principle the recoil lengths and directions could be deduced from microscope measurements of the images from two of the cameras. However for the present camera arrangement the necessary calculations were very involved (time required was hours per track) and therefore subject to error. A camera arrangement suitable for measuring recoil lengths and directions was introduced for the Neon experiment. (See Chapter V, §1(b), p.116).

Since the proton momentum is small the direction of motion of the N^{13} recoil will be very nearly that of the C^{12} recoil and therefore events of the type sought with $\phi_{Rp} \lesssim 90°$ will have $E_p \gtrsim E_p$ (c of m) respectively, i.e. for events which look like

	$E_p \sim E_p$ (c of m)	$E_p > E_p$ (c of m)	$E_p < E_p$ (c of m)
2.36 Mev level	$l_p \sim$ 0.4 cm.	$0.4 < l_p < 1.1$ cm.	$0.16 < l_p < 0.4$ cm.
3.51 and 3.56 Mev levels	$l_p \sim$ 3.0 cm.	$3.0 < l_p < 5.3$ cm.	$1.6 < l_p < 3.0$ cm.

Using the two criteria of appearance and proton range the non-collinear flags for which the proton stopped in the chamber were classified into three groups depending on whether their identification as (γ,np) events proceeding via one of the above three levels in N^{13} was

(a) probable or possible

(b) doubtful to very doubtful

(c) not possible.

The number of tracks in group (a) gives an "estimate" of the number of (γ,n) disintegrations leaving N^{13} in one of these levels which is expected to be high rather than low, possibly by a considerable factor. Limiting the analysis to the 23 Mev irradiation and correcting for the fraction of protons which do not stop in the chamber this gives 5 and 22 for the number of (γ,n) disintegrations leaving N^{13} in the 2.36 Mev and (3.51 and 3.56 Mev) levels respectively. The number of (γ,n) disintegrations leaving N^{13} in the ground state is given by the (γ,n)

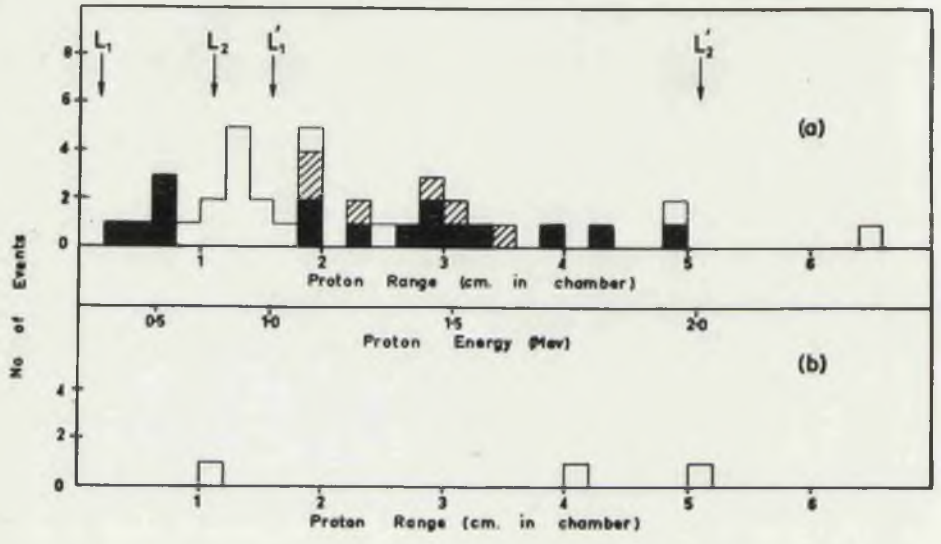

Fig. 4.7

(a) Proton range distribution for (γ,pn) events, from the 23 Mev run, with origins in the X-ray beam. Events whose identification as (γ,n) disintegrations leaving N^{13} in the 2.36, 3.51 and 3.56 Mev levels is probable or possible are indicated by solid rectangles, those for which this identification is doubtful to very doubtful by shaded rectangles and those for which this identification is not possible by open rectangles. (L_1, L_2) and (L_1', L_2') are the (min., max.) ranges in the chamber for protons from the 2.36 Mev and (3.51 Mev + 3.56 Mev) levels in N^{13}.

(b) Corresponding distribution for non-collinear flags with origins outside the X-ray beam.

yield calculated from the measurement of the N^{13} activity and is 75.

The range distribution of protons for the above three groups is given in Fig. 4.7 which also contains the range distribution for protons from non-collinear flags with origins outside the X-ray beam. The latter distribution shows that the background from $N^{14}(n,p)$ events is negligible. Fig. 4.7 (a) shows that there are a number of events which either cannot be or are most probably not (γ,n) disintegrations to the above levels. With the information now available on the expected proton peaks it is natural to interpret the group (c) events with ranges between 1 and 2 cm. as (γ,n) events leaving N^{13} in the 7.42 Mev level. Since only a fraction of these (γ,n) disintegrations are observed this would imply that the total number of (γ,n) disintegrations leaving N^{13} in the 7.42 Mev level could be quite appreciable. However it should be noted that the (γ,pn) events were not re-examined in the light of the higher levels of N^{13} and no allowance has been made for the possibility that some of the (γ,pn) events may be (γ,p) events leaving C^{13} in highly excited states. Hence these suggestions are quite speculative and/are intended primarily as a stimulus for further investigation. A further consequence of the consideration of higher levels is that the five events above are more properly classified as probable or possible (γ,n) events leaving N^{13} in either the 2.36 Mev or 6.91 Mev levels. This gives upper limits of 5 (γ,n) disintegrations to the 2.36 Mev level (assuming that there are no (γ,n) disintegrations to the 6.91 Mev level) and 10 (γ,n) disintegrations to the 6.91 Mev level (assuming that there are no (γ,n) disintegrations to the 2.36 Mev level).

It is worth noting that a study of (γ,pn) events should also provide some information on the number (if any) of low energy photoprotons ($E_p \leq 2$ Mev) for (γ,p) disintegrations due to quanta in the giant resonance region. These disintegrations will appear as (γ,pn) events and hence events due to high energy quanta can be selected using the values of $E_p + E_n + E_{C^{12}}$. They can be distinguished from the (γ,n) events discussed above by the fact that they do not belong to the sharp peaks in the corrected proton energy distribution. This should be a sufficient identification since it is reasonable to assume that the simultaneous emission of a low energy photoproton and a high energy photoneutron is a much less likely process. Because of the expected finite width of the peaks in the corrected proton energy distribution it is probable that, in practice, it will only be possible to identify a fraction of these (γ,p) events, namely those with corrected proton energies in the range 0.65 - 0.85 Mev, 1.1 - 1.35 Mev and above 1.65 Mev. However, since corresponding photoproton energies can range from 0.3 Mev to the experimental upper limit (say 3 Mev) this should lead to a reasonable estimate of the number of photoprotons with energies less than 2 Mev*.

Since there is, at present, no information on photoproton

*It will be remembered that the corrected proton energy is calculated on the assumption that the event is a (γ,n) disintegration and is therefore a fictitious energy for these (γ,p) disintegrations. The photoproton energy is very nearly the proton energy in the laboratory system and hence the range of photoproton energies can be judged from the figures in Table 4.5. The fraction of (γ,p) events identified could be calculated from the distribution of θ_{pn} (the angle between proton and neutron).

spectra below 2 Mev it would be of value to get this information for one nucleus at least. Since all other techniques for detecting photoprotons are limited to energies greater than 2 Mev by background difficulties it seems clear that this information could only be obtained in a cloud chamber experiment similar to that proposed above.

6. DISCUSSION

We are now in a position to discuss all the photonuclear reactions in N^{14} up to an energy of 23 Mev, with the exception of the (γ,d) and (γ,γ) reactions. It is convenient to separate this energy range into two sections with the dividing line at the (γ,n) threshold (10.54 Mev). Neglecting γ-ray scattering, the (γ,p) process is the only reaction which can occur in the lower energy region where its cross section is known in very great detail. In the higher energy region a considerable number of photonuclear reactions can take place.

6(a) $N^{14}(\gamma,p)$ Cross Section between 7.5 and 10.5 Mev.

The range distribution of protons of energy up to 3 Mev (see Figs. 4.1 and 4.2) gives the (γ,p) cross section below 10.5 Mev with an energy resolution of approximately 50 kev. This is to be compared with the energy resolution of 1 Mev or more of previous methods of measuring photonuclear cross sections. The results show that this cross section consists of a series of well defined resonances and provide a convincing demonstration of level structure in photonuclear cross sections. The occurrence of such level structure had been suggested by Goward and Wilkins (Go 53), Titterton and Brinkley (Ti 53) and Katz et al. (Ka 54) from results using methods of moderate energy

resolution and, in the present case, would be anticipated from an application of the principle of detailed balancing to the measurements on the $C^{13}(p,\gamma)$ reaction. The present results confirm the predictions of the principle of detailed balancing in respect of both the shape and magnitude of the (γ,p) cross section and therefore show that the measurement of (p,γ) cross sections is a powerful method of studying, in detail, the characteristics of photonuclear cross sections.

Prior to this result the only experimental information on the validity of the principle of detailed balancing was provided by a comparison of Fuller's measurement of the $He^4(\gamma,p)$ cross section (Fu 54) with the best measurement of the $H^3(p,\gamma)$ cross section (Pe 55). Both these results were published when the nitrogen experiment was nearing completion. In the energy region common to both measurements (E_γ = 20 - 25 Mev) Fuller's cross section rises in a similar, though not identical, manner to the $He^4(\gamma,p)$ cross section deduced from the $H^3(p,\gamma)$ cross section. Fuller's integrated cross section is approximately 80% of the integrated cross section deduced from the $H^3(p,\gamma)$ measurement. As Fuller points out (see Pe 55) these differences are well within the errors in the $He^4(\gamma,p)$ measurement which are expected to be rather large below 26 Mev. The confirmation of the principle of detailed balancing is thus less complete than that provided by the comparison of the $N^{14}(\gamma,p)$ and $C^{13}(p,\gamma)$ measurements.

Independent confirmation of the correspondence between the $N^{14}(\gamma,p)$ and $C^{13}(p,\gamma)$ reactions has been provided by subsequent experiments in which the cross sections at the 8.06 and 9.17 Mev resonances in the $N^{14}(\gamma,p)$ reaction have been measured using the radiation from the corresponding resonance in the $C^{13}(p,\gamma)$ reaction.

Griffiths (Gr 58) used the γ-rays from the 554 kev $C^{13}(p,\gamma)$ resonance (E_γ = 8.06 Mev) and detected the photoprotons produced in a nitrogen filled proportional counter. He obtains a value of 10.5 ± 0.6 ev for Γ_γ (which is proportional to $\sigma_{int}(\gamma,p)$ for the resonance). The value of Γ_γ obtained from $\sigma_{int}\{C^{13}(p,\gamma)\}$ is 10.2 ev (Se 52, Wo 53). Hanna and Meyer-Schützmeister (Ha 59) determined the cross section for $N^{14}(\gamma,p)$ at the 9.17 Mev resonance by measuring the absorption in liquid nitrogen of the γ-rays from the 1.75 Mev resonance in $C^{13}(p,\gamma)$. From this cross section and the principle of detailed balancing they calculate the expected yield of γ-rays from the 1.75 Mev resonance in the $C^{13}(p,\gamma)$ reaction and obtain a value of $(7.7 \pm 1.5) \times 10^{-9}$ ground state γ-rays/proton. This is to be compared with the directly measured value of $(7.4 \pm 3) \times 10^{-9}$ ground state γ-rays/proton obtained in the same experiment and the value of 10.4×10^{-9} ground state γ-rays/proton from earlier experimental measurements (Se 52, Wo 53).

Further evidence on the validity of the principle of detailed balancing in photonuclear reactions has been provided by Mann and Titterton's measurement of the $C^{12}(\gamma,p)$ cross section for monochromatic 17.6 Mev radiation (Ma 56). Their value of $(1.19 \pm 0.21) \times 10^{-27}$ cm^2 is in agreement with the cross section deduced from the measurements on the $B^{11}(p,\gamma)$ reaction (Hu 53, Go 55b) which is $(1.09 \pm 0.16) \times 10^{-27}$ cm^2.

Blatt and Weisskopf (Bl 52, p. 651) have suggested that an energy dependence of the total photonuclear cross section such as is obtained for N^{14} (see Fig. 4.8) might be due to a change in the character of the radiation absorbed above 15 Mev. They postulated that

only electric quadrupole and magnetic dipole absorption were effective below 15 Mev and that the sharp rise above this was due to the onset of electric dipole absorption. It is known that the greater part of the absorption in the giant resonance region must be electric dipole (Le 50). It is therefore of interest to note that in the energy region where this process has been studied in detail, i.e. from 7.5 - 10.5 Mev, a large proportion of the absorption is by electric dipole transitions. The spins and parities of the levels in N^{14} corresponding to the observed proton groups are as follows 1^-, 0^-, $(2^+$ or $1^+)$ and 2^+ (Ka 60) (Aj 59). The ground state of N^{14} is 1^+. Hence for two out of the four levels the transitions involved are electric dipole. This is in conflict with the above hypothesis and suggests that the giant resonance is due to a change in the probability of absorption rather than to a change in the character of the radiation absorbed.

6(b) Photonuclear Reactions in N^{14} above 10.5 Mev.

It has been shown that the cross sections for both the (γ,p) and (γ,pn) reactions in N^{14} have an energy dependence similar to that of the (γ,n) cross section, i.e, they are small below 15 Mev and large in the neighbourhood of 20 Mev. The cross sections of all other reactions are an order of magnitude smaller. The rise in the (γ,pn) cross section had also been established by the work of Ferguson et al. (Fe 54) who measured the sum of the (γ,n) and (γ,pn) cross sections by observing the total yield of neutrons from N^{14}. The (γ,pn) cross section, obtained by subtraction, resembled in shape the (γ,n) cross section obtained from measurements of the C^{13} activity and was about three times

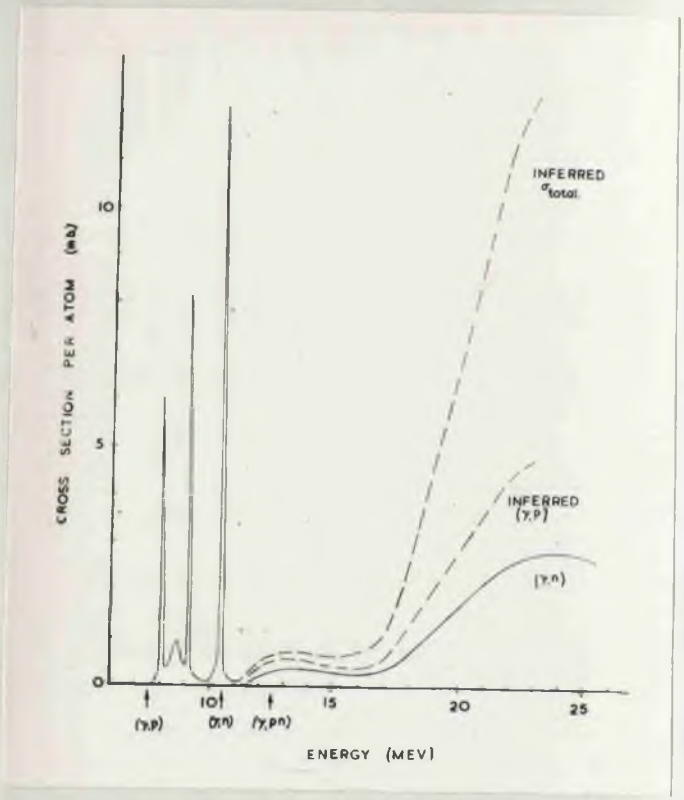

Fig. 4.8

Measured and inferred photonuclear cross sections in N^{14}. For fuller description see text (§ 6(b) p.106). For clarity the width of the narrow resonances below 10.5 Mev have been increased, but the integrated cross section remains correct.

Note - The techniques used to obtain the cross sections above 10.5 Mev were incapable of resolving levels such as those observed below this energy.

as large. Thus the cross sections of all the principal reactions in N^{14} reflect a pronounced increase in the nuclear photon absorption cross section in the vicinity of 20 Mev. This is shown in Fig. 4.8 which illustrates the characteristics of these cross sections but does not necessarily represent their exact values. This figure shows the (γ,p) cross section between 7.5 and 10.5 Mev together with the (γ,n) cross section as measured by the radioactive product technique (Ho 52). Since it has been shown that, above 10.5 Mev, the (γ,p) cross section has the same general features as the (γ,n) cross section, it is reasonable to suppose that it is a constant multiple of the (γ,n) cross section. Also, since the (γ,α) and the (γ,star) reactions have very small cross sections, the total cross section will be given by the sum of the (γ,n), (γ,p) and (γ,pn) cross sections. The (γ,pn) cross section was deduced in a manner similar to that used for the (γ,p) reaction except that, in accordance with the results discussed in § 4, the ratio of the (γ,pn) to the (γ,n) cross section was taken to increase somewhat with increasing photon energy.

As was pointed out in § 5, N^{14}(γ,n) disintegrations leaving N^{13} in low lying excited states give (γ,np) events from which it is possible to determine both the N^{13} level involved and the energy of the γ-ray producing the disintegration. A repeat experiment to measure these events would be of considerable importance. Although there are as yet no detailed theoretical calculations with which to compare the results of such an experiment it is anticipated that they would provide a significant test between the direct ejection and the compound nucleus

pictures of photodisintegration.

The following preliminary conclusions can be drawn from the data provided by the present experiment. The figures used in the following discussion are from the 23 Mev run for which most of the disintegrations will be caused by quanta in the giant resonance region and therefore the initial photon absorption will be by electric dipole transitions.

Firstly it is clear that a large fraction of $N^{14}(\gamma,n)$ and (γ,p) disintegrations leave the residual nucleus in the ground state. This is most easily seen if it is assumed that

(i) all (γ,pn) events are (γ,p) or (γ,n) disintegrations leaving the residual nucleus in highly excited states which subsequently decay by the emission of neutrons or protons respectively

(ii) half the (γ,pn) events are (γ,p) disintegrations and half (γ,n) disintegrations.

Then from the numbers of events in Table 4.3 it follows that the proportion of (γ,p) disintegrations leaving C^{13} in the ground state or one of the first three excited states $= \frac{127}{127 + 66} \simeq \frac{2}{3}$, while the proportion of (γ,n) disintegrations leaving N^{13} in the ground state $= \frac{75}{75 + 66} \simeq \frac{1}{2}$. The results of § 5 show that the number of (γ,n) disintegrations leaving N^{13} in one of the first three excited states is $\lesssim$ 1/3rd the number of (γ,n) disintegrations leaving N^{13} in the ground state. Since C^{13} and N^{13} are mirror nuclei and the particle energies are much greater than the barrier heights the corresponding ratio for (γ,p) disintegrations is expected to be very similar. Hence the

proportion of (γ,p) disintegrations leaving C^{13} in the ground state is also $\sim \frac{1}{2}$. While the figures given for the proportion of (γ,n) and (γ,p) disintegrations leaving the residual nuclei in the ground state will be influenced by the validity of assumptions (i) and (ii) the general conclusion that these disintegrations are dominant is clearly independent of these assumptions.

Also the upper limits to the number of (γ,n) disintegrations leaving N^{13} in the 2.36, (3.51 and 3.56) Mev levels (see § 5) indicate that the number of (γ,p) disintegrations leaving C^{13} in the ground state or one of the first three excited states is most probably greater than the number of (γ,n) disintegrations leaving N^{13} in one of the corresponding states. Since the energy of the fourth excited state of C^{13} is greater than the neutron binding energy the total number of these (γ,p) disintegrations is given by the number of collinear flags (see Fig. 4.6)*. The total number of these (γ,n) disintegrations lies

*This discussion assumes that

(i) there are no undiscovered levels of C^{13} or N^{13} in the appropriate energy region. This seems very reasonable since this energy region has been searched by a number of different reactions (see Aj 59);

(ii) the number of (γ,pn) events for which the neutron energy is less than $^1/_2$ Mev is small and can be neglected. Because of the small neutron momentum an event of this type will have a recoil direction falling within the acceptable range for collinear flags. Events of this type would be produced by low energy (γ,n) disintegrations leaving N^{13} in highly excited states but their number would have to be unreasonably large to significantly alter the number of collinear flags. (γ,p) disintegrations to a level in C^{13} just above the neutron binding energy appear to be very unlikely. The first well established higher level is 1.91 Mev above the neutron binding energy. Transitions to a recently reported level (Mo 58) at 5.51 Mev (0.56 Mev above C^{12} + n) would lead to some events being wrongly classified as collinear flags. However this level gave only a small group in the product spectrum for one reaction ($B^{11}(He^3,p)$) and did not give a detectable group for a number of other reactions. Hence if this level exists the probability for transitions to it is expected to be small.

between the (γ,n) yield calculated from the measurements of the induced N^{13} activity and the sum of this yield and the upper limit to the number of (γ,n) disintegrations leaving N^{13} in one of the first three excited states. Thus the ratio of (γ,p) disintegrations to (γ,n) disintegrations lies between 1.25 and 1.7. The experimental error in these limits is ± 25%. Barker and Mann (Ba 57) have pointed out that a difference of this magnitude in the yields of corresponding (γ,p) and (γ,n) disintegrations of a self conjugate nucleus is an expected consequence of the isotopic spin impurity in the excited states. They noted that the, not very accurate, experimental values of the $C^{12}(\gamma,p)$ and (γ,n) cross sections were in the ratio of 2:1 and that this ratio could be fitted with a reasonable isotopic spin impurity. The result reported here provides further evidence for a real difference in the two yields.

Chapter V

THE (γ,α), $(\gamma,2\alpha)$ AND $(\gamma,\alpha p)$ REACTIONS IN Ne^{20}

As was pointed out in Chapter I the star producing reactions are of particular interest since they can be expected to provide information about the mechanism of photonuclear reactions which is not obtainable from studies of other reactions. To date a number of star producing reactions have been studied with nuclear emulsions. Star events have been observed with the cloud chamber but not studied in detail. A feature of the star producing reactions most extensively studied, $C^{12}(\gamma,3\alpha)$ and $O^{16}(\gamma,4\alpha)$, is that their cross sections are small in the vicinity of the giant resonance and hence they give little information about the reaction mechanism in this important energy region. As is shown below there are good reasons for expecting that the reactions $Ne^{20}(\gamma,2\alpha)$ and $Ne^{20}(\gamma,\alpha p)$ will have appreciable cross sections in the vicinity of the giant resonance (at approximately 21.5 Mev for Ne^{20}). Hence a study of these reactions (which can only be made using the cloud chamber technique) would be of considerable value and would also provide a further test of the potentialities of the cloud chamber in photonuclear studies. In this connection it is of interest to note that star producing reactions make good use of the strong points of the cloud chamber technique. As the nitrogen experiment showed, the cloud chamber gives very accurate results providing the energies of the product particles are small enough to be determined from range measurements. For (γ,p) reactions the energy region which can be studied in this way is limited to the first few

Mev above threshold. For star producing reactions accurate results can be obtained over a much larger energy region since the available energy is shared between a number of particles and, in general, at least one of these is an α particle.

The reasons for expecting the $Ne^{20}(\gamma,2\alpha)$ and $Ne^{20}(\gamma,\alpha p)$ reactions to have an appreciable cross section are as follows. Firstly the thresholds for these reactions (11.90 Mev and 16.86 Mev respectively) are particularly low, while the (γ,p) and (γ,n) thresholds are high. Hence, from the standpoint of the energy available, the $(\gamma,2\alpha)$ and $(\gamma,\alpha p)$ reactions are expected to compete favourably with these latter reactions in the energy region near 20 Mev. Other factors affecting the cross sections can be assessed by considering the various ways in which these reactions could take place. In principle these are the simultaneous emission of the two particles concerned and the following two stage reactions.

$$Ne^{20} + \gamma \longrightarrow \alpha + O^{16*} \longrightarrow \alpha + \alpha + C^{12} \qquad (1a)$$

$$Ne^{20} + \gamma \longrightarrow \alpha + O^{16*} \longrightarrow \alpha + p + N^{15} \qquad (1b)$$

$$Ne^{20} + \gamma \longrightarrow p + F^{19*} \longrightarrow p + \alpha + N^{15} \qquad (2)$$

i.e. Reactions (1a) and (1b) are special cases of the (γ,α) reaction and reaction (2) is a special case of the (γ,p) reaction. The measurements on the $C^{12}(\gamma,3\alpha)$ reaction have shown that for C^{12} the simultaneous emission of two α particles is improbable. Hence, in the following discussion, only contributions from the two stage

reactions are considered. Any error in this assumption can only lead to an underestimate of the cross section.

Reaction (2) will be considered first. Since the α particle binding energy in F^{19} is 4.0 Mev, (γ,p) disintegrations leaving F^{19} in an excited state of energy greater than ~ 4.5 Mev will generally lead to (γ,pα) disintegrations. For E_γ greater than ~ 18 Mev such disintegrations are expected to form an appreciable and increasing fraction of the total (γ,p) cross section. (γ,p) disintegrations leaving F^{19} in an excited state of energy greater than 8 Mev will lead to both (γ,pα) and (γ,2p) disintegrations. For $E_{\gamma\ max.}$ = 23 Mev such (γ,p) disintegrations should be a very small fraction of the total number.

The (γ,α) reactions in Ne^{20} are analogous to the (γ,α) reactions in C^{12} and O^{16} whose general features are in good agreement with the predictions of the isotopic spin selection rules (Ge 53) (see Chapter I, p. 40). For the α particle nuclei (i.e. N = Z - even number), these rules predict that, for the energy region in which proton and neutron emission is possible, the (γ,α) cross section will be appreciable only if the emission of an α particle leaves the residual nucleus in a T = 1 state. The first T = 1 level of O^{16} is expected at 13.2 ± 0.7 Mev* which is greater than both the α particle and proton binding energies. Hence the "isotopic spin allowed" (γ,α) disintegrations will appear as either (γ,2α) or (γ,αp) stars (see

*This was the case at the time the neon experiment was planned. The first T = 1 level is now known to be at 12.78 Mev (Aj 59).

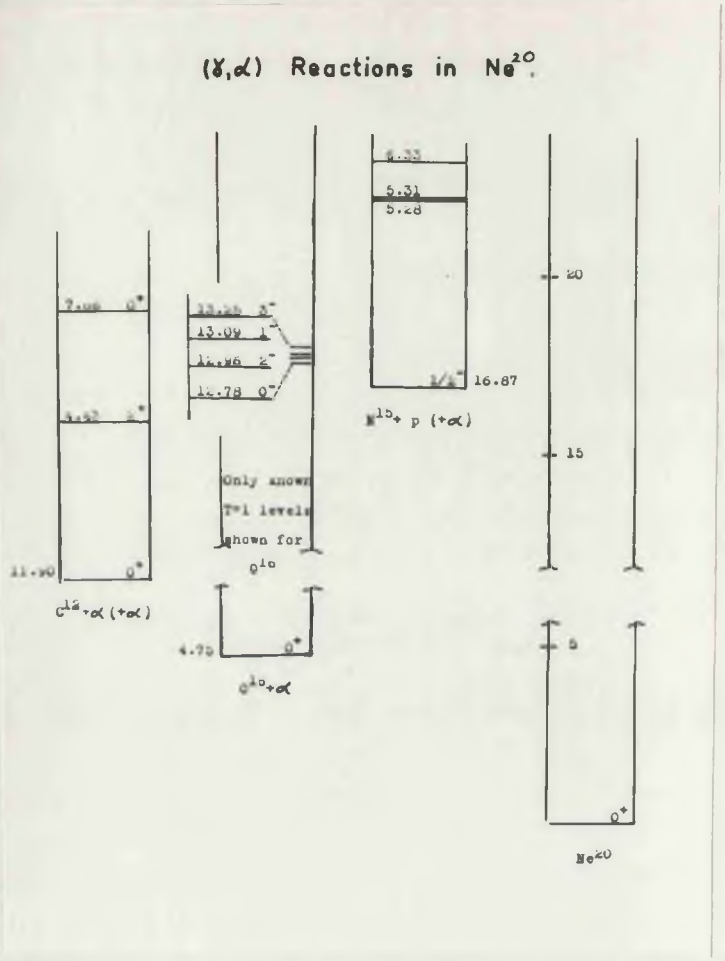

Fig. 5.1

Energy level diagram for the (γ,α) reactions in Ne^{20}. The level data is taken from Ajzenberg-Selove and Lauritsen (Aj 59).

Table 5.1

Characteristics of (γ,α) Reactions in α Particle Nuclei

Nucleus	Thresholds		Data for Residual Nucleus		
	(γ,α)	Allowed (γ,α) (approx.)	1st T = 1 level (Estimated Energy)	Binding Energies	
				α	p
	Mev	Mev	Mev	Mev	Mev
C^{12}	7.37	24.0	16.7	- 0.09	17.2
O^{16}	7.19	22.2	15.1	7.39	16.0
Ne^{20}	4.78	18.0	13.2	7.19	12.1
Mg^{24}	9.33	20.0	10.7	4.78	12.9
Si^{28}	10.00	19.5	9.5	9.33	11.7
S^{32}	6.94	16.2	9.3	10.00	11.6
A^{36}	6.6	14.0	7.4	6.94	8.9
Ca^{40}	7.2	13.7	6.5	6.6	8.5

Note - The figures in this table represent the data available at the time the Neon experiment was planned. The energies of the first T = 1 levels are derived from the masses of the isobaric nuclei and may be in error by a few tenths of an Mev.

Fig. 5.1). The threshold for the isotopic spin allowed (γ,α) reaction is 17.9 Mev (i.e. 13.2 + 4.7 Mev). Allowing for the effect of the coulomb barrier the cross section can be expected to be appreciable above 20 Mev (say) which is well within the giant resonance region.

It should be noted that in this respect Ne^{20} is unique among the lighter α particle nuclei. This can be seen from Table 5.1 which lists the thresholds for the (γ,α) reaction and the allowed (γ,α) reaction and data for the residual nuclei. For C^{12}, O^{16}, Mg^{24} and Si^{28} the energy at which the probability for α emission to a T = 1 state of the residual nucleus becomes significant (i.e. threshold plus allowance for the coulomb barrier), is above the energy of the giant resonance and hence the maximum cross section for the allowed (γ,α) reaction (appears as $(\gamma,2\alpha)$ reaction) will be less than that for Ne^{20} by an amount corresponding to the smaller nuclear photoabsorption at the higher energy. The remaining α particle nuclei seem unlikely to have large $(\gamma,2\alpha)$ and $(\gamma,\alpha p)$ cross sections*. Hence the cross sections for the $(\gamma,2\alpha)$ and $(\gamma,\alpha p)$ reactions in Ne^{20} are probably considerably larger than the corresponding cross sections in other α particle nuclei.

*The reasons for this are

(i) The lowest T = 1 levels of the residual nuclei have insufficient or only just sufficient energy to emit an α particle. This and the larger coulomb barrier make it most probable that transitions to these levels will appear as (γ,α) and not $(\gamma,2\alpha)$ disintegrations.

(ii) The larger coulomb barrier will also lead to a reduction in the probability of emission of the first α particle.

(iii) In any case it is by no means certain that the isotopic spin selection rules will channel all (γ,α) disintegrations to T = 1 levels since their effectiveness will be reduced by the increasing coulomb force.

It follows that these cross sections are probably considerably larger than the corresponding cross sections in any other nucleus. For nuclei other than the α particle nuclei either one or both of the (γ,n) and (γ,p) reactions will have a comparatively low threshold and hence competition from these reactions can be expected to result in a smaller cross section for the star producing reactions. Also for these nuclei there is no mechanism tending to make the (γ,α) reaction lead to highly excited states of the residual nucleus* and hence it is to be expected that only a small proportion of (γ,α) disintegrations will appear as star events.

An additional reason for studying the (γ,α), (γ,2α) and (γ,αp) reactions in Ne^{20} is that they provide a test of the isotopic spin selection rules in a nucleus for which any deviations due to the coulomb force will be greater than those for C^{12} and O^{16}.

A desirable feature of this experiment is that significant results can be obtained with only a few events and these results can be used to determine if it is worthwhile collecting more data to study the other results of interest. Only a few events are required to show if the (γ,2α) and (γ,αp) cross sections are large as expected and if the (γ,α), (γ,2α) and (γ,αp) cross sections have the general form predicted by the isotopic spin selection rules. Rather more

*For nuclei with $N \neq Z$ the isotopic spin selection rules do not restrict the states in which the residual nucleus may be left following α emission. For nuclei with $N = Z$ (equals an odd number in this case) the isotopic spin selection rules predict a strong preference for $T = 1$ states in the residual nucleus, but the first $T = 1$ state in these nuclei is at a low energy.

events are required to determine which levels of the intermediate nuclei (if any) are involved in the $(\gamma,2\alpha)$ and $(\gamma,\alpha p)$ reactions. If only one or two levels are involved then it may well be worthwhile collecting the number of events required to determine the angular distributions and hence the type of radiative transitions involved.

The experiment described in this chapter covers the first stage of this program. It shows that the $(\gamma,2\alpha)$ and $(\gamma,\alpha p)$ cross sections are indeed large and, in addition to the results of physical interest which are discussed later, it provides considerable information on the accuracy of star measurements in a cloud chamber.

1. NOTES ON EXPERIMENTAL METHOD

1 (a) Summary of Cloud Chamber Conditions.

The cloud chamber filling (with the chamber expanded) was 87 cm. neon (spectroscopically pure) + 1 cm. oxygen + water. The cloud chamber was fitted with a butyl rubber diaphram to reduce diffusion (the diffusion rate for air was 0.05 cm./day/atmosphere pressure difference) and therefore the gas composition did not change significantly during the 10 day period in which the photographs were taken. The stopping power of the gas was obtained from the range of the Po α particles and also from the pressure which was measured before and after the run. The two methods gave values of 0.72 and 0.727 respectively for the stopping power relative to air at S.T.P.

The electrostatic clearing field was turned off during the expansion. This produced very sharp recoil tracks but caused some reduction in contrast between the tracks of the reaction product and

recoil nucleus. As a result the origin of some (γ,α) events could not be clearly distinguished. The recoils from (γ,p) events were always clearly visible (see Plate 14).

Approximately 1000 photographs were taken at a peak X-ray energy of 23 Mev. The total X-ray dose was measured with an ionization chamber (see p. 59) which was calibrated by comparison with a Victoreen r meter placed at the centre of a perspex cylinder 8 cm. in outside diameter.

1 (b) Camera Arrangement for Microscope Measurement of Cloud Chamber Tracks.

The nitrogen experiment showed that valuable and reliable data could be obtained from the measurement of recoil tracks (1/3rd - 3 mm. long) provided the films were measured with a microscope. A limitation on the results was that, with the camera arrangement used, it was only practicable to use the microscope to measure the length of recoil tracks whose direction was known from the direction of the associated photoproton. The determination of both track length and direction from measurements of the images on the films involved calculations requiring hours per track. For the analysis of the star events expected in the Neon experiment it is essential to obtain both recoil lengths and directions from the microscope data. The modification to the camera arrangement described below enabled these to be determined in a straightforward and convenient way. A desirable additional feature was that the lengths and directions of longer tracks could be obtained using the set up for measurement by microscope

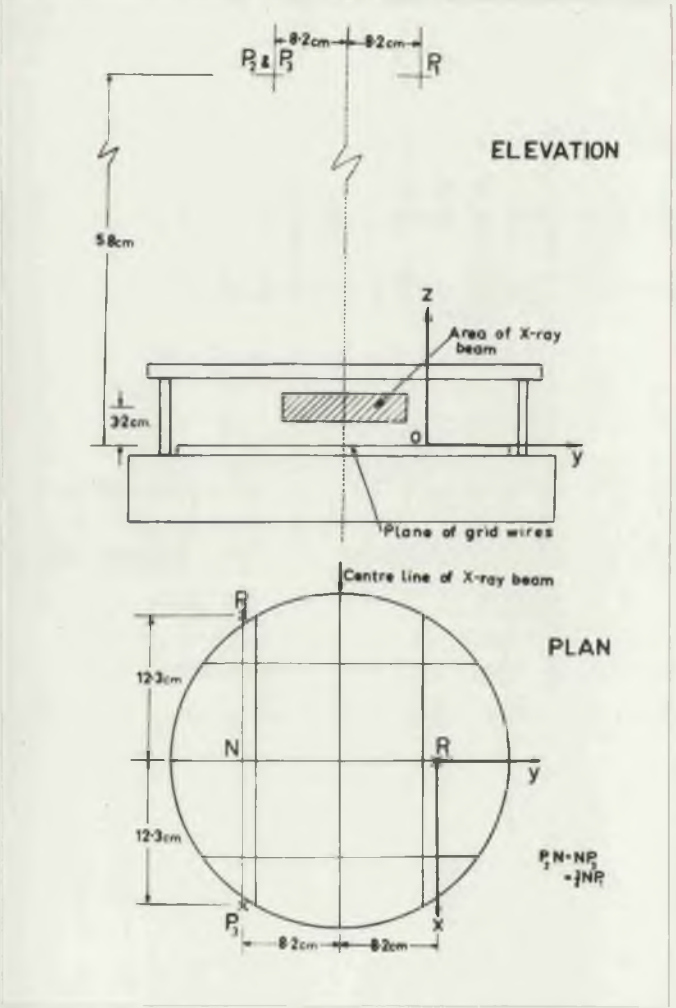

Fig. 5.2

Arrangement of the cloud chamber cameras for the Neon experiment. P_1, P_2 and P_3 are the principal points of the camera lenses. The rectangular axes (Ox, Oy, Oz) define the coordinate system used in the analysis.

with an accuracy as good as that obtained by reprojection and hence all the analysis could be completed in one operation. The time required for a track measurement was about the same as that required for a track measurement by reprojection.

The essential feature of the new arrangement is that, for all cameras, the lens axis is vertical and the film plane horizontal. The image on the film is then an exact reprojection of the (conical) projection of the track onto the (horizontal) plane of the grid wires built into the chamber. The formulae relating measurements on the films to positions in the chamber are then very simple while those giving directions and lengths of cloud chamber tracks are relatively simple.

The positions of the three cameras are indicated in Fig. 5.2 where P_1, P_2 and P_3 are the principal points of the three camera lenses. For all cameras the centre of the cloud chamber image was an appreciable distance off the lens axis and therefore it was expected that the effect of lens abberations would be correspondingly greater. Because of this the camera lenses were checked for distortion and it was found that, while they produced measureable barrel distortion at a distance from the axis, the errors were small and did not affect the accuracy of the measurements. The accuracy of the analysis was therefore determined by the quality of the track and, to some extent, by the characteristics of the microscopes used in the analysis. The maximum errors were

	Max. error
Position within chamber	
Horizontal coordinates	1/3 mm.
Vertical coordinates	1 mm.
Track direction (for proton or α particle tracks)	
Projected angle	1/3°
Vertical angle	1°
Track length (all tracks)	
Tracks shorter than 2-1/2 cm. (equivalent to diameter of microscope field of view)	0.1 mm.
Tracks longer than 2-1/2 cm.	0.5 mm.

This accuracy was quite adequate for the neon experiment but if it were necessary it could be improved by using better microscope equipment. A further description of this method of analysis is given in Appendix III which contains the formulae for analysing the measurements, the figures for the lens distortion and a discussion of the accuracy achieved and the ultimate accuracy of the method.

The only previously reported method for analysing cloud chamber tracks by microscope measurement of the camera films is that due to Blackett (Bl 22, Bl 23, Bl 25, described in Wi 51, p. 105-109). Blackett used an arrangement of two cameras whose film planes were each at an angle of 45° to the horizontal and at right angles to one another. In comparison with this the camera arrangement developed for the neon experiment has two advantages. Less time is required for the analysis since the equations used are simpler. Greater flexibility in

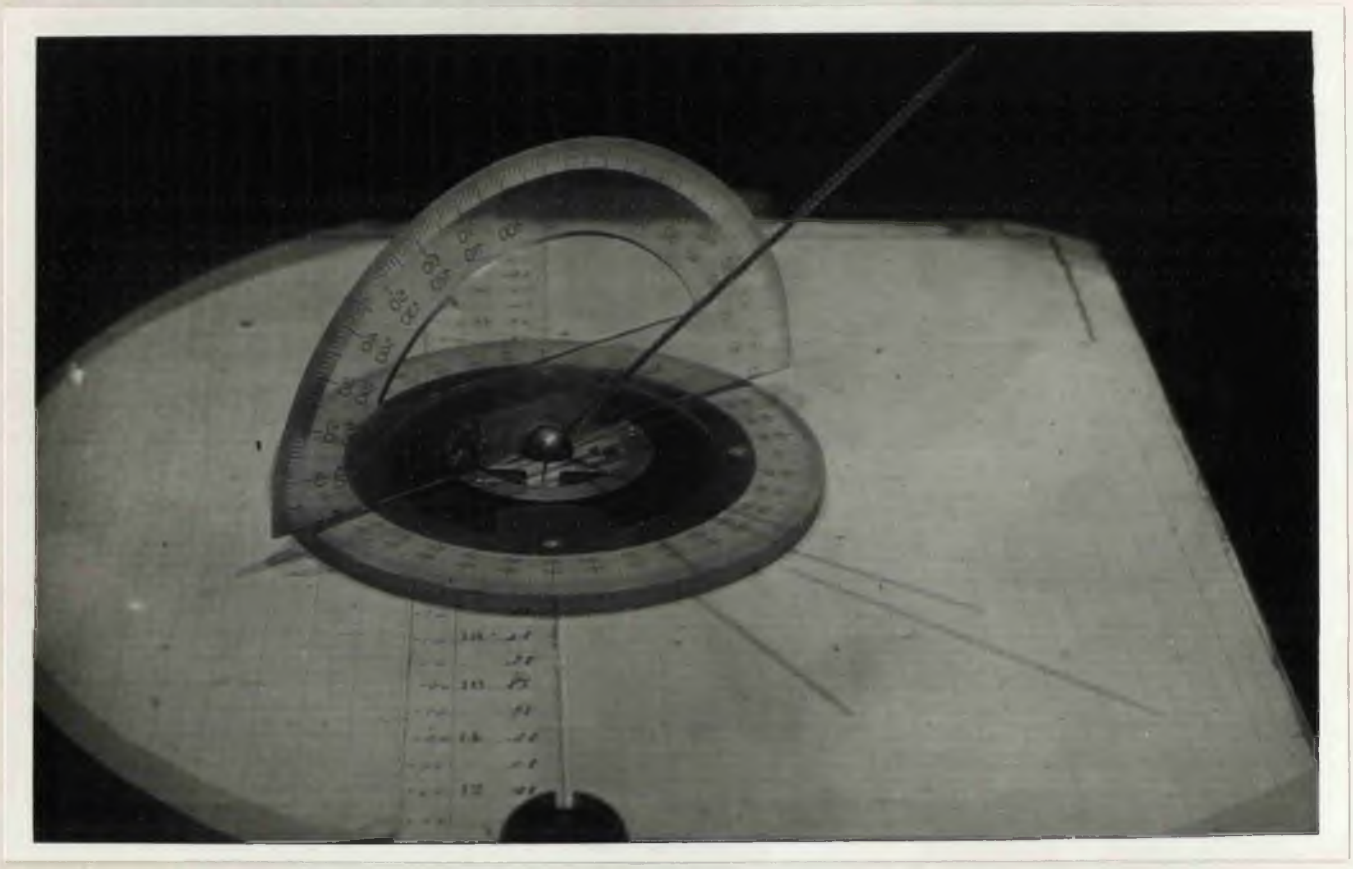

Fig. 5.3

Model used to determine directions and lengths of cloud chamber tracks from measurements on the three camera films. The diameter of the circular protractor is 5" and the length of the pointer is 6".

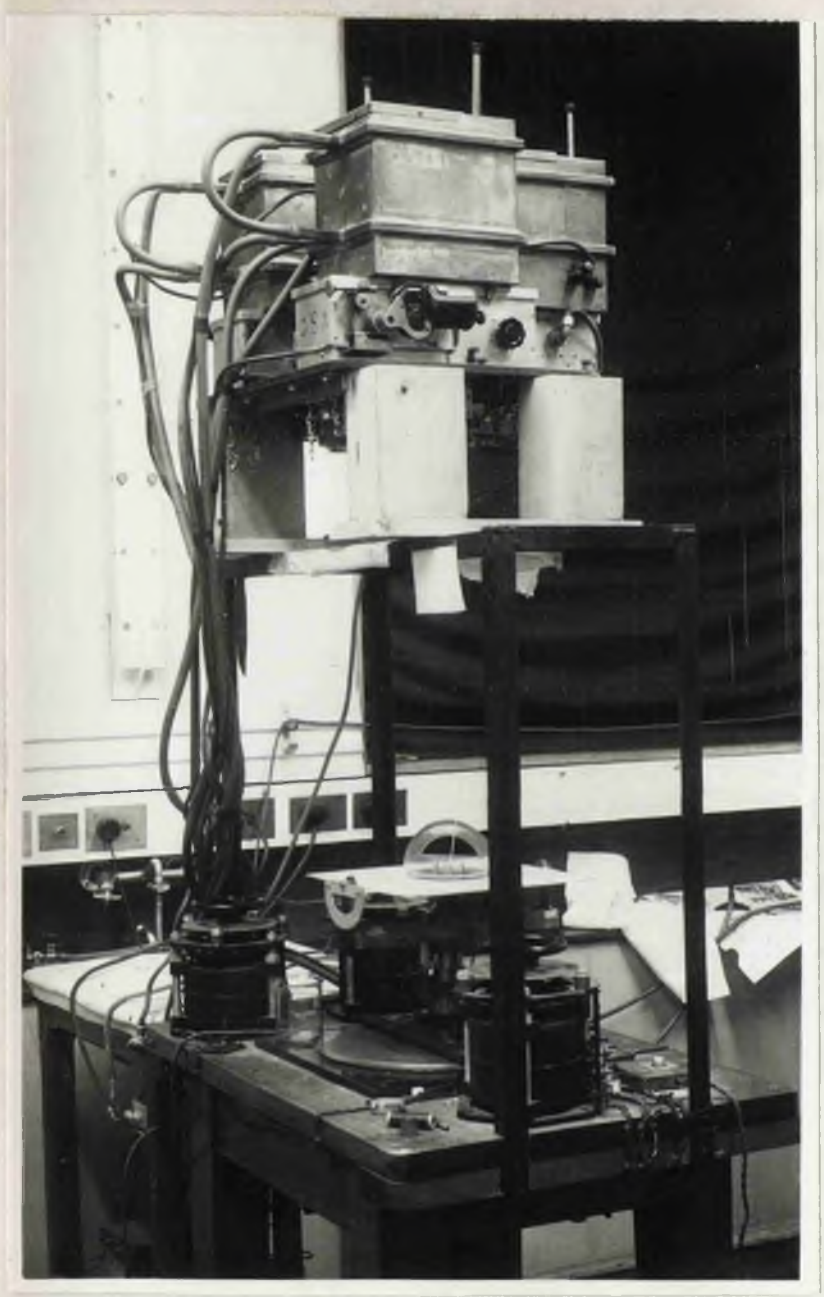

Fig. 5.4

Photograph showing cameras and reprojection table as used for track analysis in the neon experiment.

design is possible, since the horizontal separation of the cameras can be varied within quite wide limits. For the Blackett arrangement the position of the cameras in uniquely determined by the characteristics of the camera lenses and the size of the cloud chamber image. The new arrangement has the disadvantage that the centre of the cloud chamber image is displaced from the axis of the camera lens but, as was found here, the requirement for freedom from errors due to distortion can be met without difficulty. At the same time it is clear that the lenses should always be tested for freedom from distortion.

The process of analysis was further simplified by using a model which makes use of the fact that the images on the films are projections onto a horizontal plane from the camera lenses. This model consists of a pointer fixed in a ball joint and fitted with angular scales as shown in Fig. 5.3. It was used in conjunction with the existing reprojection equipment and rested on the reprojection table which was kept horizontal. The positions of model and reprojection table were adjusted so that the centre of the ball joint was at the point corresponding to the origin of the track being studied and the pointer moved until the shadows cast by the three combinations of projection lamp and camera were in the same directions as the images on the three films (see Fig. 5.3 and 5.4). The angle of dip and the horizontal projected angle of the pointer and track were measured directly with the aid of the vertical protractor. The length of the track was also obtained from this model since

$$\text{length of track} = \text{length of image} \times \frac{\text{length of pointer}}{\text{length of shadow}} + \text{small correction}$$

(see Appendix III).

In addition to saving time the use of the model had the further advantage that the data from all three films was displayed and analysed simultaneously. Hence any inconsistencies in the measurements could be seen and checked immediately.

An important observation following from the above is that by using a similar though somewhat more complicated model this type of analysis can be used with any stereographic camera arrangement. For any camera the image on the film is a reproduction of the projection of the track onto a plane parallel to the film plane. Thus microscope measurements with any camera arrangement can be analysed using a model designed to measure for each shadow the angle and length of the shadow cast on the plane parallel to the film plane of the corresponding camera. A model of this type could be built by using a set of open protractors. This type of model was not used to analyse the results of the nitrogen experiment for the good reason that the idea of using it only occurred during and as a consequence of the neon experiment. The possibility of analysing microscope measurements made with any camera arrangement will modify the case for adopting the "horizontal film plane" camera arrangement in any future experiment. There is a good case for using this camera arrangement for all experiments in which it is necessary or desirable to measure a large number of the tracks of interest with a microscope. The coordinates of some point on the track must be known before the model can be used and the determination of these from microscope

Table 5.2

Possible Photoreactions in the Neon Experiment

Target Nucleus	Particles Emitted	Threshold		
		Short Singles	Flags	Stars
		Mev	Mev	Mev
Ne^{20}	α		4.75	
	α + α			11.90
	p		12.87	
	α + p			16.86
	n	16.91		
	5α			19.17
	α + n		20.34	
	p + p			20.82
	d		21.05	
	He^3		21.17	
Ne^{22}	α		9.66	
	n	10.36		
	p		15.31	
	α + α			15.90
	α + n		17.72	
	d		21.16	
	t		21.51	
O^{16}	α		7.15	
	p		12.11	
	4α			14.43
	n	15.60		
	d		20.72	

measurements is much easier for the "horizontal film plane" camera arrangement.

1 (c) Analysis.

(i) Inspection and Classification of Events.

The reactions which can be produced in the gas of the cloud chamber are listed in Table 5.2 together with their thresholds and expected classification. Reactions in Ne^{21} can be safely neglected. The thresholds for the reactions of interest ((γ,α), $(\gamma,2\alpha)$ and $(\gamma,\alpha p)$) are all higher than the corresponding thresholds in Ne^{20} while the $Ne^{21}(\gamma,n)$ threshold is 10 Mev lower than that for $Ne^{20}(\gamma,n)$. Hence, for these two nuclei, the ratio of events of interest can confidently be taken as less than the ratio of their relative abundances (0.28% and 90.51% respectively).

The films from all three cameras were scanned concurrently using an eyeglass and, for closer examination, a low powered microscope. The events found were classified directly into reaction groups. This was possible since events due to the (γ,n)*, (γ,p), (γ,α), $(\gamma,2\alpha)$ and $(\gamma,\alpha p)$ reactions were easily distinguished and there were no events due to other reactions.

The evidence for the absence of other events is as follows. Four of the reactions give distinctive events which were not observed. These are $(\gamma,4\alpha)$ (4 pronged star), $(\gamma,\alpha n)$ (non collinear flag with long

*The recoil tracks from the (γ,n) reaction have a maximum length of 2 mm. Such tracks were observed and noted but not measured or counted since it is probable that some of them were overlooked.

Table 5.3

Q Values for Background Events

	Q
Neon Experiment	
$Ne^{20}(n,\alpha)$	- 0.60 Mev
$Ne^{20}(n,p)$	- 6.26 Mev
$Ne^{22}(n,\alpha)$	- 5.70 Mev
$Ne^{22}(n,p)$	Not known but certainly large
$O^{16}(n,\alpha)$	- 2.20 Mev
$O^{16}(n,p)$	- 9.62 Mev
Nitrogen Experiment	
$N^{14}(n,\alpha)$	- 0.15 Mev
$N^{14}(n,p)$	+ 0.63 Mev

Table 5.4

Classification of Events for Neon Experiment

Reaction Group	Number of Events	Approximate Integrated Cross Section Mev-mb.
(γ,p)	316	30
($\int_{23\ Mev}^{} (\gamma,n)dE$ from reference Fe 54		30)
Doubtful (γ,pn)[i]	6	-
(γ,α)	28	1
$(\gamma,2\alpha)$	20	2
$(\gamma,\alpha p)$	40	4
Unclassified[ii]	5	-

Notes

(i) On the criteria of the nitrogen experiment (see p. 84) these events were non-collinear flags and were therefore classified thus even though the (γ,pn) reaction is energetically impossible for neon and oxygen. They are probably (γ,p) events in which the recoil was scattered close to the origin. The expected number of (γ,pn) disintegrations in the small amount of nitrogen which would have diffused into the chamber during the experiment is $^2/_3$ of an event.

(ii) These events are all short tracks resembling α tracks and somewhat buckled in appearance. They are possibly α particles emitted just before the expansion from slight radioactive contamination from the Po source.

recoil and short dense fragment track), $(\gamma,5\alpha)$ (5 pronged star) and $(\gamma,2p)$ (two low energy proton tracks and short recoil (total proton energy less than 2.2 Mev)). (γ,d), (γ,t) and (γ,He^3) events are unlikely because of the high thresholds for these reactions. They were definitely excluded by later measurements since, with the X-ray energy available, the emitted particles would be of short range with a high probability of stopping in the chamber. $((R_d)_{max.} = 5.2$ cm., $(R_t)_{max.} = 1.9$ cm. and $(R_{He}3)_{max.} = 1.0$ cm.). Such events would resemble (γ,p) and (γ,α) events but be distinguished from them by the recoil range. As it happened there were no "(γ,p)" events of range less than 5 cm. or "(γ,α)" events of range less than 1 cm. None of the events originated outside the X-ray beam. Hence the number of background events due to (n,α) and (n,p) reactions in the gas is negligible. This reduction in background as compared with the (small) background found in the nitrogen experiment is to be expected since neutrons of all energies produced background events in the nitrogen experiment while only neutrons of energy greater than 2 Mev could produce background events in the Neon experiment. (See list of Q values in Table 5.3 remembering that the coulomb barrier for α particles in neon is 7 Mev). The expected mean energy of the background neutrons (mainly photoneutrons from the lead collimator) is about 1 Mev.

The numbers of events for each reaction are given in Table 5.4. The reliability of the classification is indicated by the following notes. Events due to the four possible reactions will be either collinear flags

((γ,p) and (γ,α)) or three pronged stars ((γ,2α) and (γ,αp)). (γ,p) events were distinguished from (γ,α) events (see Plates 14 and 15) by the fact that the proton was much more lightly ionizing and the recoil track (clearly visible in all (γ,p) events) was very short. The maximum range of the recoil for (γ,p) events was $2\text{-}1/2$ mm. and only four (γ,α) events had a recoil range as short as this. With the exceptions noted in the table all flag events not obviously (γ,p) events had the appearance expected for (γ,α) events (though for some the origin could not be clearly distinguished) and were classified as such.

(γ,αp) events were distinguished from (γ,2α) events by the lighter ionization of the proton track, which was very marked for protons of 2 Mev or more. Lower energy protons were sometimes slightly more difficult to distinguish but in these cases the direction of the recoil track clearly showed the lower momentum associated with the proton track. (Compare Plates 13 and 16). For many of the stars the measurements made later gave an independent identification. In every case this agreed with the visual identification.

In measuring these events three microscopes were used, one for each image, and any uncertainties were clarified immediately by inspection of the other images. The quantities determined in the measurement of an event were

(1) The coordinates of the origin and of the end point of each track. These were used to check that the event originated within the X-ray beam and to determine which tracks stopped within the chamber.

(2) The direction in space of each track.

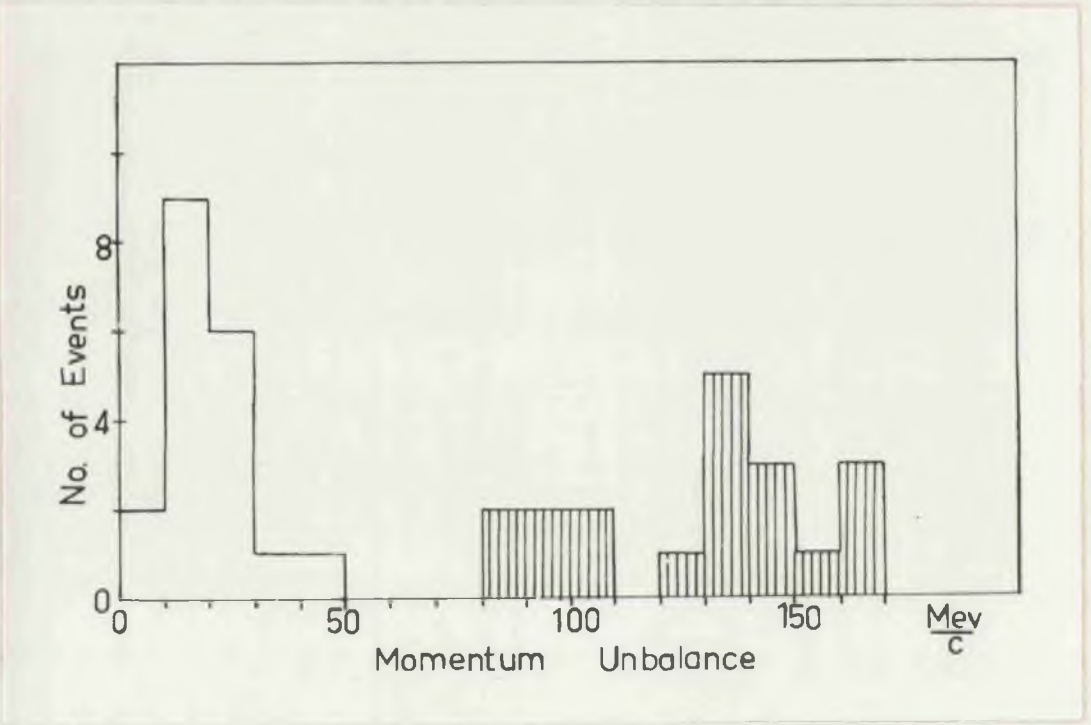

Fig. 5.5

Momentum unbalance distributions for the (γ,2α) and (γ,αp) stars in which all tracks stop in the chamber. The open histogram represents the values obtained for the visual identifications of the star tracks. The shaded histogram represents the smallest values (one for each star) for any other identification.

(3) The length of each track.

The determination of these quantities from the image measurements was made immediately so that inconsistencies in the measurements could be detected and checked. The initial measurements were confined to the star events and (γ,α) events.

(ii) Momentum Balance Test of the Accuracy of the Star Measurements.

Since only charged particles are emitted in the star producing reactions, the momentum unbalance (i.e. the difference between the vector sum of the measured momenta of the three particles and the momentum of the incoming quantum) is a direct measure of the accuracy of the measurements. This was calculated for the 19 stars (11 $(\gamma,2\alpha)$ and 8 $(\gamma,\alpha p)$) in which all three tracks stopped in the chamber. It was assumed that all $(\gamma,2\alpha)$ stars were due to the $Ne^{20}(\gamma,2\alpha)$ reaction*. The $(\gamma,\alpha p)$ stars must be due to the $Ne^{20}(\gamma,\alpha p)$ reaction. The values of the momentum unbalance are plotted in Fig. 5.5 (open histogram). The average value of the momentum unbalance is 21 Mev/c which is 12% of the average recoil momentum.

The expected range straggling and multiple scattering of the recoil track accounts for most of the observed momentum unbalance. The errors introduced by the cloud chamber analysis are therefore small

*This assumption is reasonable since the $Ne^{20}(\gamma,2\alpha)$ threshold is 4 Mev lower than the $Ne^{22}(\gamma,2\alpha)$ threshold and the relative abundances of the two nuclei are 90.51% and 9.21% respectively. As the momentum unbalance obtained for any $Ne^{22}(\gamma,2\alpha)$ star will be close to the true value this assumption cannot affect the momentum balance analysis.

compared with these. The average momentum unbalance in the direction of the recoil is approximately twice the average momentum unbalance at right angles (in the plane of the star) which indicates that range straggling is rather more important than multiple scattering.

The calculation of the momentum unbalance also gave an independent identification of the nature of the star event. The apparent momentum unbalance was calculated for all possible "identifications" of the three tracks, these "identifications" being made without reference to the appearance of the tracks. For all events only one value of the apparent momentum was less than the value allowed by experimental error. This identified the events uniquely and these identifications corresponded exactly with the visual identifications. The second-best values for the momentum unbalance are plotted in Fig. 5.5 (shaded histogram) and are very clearly separated from those calculated for the visual identification.

Because of the limited amount of data available for the recoil range-energy relations the procedure actually followed was somewhat more complicated than that indicated above. Mr. D.R.O. Morrison had deduced range-energy relations for C^{12} and N^{15} ions in neon based on a review of all the data available (see D.R.O. Morrison, Ph.D. Thesis, University of Glasgow). These relations were used for the identification of events by momentum balance and this gave a clear confirmation of the visual identification only slightly less marked than that indicated by Fig. 5.5. Since the recoil energies were known from measurements on the other

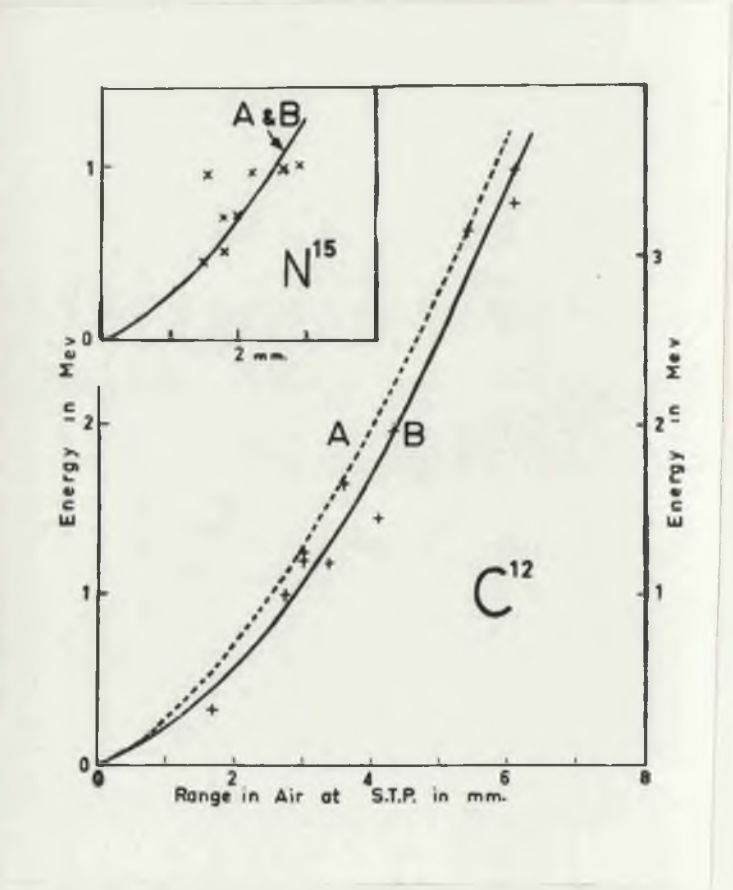

Fig. 5.6

Range Energy Relations for N^{15} and C^{12} ions in neon.

A. Range energy relations deduced from previous experiments.

B. Range energy relations indicated by the present results and used in the analysis.

The experimental points are the ranges found in the present experiment for stars in which all tracks stopped in the chamber.

tracks the measured ranges were compared directly with the proposed range-energy relations (see Fig. 5.6). There was good agreement for N^{15} recoil ranges. For C^{12} recoils the measured ranges were within the uncertainties of the proposed relation but consistently higher than the curve chosen. Since there were good reasons for preferring the new data** a range-energy relation based on these experimental points was adopted for C^{12} recoils and the momentum unbalance figures plotted in Fig. 5.5 were calculated from this.

The data ultimately required from the analysis of a star event was E_T, the total energy release, and E_1^* and E_2^*, the estimates of the excitation energy of the intermediate nucleus through which the reaction was assumed to pass. As can be seen from the following comments the accuracy with which these were determined depended on the number of tracks which stop in the chamber.

(1) 2 + R Stars - all tracks stopped in the chamber. For these the errors were small since the characteristics of the star were determined from the range and direction of the two fragment tracks.

(2) 1 + R Stars - one fragment track passed out of the chamber. The characteristics of the star were determined from the range and direction of the recoil and the fragment which stopped in the chamber. The accuracy of the recoil measurement was checked by calculating the

**The proposed range energy relation for C^{12} ions was based on the ranges of ions of lower energy in other gases. The calculation of the equivalent ranges in neon was somewhat uncertain since part of the energy loss is by nuclear scattering and part by ionization.

Table 5.5

Estimated Errors in Quantities Determined from Star Measurements

Quantity Measured	Type of Star		
	2 + R	1 + R	0 + R
E_T	100 kev	1 Mev	2 - 3 Mev
E^*	100 kev	250 kev(1) or 1 Mev(2)	2 Mev

Notes - (1) for f_2 stopping in the cloud chamber

(2) for f_2 passing out of the cloud chamber

where f_2 is the fragment which is assumed to be emitted second.

momentum unbalance at right angles to the direction of the fragment leaving the cloud chamber. Thirteen 1 + R stars (5 (γ,2α) and 8 (γ,αp)) were analysed in this way. Three other stars in which the recoil tracks were scattered were rejected because of a large momentum unbalance.

(3) 0 + R Stars - both fragment tracks passed out of the chamber. The characteristics of a 0 + R star can be determined from the recoil range and the directions of the three tracks. These stars were not measured in the present experiment since, with the accuracy that can be achieved (see Table 5.5), such measurements would add little to what is already implied by the fact that the peak X-ray energy is 23 Mev.

The estimated errors in the measurements of E_T and E^* are listed in Table 5.5 for the three classes of star. These estimates are based on the errors in the track measurements quoted above, the expected range straggling for protons and α particles and the errors in recoil measurements indicated by the mean momentum unbalance for 2 + R stars.

2. RESULTS

The approximate integrated cross sections for the reactions observed are given in Table 5.4 on p.122b. For the (γ,p), (γ,2α) and (γ,αp) reactions these values were deduced directly from the number of events assuming that the mean energy of the quanta producing these events was 20 Mev. The integrated cross section for the (γ,α) reaction was deduced from the energy distribution discussed below. The failure

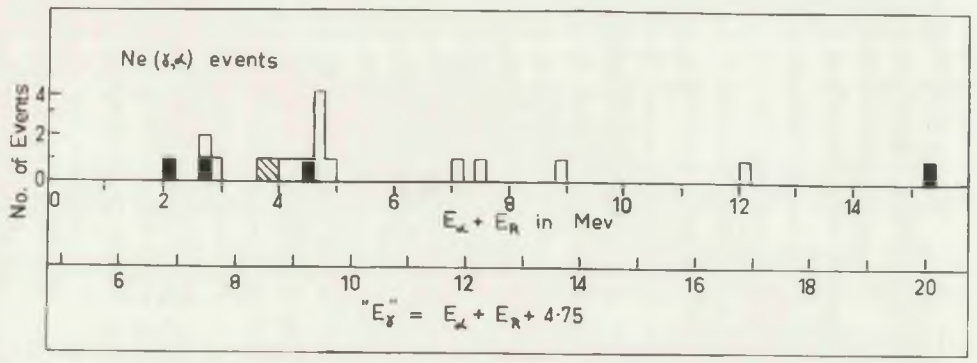

Fig. 5.7

Total energy of α particle and recoil for (γ,α) events in neon. The lower scale gives the energy of the quanta producing the disintegrations, if these events are due to the reaction $Ne^{20}(\gamma,\alpha)O^{16}$ (ground state). The solid rectangles represent events for which both α particle and recoil ranges were measured. The open rectangles represent events for which only the recoil range could be measured since the α particle passed out of the chamber. The shaded rectangles represent events for which only the sum of the α particle and recoil ranges were measured, i.e. the origin was not clearly visible. In this case there is an ambiguity of ~ 0.5 Mev in the value of $E_\alpha + E_R$.

to observe any events due to other reactions leads to the following upper limits for the average cross sections of these reactions below 23 Mev. These upper limits were calculated for the 95% confidence level.

$Ne^{22}(\gamma,\alpha n)$ < 1 mb.

$Ne^{20}(\gamma,5\alpha)$, $Ne^{20}(\gamma,\alpha n)$ $< 1/5$ mb.

$Ne^{20}(\gamma,2p)$, $Ne^{20}(\gamma,d)$, $Ne^{20}(\gamma,He^3)$ $< 1/4$ mb.

The results for the four reactions observed are discussed below.

2 (a) $Ne^{20}(\gamma,\alpha)$ Reaction.

The total energy of the α particle and recoil, was determined for 19 (γ,α) events and these energies are plotted in Fig. 5.7. The error in these energies is less than 100 kev for those events in which both the α particle and recoil could be measured and from $^1/_2$ - 1 Mev for those events in which only the recoil could be measured. Nine events were not measured as the α particle passed out of the cloud chamber and the origin of the event was not clearly visible in all three films. These events have been neglected in the following discussion, which also neglects the possibility that some of the (γ,α) events may be due to the $Ne^{22}(\gamma,\alpha)$ reaction. These assumptions should not affect the validity of the conclusions drawn since the discussion is, in any case, limited to approximate cross sections by the small number of events available.

Fig. 5.7 shows that there are very few (γ,α) events for

Table 5.6

$Ne^{20}(\gamma, \alpha)$ Cross Sections

Cloud Chamber Measurement

Levels of Residual Nucleus	AVERAGE Cross Section	E_γ
	10^{-28} cm^2	Mev
Ground State	~ 0.3	17 - 23
Ground State	$\lesssim 0.3$	10 - 17
6 - 7 Mev	$\lesssim 0.6$	16 - 23

Ionization Chamber Measurement

by Hay and Warren

Levels of Residual Nucleus	Cross Section	E_γ
	10^{-28} cm^2	Mev
Ground State	0.50	17.6
6.06, 6.14 Mev	6.7	17.6
6.91, 7.12 Mev	18	17.6
Ground State	0.86	14.8
6.06, 6.14 Mev	~ 1	14.8

which $E_\alpha + E_R$ is greater than 5 Mev. The reactions which could produce these events are

$E_\alpha + E_R > 12$ Mev

$Ne^{20}(\gamma,\alpha)O^{16}$ (ground state) 17 Mev $< E_\gamma <$ 23 Mev

5 Mev $< E_\alpha + E_R <$ 12 Mev

Either $Ne^{20}(\gamma,\alpha)O^{16}$ (ground state) 10 Mev $< E_\gamma <$ 17 Mev

or $Ne^{20}(\gamma,\alpha)O^{16*}$ (6 - 7 Mev) 16 Mev $< E_\gamma <$ 23 Mev.

The cross section data deduced from the numbers of events found in this experiment is given in Table 5.6.

Hay and Warren (Ha 50a) have obtained $Ne^{20}(\gamma,\alpha)$ cross sections for a number of states of the residual nucleus, by irradiating a neon filled ionization chamber with γ-rays from the $p + Li^7$ reaction and measuring the resulting pulse height distribution. Their cross sections are also given in Table 5.6. Their cross sections for disintegrations leaving O^{16} in the ground state are close to the average cross sections found in the cloud chamber experiment. However their 17.6 Mev cross section for disintegrations leaving O^{16} in excited states near 6 and 7 Mev is 40 times the upper limit given by the cloud chamber for the average value of this cross section in this energy region. Taken at its face value this would indicate that the cross section for $Ne^{20}(\gamma,\alpha)O^{16*}$ (6 - 7 Mev) has a pronounced and very sharp maximum close to 17.6 Mev. However, the author believes that the difference is more likely to be due to experimental error in the ionization chamber measurements. The peaks in the pulse height

distribution at 6.8 and 5.9 Mev, corresponding to α particles leaving O^{16} in the pairs of states near 6 and 7 Mev, are in fact unresolved bumps on the high energy side of a large peak at 4.7 Mev due to the $Ne^{20}(\gamma,p)$ reaction. Hence they could conceivably be due to some spurious effect. This suggestion is supported by the fact that the one α particle peak which is well resolved, the 12.9 Mev peak corresponding to 17.6 Mev disintegrations leaving O^{16} in the ground state, gives a cross section which is close to the average cross section indicated by the cloud chamber results.

If the events with $E_\alpha + E_R$ less than 5 Mev are assumed to be due to disintegrations produced by quanta of energy less than 10 Mev*, then the integrated cross section for the (γ,α) reaction in this energy region will be $\sim 1/3$ Mev-mb.

2 (b) <u>$Ne^{20}(\gamma,p)$ Reaction</u>.

This reaction was not studied in any detail but the following observations are of interest. Only three proton tracks from (γ,p) events were observed to stop in the chamber. This implies that the $Ne^{20}(\gamma,p)$ cross section is small for quantum energies below 15 Mev. The results of Sinclair (Si 54) show that the cross section for the inverse reaction, $F^{19}(p,\gamma)Ne^{20}$ (ground state), is very small for proton energies below 1.5 Mev. This also implies that the $Ne^{20}(\gamma,p)$ cross section is small below 14.3 Mev.

There are not sufficient (γ,p) events to give a meaningful angular distribution. The experimental points suggest an isotropic

*This seems to be most likely: see discussion on p. 134

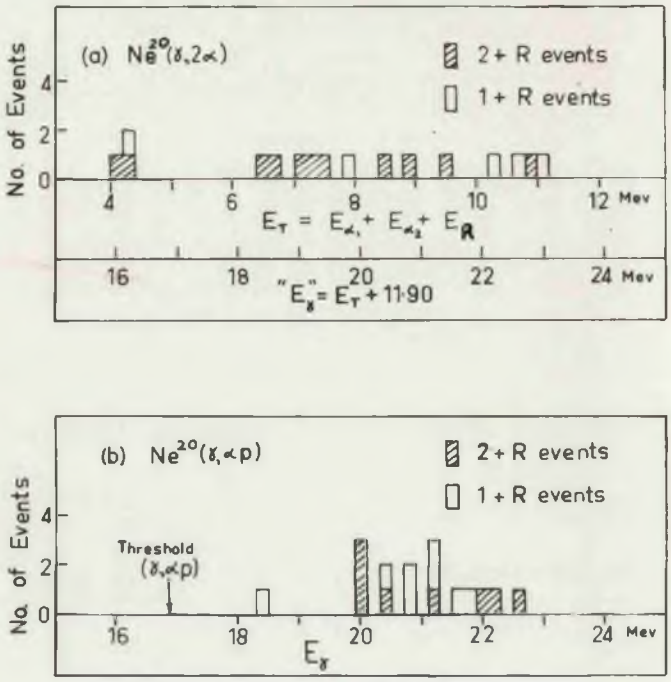

Fig. 5.8

(a) Distribution of the total energy release (i.e. $E_{\alpha_1} + E_{\alpha_2} + E_R$) for the $Ne^{20}(\gamma,2\alpha)$ stars. The lower energy scale gives the energy of the quanta producing these disintegrations if they are due to the reaction $Ne^{20}(\gamma,2\alpha)C^{12}$ (ground state). The energetics show that stars with $E_{\alpha_1} + E_{\alpha_2} + E_R > 6.7$ Mev must be due to this reaction.

(b) Distribution of the E_γ values obtained from the measurements of $E_\alpha + E_p + E_R$ for $Ne^{20}(\gamma,\alpha p)$ stars.

distribution but the difference from a $1 + \sin^2\theta$ or a $1 + 3/2 \sin^2\theta$ distribution is not statistically significant.

2 (c) $Ne^{20}(\gamma,2\alpha)$ and $Ne^{20}(\gamma,\alpha p)$ Reactions.

The results for these two reactions will be considered together. As has been noted $(\gamma,\alpha p)$ events must be due to the $Ne^{20}(\gamma,\alpha p)$ reaction; $(\gamma,2\alpha)$ events could be due to either the $Ne^{20}(\gamma,2\alpha)$ reaction or to the $Ne^{22}(\gamma,2\alpha)$ reaction. These $(\gamma,2\alpha)$ events cannot be distinguished experimentally and it has been assumed that all $(\gamma,2\alpha)$ events are due to the $Ne^{20}(\gamma,2\alpha)$ reaction. This is reasonable since the relative abundance of Ne^{22} is small (9.21% compared with 90.51% for Ne^{20}) and the cross section for $Ne^{22}(\gamma,2\alpha)$ is expected to be less than the cross section for $Ne^{20}(\gamma,2\alpha)$ (see general argument on p. 114). The results discussed below are based on measurements on 16 of the 20 $(\gamma,2\alpha)$ stars (11, 2 + R stars and 5, 1 + R stars) and 16 of the 40 $(\gamma,\alpha p)$ stars (8, 2 + R stars and 8, 1 + R stars).

The distribution of E_T ($= E_{\alpha_1} + E_{\alpha_2} + E_R$) for the $(\gamma,2\alpha)$ events is given in Fig. 5.8 (a). Events with E_T greater than 6.7 Mev must be due to disintegrations leaving C^{12} in the ground state; for the four events of lower energy the residual C^{12} nucleus could have been left in either the ground state or the 4.43 Mev excited state. The lower energy scale gives the value of E_γ for events in which the C^{12} nucleus is left in the ground state. The corresponding distribution for the $(\gamma,\alpha p)$ events is plotted in Fig. 5.8 (b). In this case the

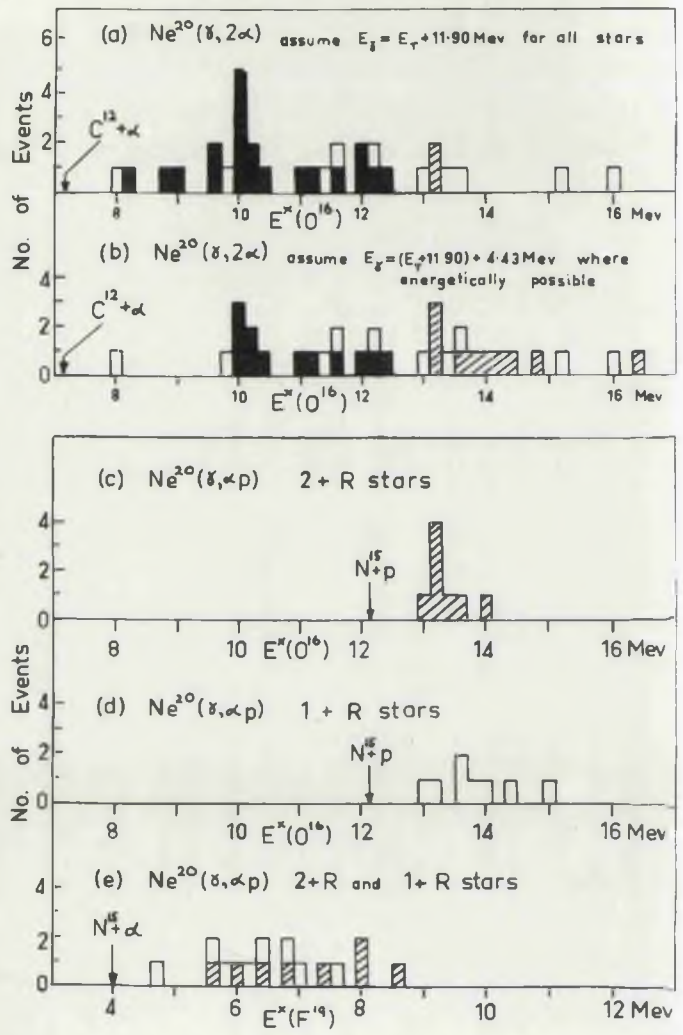

Explanation of Shading

(a) & (b)

Solid rectangles - both values of $E^* < 12.5$ Mev

Shaded rectangles - both values of $E^* > 12.5$ Mev

Open rectangles - one value of $E^* < 12.5$ Mev, one value of $E^* > 12.5$ Mev

(c), (d) & (e)

Shaded rectangles - 2 + R events

Open rectangles - 1 + R events

Fig. 5.9

(a), (b) Distribution of $E^*(O^{16})$ values (two for each star) for (γ ,2α) stars (both 2 + R and 1 + R). For distribution (a) it is assumed that, for all stars, the residual C^{12} nucleus is left in the ground state. For distribution (b), it is assumed that the residual C^{12} nucleus is left in the first excited state, at 4.43 Mev, for the four stars where this is energetically possible.

(c), (d) Distributions of the $E^*(O^{16})$ values for the 2 + R, (γ ,α p) stars and 1 + R, (γ ,α p) stars.

(e) Distribution of $E^*(F^{19})$ values for (γ ,α p) stars.

values of E_γ are uniquely determined since, for all the events, it is energetically impossible for N^{15} to be left in its first excited state at 5.28 Mev. These distributions show that the cross sections for both these reactions are appreciable between 19 Mev and 23 Mev and hence that the average cross sections in this energy region are $\sim 1/2$ mb. for $Ne^{20}(\gamma,2\alpha)$ and ~ 1 mb. for $Ne^{20}(\gamma,\alpha p)$. For comparison the average cross sections for the $Ne^{20}(\gamma,n)$ (Fe 54) and (γ,p) reactions in this energy region are each ~ 6 mb.

If the neon stars are assumed to involve a level of an intermediate nucleus, then each star will give two possible values for E^*, its excitation energy, only one of which is significant**. With the small number of events available it is not possible to carry through the kind of analysis made of the $C^{12}(\gamma,3\alpha)$ stars (see Chapter I, p. 38) but, nevertheless, an examination of the E^* distributions leads to some useful conclusions. These distributions are given in Fig. 5.9.

The E^* distribution for the $(\gamma,2\alpha)$ stars will depend on the assumption made about the four events for which the C^{12} nucleus may be left in either the ground state or the first excited state. In Fig. 5.9 the distribution has been plotted for the two limiting assumptions; namely that the C^{12} nucleus is left in the ground state for all four events or is left in the first excited state for all four

**For the $(\gamma,\alpha p)$ reaction one of these values will be an "excitation energy" of the F^{19} nucleus (corresponding to the assumption that the reaction is $Ne^{20}(\gamma,p)F^{19*}(\alpha)N^{15}$) and the other will be an "excitation energy" of the O^{16} nucleus (corresponding to the assumption $Ne^{20}(\gamma,\alpha)O^{16*}(p)N^{15}$).

events.

Although the statistics are very poor these distributions strongly suggest the following conclusions:

(1) In the energy region where the (γ,α) reaction is allowed by the isotopic spin selection rules, the emission of an α particle from Ne^{20} does not generally leave the O^{16} nucleus in the same excited state**. This is in contrast to the $C^{12}(\gamma,3\alpha)$ reaction above 26 Mev, for which most α particles emitted leave the Be^{8} nucleus in a level at 16.8 Mev.

(2) For a large fraction of $(\gamma,2\alpha)$ stars both values for $E^*(O^{16})$ are less than 12.5 Mev. This implies that O^{16} is left in an excited state below the first T = 1 level (at 12.8 Mev (Aj 59)) for an appreciable fraction of the $Ne^{20}(\gamma,\alpha)$ disintegrations which appear as $(\gamma,2\alpha)$ events***. This result cannot be explained away by assuming that the events indicated by solid rectangles are, in fact, $Ne^{22}(\gamma,2\alpha)$ events, since this is energetically impossible for four of the six such

**It should be noted that the apparent peak in the $E^*(O^{16})$ distribution for 2 + R stars from the $(\gamma,\alpha p)$ reaction could be due to instrumental bias. The probability of observing these 2 + R stars depends on the probability that the proton will stop in the chamber. This decreases from 0.62 to 0.14 as the proton energy is increased from 1 to 2 Mev. Hence, for $(\gamma,\alpha p)$ stars, measured under the conditions of the present experiment, a peak in the $E^*(O^{16})$ distribution at $\sim$13 Mev cannot be regarded as real unless it appears in the distributions for both 1 + R and 2 + R stars.

***For the sake of definiteness it is assumed, both here and in the following discussion, that the star producing reactions proceed via a level of an intermediate nucleus. This seems to be most likely. The discussion can always be made quite general by including the simultaneous emission of the two particles concerned as an additional alternative.

events in Fig. 5.9(b).

3. DISCUSSION

The number of (γ, 2α) and (γ,αp) stars show that, as was expected, both the Ne^{20}(γ,2α) and the Ne^{20}(γ,αp) reactions have appreciable cross sections in the region of the giant resonance. This result and the observations on the (γ, α) reaction show that the general form of these cross sections is in agreement with the predictions of the isotopic spin selection rules.

For Ne^{20} these predictions are - at energies below the first T = 1 level in Ne^{20} (at $\sim$10.7 Mev) absorption of quanta will be by E2 or M1 transitions. M1 absorption must lead to the re-emission of a γ-ray, but, at energies above $\sim$ 6 Mev, E2 absorption should lead to a (γ, α) disintegration. 1^-, T = 1 states in Ne^{20} can occur above 10.7 Mev and these should give rise to strong absorption. Such absorption will produce (γ,α) disintegrations (if $E_\gamma < 13.5$ Mev (say)), (γ,p) disintegrations (if 13.5 Mev$< E_\gamma <$ 17 Mev) and (γ,p) and (γ,n) disintegrations (if $E_\gamma > 17$ Mev). The cross section for (γ,α) disintegrations leaving O^{16} in the ground state or in the excited states near 6 and 7 Mev will be small at all energies above 13.5 Mev. The cross section for (γ,α) disintegrations leaving O^{16} in T = 1 levels should be appreciable above 20 Mev. These disintegrations will appear as (γ,2α) or (γ,αp) events. (Because the emission of α-particles from T = 1 states in O^{16} is inhibited by their isotopic spin, it is expected that, in general, these states will decay by proton emission: i.e., the (γ,α p) cross section will be greater than the (γ,2α) cross section.)

With this picture in mind it is natural to identify the group of (γ,α) events with $E_\alpha + E_R < 5$ Mev as disintegrations produced by quanta of energy less than 10 Mev. If this is done then the cross section obtained is a reasonable one for E2 transitions. This can be seen if, for example, the group of 8 events with $E_\alpha + E_R$ between 4 and 5 Mev is assumed to be due to a single level. The value of Γ_γ for this level is then 0.4 ev which is equal to three Weisskopf units for E2 transitions. Further points of agreement between the above picture and the experimental results are the small (γ,α) cross section at higher energies and the appreciable cross sections for the $(\gamma,2\alpha)$ and $(\gamma,\alpha p)$ reactions. The absence of any large groups of α-particles or protons implies that there are no 1^-, T = 1 states below 15 Mev in Ne^{20}.

However, since this experiment does not identify the levels in which O^{16} is left following α-emission, it cannot be said that these results confirm the isotopic spin selection rules, although they are compatible with them. The result that, for a fraction of the $(\gamma,2\alpha)$ stars, the O^{16} nucleus must be left in an excited state below the first T = 1 level is an apparent exception to this statement. However, as is shown below, this result is consistent with the expected small departures from the isotopic spin selection rules due to the coulomb force. Because of this force there will be a small number of (γ,α) disintegrations which

leave O^{16} in T = 0 levels at energies somewhat below the first T = 1 level. These disintegrations can only lead to (γ,2α) events. On the other hand disintegrations which leave O^{16} in T = 1 levels can lead to both (γ,2α) events or (γ,αp) events. It is expected that these T = 1 states will decay by proton emission more frequently than by α-emission* i.e., for these latter disintegrations (γ,αp) events will be more frequent than (γ,2α) events. Hence, although the proportion of (γ,α) disintegrations leaving O^{16} in T = 0 levels is expected to be small, it can be an appreciable fraction of the number of (γ,2α) events. The value of one third required to explain the present results is not unreasonable. It is emphasized that these results do not provide positive evidence for the isotopic spin selection rules. It is just as easy to show that the experimental data is also compatible with the assertion that (γ,α) disintegrations in Ne^{20} do not leave O^{16} in T = 1 levels.

As has been pointed out Ne^{20} is the only α-particle nucleus likely to have an appreciable cross section for α-particle emission in the giant resonance region. Unfortunately it is not possible to determine this cross section at present, since the

*This follows since the residual state of C^{12} has T = 0 and the emission of an α-particle is subject to the selection rule $\Delta T = 0$. Recent experimental results (see Aj 59) indicate that, for the first four T = 1 levels in O^{16} (at 12.78, 12.96, 13.09 and 13.25 Mev), the probability of decay by proton emission is $\sim$100%, 55%, 80% and 20% respectively.

above results do not allow the (γ, α p) events to be separated into "(γ, α)" disintegrations and "(γ ,p)" disintegrations. However, the argument of the previous paragraph shows that, if the isotopic spin selection rules are valid, then a large fraction of the 40(γ, α p) events must be "(γ, α)" disintegrations. Assuming a value of one half for this ratio then

$$\frac{\sigma\text{"}(\gamma,\alpha)\text{"}}{\sigma\text{"}(\gamma,p)\text{"}} = \frac{20 + 20}{300 + 20} = \frac{1}{8} \quad \text{for } E_\gamma \sim 20 \text{ Mev.}$$

This is quite a large value and, if confirmed, will provide an additional test for any theory of the giant resonance. A ratio of 1/8 seems to be quite compatible with any theory of the giant resonance involving the formation of a compound nucleus. As far as is known the expected value of this ratio has not been calculated for the Wilkinson theory of the giant resonance (Wi 56).

The precision of the above conclusions would be improved if the levels of the ~~individual~~ intermediate nuclei assumed to be involved in the star reactions could be identified. The necessary conditions for such an identification, with a reasonable number of events, are

(a) only a few levels be involved and

(b) the error in the determination of the E* values be much less than the spacing between levels.

It is clear from the wide spread of E* values for (γ ,2α) events that a number of levels are involved and hence that their identification will require a much larger number of events. The same is

true for the identification of the F^{19} levels involved in the (γ,p) disintegrations leaving F^{19} in highly excited states. However, the prospects are brighter for the (γ,αp) reaction. Although it cannot be determined beforehand, it is possible that condition (a) will be satisfied since the levels involved are expected to be limited to those with T = 1. The error in the measurement of E* depends on the error in the measurement of the proton energy and hence condition (b) will be satisfied if (and only if) the proton stops in the chamber. For the present experiment the range of E* energies for which this was probable was very small (see footnote on p. 133), but this energy range could be increased substantially by using a chamber with a greater illuminated depth and by increasing the stopping power of the cloud chamber gas. Under these conditions it is possible that the levels involved in the (γ,αp) reaction would be identified with a reasonable number of events. The identification of these levels in O^{16} and of the corresponding (γ,α p) events would provide a significant test of the isotopic spin selection rules and would also provide further information on the ratio $\sigma''(\gamma,\alpha)''/\sigma''(\gamma,p)''$ discussed in the preceeding paragraph.

Subsequent to the completion of the above experiment Komar and Iavor (Ko57) have published preliminary results from a cloud chamber investigation of photonuclear reactions in neon irradiated with 80 Mev X-rays. The number of events for each of the reactions

Table 5.7

Cloud Chamber Measurement of

Photonuclear Yields for Neon Using

80 Mev X-rays (Komar and Lavor (Ko 57))

Reaction	No. of Events
(γ,p)	352
(γ,pn)	137
$(\gamma,2p)$	64
$(\gamma,2\alpha)$	21
$(\gamma,\alpha p)$	143
$(\gamma,5\alpha)$	2

observed is given in Table 5.7. It should be noted that Komar and Iavor do not give a figure for the number of (γ ,α) events although they state that, "...reactions (γ ,p) and (γ , α) were distinguished by the ionization density and the tracks of the recoil nuclei." Komar and Iavor also report that the integrated cross section for the (γ ,p) reaction is 160 $\pm$ 80 Mev-mb. and that the angular distribution of photoprotons with energies between 1 and 15 Mev is of the form a + b $\sin^2\theta$ with b/a $\simeq$ 2.5. The integrated (γ ,p) cross section found by Komar and Iavor is very much larger than the (γ ,p) cross section integrated up to 23 Mev (see Table 5.4 on p. 122b) which implies that most of the integrated (γ ,p) cross section is due to quanta of energy greater than 23 Mev. The relatively large numbers of (γ ,pn), (γ ,2p) and (γ ,pα) events found by Komar and Iavor imply a similar result for the cross sections for these reactions and show further that the star producing reactions contribute a substantial fraction of the total photonuclear cross section in Ne^{20}.
In a recent private communication Professor Komar stated that they have since extended their investigations by studying photonuclear reactions in neon enriched in Ne^{22}. He stated that the results for the star producing reactions in Ne^{22} are quite different to those for the corresponding reactions in Ne^{20} but gave no details.

As has been noted the Neon experiment showed that the lengths and directions of recoil nuclei could be measured with fair accuracy and provided quantitative information on the accuracy of

measurements on stars produced in a cloud chamber by photonuclear reactions. This information is summarized in Table 5.5 on p. 127a and refers to stars produced by the emission of two charged fragments and no neutrons. It shows that, compared with the accuracy of the results that can be obtained by measuring stars in nuclear emulsions, the cloud chamber results are much more accurate when all tracks stop in the chamber and of comparable accuracy when one or both charged particles pass out of the chamber. Stars from reactions involving the emission of a neutron can only be analysed when all the charged particles stop in the chamber. The expected accuracy corresponds to that for 1 + R stars. The consequences of these results will be discussed first for stars produced by quanta whose energy is only a few Mev above the threshold and then for stars produced by quanta of higher energies.

For an appreciable fraction of the first group of stars the tracks of all charged particles will stop in the chamber. For these stars calculation of the momentum balance provides positive identification for all events and the characteristics of the star (i.e., the total energy release and the energies and directions of all the product particles) can be determined with considerable accuracy for all reactions*

*Reactions involving the emission of two or more neutrons are an exception. However it is expected that, in practice, these reactions will not cause appreciable ambiguity since they are likely to have small cross sections. This can be checked directly for a large number of these reactions since they lead to radioactive product nuclei.

For stars produced by higher energy quanta one or more of the charged fragments will pass out of the chamber. In this case measurements on stars from reactions involving the emission of a neutron give only a lower limit for the neutron energy and the total energy release. On the other hand, if (γ,2α), (γ,αp) and (γ,2p) stars can be identified, then, since 1 + R and 0 + R events can be analysed with fair accuracy, the characteristics of these stars can be determined over the whole range of quantum energies in which they are produced. Since the Neon experiment has demonstrated that (γ,2α), (γ,α p) and, by implication, (γ,2p) events can be reliably distinguished by visual observation this identification can be made if the three-prong stars involving the emission of a neutron can be separated from those not involving the emission of a neutron. This separation should be quite straightforward. For stars involving a neutron the tracks of the three charged particles will be non-coplanar, while for stars not involving a neutron the tracks will depart from exact coplanarity by a small and calculable amount determined by the momentum of the incoming quantum.

The above discussion assumes that the number of events due to reactions such as (γ,pd), (γ,α d), (γ,pt) . . . is neglible. This is a reasonable first approximation. It should be possible to obtain some indication of its validity from the number of such events in the energy region just above threshold and from the number of events due to reactions such as (γ,2pn) and (γ,α pn) in this energy region and at higher energies. The numbers of these latter events are almost

certainly related to, and probably larger than, the number of (γ ,pd) and (γ ,α d) events.

The cloud chamber can therefore provide a considerable amount of information on the star producing reactions over the whole energy range in which they occur. There is good evidence that, for light nuclei at energies above the giant resonance, these reactions have appreciable cross sections and contribute a good fraction of the total photonuclear cross section but there is virtually no information on the energy dependence and exact magnitude of their cross sections. The absence of this information is attributable to the fact that these cross sections are not easily measured by the other techniques which have been used to study photomuclear reactions. Hence a cloud chamber measurement of (γ ,2p), (γ ,pα) and (γ ,2α) cross sections and of the yields of other events would be of considerable importance. This point is discussed at greater length in Chapter VI (Summary and Conclusion).

Chapter VI

SUMMARY AND CONCLUSION

The work described in this thesis has shown that a conventional volume defined expansion chamber is suitable for use in a cloud chamber investigation of photonuclear reactions. As far as is known the track quality obtained has not been bettered in any similar investigation. This work has also demonstrated that the cloud chamber method gives very accurate results for the energy region in which the energies of the fragments can be determined from range measurements* and further that the tracks of recoil nuclei can be measured with a total error which is only slightly greater than the unavoidable error due to range straggling and multiple scattering. For (γ,p), (γ,d) and (γ,α) events the measurement of recoil tracks provides the same information as a measurement of the curvatures of the fragments in a magnetic field and has the advantage that a measurement can be made on all such events occuring in the cloud chamber. For (γ,pn) and star events the measurement of the recoil is an essential part of the analysis. In particular, measurement of the recoils will enable $(\gamma,2p)$, $(\gamma,p\alpha)$ and $(\gamma,2\alpha)$ events to be analysed with fair accuracy over the whole range of quantum energy for which they occur.

Although its usefulness was limited by the peak X-ray energy of the available synchrotron, the Helium experiment showed that the

* i.e., $E_p \lesssim 3$ Mev, $E_\alpha \lesssim 12$ Mev.

cross section for the $He^4(\gamma,p)$ reaction was approximately 1/10th of the value implied by the existing measurements of the $H^3(p,\gamma)$ cross section and that the measurement of the recoil triton could give an accurate measurement of the $He^4(\gamma,p)$ cross section up to 45 Mev. The Nitrogen experiment gave the first clear cut demonstration of level structure in photonuclear reactions, the first confirmation of the principle of detailed balancing for photonuclear reactions and showed that the $N^{14}(\gamma,p)$ and $N^{14}(\gamma,pn)$ cross sections have shapes which are similar to the giant resonance shape of the (γ,n) cross section. The Neon experiment showed that the $Ne^{20}(\gamma,2\alpha)$ and $Ne^{20}(\gamma,\alpha p)$ reactions have significant cross sections in the region of the giant resonance and that the general features of the (γ,α), $(\gamma,2\alpha)$ and $(\gamma,\alpha p)$ reactions in Ne^{20} are compatible with the isotopic spin selection rules. However, since this experiment did not identify the O^{16}, T = 1 levels which are assumed to be involved, it does not provide a confirmation of the isotopic spin selection rules.

The potentialities of the cloud chamber method can be judged by considering possible experiments for which its use is either necessary or desirable. The following experiments have been suggested as a continuation of work described in this thesis.

(1) A study of the $He^4(\gamma,p)$ and $He^4(\gamma,n)$ reactions using range measurements of the recoil tritons and He^3 nuclei to determine the energies of the quanta producing the disintegrations. This experiment would provide a more accurate measurement of the (γ,p)

cross section up to ~ 45 Mev and the (γ,n) cross section up to ~ 70 Mev than do published experiments. It can be expected to clear up discrepancies between these experiments and to determine if there is a significant difference between the (γ,p) and (γ,n) cross sections.

(2) An analysis of $N^{14}(\gamma,pn)$ events. As is explained in Chapter IV, § 5 the measurement of the proton ranges and of the ranges and directions of the associated C^{12} recoils can be expected to provide the following results

(a) the respective cross sections for $N^{14}(\gamma,n)$ disintegrations leaving N^{13} in the following levels - 2.36 Mev, (3.51 and 3.56 Mev), 6.91 Mev and 7.42 Mev.

(b) the number (and, if this is large, the energy distribution) of low energy photoprotons ($E_p < 2$ Mev) from $N^{14}(\gamma,p)$ disintegrations due to quanta in the giant resonance region.

Both these results would provide information of a type which is not available for any nucleus.*

(3) Further measurement of $Ne^{20}(\gamma,\alpha p)$ stars, using

*There is however some information on the cross sections for (γ,p) reactions leaving the residual nucleus in particular excited states. This is limited to a few target nuclei - Na^{23}(Op 58), K^{39}(Op 58a), I^{127} and Cs^{133}(I.F. Wright - to be published) - and to a single gamma ray energy (17.6 Mev). Although it is conceivable that these measurements could be extended to higher energies by using monochromatic γ-rays from the $p + H^3$ reaction (or, possibly, monochromatic quanta obtained from positron annihilation in flight) such an extension is difficult and has yet to be done.

a deeper chamber and a higher stopping power than were used in the experiment described in Chapter V., in an attempt to identify the O^{16}, T = 1 levels which are expected to be involved in the Ne^{20} (γ, α) reaction.

An important experiment for which the cloud chamber is well suited is the measurement of the He^3 photonuclear cross sections. Gunn and Irving (Gu 51) have shown that their shape is a sensitive function of the nuclear wave function and the nuclear size parameter, and hence the measurement of these cross sections will provide a good test for the values of these quantities. The experimental conditions required for this measurement are quite straightforward, as can be seen from the following comments. The two possible reactions are

$He^3(\gamma,p)H^2$ Threshold 5.49 Mev

$He^3(\gamma,2pn)$ Threshold 7.71 Mev

For both reactions the cross sections calculated by Gunn and Irving reach a maximum from 5 - 15 Mev above the threshold. Using these calculated cross sections, the expected yield, for the cloud chamber and synchrotron used in the present work and a He^3 partial pressure of 1 atmosphere,* is approximately 1 event per 5 photos for $He^3(\gamma,p)H^2$ and 1 event per 2 photos for $He^3(\gamma,2pn)$. Events due to these two reactions are readily distinguished from photonuclear disintegrations in heavier nuclei and can be

*At the quoted price of 15 cents/cc. at atmospheric pressure the cost of filling the cloud chamber to a pressure of one atmosphere is $900.

separated from one another by simply measuring the angle between the two tracks. For the $He^3(\gamma,p)H^2$ reaction, the angle between the proton and the deuteron is a characteristic of the reaction since it is practically independent of the energy of the quantum producing the disintegration.* For the $He^3(\gamma,2pn)$ reaction, the angle between the two protons is expected to vary over the whole range from 0° - 180°. The energy of the quantum producing a $He^3(\gamma,p)H^2$ disintegration can be determined from the energy of either the proton or the deuteron. If a heavier gas is added to give a total stopping power equivalent to three atmospheres of air, deuteron range measurements can be made up to an energy corresponding to an E_γ of 25 Mev. The determination of E_γ for a $He^3(\gamma,2pn)$ disintegration requires the measurement of the energies of both protons. For the above total stopping power, range measurements are possible for values of E_γ up to about 15 Mev. Higher energy events can be analysed by measuring radii of curvature in a magnetic field.

A further application of the cloud chamber is to a study of the star producing reactions in light nuclei. There is a need for more information on these reactions which, with the exception of the $C^{12}(\gamma,3\alpha)$ reaction, have been largely neglected. The available experimental evidence indicates that, for light nuclei,

*The greatest variation with energy is when the proton is emitted at right angles to the incoming quantum. In this case the angle between the proton and deuteron is within 1° of 172° for quantum energies between 7 and 25 Mev.

the cross section for star producing reactions is largest at energies somewhat above the giant resonance and that, in this energy region, this cross section is an appreciable fraction of the total photonuclear cross section.* Hence a study of these reactions is likely to be a fruitful way of investigating the photonuclear process in the energy region between the giant resonance and the energies at which the 'pseudo-deuteron' theory of Levinger (Le 51) has been shown to be appropriate. An advantage of studying star producing reactions is that the distribution of energy between the product particles can provide valuable information on the nature of the reaction. Also, since the energy of any one particle will be only a fraction of the total energy release, information on these reactions will compliment published experimental results on higher energy photoprotons (Wh 58, Ch 57, Ch58).

As was noted in Chapter V the cloud chamber can provide the following information on these reactions.

(1) Accurate values for the total energy release and energies and angles of the emitted particles for all star events in the energy region just above the reaction thresholds.

(2) Moderately accurate values of the same quantities for $(\gamma, 2p)$, $(\gamma, \alpha p)$ and $(\gamma, 2\alpha)$ events produced by quanta of any

*See discussion of results of Gaerttner and Yeater for C^{12}, N^{14} and O^{16} on p. 19-22, and of Komar and Iavor for neon on p.138f. Iavor (Ia 58) has also made a cloud chamber study of the photodisintegration of A^{40} and finds that for this nucleus the integrated cross section for star producing reactions is very small. This suggests that star producing reactions may be less important for the medium weight nuclei.

energy.

(3) The reaction yields for other star producing reactions and quanta of higher energy.

This method can therefore provide a general picture of the star producing reactions.

Other methods that could be used to study these reactions are the radioactive product method, measurements on stars produced in nuclear emulsions, the use of counters in conjunction with a cloud chamber and the use of counters in coincidence. The radioactive product method is useful for cross section measurements but does not give any information on the distribution of energy between the product particles. Another limitation is that the reactions which lead to radioactive products are inevitably less favoured energetically and will therefore tend to have smaller cross sections than the reactions leading to stable products. This will be especially true if star producing reactions involve the evaporation of several particles in cascade. Thus this method cannot be expected to give a general picture of the star producing reactions, although it ought to be exploited to the full. The information it provides would be a valuable supplement to that provided by the cloud chamber.

The nuclear emulsion method has been used in extensive studies of the $C^{12}(\gamma, 3\alpha)$ and $O^{16}(\gamma, 4\alpha)$ reactions and has also been used to study reactions in Li^6, Li^7, Be^9, B^{10} and B^{11} at energies below 30 Mev (for discussion and references see Ti 55), the

Table 6.1

Nuclear Emulsion Results for (γ ,pα) Integrated Cross Sections

E_γ	25 - 40 Mev		40 - 55 Mev	55 - 70 Mev	70 - 85 Mev
	25-35	35-40			
	Integrated Cross Sections in Mev-mb				
Maikov's Results					
$C^{12}(\gamma,p\alpha)$	2.10	1.75	1.78	0.82	0.38
$N^{14}(\gamma,p\alpha)$ (1)	~5.0	~0.9	~1.2	~0.2	
$O^{16}(\gamma,p\alpha)$	1.89	1.22	1.64	0.64	0.16
Livesey's Results					
$C^{12}(\gamma,p\alpha)$	0.68	0.65			
$N^{14}(\gamma,p\alpha)$	1.3				
$O^{16}(\gamma,p\alpha)$	Small compared with cross sections for $C^{12}(\gamma,p\alpha)$ and $N^{14}(\gamma,p\alpha)$				

Note (1) The cross sections for $N^{14}(\gamma,p\alpha)$ are approximate estimates by the author from the energy distribution of N^{14} events assuming an integrated cross section of 7.35 Mev-mb for the energy range E_γ = 20-70 Mev. The English translation (Soviet Phys. JETP 7,973 (1958)) gives this figure as 7.35 Mev-mb for E_γ = 30-80 Mev but, from the context, this seems to be a typographical error.

Table 6.2

Nuclear Emulsion Measurement of the $C^{12}(\gamma,pt2\alpha)$ Cross Section by Maikov (Ma 58).

E_γ	30 - 40 Mev	40 - 55 Mev	55 - 70 Mev	70 - 85 Mev
σ_{int}(Mev-mb)	0.64	1.74	1.25	0.54

(γ,pα) reactions in C^{12}, N^{14} and O^{16} and the C^{12}(γ,pt2α) reaction (Li 56, Ma 58). This method is very satisfactory for disintegrations (in the very lightest nuclei) in which the heaviest product particle is an α-particle. However a comparison of the results of Livesey (Li 56) and Maikov (Ma 58) for the (γ,pα) reactions in C^{12}, N^{14} and O^{16} indicates that it is less satisfactory for reactions involving heavier recoil nuclei. In these measurements both Livesey and Maikov separated the C^{12}(γ,pα), N^{14}(γ,pα) and O^{16}(γ,pα) events produced in the emulsion by a momentum balance analysis using the measured ranges of the recoil nuclei. Their cross section results are summarized in Table 6.1 which shows that there is a considerable discrepancy between the two measurements. The measured energy distributions for protons and α-particles are also in disagreement. Livesey reports that, for C^{12}(γ,pα) stars and $E_\gamma < 40$ Mev, the mean energy of the α-particles is 5/3 times the mean energy of the protons. For the same reaction and the same range of quantum energies, Maikov finds that the mean energies of the two particles are approximately equal. Maikov suggests that Livesey's failure to find any significant number of O^{16}(γ,pα) events was due to an error in his recoil range energy relations such that O^{16}(γ,pα) events were wrongly classified as N^{14}(γ,pα) events. While this may be true it cannot account for all the discrepancy since all of Maikov's cross sections are considerably larger than those reported by Livesey. The above comparison implies that one or both workers

have made large errors in the detection and identification of (γ, pα) events and points to the need for a more reliable method of studying these reactions.

Because of this difference in detection efficiency these nuclear emulsion results were not included in the evidence for the conclusion that the cross section for the star producing reactions is largest at energies above the giant resonance. For this reason it might be noted that, if taken at their face value, both sets of results are in agreement with this conslusion. In particular Maikov finds that the (γ,pα) cross sections have maxima at $\sim$ 35 Mev and appreciable cross sections at higher energies. (See also Maikov's cross section data for C^{12}(γ,pt2α) which is given in Table 6.2).

Reid and Turnbull (Re 60) have extended the cloud chamber method by adding scintillation counter telescopes, placed at the side of the chamber, to determine the energy of high energy protons produced in the chamber. Their counter telescopes detected protons with energies between 80 and 120 Mev and these proton pulses were used to trigger the expansion chamber. This arrangement was used to study the photodisintegration of O^{16} between 100 Mev and 240 Mev. The application of a similar technique to stars produced by lower energy quanta could be of value for

(1) the analysis of stars involving the emission of a neutron

(2) a more exact measurement of the energies of energetic protons and α-particles from (γ,2p), (γ,pα) and (γ,2α) events.

(3) the selection of infrequent events.

The usefulness of this technique will depend on the electron background in the counters. This background will place a lower limit on the energy of the protons that can be detected and, possibly, produce some uncertainty in the measured value of the proton energy. Information on this background is not available to the author at the time of writing.

Counter measurements of particles emitted in coincidence would provide information on the star producing reactions. The use of this technique with a high intensity electron accelerator seems to be the ultimately desirable method of studying these reactions since this is the only way in which results of good statistical accuracy could be obtained. Measurements of this kind have not yet been made and therefore it is not known how complicated an arrangement is required to eliminate the effects of the electron background. However it is clear that the experiment itself would be involved, since the description of a star producing reaction requires the measurement of several angular distributions and angular correlations. Also, since the recoil nucleus is not detected, there may be some difficulty in determining whether a further particle is emitted in coincidence with those detected.

From these considerations it seems clear that the best approach to the study of the star producing reactions in light nuclei, in the energy region 20 - 80 Mev, is to use the cloud chamber method to

obtain a general picture of these reactions and then to use either coincidence measurements of the combination of counters and cloud chamber for particular reactions of interest.

Because of the analysis time required, the cloud chamber is an instrument for special rather than general use. The above discussion shows that there are still a number of photonuclear experiments for which it is both appropriate and desirable to use a cloud chamber.

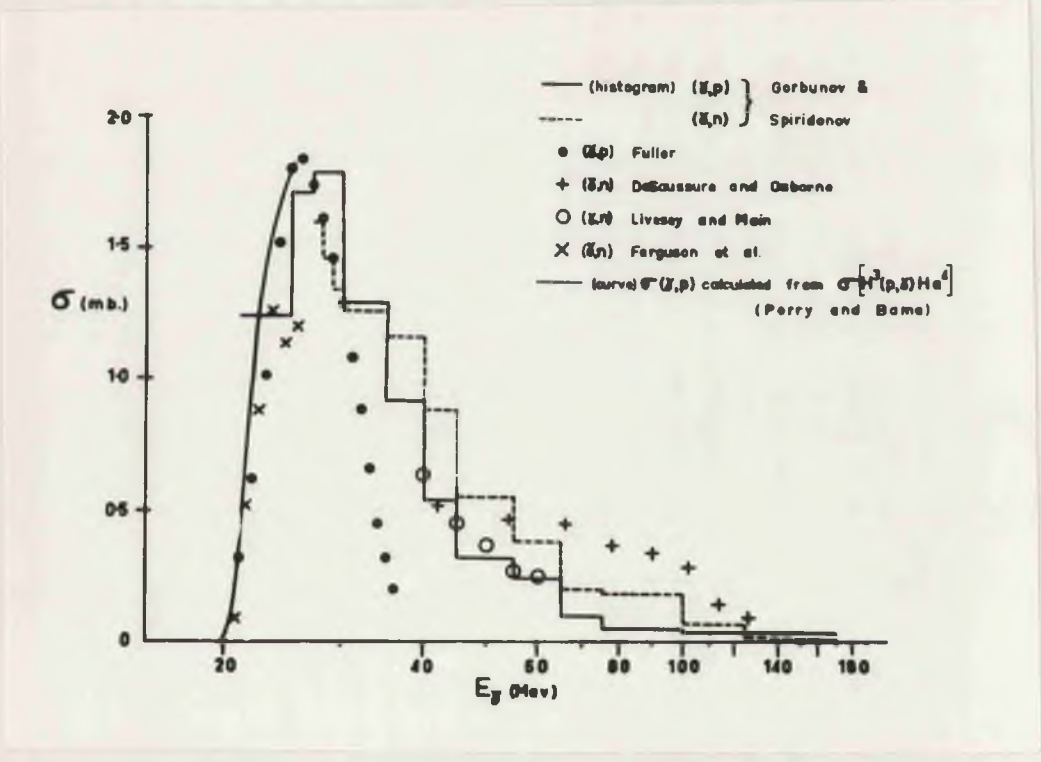

Fig. A 1.1

Experimental measurements of $He^4(\gamma,p)$ and $He^4(\gamma,n)$ cross sections.

Appendix I

SOME REMARKS ON RECENT MEASUREMENTS OF THE $He^4(\gamma,p)$ AND $He^4(\gamma,n)$ CROSS SECTIONS

There are now a number of measurements of the $He^4(\gamma,p)$ cross section and of the (γ,n) cross section, which is expected to be very similar. There is good evidence that these cross sections have a pronounced maximum at approximately 26 Mev* but there are large discrepancies between the values given for the cross sections above 30 Mev. The results are summarized in Fig. A1.1 and the methods used are as follows.

(1) Gorbunov and Spiridonov. (Go 57), (Go 58a) and (Go 58b). These workers measured the cross sections up to 170 Mev for all photonuclear reactions in helium using an expansion chamber of illuminated volume 30 cm. by 8 cm. deep filled with helium at a pressure of 1.7 atmospheres (not stated but can be calculated from ranges quoted in (Go 58a)). The energies of the charged particles produced (and hence E_γ) were obtained from their radii of curvature in the magnetic field of 5500 gauss. For (γ,n)

*The theoretical implications of this result are of interest. In a continuation of the calculations of Gunn and Irving (Gu 51) Bransden et al. (Br 57) show that, for a variety of types of wave function, parameters which give the correct energy for the (γ,p) cross section maximum lead to too small a value for the He^4 binding energy and too large a value for the r.m.s. radius of He^4. In particular, allowance for the proton-triton interaction in the final state and for tensor forces does not affect this result. These workers suggest that the use of wave functions based on a nuclear potential with a repulsive core may remove this inconsistency. If this is so it would be evidence for such an interaction. A further result of interest is that the shape of the cross section above the maximum shows a considerable dependence on the nature of the proton-triton interaction in the final state.

disintegrations with E_γ less than about 30 Mev the He^3 recoil nuclei are of short range and their energies were determined from the observed ranges. For the cross sections not given in Fig. A1.1 Gorbonov and Spiridonov find that the (γ,pn) cross section (Go 58b) has a maximum at 50 Mev and an integrated value (to 170 Mev) of approximately $1/4\ \sigma_{int}(\gamma,p)$, that the yield of the $(\gamma,2p2n)$ reaction is not more than 10% of the (γ,pn) yield and that the (γ,d) yield is also small (less than 2% of the (γ,p) yield).

(2) Fuller (Fu 54) used nuclear emulsions to detect the charged particles emitted from a helium gas target irradiated with 25, 29, 32 and 40 Mev X-rays. Tracks of photoprotons from the $He^4(\gamma,p)$ reaction were identified with certainty when their length was greater than the maximum range of the recoil tritons or the particles from other reactions. Hence each irradiation gave the $He^4(\gamma,p)$ cross section from the maximum energy down to some experimental cut off and the cross section from 24 Mev to 40 Mev was obtained from a combination of these four results.

(3) De Saussure and Osborne (De 55) measured the $He^4(\gamma,n)$ cross section from 40 - 160 Mev by detecting the He^3 recoil nuclei emitted from a helium gas target with nuclear emulsions. The type of emulsion and method of development were chosen to give best discrimination between proton and triton tracks and He^3 tracks, which were identified by visual examination.

(4) Livesey and Main (Li 58) used the same method to measure the (γ,n) cross section from 40 - 70 Mev. To facilitate the visual discrimination they irradiated the emulsion with α particles from a radioactive source placed so that the α particles entered the emulsion at

a similar angle to the He^3 tracks but from the opposite direction. Tracks were identified as He^3 tracks only if they were as dense as or more dense than the nearest α track.

(5) Ferguson et al. (Fe 54) measured the neutron yield from a helium gas target with BF_3 counters embedded in paraffin and hence obtained the (γ,n) cross section up to 26 Mev by the activation curve method.

Preliminary reports without experimental details of cloud chamber measurements of the $He^4(\gamma,p)$ cross section have been published by Nicolai and Goldwasser (Ni 54) and Reid et al. (Re 56, also private communication from J.M. Reid (1959)). The data given by both sets of workers indicate a cross section in general agreement with that reported by Fuller.

The results below 30 Mev are all in agreement within the errors expected for the various experiments. The most accurate data in this energy range is that obtained from the measurements of the $H^3(p,\gamma)$ reaction (Pe 55). The following comments are relevant to the evident disagreement above 30 Mev.

It seems likely that de Saussure and Osborne have included a number of proton and triton tracks with the He^3 tracks. Because they correspond to a lower E_γ the number of proton and triton tracks in the appropriate range interval is some seven times the number of He^3 tracks*

*The results obtained by de Saussure and Osborne for the $He^4(\gamma,\pi_o)$ He^4 reaction are of interest in this connection. This measurement was made in association with the (γ,n) experiment using 300 Mev X-rays and the same apparatus to measure the He^4 recoil nuclei. Their cross section is an order of magnitude greater than that of other workers ((Go 56) and (Pa 58)) who used quite different and apparently reliable experimental methods. The only obvious explanation for such a large overestimate of the cross section is a similar inclusion of proton and triton tracks with the (short) He^4 tracks.

(see Li 58). Because of their procedure of comparison with a nearby α particle the measurement of Livesey and Main should be more reliable in this respect but it is clearly desirable that their result should be confirmed by an independent method. The fact that for E_γ between 45 Mev and 50 Mev their angular distribution for the He^3 nuclei has a strong forward asymmetry not found at higher energies or by other workers suggests that their selection criterion may have varied somewhat.

Gorbunov and Spiridonov obtained their (γ,p) cross section from the measured curvatures of both the protons and tritons which were analysed independently. The two results are in very good agreement. These authors are not prepared to claim that the difference between the (γ,n) and (γ,p) cross sections is real. They note (Go 58a) that it may be due to errors in curvature measurements arising from multiple scattering* or in the correction to the measured curvatures for the energy loss of the He^3 along the track length. They promise further measurements at a lower gas pressure and twice the magnetic field.

When considered by themselves the (γ,p) measurements of Fuller and of Gorbunov and Spiridonov both appear to be reliable and hence the difference above 30 Mev is an unexplained discrepancy.

For any repeat measurement of the He^4(γ,p) and He^4(γ,n) cross sections there is a lot to recommend the use of the cloud chamber (since it is the method by which these reactions can be most clearly separated

*For disintegrations with E_γ = 40 Mev and $\theta_{\gamma p}$ = 90°, the expected errors due to multiple scattering (estimated from the Bethe formula (Be 46)) are - proton curvature 4%, triton and He^3 curvature 11%. The corresponding errors in E_γ are 1.5 and 4.5 Mev.

from other reactions) and, with it, the method of determining E_γ from the ranges of the recoil tritons or He^3 nuclei. Values of E_γ determined in this way are expected to be more accurate than those determined from curvature measurements. For E_γ = 40 Mev the expected error for both (γ,p) and (γ,n) events is 0.4 Mev whereas the corresponding estimated errors in the measurements of Gorbunov and Spiridonov due to multiple scattering are 1.5 and 4.5 Mev respectively for (γ,p) and (γ,n) events. The energy region which can be investigated in this way depends on the stopping power of the gas in the chamber. By adding a heavier gas to increase the stopping power (γ,p) events up to 45 Mev and (γ,n) events up to 70 Mev could be measured with a reasonable total pressure. For a stopping power of four times air at N.T.P. (obtained by adding, say, 2 atmospheres of CO_2) and E_γ = 45 Mev the ranges of triton emitted at 90°, 0° and 180° are 6.0 cm., 10.1 cm. and 3.0 cm. respectively while for E_γ = 70 Mev the corresponding He^3 ranges are 4.7 cm., 8.6 cm. and 3.9 cm. respectively. As has been pointed out in Chapter III (see p.76f) the photonuclear events in carbon and oxygen are clearly distinguished from those in helium and are therefore no problem. Such a measurement would determine the (γ,p) cross section by an independent method and, since the errors in the two measurements would be comparable, show clearly if there is a real difference between the (γ,p) and (γ,n) cross sections.

Appendix II

EXAMINATION OF THE NITROGEN PHOTOPROTON SPECTRUM REPORTED BY SPICER

As was noted in Chapter IV a measurement by Spicer (Sp 53) of the spectrum of photoprotons from nitrogen irradiated with 11.5 Mev X-rays is in conflict with both the cloud chamber results reported in this thesis and the measurements on the $C^{13}(p,\gamma)$ reaction. This appendix seeks an explanation of the observed discrepancy by examining Spicer's nitrogen experiment and also his experiments on oxygen and argon, which used the same technique.

Spicer irradiated a nitrogen gas target with a narrow beam of X-rays and detected the photoprotons with nuclear emulsions placed to the side of the X-ray beam. The gas pressure used (1 atmosphere) was sufficient to ensure that particles from the $N^{14}(\gamma,d)$, $N^{14}(\gamma,\alpha)$ and $N^{14}(\gamma,pn)$ reactions would be stopped before they reached the emulsion. The measurements made on the proton tracks were the range in the emulsion, the angle to the beam direction and the depth in the emulsion at the end of the track. To be accepted a track was required to start at the surface of the emulsion and have a direction compatible with an origin within the irradiated volume. The angular range covered was 40° - 140°. The number of background tracks was determined in a second irradiation for which the collimator was blocked by a lead plug. The photoproton energy distribution was obtained directly by allowing for the energy lost by each proton before it reached the surface of the emulsion and the angular distribution by dividing the observed

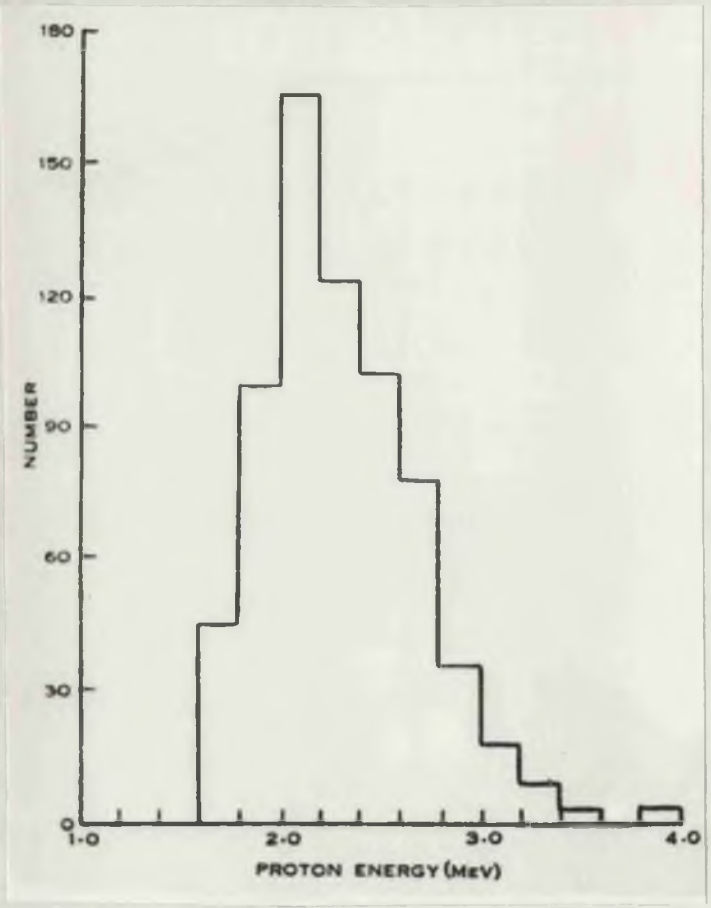

Fig. A 2.1

Energy distribution of photoprotons from nitrogen irradiated with 11.5 Mev X-rays, as measured by Spicer (Sp 53).

160b

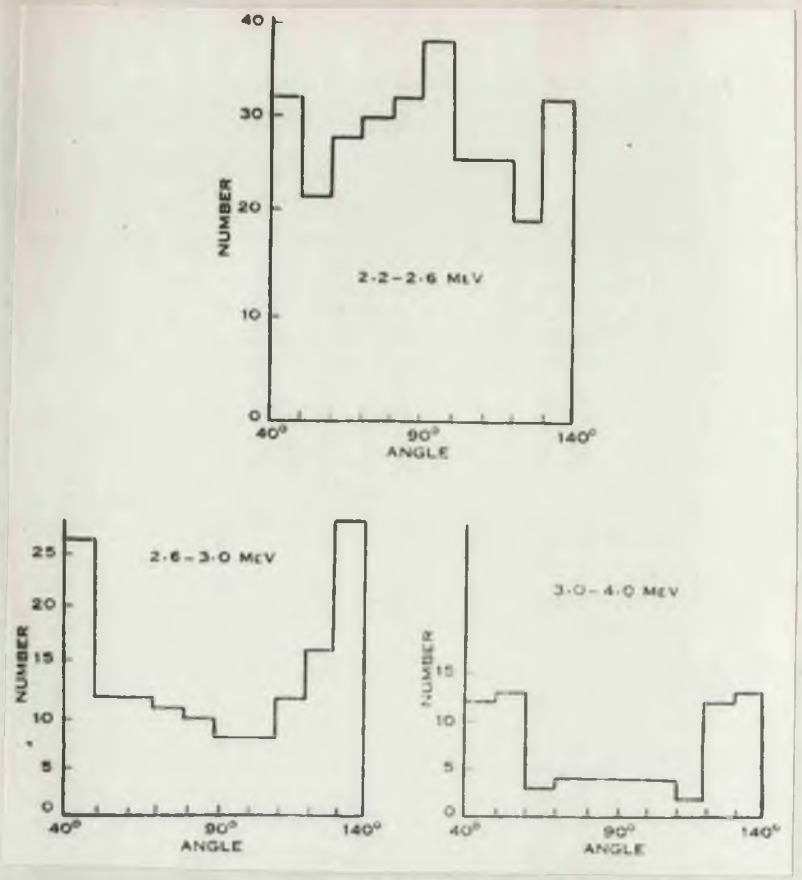

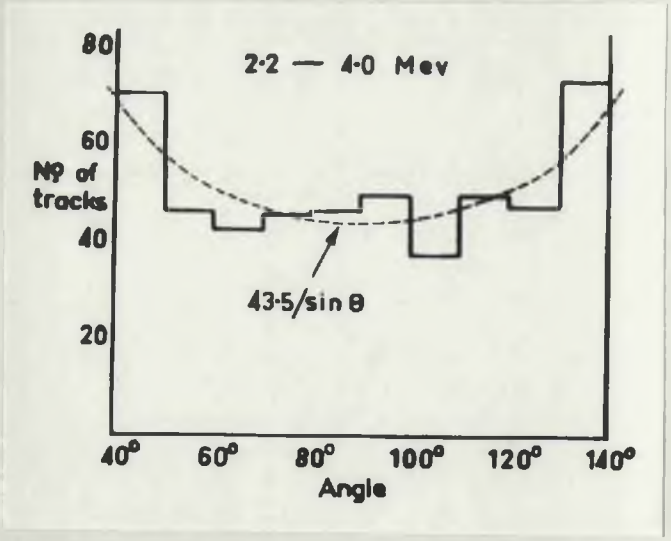

Fig. A 2.2

(a) Angular distribution of photoprotons from nitrogen as measured by Spicer.

(b) Angular distribution obtained by adding the individual distributions of fig. (a).

number of protons in a given angular interval by the appropriate geometrical factor, $\frac{1}{\langle \sin \theta \rangle_{av.}}$, where the average is over the angular interval concerned. The energy distribution is given in Fig. A2.1 and should be cut off at 2.2 Mev since protons with energy less than this may fail to reach the emulsion. The angular distributions are given in Fig. A2.2. In this energy interval the energy distribution given by the cloud chamber and predicted from the inverse reaction is a single sharp peak at a proton energy of 2.7 Mev. Because of the small number of tracks the cloud chamber experiment does not give an angular distribution for this peak; the angular distribution obtained from the inverse reaction is of the form $1 + \sin^2\theta$. Thus both Spicer's energy distribution and angular distribution are in conflict with the other experimental results which are consistent between themselves.

It is of interest to examine the form of the results which would be obtained in a nuclear emulsion experiment if the tracks measured were simply a background of short tracks uniformly distributed in angle. Since the correction for the initial energy loss is greatest at large and small angles and a minimum at 90°, tracks entering the emulsion at large and small angles will give higher values for the apparent photoproton energy than those entering at 90°. Consequently the angular distribution for low energies will be peaked at 90° while that for higher energies will peak at large and small angles. The angular distribution of all tracks will reflect the geometrical correction, i.e. be proportional to $\frac{1}{\sin \theta}$. The angular distributions obtained by Spicer (Figs. A2.2 (a) and A2.2 (b)) correspond

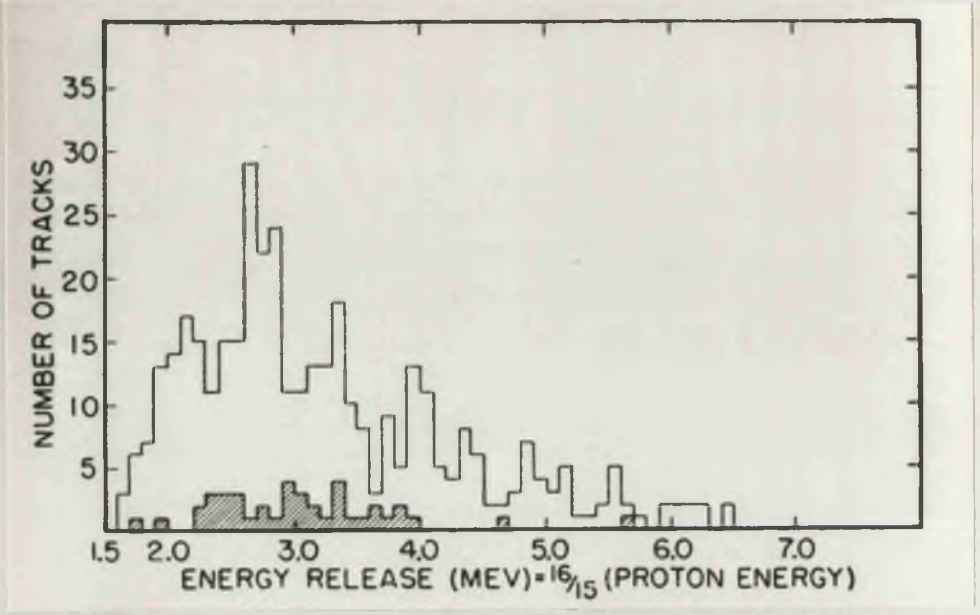

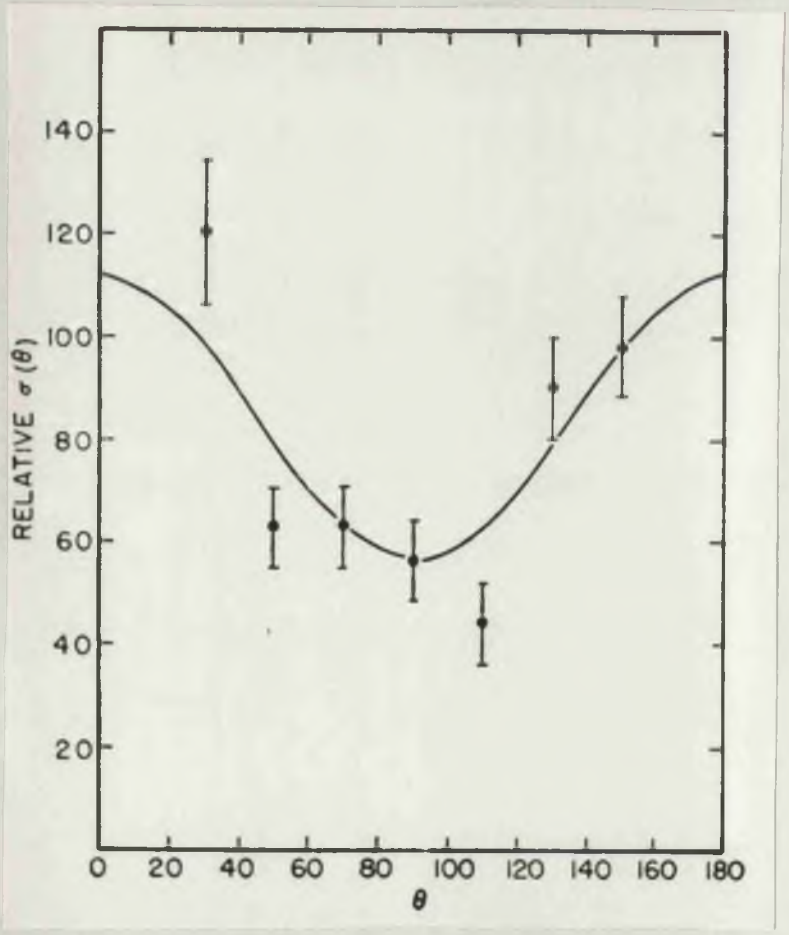

Fig. A 2.3

(a) Energy distribution of photoprotons from oxygen irradiated by 18.7 Mev X-rays as measured by Spicer (Sp 55). The background which was subtracted is indicated by the shaded histogram.

(b) The angular distribution of the photoprotons in fig. (a). The line, 56 $(1 + \cos^2\theta)$, is Spicer's fit to these points.

closely with these expectations and hence his results could be explained as a background not detected in the background run.

In a similar experiment on oxygen Spicer (Sp 55) used an essentially identical target chamber filled with oxygen at a pressure of 1 atmosphere and irradiated with 18.7 Mev X-rays. For this experiment the background was obtained by measuring tracks which entered the emulsion within the allowed range of dip angles but came from directions opposite to those of photoprotons from the irradiated volume. An important feature of this experiment is that, since the first excited state of N^{15} is at 5.28 Mev only photoprotons which leave N^{15} in the ground state can be detected. Hence the photoproton energy distribution yields directly the (γ,p) cross section and also the reaction studied is the exact inverse of the $N^{15}(p,\gamma)O^{16}$(ground state) reaction. The energy distribution found by Spicer (Fig. A2.3 (a)) has a peak at 2.7 Mev which corresponds to a peak in the (γ,p) cross section at 14.8 Mev with a maximum value of 4.8 mb. The photoproton angular distribution is given in Fig.A2.3 (b).

These results are also in conflict with other data and in particular with the $N^{15}(p,\gamma)$ cross section, which has been measured by Wilkinson and Bloom up to a proton energy of 4 Mev (Wi 57a). They find no sign of a peak at 2.8 Mev (the proton energy corresponding to E_γ = 14.8 Mev) where the cross section is less than 10% of the cross section obtained from Spicer's results using the principle of detailed balancing. A number of other workers have measured O^{16} photoproton spectra using X-rays with peak energies from 20 - 30 Mev. Their results for proton energies between

2 and 3 Mev are as follows. Milone et al. (Mi 58) detected the photoprotons from an oxygen gas target with nuclear emulsions placed directly behind the irradiated volume which gave them a large detection efficiency over a limited range of angles ($90° \leq \theta \leq 115°$). They find very few photoprotons between 2 and 3 Mev. Johansson et al. (Jo 57) used an experimental arrangement similar to Spicer's and made a careful study of the various sources of background. They find a peak at 2.2 Mev whose magnitude is only one-third that reported by Spicer. Cohen et al. (Co 56) also used an experimental arrangement similar to Spicer's and note that, "the background was estimated from experimental observations to be small ($\sim 1\%$) and of low energy (~ 2 Mev) and was therefore neglected". They find a peak at 2.4 Mev of magnitude approximately two-thirds that reported by Spicer. Both Johansson et al. and Cohen et al. find that the angular distribution for these low energy photoprotons is approximately isotropic. All three groups of workers reported very similar results for the spectrum of photoprotons above 3 Mev.

Spicer (Sp 55a) has also used the same apparatus to measure the spectrum of photoprotons from argon irradiated with 22.5 Mev X-rays. He finds a photoproton energy spectrum which is peaked at 2.6 Mev with an angular distribution of the form $0.15 + \sin^2\theta\,(1 + \cos\theta)$ which is good evidence that the particles measured were photoprotons. The photoproton yield in this experiment was 6.6×10^5 protons/mole/r. and therefore a background comparable with the photoproton yield in the oxygen experiment (4×10^4 protons/mole/r.) would have little effect on the results.

Taking all this evidence together and noting, in particular, the

close similarity between Spicer's results for both nitrogen and oxygen there seems to be no doubt that in these experiments Spicer has simply measured a background which he failed to detect in the background measurements. It seems likely that this background is present to a lesser extent in the measurements of Johansson et al. and Cohen et al. However this cannot be asserted with certainty since these results are not necessarily in conflict with the $N^{15}(p,\gamma)$ cross section measurements. Because of the higher X-ray energies it is possible that the photoproton groups reported by these workers correspond to protons which leave N^{15} in an excited state.

Although it has not been possible to identify the source(s) of this background it is probable that part of Spicer's background came from the walls of the target chamber. Lasich et al. (La 55) used the target chamber from Spicer's nitrogen experiment for a measurement of the photoproton spectrum from CF_4 irradiated with 16.5 Mev X-rays and reported that, "Preliminary runs showed that a significant number of tracks recorded came from the brass walls of the reaction chamber; accordingly the latter was lined with graphite $\frac{1}{8}$" thick". However since Johansson et al. were careful to eliminate protons from the wall of their chamber, it is likely that there are other sources of background as well.

It is concluded that nuclear emulsion measurements of photoproton spectra with moderate or low yields ($< 10^5$ protons/mole/r.) are liable to be in error at the low energy end ($E_p < 3$ Mev) and that the methods used to date to measure background are not adequate in this energy region.

Appendix III

ANALYSIS OF CLOUD CHAMBER TRACKS BY MICROSCOPE MEASUREMENT OF THE CAMERA FILMS

This appendix supplements the description of the method of analysing cloud chamber tracks used in the neon experiment given in Chapter V on p.116ff. It contains the analytical formulae used in this analysis and a description of the experimental measurements on the accuracy of the method.

1. FORMULAE FOR ANALYSING TRACK MEASUREMENTS WHEN ALL CAMERA FILM PLANES ARE HORIZONTAL

For this camera arrangement the images on all camera films are projections onto a horizontal plane. The measurements of a track image are most conveniently made by using the image of grid wires to provide fixed reference points and directions (see set of stereo photographs in Plate 13). Hence the formulae for analysing these measurements are those relating the coordinates and directions of a track to the coordinates and directions of its projections onto the plane of the grid wires from the principal points of the camera lenses.

These formulae are given below in the order and form in which they were used for the analysis of the neon results. The information required from a track measurement was

(a) the coordinates of the origin and end point,

(b) the track direction,

and (c) the track length.

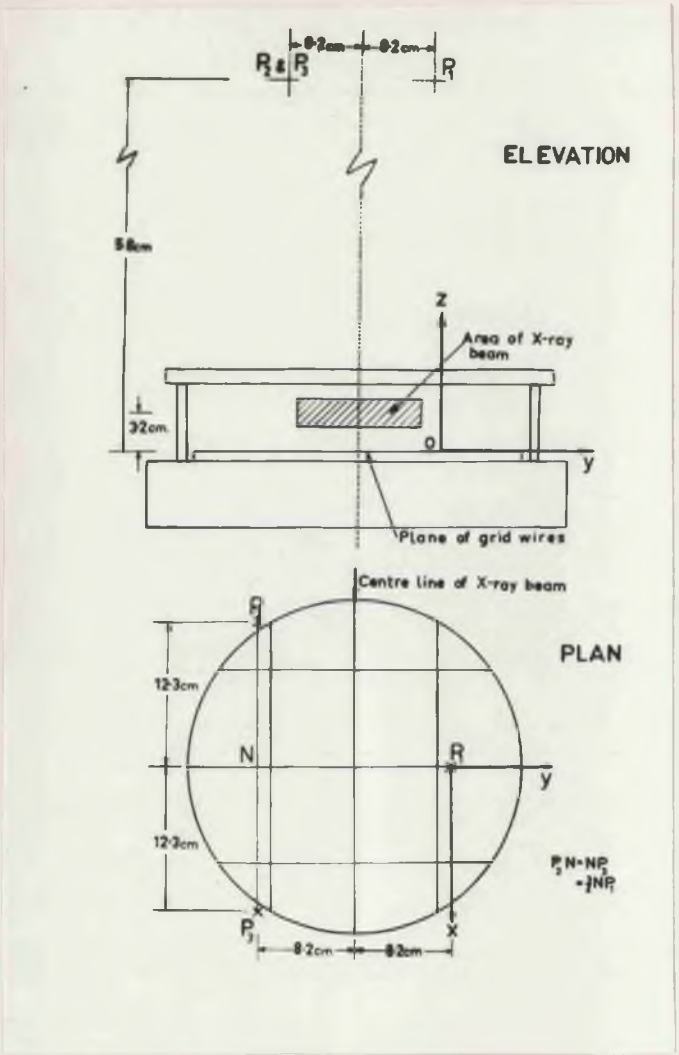

Fig. A 3.1

Arrangement of the cloud chamber cameras for the Neon experiment. P_1, P_2 and P_3 are the principal points of the camera lenses. The rectangular axes (Ox, Oy, Oz) define the coordinate system used in the analysis.

1 (a) Measurement of Track Position.

The position of any point within the chamber can be obtained with any two of the three cameras. For convenience let these be cameras 1 and 2 and use the coordinate system shown in Fig. A3.1.

Then $$x = x_1(1 - z/h) \qquad (1)$$

$$y = y_1(1 - z/h) \qquad (2)$$

$$z = \frac{h}{a}(1 - z/h)(x_2 - x_1) \qquad (3a)$$

and $$z = \frac{h}{b}(1 - z/h)(y_2 - y_1) \qquad (3b)$$

Where (x_1,y_1) and (x_2,y_2) are the (measured) projections of (x,y,z) onto the plane of the grid from P_1 and P_2, the principal points of cameras 1 and 2 respectively and h, a and b specify the positions of the two cameras since the coordinates of P_1 are (0,0,h) and of $P_2(-a,-b,h)$.

Since equations (3a) and (3b) are independent the relationship

$$(x_2 - x_1) = \frac{a}{b}(y_2 - y_1)$$

$$= \frac{3}{4}(y_2 - y_1) \text{ in the present case, was used}$$

to check the consistency of the measurements.

A best value for z was calculated using

$$z = \frac{h}{a+b}(1 - z/h)\left[(x_2 - x_1) + (y_2 - y_1)\right]$$

Since z/h is small ($< 1/10$) this was solved by calculating

$$z' = \frac{h}{a+b}\left[(x_2 - x_1) + (y_2 - y_1)\right]$$

Then $z \simeq z'(1 - z'/h)$

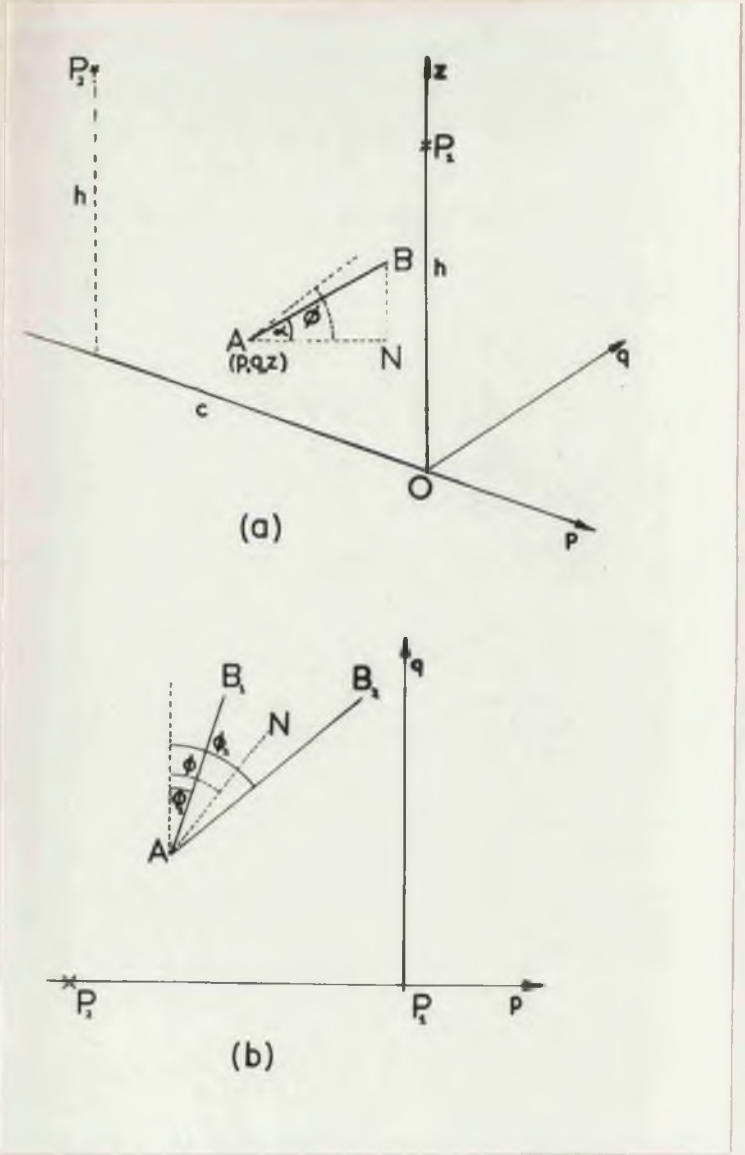

Fig. A 3.2

(a) Coordinate system used in the determination of track directions. α and ϕ specify the direction of the track in the cloud chamber. P_1 and P_2 are the principal points of the lenses of cameras 1 and 2.

(b) Projections of track AB on to the horizontal plane $Z = Z_o$ from cameras 1 and 2 respectively.

1 (b) Measurement of Track Direction.

The formulae for determining the direction of a cloud chamber track from measurements with a few cameras are most conveniently expressed in terms of a coordinate system (Op, Oq, Oz) where Oz is vertical and Op and Oq are horizontal axes in the plane of the grid wires, with Op along the line joining the two cameras.

Then α, the angle between the track and the horizontal and ϕ, the angle between Oq and the horizontal projection of the track (see Fig. A3.2(a)) are given by

$$\tan\phi = \frac{\tan\phi_1 - \frac{p}{c}(\tan\phi_1 - \tan\phi_2)}{1 - \frac{q}{c}(\tan\phi_1 - \tan\phi_2)} \qquad (4)$$

$$\tan\alpha = \frac{h-z}{c}\,\frac{\cos\phi(\tan\phi_1 - \tan\phi_2)}{1 - \frac{q}{c}(\tan\phi_1 - \tan\phi_2)} \qquad (5)$$

where ϕ_1 and ϕ_2 are the measured angles of the images in the cameras 1 and 2; (p, q, z) the coordinates of the track origin; h the height of the cameras above the grid and c, their horizontal separation (see Fig. A3.2). Clearly the values of ϕ and α are most accurately determined when ϕ_1 and ϕ_2 are small and are indeterminate when ϕ_1 or $\phi_2 = 90°$.

Hence the procedure used when calculating track directions was to select, for measurement, the films from the two cameras for which the line joining them was most nearly at right angles to the track images. The values of p, q, z, ϕ_1 and ϕ_2 appropriate to the pair of cameras chosen

were then calculated from the already determined coordinates and the measured angles and the analysis completed as above.

1 (c) Measurement of Track Lengths.

(i) By Calculation from Measured Image Lengths -

Since the coordinates and direction of a track had been determined the length of the track could be obtained from the length of the image in any one of the cameras. The formulae connecting ℓ, the length of the track with ℓ_i the length of the projections from the camera onto the plane of the grid are

$$\ell = \frac{\ell_i}{\cos\alpha} \frac{\cos\theta_i}{\cos\theta} \frac{1 - z_0/h}{1 + \frac{\tan\alpha}{\cos\theta} \frac{x_a - A_i}{h - z_a}} \qquad (6a)$$

which is useful when $\cos\theta$ is large

and

$$\ell = \frac{\ell_i}{\cos\alpha} \frac{\sin\theta_i}{\sin\theta} \frac{1 - z_0/h}{1 + \frac{\tan\alpha}{\sin\theta} \frac{y_a - B_i}{h - z_a}} \qquad (6b)$$

which is useful when $\cos\theta$ is small.

In these formulae

α is the angle between the track and the horizontal,

θ_i the angle between Ox and the track projection from the i^{th} camera,

θ the horizontal angle between Ox and the horizontal

projection of the track,

$(x_o\ y_o\ z_o)$ the coordinates of the track origin,

$(x_a\ y_a\ z_a)$ the coordinates of the track end point,

and $(A_i\ B_i\ h)$ the coordinates of P_i the principal point of the lens of the i^{th} camera.

Since h is large the value obtained for ℓ is insensitive to small changes in the track coordinates and therefore their values need only be approximate. In particular for recoil and other short tracks x_o and y_o can be used instead of x_a and y_a.

(ii) From the Length of the Shadow Cast by the Model -

To analyse a track the model was placed so that the pointer was in the same position as the origin of the track and the pointer adjusted until the shadows were at the same angles as the images in the three cameras (see Fig. 5.3, on p. 119a). The length of the track could then be obtained from the length of these shadows which were measured in the horizontal plane through the track origin. The relationship between these quantities is

$$\ell = \ell_i \frac{L}{L_i}\left[\frac{\left(1-\frac{z_a-z_o}{h-z_o}\right)\left(1-\frac{z_o}{h}\right)}{1-\frac{L\sin\alpha}{h-z_o}}\right] \qquad (7)$$

where L is the length of the pointer, and L_i the length of the shadow cast by the i^{th} camera in the plane $Z = Z_o$.

For obvious constructional reasons tracks dipping downwards

(i.e. $\alpha < 0$) were analysed with the model pointing in the reverse direction. Formula (7) applies equally to this case providing the value used for α is that appropriate to the pointer (i.e. α is always positive).

Formula (7) is derived directly from the expressions for ℓ and L in terms of the positional and angular coordinates of the track and pointer. These are

$$\ell = \ell_i \left(1 - \frac{\ell \sin\alpha}{h - z_0}\right)\left(1 - \frac{z_0}{h}\right)\Big\} \qquad \Big\}$$

where $\Big\{ \quad \Big\}$

$$= \frac{1}{\cos\alpha \sqrt{\left\{1 + 2\tan\alpha \frac{[(x_0 - A_i)\sin\theta + (y_0 - B_i)\cos\theta]}{h - z_0} + \tan^2\alpha \frac{[(x_0 - A_i)^2 + (y_0 - B_i)^2]}{(h - z_0)^2}\right\}}}$$

Similarly

$$L = L_i \left(1 - \frac{L \sin\alpha}{h - z_0}\right)\Big\} \qquad \Big\}$$

2. MEASUREMENT OF CAMERA LENS DISTORTION

The lenses used in the cameras were "Ental" enlarging lenses* of actual focal length 78 mm. and maximum aperture f/4.5. The makers claim that these lenses should cover a 60 mm. x 60 mm. plate at full aperture. The images of the cloud chamber recorded by the cameras were circles 4.8 cm. in diameter. For the camera arrangement used in the Nitrogen experiment these images were centered on the lens axes. For the

*Manufactured by Taylor, Taylor and Hobson.

Table A3.1

Maximum Errors due to Distortion at Various Distances from the Lens Axis

Distance from Lens Axis cm.	Maximum Error in Angle	Maximum Error in Magnification	Upper Limit to Error in Coordinates	
			On Film mm.	Equivalent distance in Chamber mm.
2.4	-	0.04%	0.003	0.02
3	1/60°	0.15%	0.015	0.09
3.5	1/20°	0.5%	0.06	0.4
4	1/10°	1.3%	0.18	1.1
4.5	1/4°	2.8%	0.4	2.4

Neon experiment the centre of the image was displaced from the axis by 1.4 cm. for camera 1 and 2.4 cm. for cameras 2 and 3 (i.e. the furthest edges of these images were 3.8 cm. and 4.8 cm. respectively from the lens axis).

The lenses were tested by photographing a straight edge and showed measurable barrel distortion when the perpendicular distance from axis to image was greater than 2.4 cm. This type of distortion is produced by the displacement of the image inwards from its ideal position by an amount which increases with d, the distance from the axis.

This displacement will produce an error in the coordinates deduced from the position of the image and will also lead to the following errors in the other quantities measured in the analysis. An error in angle which will be zero for a track image at right angles to the radius from the axis or along this radius and have a maximum at some angle between these. An error in magnification (i.e. track length) which will be a maximum for a track along the radius and very nearly zero for a track at right angles to the radius. Maximum values for these errors were deduced from the measured radii of curvature of the straight line images and are given in Table A3.1. For these measurements the lens aperture was set to f/11, the maximum aperture used in this experiment. For larger apertures the errors due to distortion are slightly greater. The errors in magnification and coordinates were deduced assuming that, as stated in optics text-books, the image displacement is proportional to d^3, although, from the observed dependence of the barrel distortion on d, the image

displacement varied as some higher power of the distance. In consequence the formulae used overestimated the image displacement but gave a good estimate of the error in magnification. No attempt was made to obtain more exact figures since these estimates showed that the lenses could be used satisfactorily.

Table A3.1 shows that the errors due to distortion were quite negligible over most of the area covered by the cloud chamber images. For angular measurements the errors due to distortion were always less than the errors from other sources. As expected all errors increased rapidly with distance from the axis and as a result the errors in magnification and coordinates were significant at the edge of the image for cameras 2 and 3. However for any point in the cloud chamber these distortion errors were only large for one of the three camera images. Since only two cameras were required for coordinate and length determinations all errors were avoided by using camera 1 and the most appropriate of either cameras 2 or 3 for these measurements.

It is worth noting that the makers claim that the lenses will cover a plate 60 mm. x 60 mm. allows for some distortion at the corners of the image and cannot be taken to mean that the lenses are completely satisfactory for cloud chamber measurements out to a distance of 4.5 cm.

3. NOTES ON THE ACCURACY OF THE MICROSCOPE MEASUREMENTS

The microscopes used for measuring the films were of standard design and were fitted with standard moveable stages and goniometer heads. Objectives and eyepiece magnifications were x 2.75 and

Table A3.2

Errors in Microscope Measurements

Quantity Measured	Error on Film	Equivalent Error in Chamber	Error due to Track Quality*
Position Within Chamber			
Horizontal Coord.	1/20 mm.	1/3 mm.	1/10 mm.
Vertical Coord.	-	1 mm.	1/3 mm.
Track Direction			
Projected Angle	1/3°	1/3°	
Vertical Angle	1°	1°	
Track Length			
Tracks shorter than 2.5 cm.	1/60 mm.	0.1 mm.	0.1 mm.
Tracks longer than 2.5 cm.	1/12 mm.	0.5 mm.	0.1 mm.

*Expressed as equivalent error in chamber.

x 7 respectively.

The accuracy of the measurements made with this equipment can be seen from the errors given in Table A3.2. For short tracks these measurements take full advantage of the track quality. For longer tracks the accuracy is a little less than the track quality limit but is always as good as the accuracy obtained by reprojection. For longer tracks the accuracy of the energy determination is limited by range straggling rather than by the length measurements and hence for this experiment nothing would have been gained from the slightly greater accuracy with improved equipment. The factors affecting the accuracy are discussed in the following notes.

(i) Position Measurements.

Positions in the cloud chamber were determined by using the moveable stage to measure the distances between the images of track and grid wires. The movement of the stage and the track quality enabled the eyepiece cross wires to be set on the image of the track origin (for example) with an accuracy of 1/60 mm. but the verniers with which the stage was fitted only gave its position to the nearest 1/20 mm.

(ii) Angle Measurements.

Tests on proton tracks and straight lines ruled on the film showed that the consistency of setting the goniometer head was 1/3°. Most of this error came from flexing of the microscope mounting.

(iii) Length Measurements.

For track images shorter than the diameter of the

microscope field of view (slightly larger than 4 mm. and equivalent to 2.5 cm. in the chamber), the error in image length is 1/60 mm. for proton and α tracks and probably slightly more for recoil tracks. The figure quoted for longer lengths assumes that these were computed from coordinates of the end points.

REFERENCES

Ar 50 H. V. Argo et al., Phys. Rev. 78, 691 (1950).

Aj 59 F. Ajzenberg-Selove & T. Lauritsen, Nuclear Physics 11, 1 (1959).

Ba 48 G. C. Baldwin & G. S. Klaiber, Phys. Rev. 73, 1156 (1948).

Ba 57 F. C. Barker & A. K. Mann, Phil. Mag. 2, 5 (1957).

Be 46 H. A. Bethe, Phys. Rev. 70, 821 (1946).

Bl 22 P. M. S. Blackett, Proc. Roy. Soc. A 102, 294 (1922).

Bl 23 P. M. S. Blackett, Proc. Roy. Soc. A 103, 62 (1923).

Bl 25 P. M. S. Blackett, Proc. Roy. Soc. A 107, 349 (1925).

Bl 50 W. Blocker et al., Phys. Rev. 79, 419 (1950).

Bl 52 J. M. Blatt & V. F. Weisskopf, Theoretical Nuclear Physics (John Wiley and Sons, 1952).

Br 56 C. P. Browne & J. R. Lamarsh, Phys. Rev. 104, 1099 (1956).

Br 57 B. R. Bransden et al., Phil. Mag. 2, 1211 (1957).

By 51 P. R. Byerly & W. E. Stephens, Phys. Rev. 81, 473 (L) (1951).

By 51a P. R. Byerly & W. E. Stephens, Phys. Rev. 83, 54 (1951).

Ch 37 J. Chadwick, W. Feather & E. Bretscher, Proc. Roy. Soc. A 163, 366 (1937).

Ch 57 I. V. Chuvilo & V. G. Shevchenko, J. Exptl. Theor. Phys. (U.S.S.R.) 32, 1335(1957).

Ch 58 I. V. Chuvilo & V. G. Shevchenko, J. Exptl. Theor. Phys. (U.S.S.R.) 34, 593 (1958).

Co 51 E. D. Courant, Phys. Rev. 82, 703 (1951).

Co 56 L. Cohen et al., Phys. Rev. 104, 108 (1956).

De 48 A. J. Dempster, Phys. Rev. 74, 1225(a) (1948).

De 55 G. DeSaussure & L. S. Osborne, Phys. Rev. 99, 843 (1955).

Di 50 B. C. Diven & G. M. Almy, Phys. Rev. 80, 407 (1950).

Du 50 H. E. Duckworth et al., Phys. Rev. 79, 188 (1950).

Du 50a R. B. Duffield et al., Phys. Rev. 79, 1011 (L) (1950).

Ey 51 L. Eyges, Phys. Rev. 81, 981 (1951).

Fe 54 G. A. Ferguson et al., Phys. Rev. 95, 776 (1954).

Fl 51 B. H. Flowers & F. Mandl, Proc. Roy. Soc. A 206, 131 (1951)

Fo 48 W. A. Fowler et al., Rev. Mod. Phys. 20, 236 (1948).

Fo 49 W. A. Fowler et al., Phys. Rev. 76, 1767 (1949).

Fu 54 E. G. Fuller, Phys. Rev. 96, 1306 (1954).

Ga 49 E. R. Gaerttner & M. L. Yeater, Rev. Sci. Inst. 20, 588 (1949).

Ga 50a E. R. Gaerttner & M. L. Yeater, Phys. Rev. 77, 570 (L) (1950).

Ga 50b E. R. Gaerttner & M. L. Yeater, Phys. Rev. 77, 714 (L) (1950).

Ga 50c E. R. Gaerttner & M. L. Yeater, Phys. Rev. 79, 401 (L) (1950).

Ga 51a E. R. Gaerttner & M. L. Yeater, Phys. Rev. 82, 461 (L) (1951).

Ga 51b E. R. Gaerttner & M. L. Yeater, Phys. Rev. 83, 146 (1951).

Ge 53 M. Gell-Mann & V. L. Telegdi, Phys. Rev. 91, 169 (1953).

Ge 54 W. Gentner, H. Maier-Leibnitz and W. Bothe, "An Atlas of Typical Expansion Chamber Photographs", p. 122-125 (Pergamon Press, 1954).

Gh 50 S. N. Ghoshal, Phys. Rev. 80, 939 (1950).

Go 48 M. Goldhaber & E. Teller, Phys. Rev. 74, 1046 (1948).

Go 49 F. K. Goward, E. W. Titterton & J. J. Wilkins, Proc. Phys. Soc. A 62, 460 (1949).

Go 50 F. K. Goward, V. L. Telegdi & J. J. Wilkins, Proc. Phys. Soc. A 63, 402 (1950).

Go 50a F. K. Goward & J. J. Wilkins, Proc. Phys. Soc. A 63, 1171 (1950).

Go 50b F. K. Goward et al., Proc. Phys. Soc. A 63, 172 (L) (1950).

Go 51 F. K. Goward & J. J. Wilkins, Proc. Phys. Soc. A 64, 94 (1951).

Go 51a F. K. Goward & J. J. Wilkins, Proc. Phys. Soc. A 64, 313 (L) (1951).

Go 53 F. K. Goward & J. J. Wilkins, Proc. Roy. Soc. A 217, 357 (1953).

Go 55 F. K. Goward & J. J. Wilkins, Proc. Roy. Soc. A 228, 376 (1955).

Go 55a E. L. Goldwasser & V. O. Nicolai, "Conference on Recent Developments in Cloud Chamber and Associated Techniques", p. 152 (Ed. M. Morris & M. J. Duff - University College, London, 1955).

Go 55b H. E. Gove & E. G. Paul, Phys. Rev. 97, 104 (1955).

Go 56 E. L. Goldwasser & L. J. Kaester, Nuovo Cimento Supl. 4, 950 (1956).

Go 57 A. N. Gorbunov & V. M. Spiridonov, J. Exptl. Theor. Phys. (U.S.S.R.) 33, 21 (1957).

Go 58a A. N. Gorbunov & V. M. Spiridonov, J. Exptl. Theor. Phys. (U.S.S.R.) 34, 862 (1958).

Go 58b A. N. Gorbunov & V. M. Spiridonov, J. Exptl. Theor. Phys. (U.S.S.R.) 34, 866 (1958).

Gr 58 G. M. Griffiths, Proc. Phys. Soc. 72, 337 (1958).

Gu 51 J. C. Gunn & J. Irving, Phil. Mag. 42, 1353 (1951).

Ha 47 A. O. Hanson & J. L. McKibben, Phys. Rev. 72, 673 (1947).

Ha 48 H. Hanni et al., Helv. Phys. Acta 21, 203 (1948).

Ha 51 J. Halpern & A. K. Mann, Phys. Rev. 83, 370 (1951).

Ha 51a R. N. H. Haslam et al., Phys. Rev. 81, 479 (L) (1951).

Ha 51b R. N. H. Haslam et al., Phys. Rev. 83, 886 (A) (1951).

Ha 51c R. N. H. Haslam et al., Phys. Rev. 82, 270 (L) (1951).

Ha 59 S. S. Hanna & Luise Meyer-Schützmeister, Phys. Rev. 115, 986 (1959).

Ha 59a H. J. Hay & J. B. Warren, Can. J. Phys. 37, 1153 (1959).

He 51 J. Heidmann & H. A. Bethe, Phys. Rev. 84, 274 (1951).

Hi 47 O. Hirzel & H. Wäffler, Helv. Phys. Acta 20, 373 (1947).

Ho 51 R. J. Horsley et al., Phys. Rev. 83, 886 (A) (1950).

Ho 52 R. J. Horsley et al., Can. J. Phys. 30, 159 (1952).

Hu 43 O. Huber et al., Helv. Phys. Acta 16, 33 (1943).

Hu 44 O. Huber et al., Helv. Phys. Acta 17, 195 (1944).

Hu 53 T. Huus & R. B. Day, Phys. Rev. 97, 104 (1953).

Ia 58 I. P. Iavor, J. Exptl. Theor. Phys. (U.S.S.R.) 34, 1420 (1958).

Je 48 P. Jensen, Naturwiss. 35, 190 (1948).

Je 50 J. H. D. Jensen & P. Jensen, Z. Naturforsch. 5a, 343 (1950).

Jo 50 H. E. Johns et al., Phys. Rev. 80, 1062 (1950).

Jo 55 E. J. Jones, Proceedings Glasgow Conference on Nuclear and Meson Physics, p. 151 (Pergamon Press, 1955).

Jo 57 S. A. E. Johansson & B. Forkman, Arkiv för Fysik 12, 359 (1957).

Ka 51 L. Katz & A. G. W. Cameron, Can. J. Phys. 29, 518 (1951).

Ka 51a L. Katz et al., Phys. Rev. 83, 892 (A) (1951).

Ka 51b L. Katz & A. S. Penfold, Phys. Rev. 81, 815 (1951). Erratum, Phys. Rev. 83, 169 (L) (1951).

Ka 51c L. Katz et al., Phys. Rev. 82, 271 (L) (1951).

Ka 54 L. Katz et al., Phys. Rev. 95, 464 (1954).

Ka 60 E. Kashy et al., Bull. Am. Phys. Soc. 5, 108 (1960).

Ke 51 D. W. Kerst & G. A. Price, Phys. Rev. 79, 725 (L) (1951).

Ko 48 H. W. Koch & C. S. Robinson, Rev. Sci. Inst. 19, 36 (1948).

Ko 50 H. W. Koch & R. E. Carter, Phys. Rev. 77, 165 (1950).

Ko 51 H. W. Koch et al., Phys. Rev. 81, 318 (A) (1951).

Ko 57 A. P. Komar & I. P. Iavor, J. Exptl. Theor. Phys. (U.S.S.R.) 32, 614 (1957).

Kr 52 N. M. Kroll & L. L. Foldy, Phys. Rev. 88, 1177 (1952).

La 55 W. B. Lasich et al., Aust. J. Phys. 8, 456 (1955).

Le 50 J. S. Levinger & H. A. Bethe, Phys. Rev. 78, 115 (1950).

Le 51 J. S. Levinger, Phys. Rev. 84, 43 (1951).

Li 56 D. L. Livesey, Can. J. Phys. 34, 216 (1956).

Li 58 D. L. Livesey & I. G. Main, Nuovo Cimento 10, 590 (1958).

Ma 51 L. Marshall, Phys. Rev. 83, 345 (1951).

Ma 51a L. Marshall et al., Phys. Rev. 83, 305 (1951).

Ma 51c A. K. Mann & J. Halpern, Phys. Rev. 82, 733 (1951).

Ma 51d L. Marquez, Phys. Rev. 81, 877 (L) (1951).

Ma 56 A. K. Mann & E. W. Titterton, Proc. Phys. Soc. A 69, 917 (1956).

Ma 58 V. N. Maikov, J. Exptl. Theor. Phys. (U.S.S.R.) 34, 1406 (1958).

Mc 49 J. McElhinney et al., Phys. Rev. 75, 542 (1949).

Mi 58 C. Milone et al., Nuovo Cimento 7, 729 (1958).

Mo 51 R. Montalbetti et al., Phys. Rev. 83, 892 (A) (1951).

Mo 58 C. D. Moak et al., Phys. Rev. 110, 1369 (1958).

Ni 54 V. O. Nicolai & E. L. Goldwasser, Phys. Rev. 94, 755 (A) (1954).

Op 58 T. R. Ophel & I. F. Wright, Proc. Phys. Soc. 71, 389 (1958).

Op 58a T. R. Ophel, Proc. Phys. Soc. 72, 321 (1958).

Pa 58 F. Palit & E. H. Bellamy, Proc. Phys. Soc 72, 880 (1958).

Pe 48 M. L. Perlman & G. Friedlander, Phys. Rev. 74, 442 (1948).

Pe 49 M. L. Perlman, Phys. Rev. 75, 988 (L) (1949).

Pe 55 J. E. Perry & S. J. Bame, Phys. Rev. 99, 1368 (1955).

Pe 59 A. S. Penfeld & E. L. Garwin, Phys. Rev. 116, 120 (1959).

Ph 50 J. A. Phillips et al., Phys. Rev. 80, 326 (1950).

Po 40 E. Pollard, Phys. Rev. 57, 1186 (1940).

Po 51 W. M. Powell et al., Phys. Rev. 81, 213 (1951).

Pr 50 G. A. Price & D. W. Kerst, Phys. Rev. 77, 806 (1950).

Ra 52 L. A. Radicati, Phys. Rev. 87, 521 (L) (1952).

Re 56 J. M. Reid et al., Physica 22, 1142 (A) (1956).

Re 56a C. W. Reich et al., Phys. Rev. 104, 143 (1956).

Re 60 J. M. Reid & R. M. Turnbull, Unpublished results - reported to the Karlsruhe Photonuclear Conference (1960).

Sc 48 L. I. Schiff, Phys. Rev. 73, 1311 (1948).

Sc 51 L. I. Schiff, Phys. Rev. 83, 252 (1951).

Se 52 J. D. Seagrave, Phys. Rev. 85, 197 (1952).

Si 54 R. M. Sinclair, Phys. Rev. 93, 1082 (1954).

Sp 53 B. M. Spicer, Aust. J. Phys. 6, 391 (1953).

Sp 55 B. M. Spicer, Phys. Rev. 99, 33 (1955).

Sp 55a B. M. Spicer, Phys. Rev. 100, 791 (1955).

St 50 H. Steinwedel et al., Phys. Rev. 79, 1019 (L) (1950).

St 50a H. Steinwedel & J. H. D. Jensen, Z. Naturforsch. 5a, 413 (1950).

St 51 K. Strauch, Phys. Rev. 81, 973 (1951).

St 51a M. B. Stearns & B. D. McDaniel, Phys. Rev. 82, 450 (L) (1951).

St 51b W. E. Stephens et al., Phys. Rev. 82, 511 (1951).

Sv 56 N. Svantesson, Bull. Am. Phys. Soc. 1, 28 (1956).

Te 50 V. L. Telegdi & W. Zunti, Helv. Phys. Acta 23, 745 (1950).

Te 51 K. M. Terwilliger et al., Phys. Rev. 82, 820 (1951).

Te 51a V. L. Telegdi, Phys. Rev. 84, 600 (L) (1951).

Ti 50 E. W. Titterton, Proceedings Harwell Conference, p. 65 (1950).

Ti 50a E. W. Titterton, Proc. Phys. Soc. A 63, 915 (L) (1950).

Ti 51 E. W. Titterton & T. A. Brinkley, Proc. Phys. Soc. A 64, 212 (L) (1951).

Ti 53 E. W. Titterton & T. A. Brinkley, Proc. Phys. Soc. A 66, 194 (1953).

Ti 55 E. W. Titterton, Progress in Nuclear Physics 4, 1 (1955).

To 51 M. E. Toms & W. E. Stephens, Phys. Rev. 82, 709 (1951).

Wa 48 H. Wäffler & O. Hirzel, Helv. Phys. Acta 21, 200 (1948).

Wh 58 C. Whitehead et al., Phys. Rev. 110, 941 (1958).

Wi 37 E. Wigner, Phys. Rev. 51, 106 (1937).

Wi 50 J. J. Wilkins & F. K. Goward, Proc. Phys. Soc. A 63, 1173 (L) (1950).

Wi 51 J. G. Wilson, The Principles of Cloud Chamber Technique, (C. U. P., 1951).

Wi 51a J. J. Wilkins & F. K. Goward, Proc. Phys. Soc. A 64, 201 (1951).

Wi 51b J. J. Wilkins & F. K. Goward, Proc. Phys. Soc. A 64, 1056 (1951).

Wi 51c D. H. Wilkinson & J. H. Carver, Phys. Rev. 83, 466 (L) (1951).

Wi 53 J. J. Wilkins & F. K. Goward, Proc. Phys. Soc. A 66, 661 (1953).

Wi 56 D. H. Wilkinson, Physica 22, 1039 (1956).

Wi 57 H. B. Willard et al., Phys. Rev. 105, 202 (1957).

Wi 57a D. H. Wilkinson & S. D. Bloom, Phys. Rev. 105, 683 (1957).

Wo 53 H. H. Woodbury et al., Phys. Rev. 92, 1199 (1953).

A CLOUD CHAMBER INVESTIGATION OF PHOTONUCLEAR REACTIONS IN LIGHT NUCLEI

I. F. Wright

SUMMARY

This thesis describes a series of experiments in which a number of photonuclear reactions in light nuclei were studied by passing the X-ray beam from a 23 Mev electron synchrotron through a Wilson cloud chamber. These experiments, which were carried out between 1950 and 1955, were among the first to use this method. Consequently the thesis deals with the results on these reactions and with the information obtained on cloud chamber technique.

The first chapter of the thesis contains a comprehensive review of the results of photonuclear experiments prior to this investigation. This review shows that most of these results were for (γ,n) reactions and that there was a need for further results on other reactions. It is noted that a study of photonuclear reactions in light nuclei would probably be of greatest value and that the cloud chamber method should provide more comprehensive information than other methods. The experiments chosen studied the $He^4(\gamma,p)$ reaction, a number of photonuclear reactions in N^{14} and the (γ,α), $(\gamma,2\alpha)$ and $(\gamma,\alpha p)$ reactions in Ne^{20}.

The information obtained on the $He^4(\gamma,p)$ reaction was limited since the peak energy of the synchrotron was only

3 Mev above the threshold for the reaction. However this experiment showed that the $He^4(\gamma,p)$ cross section in this energy region is approximately one-tenth of the value deduced from the first measurement of the cross section for the inverse reaction, $H^3(p,\gamma)He^4$. This lower cross section has been confirmed by subsequent measurements of both the $He^4(\gamma,p)$ and $H^3(p,\gamma)$ cross sections. In the measurements on N^{14} the (γ,p), (γ,pn), (γ,α), $(\gamma,2\alpha)$ and $(\gamma,\alpha p)$ reactions were studied. The range distribution of protons of energy up to 3 Mev shows sharp well-defined peaks at energies of 0.51, 1.63 and 2.92 Mev. These energies correspond closely to the energies of the resonances reported for the $C^{13}(p,\gamma)N^{14}$ (ground state) reaction. For these resonances the ratios of the cross sections for the (γ,p) and (p,γ) reactions are in good agreement with the predictions of the principle of detailed balancing. At higher energies the following measurements were made: (i) the (γ,p) process was investigated by measuring the range distribution of the C^{13} nuclei, (ii) both (γ,p) and (γ,pn) processes were studied by measuring the numbers of events at three different synchrotron peak energies. These measurements showed that both the (γ,p) and (γ,pn) cross sections are small at energies up to 15 Mev and large in the neighbourhood of 20 Mev. The estimated values of the integrated cross sections up to 23 Mev for the (γ,p) and the (γ,pn) reactions are both approximately 0.02 Mev-barn. The (γ,α), $(\gamma,2\alpha)$ and $(\gamma,\alpha p)$ cross sections are each about

0.1 millibarn. In addition this experiment shows that the cross sections for $N^{14}(\gamma,n)$ disintegrations leaving N^{13} in the levels at 2.36, (3.51 and 3.56), 6.91 and 7.42 Mev could be determined from an analysis of (γ,pn) events. Although the conditions of the present experiment did not permit a full analysis of these events, upper limits were obtained for the numbers of (γ,n) disintegrations leaving N^{13} in the 2.36, (3.51 and 3.56) and 6.91 Mev levels.

The following results were obtained for the (γ,α), $(\gamma,2\alpha)$ and $(\gamma,\alpha p)$ reactions in Ne^{20}. For a large proportion of the (γ,α) events the total energy of the α-particle and recoil is less than 5 Mev. If these low energy events are attributed to the $Ne^{20}(\gamma,\alpha)O^{16}$ (ground state) reaction then the cross section for this reaction, integrated up to 10 Mev, is approximately 0.3 Mev-millibarn. For quantum energies in the vicinity of 20 Mev, the average cross sections are: (γ,α) reaction, less than 0.1 millibarn; $(\gamma,2\alpha)$ reaction, approximately 0.5 millibarn and $(\gamma,\alpha p)$ reaction, approximately 1 millibarn. If the $(\gamma,2\alpha)$ and $(\gamma,\alpha p)$ stars are assumed to be due to (γ,α) and (γ,p) disintegrations leaving O^{16} and F^{19} in highly excited states then, an analysis of these stars shows that: (i) a number of O^{16} and F^{19} levels are involved and (ii) for at least one-third of the $(\gamma,2\alpha)$ stars the initial (γ,α) disintegration must leave O^{16} in excited states below the first level with an isotopic spin of one. Since the number of stars available for analysis was limited, it is not possible to identify any O^{16} or F^{19}

levels and so confirm the above assumption. These results are compatible with, although they do not prove, the predictions of the isotopic spin selection rules for (γ,α) reactions in Ne^{20}.

In obtaining these results it was shown that the cloud chamber method gives very accurate results for the energy region in which the energies of the protons and α-particles can be determined from range measurements and further that the tracks of the recoil nuclei can be measured with a total error which is only slightly greater than the unavoidable error due to range straggling and multiple scattering. The thesis contains a description of the method developed to measure the lengths and directions of these tracks which were from 0.3 to 6 mm long.

The potential of the cloud chamber method is discussed in a concluding chapter which lists a number of experiments for which its use is either necessary or desirable. In particular it is noted that an investigation of star-producing reactions could be of considerable value.

ATLAS OF CLOUD CHAMBER PHOTOGRAPHS

to accompany

A CLOUD CHAMBER INVESTIGATION OF PHOTONUCLEAR REACTIONS IN LIGHT NUCLEI

Ph.D. Thesis

submitted to

The University of Glasgow

I. F. Wright

March 1961

PLATE 1.

Helium Experiment.

$He^4(\gamma,p)$ disintegration. The triton stops within the illuminated region and the proton passes out of it.

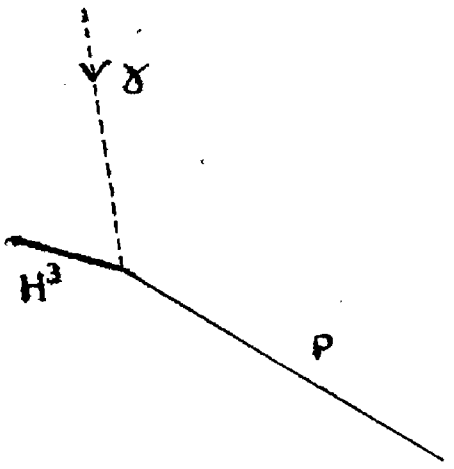

Expansion Chamber Conditions:- Gas filling (chamber expanded) 140 cm. helium + approx. 16 cm. nitrogen and air + water. Clearing field left on during expansion. X-ray beam 5.8 cm. wide x 4.6 cm. high enters chamber through 1/4" thick glass wall.

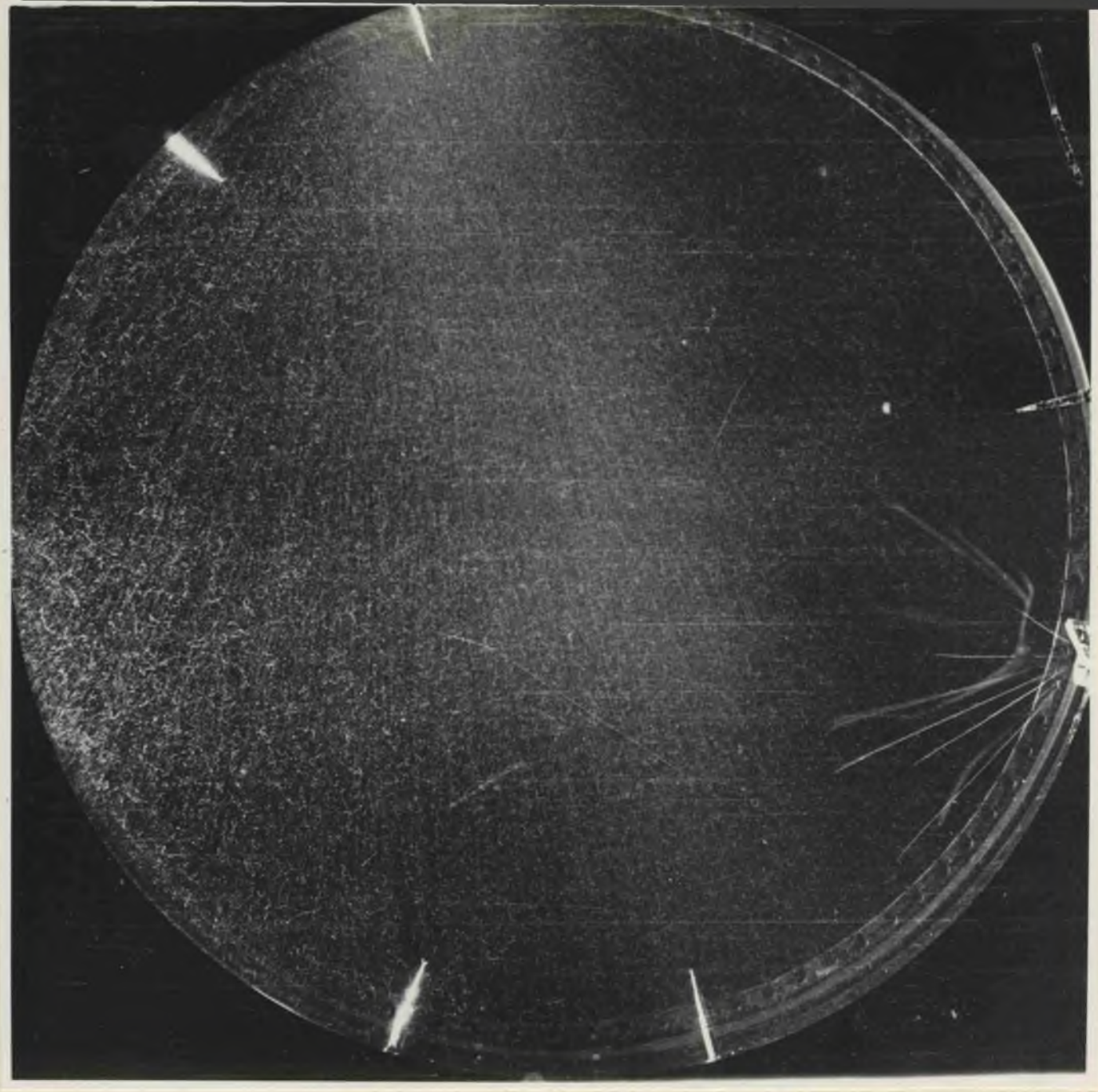

Top Camera

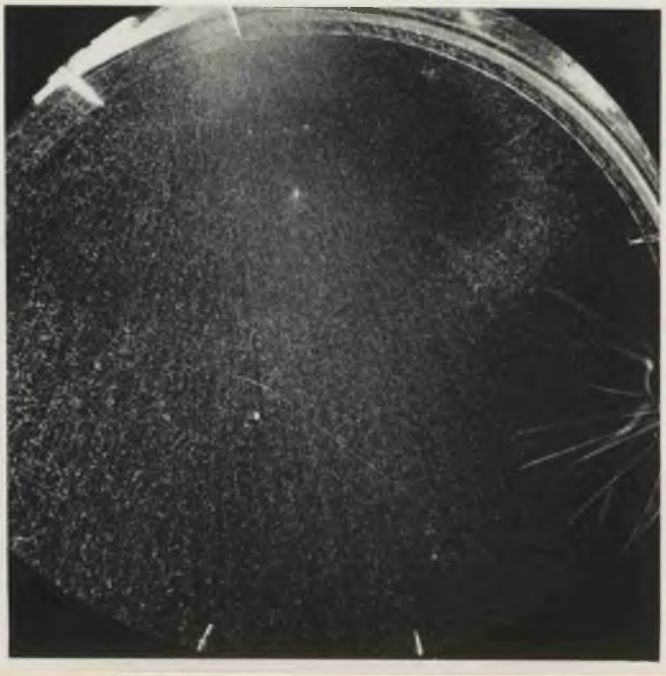

Side Camera

Plate 1

PLATE 2.

Helium Experiment.

$O^{16}(\gamma,\alpha)$ disintegration. The C^{12} recoil stops within and the alpha particle passes out of the illuminated region.

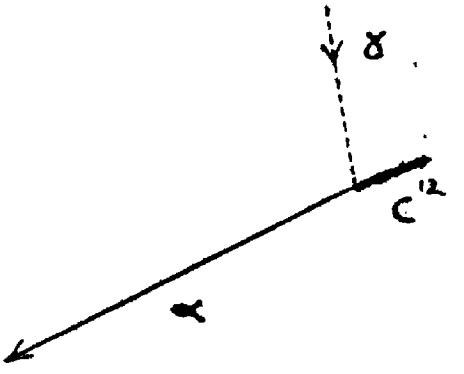

Expansion Chamber Conditions:- As for Plate 1.

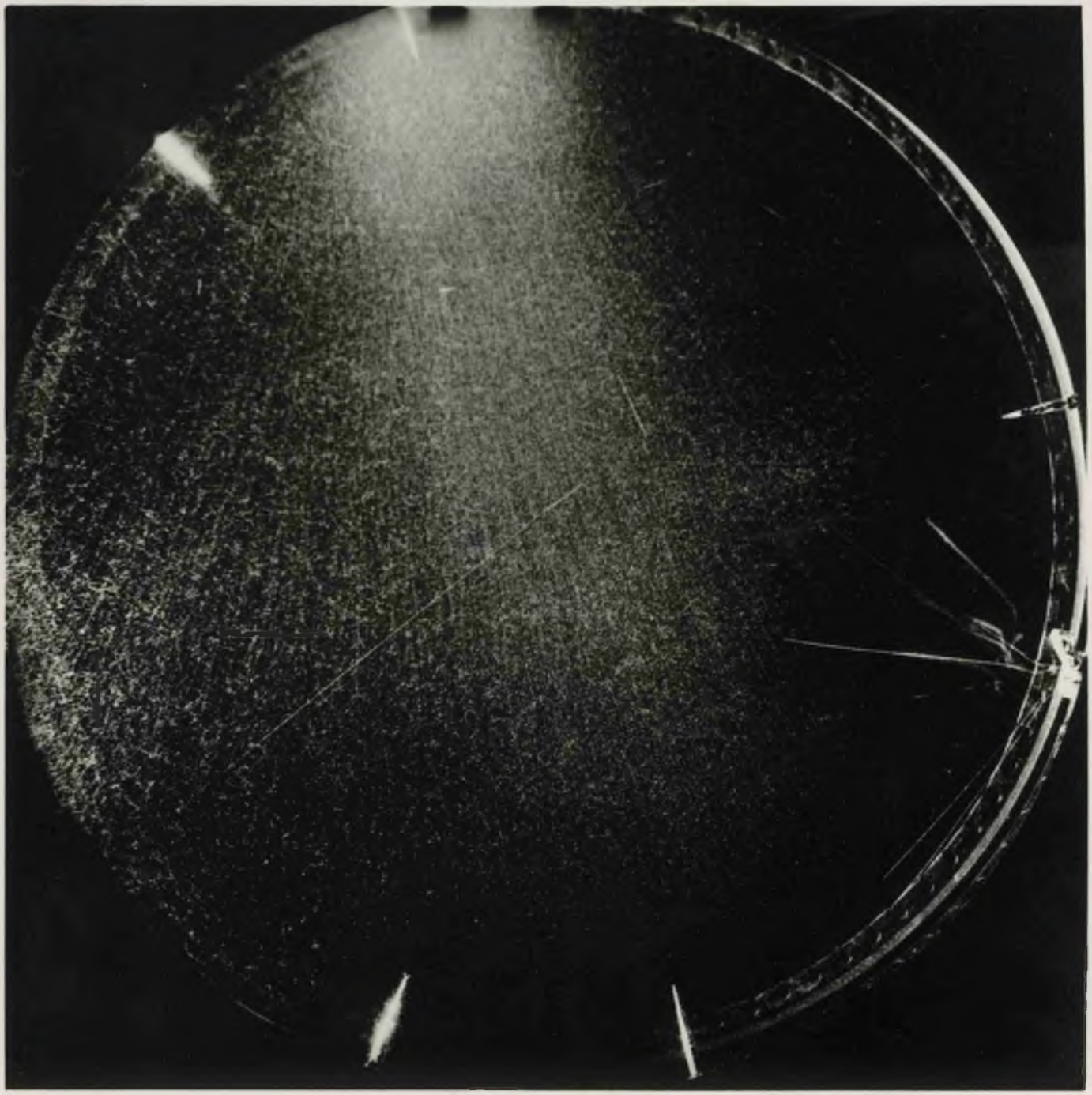

Plate 2

PLATE 3.

Helium Experiment.

Photograph showing two $N^{14}(\gamma,pn)$ disintegrations.

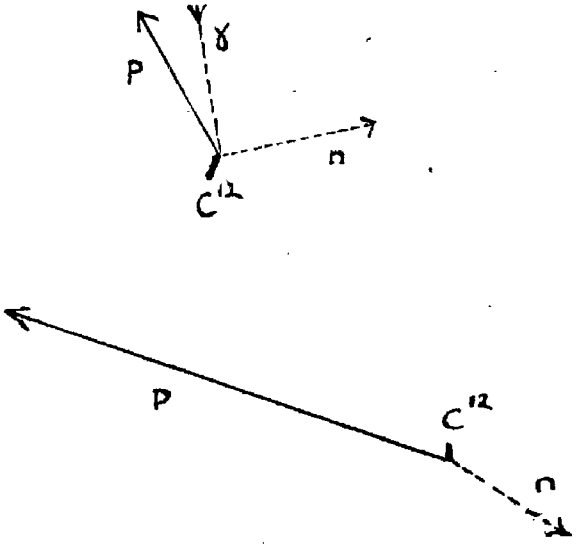

Note: Since the neutron and proton are emitted in nearly opposite directions the C^{12} recoil has very little energy.

Expansion Chamber Conditions:- As for Plate 1.

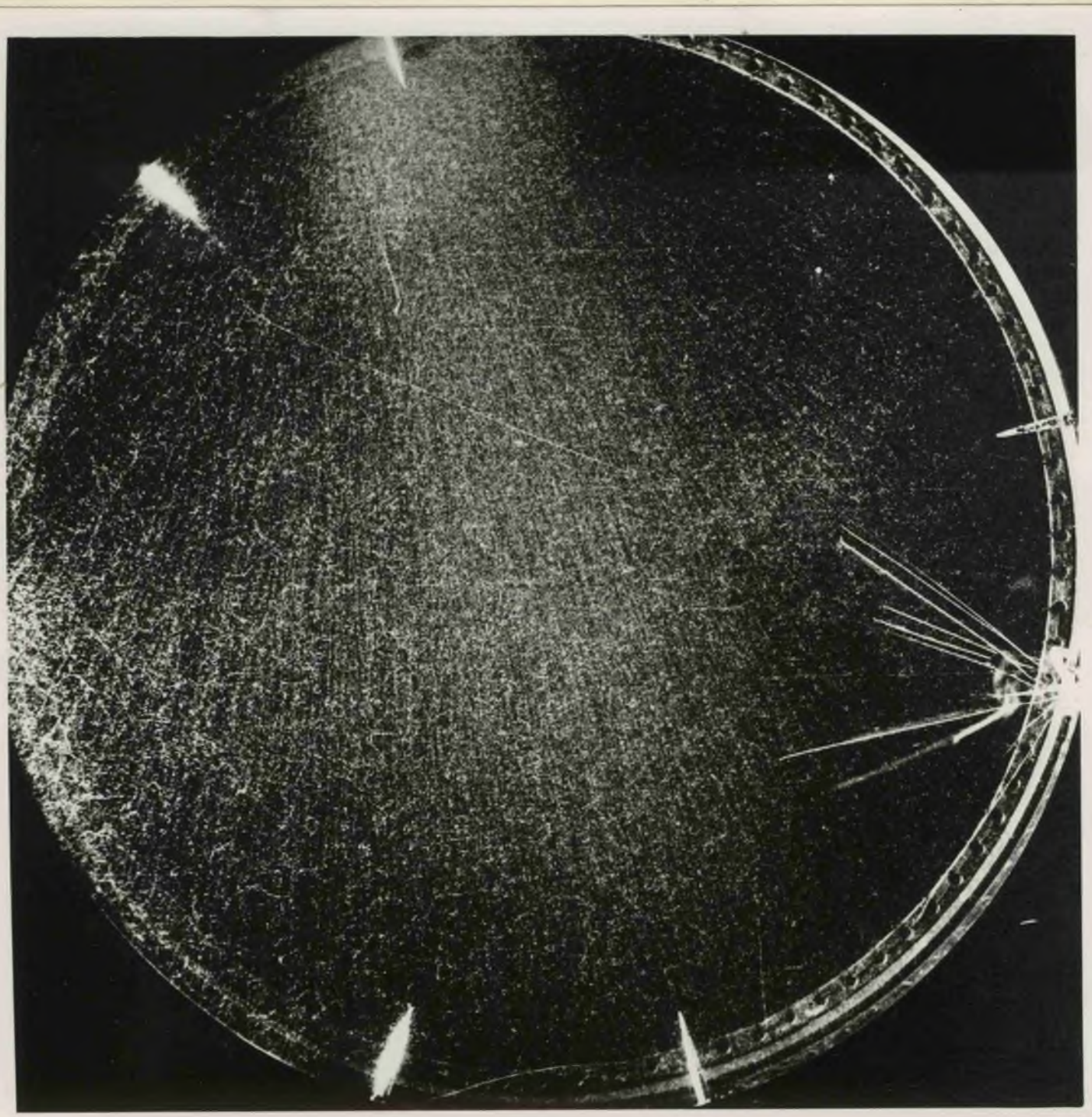

Plate 3

PLATES 4 and 5.

Nitrogen Experiment (low pressure).

(These photographs were taken during some preliminary measurements which do not form part of the experiment discussed in Chapter IV).

Plate 4. $N^{14}(\gamma,p)$ (or $N^{14}(\gamma,d)$) disintegration.

Plate 5. $N^{14}(\gamma,pn)$ disintegration.

The side camera photograph of Plate 5 shows that because of the large ion density along the recoil track some of the ions have been dragged out vertically by the clearing field. This "dragging" is not always present as can be seen from Plate 4 which was taken about 30 minutes earlier and with identical conditions except that the delay between the X-ray pulse and the flashing of the discharge lamps was 100 millisec. for Plate 4 and about 150 millisec. for Plate 5.

Expansion Chamber Conditions:- Gas filling (chamber expanded) 21 cm. nitrogen + 21 cm. helium + water. Clearing field (approx. 25v/cm.) left on during expansion. X-ray beam 10 cm. wide x 2.5 cm. high enters chamber through 0.090" Perspex window.

Top Camera

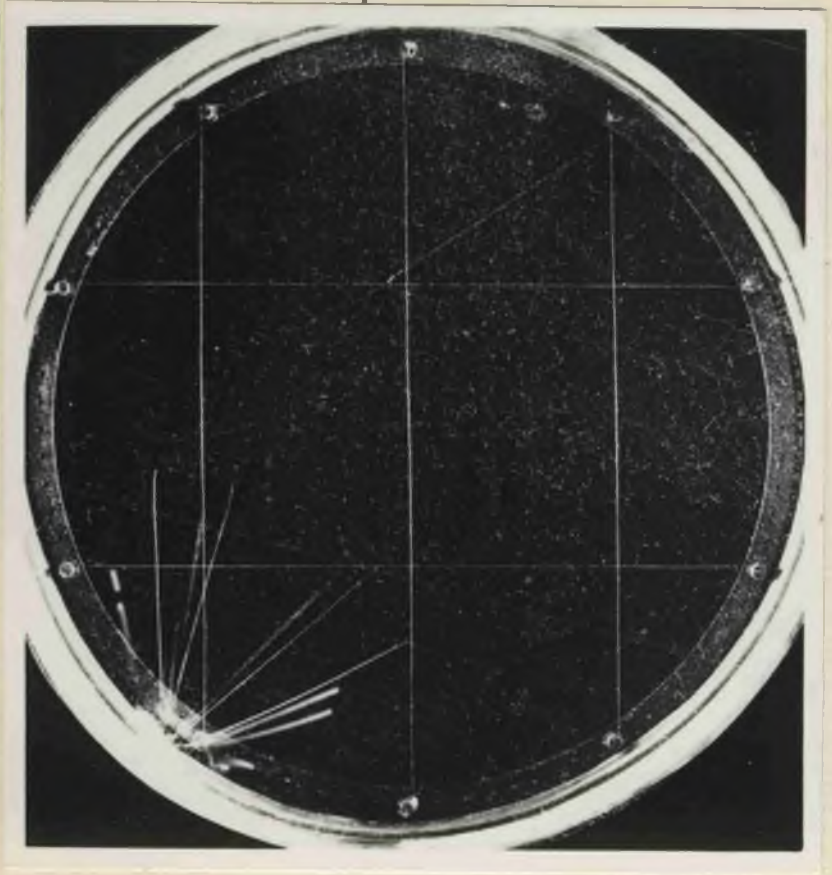

Plate 4

Top Camera

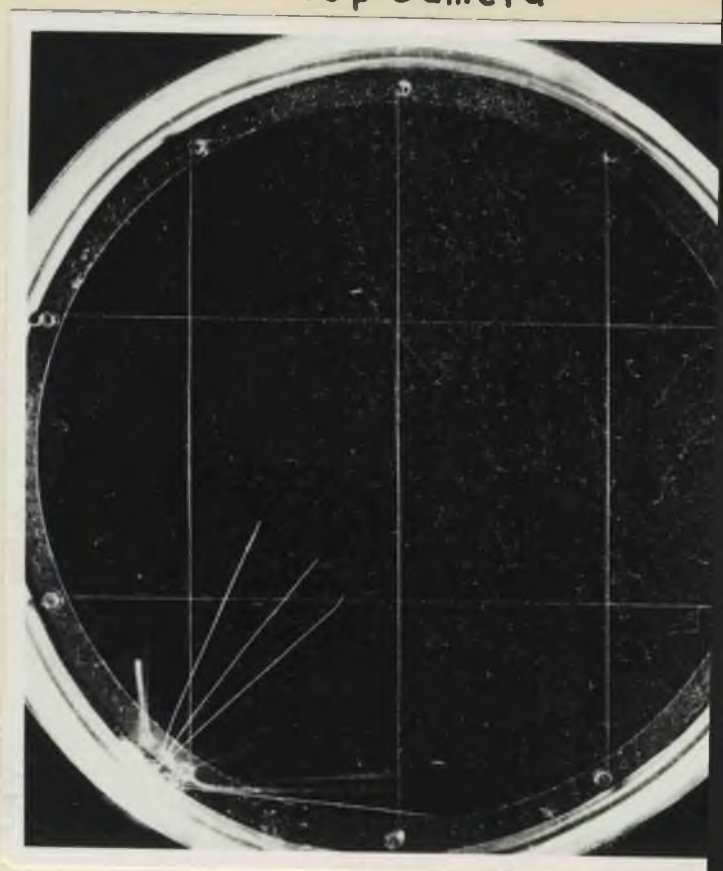

Plate 5

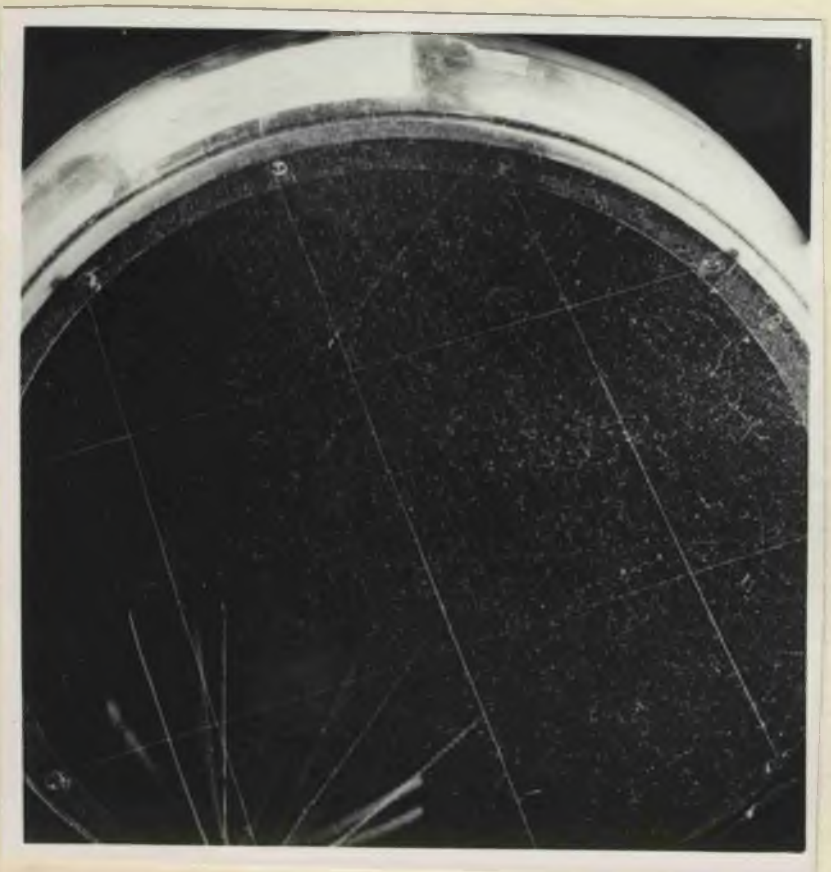

Side Camera

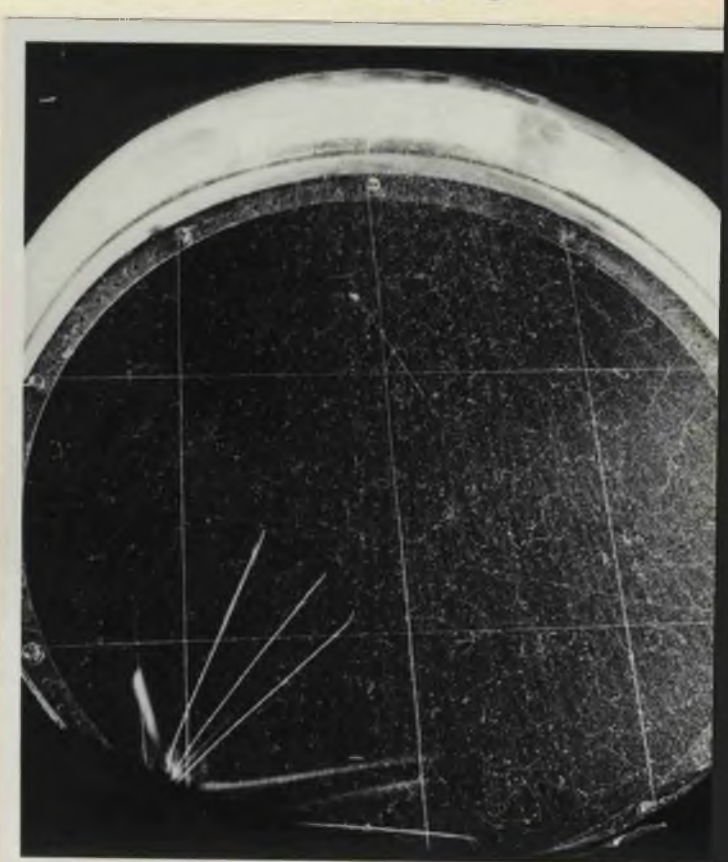

Side Camera

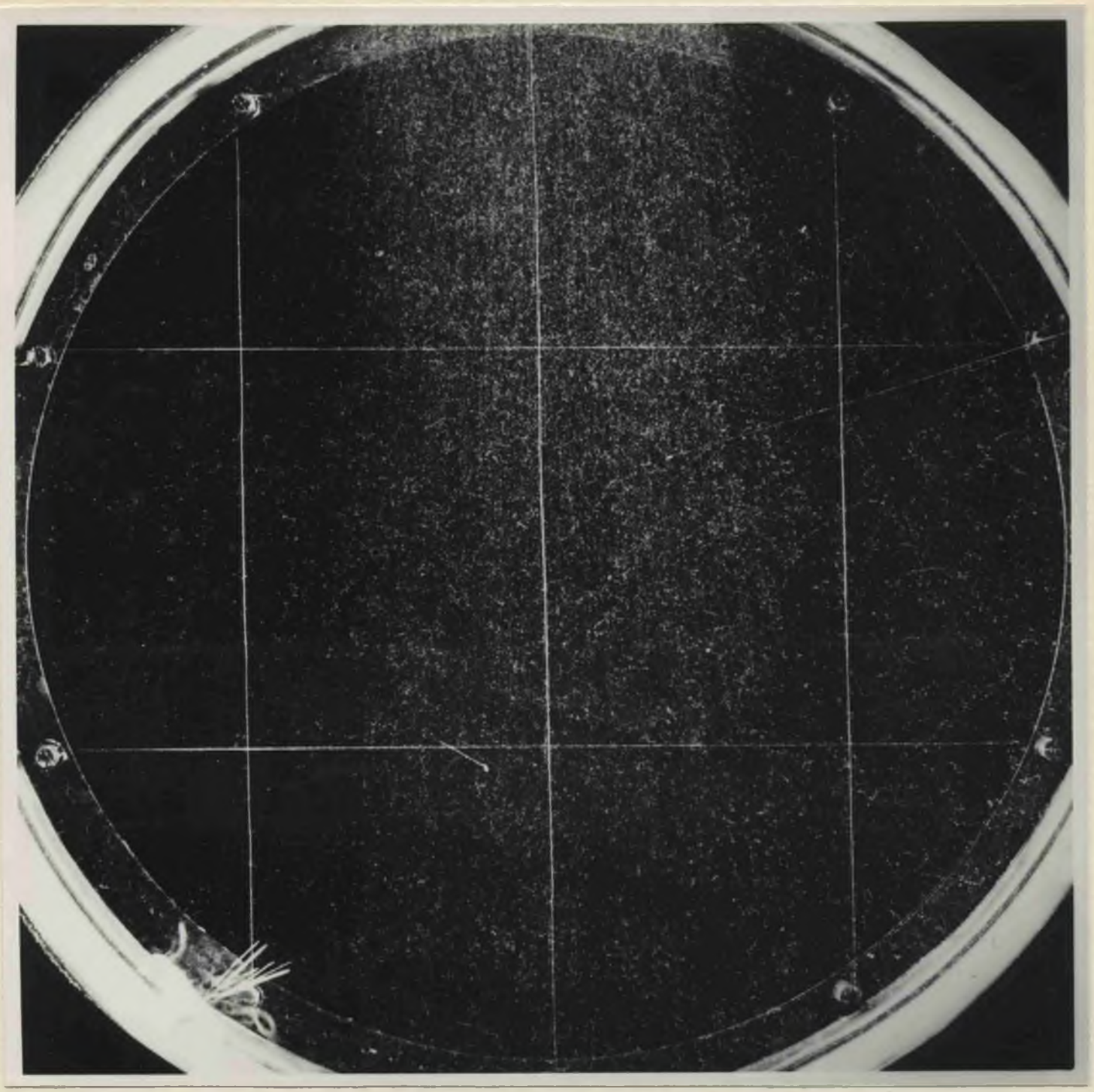

Plate 6

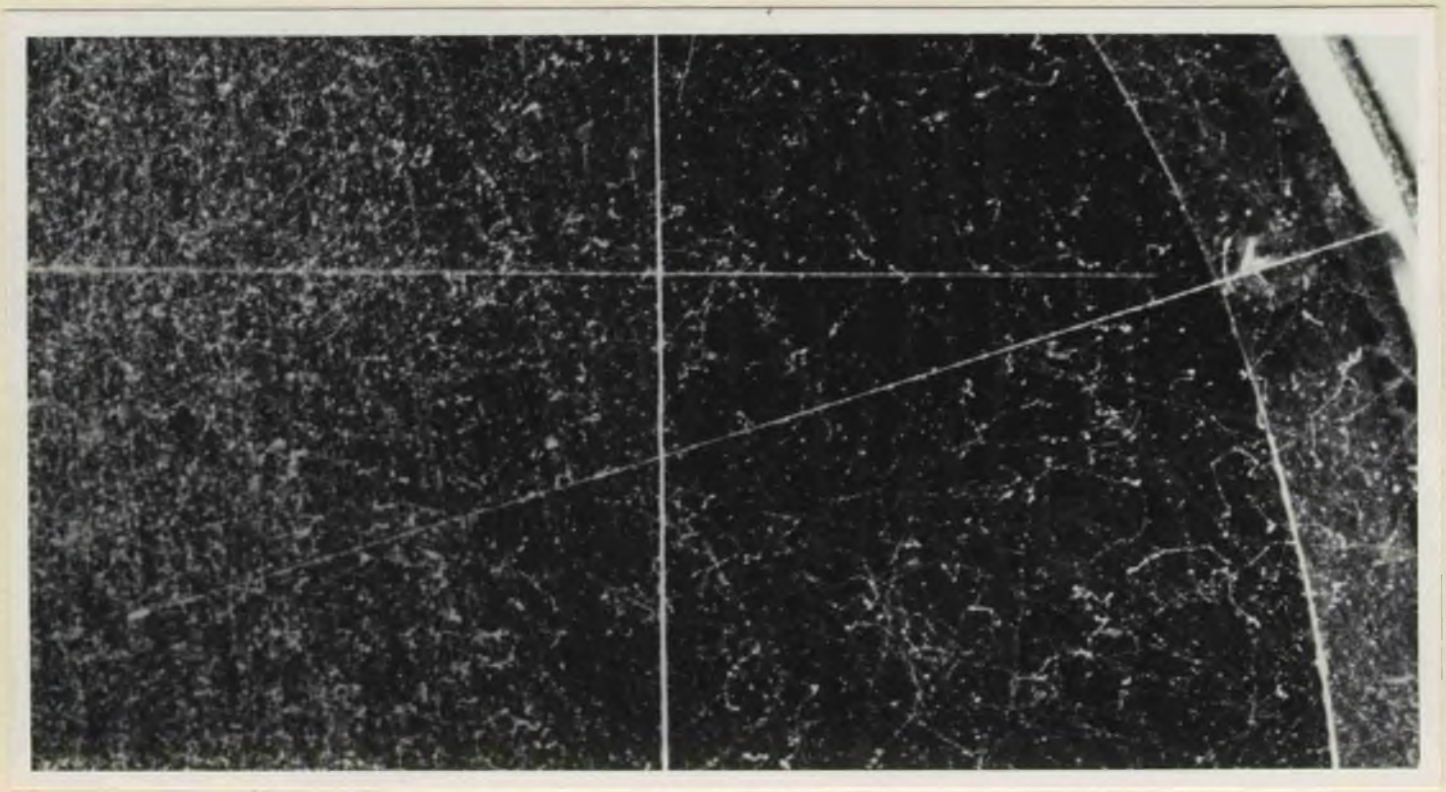

PLATE 6.

Nitrogen Experiment.

Photograph showing $N^{14}(\gamma,p)$ (or $N^{14}(\gamma,d)$) and $N^{14}(\gamma,pn)$ disintegrations with enlargement showing detail of the former. This recoil track is 1.8 mm. long.

Expansion Chamber Conditions:- Gas filling (chamber expanded) 106 cm. nitrogen + water. Clearing field on at expansion. X-ray beam 10 cm. wide x 2.5 cm. high enters chamber through 0.090" Perspex window.

PLATE 7.

Nitrogen Experiment.

$N^{14}(\gamma,p)$ disintegration in which the proton stops in the chamber (E_p = 2.7 Mev.). The C^{13} recoil can be seen on the end of the track near the centre of the chamber.

Expansion Chamber Conditions:- Gas filling and X-ray beam as Plate 6. Condition of clearing field during expansion - not known.

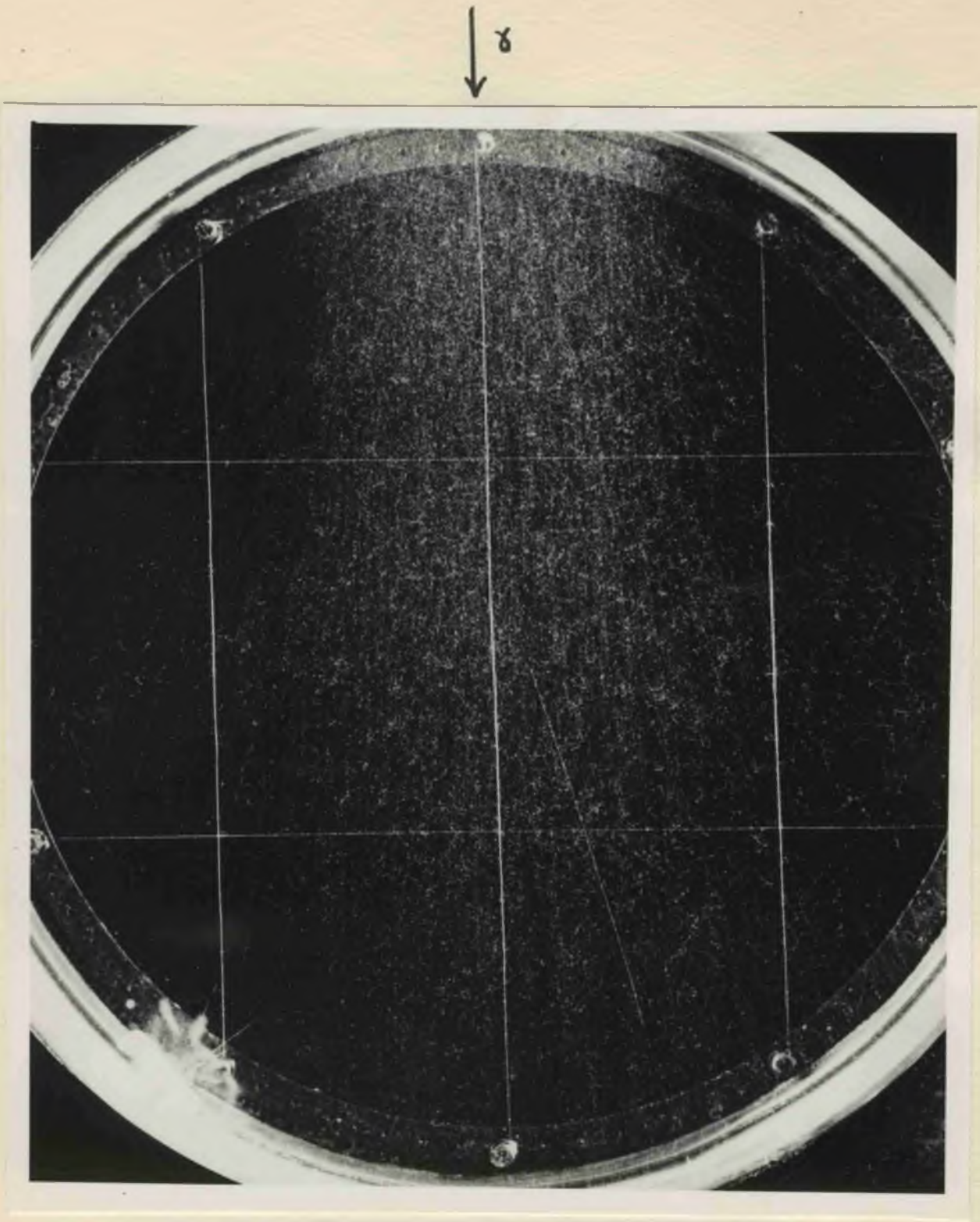

Plate 7

PLATES 8 and 9.

Nitrogen Experiment.

Plate 8. $N^{14}(\gamma,2\alpha)\ Li^{6}$ disintegration.

Plate 9. $N^{14}(\gamma,pn)$ disintegration in which the proton stops in the chamber.

Expansion Chamber Conditions:- Gas filling and X-ray beam as Plate 6. Clearing field probably turned off during expansion.

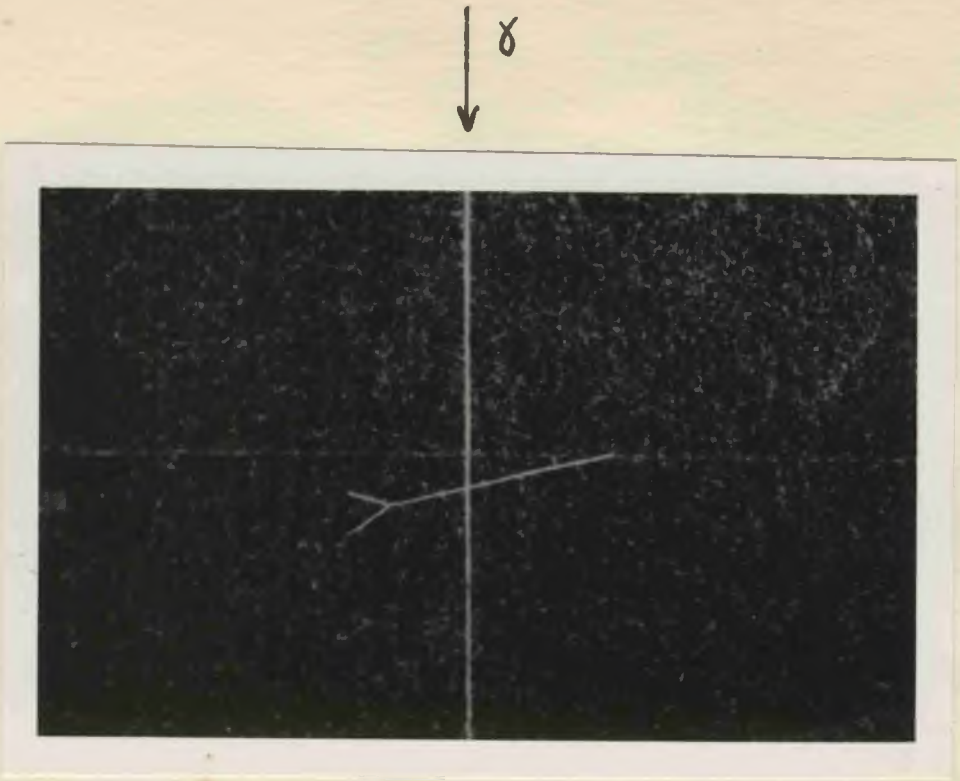

Plate 8

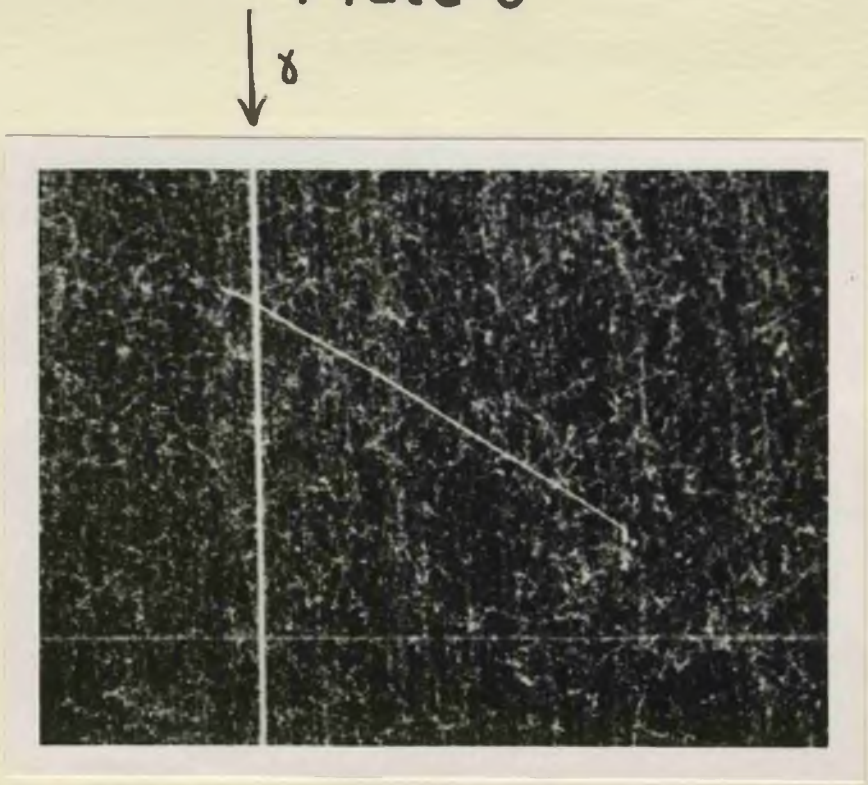

Plate 9

PLATE 10.

Nitrogen Experiment.

Set of stereo photographs showing the way in which the ions along the recoil track may be dragged out vertically when the clearing field is left on during the expansion.

Expansion Chamber Conditions:- Gas filling and X-ray beam as for Plate 6. Clearing field left on during expansion.

γ

Side Camera

γ

Top Camera

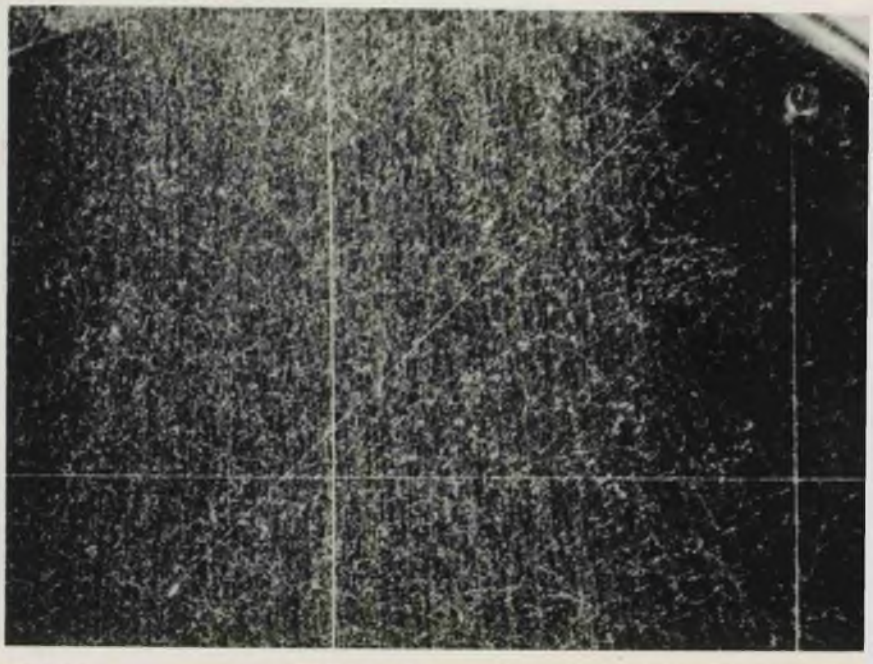

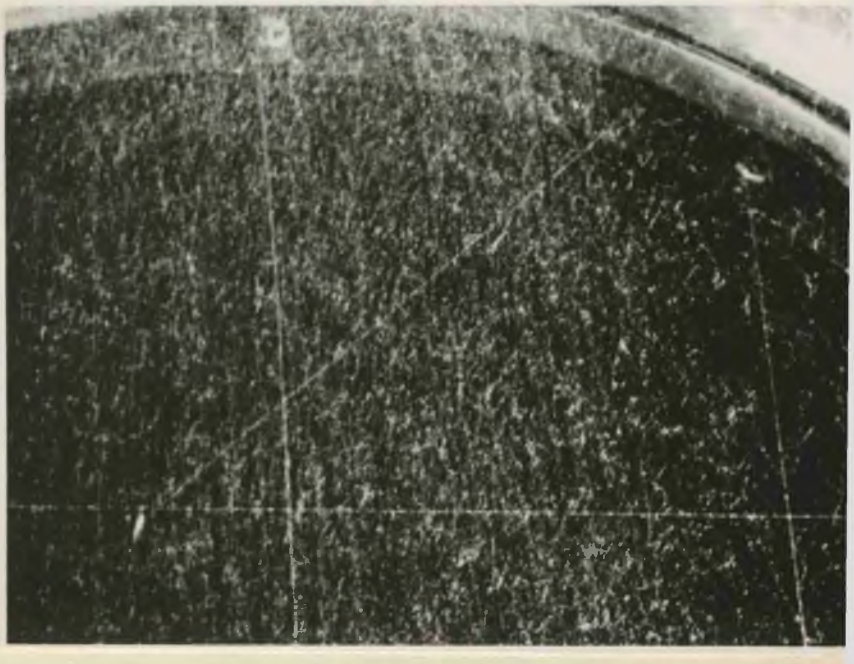

Side Camera

Plate 10

PLATE 11.

Nitrogen Experiment.

Set of stereo photographs showing the sharpness of the recoil track when the clearing field is turned off during expansion. Note the reduced contrast between recoil and proton as compared with Plate 10.

Expansion Chamber Conditions:- Gas filling and X-ray beam as Plate 6. Clearing field turned off during expansion.

Side Camera

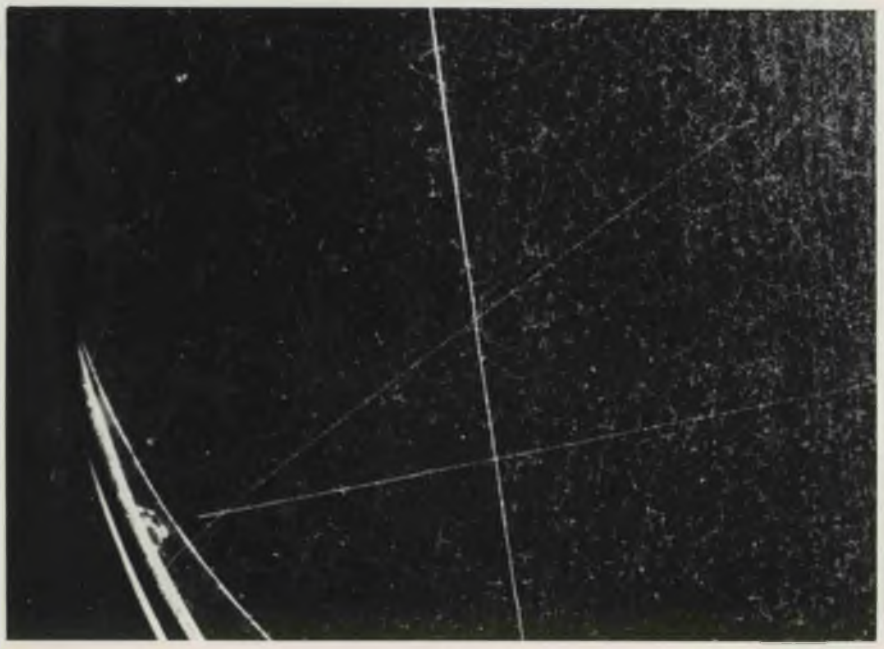

Top Camera

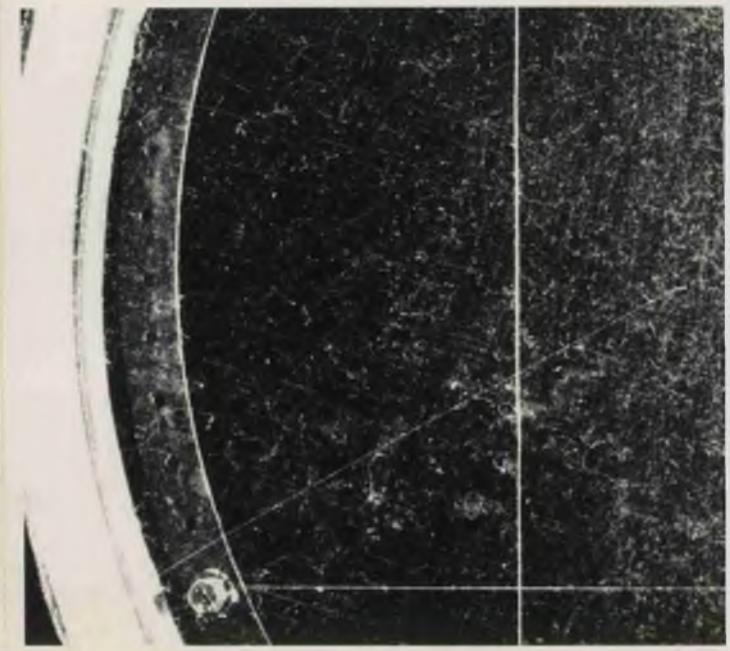

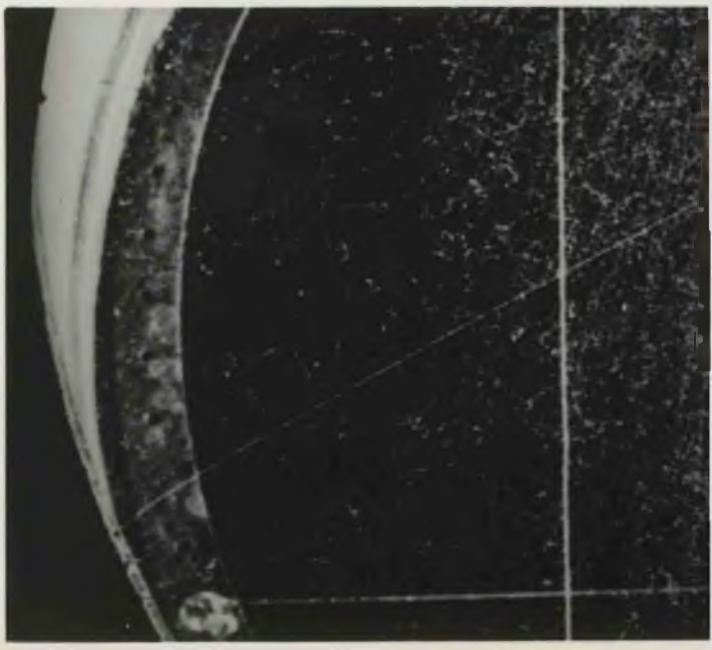

Side Camera

Plate 11

40 millisec.

45 millisec.

50 millisec.

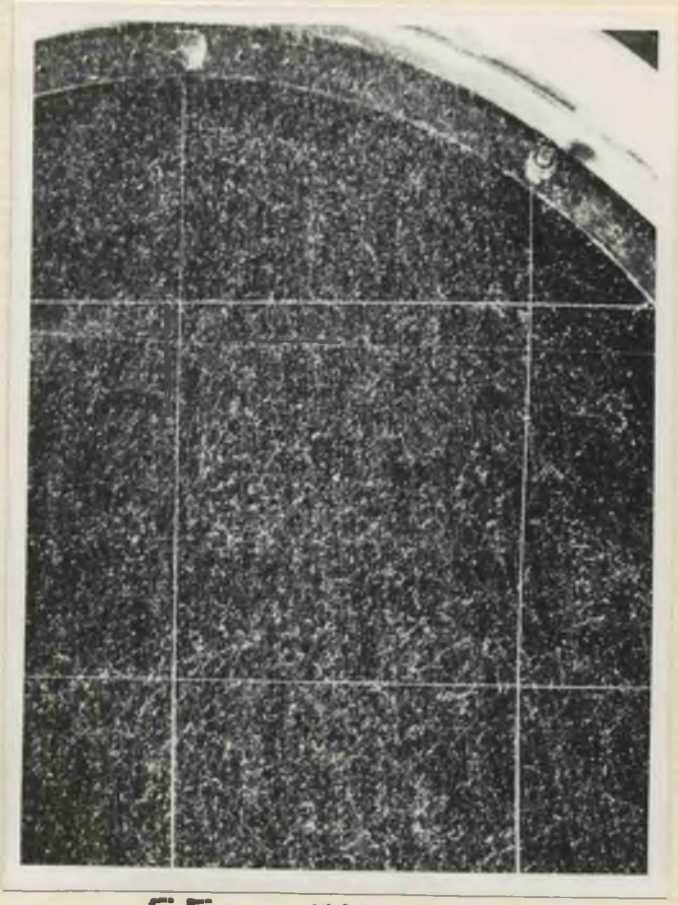

55 millisecs

PLATE 12.

Neon Experiment.

Variation in track quality with varying expansion chamber - synchrotron delay. Details on following page.

No photograph

available for

60 millisecs.

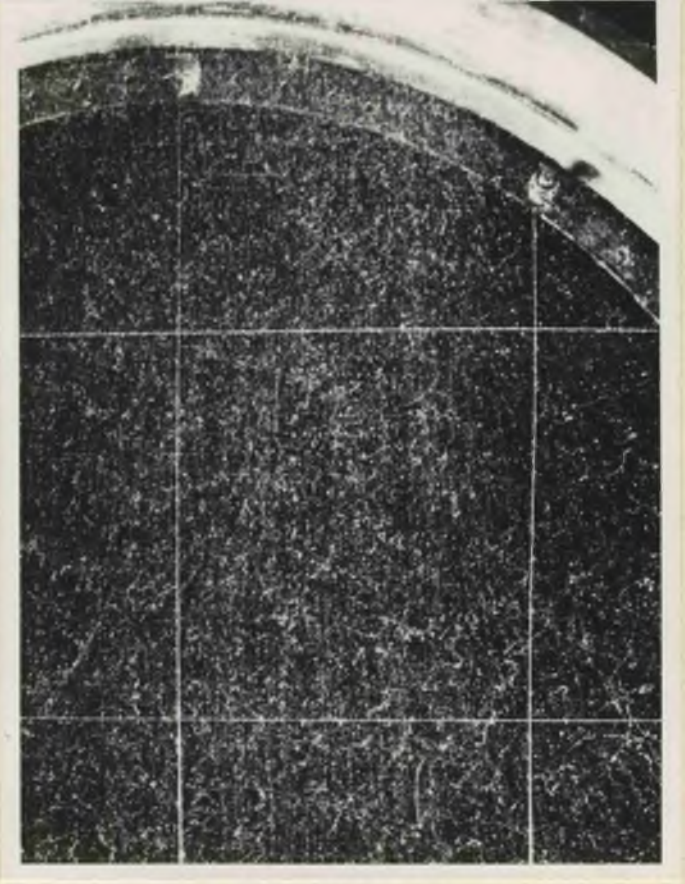

65 millisec.

70 millisec.

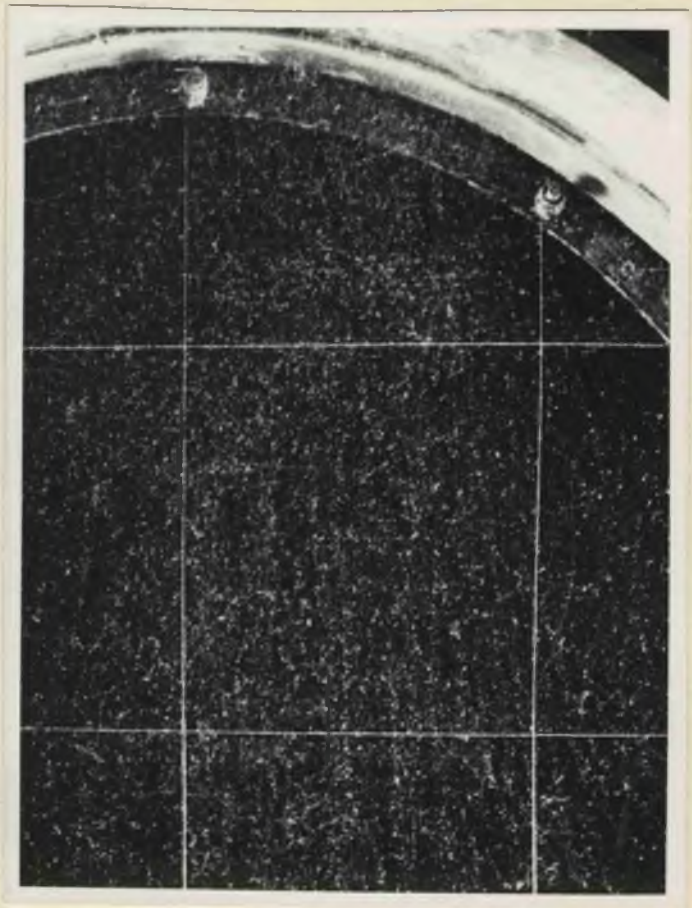

75 millisec.

PLATE 12.

Neon Experiment.

Continued from preceeding page.

Series of photographs showing the variation of track quality with the delay between the triggering of the expansion chamber and the arrival of the X-ray pulse.

Expansion Chamber Conditions:- Gas filling (chamber expanded) 87 cm. neon + water. (For these photographs the chamber contained no oxygen). Clearing field left on during expansion. X-ray beam 10 cm. wide x 2.5 cm. high enters chamber through 0.090" Perspex window.

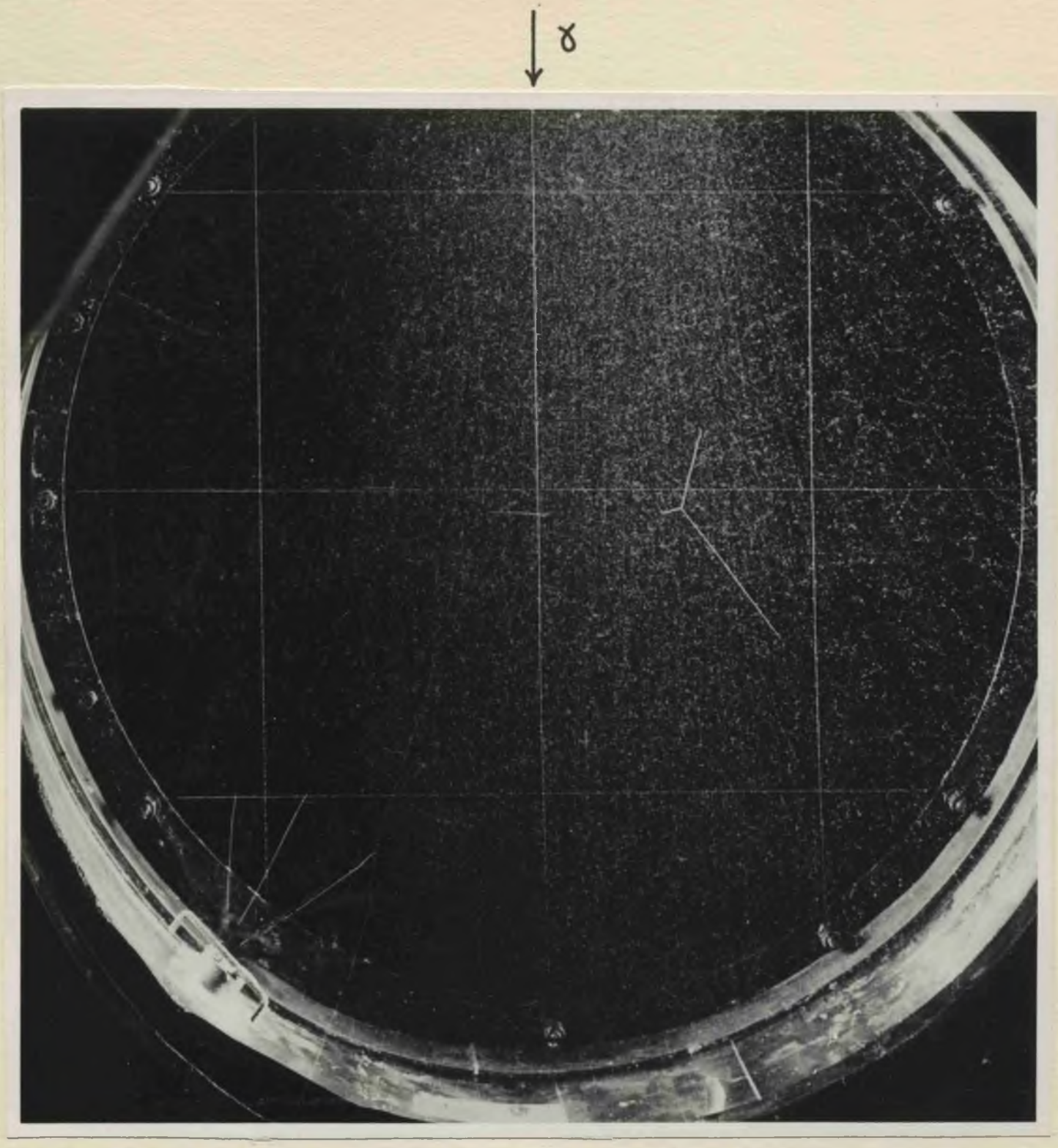

Plate 13

Side

Cameras

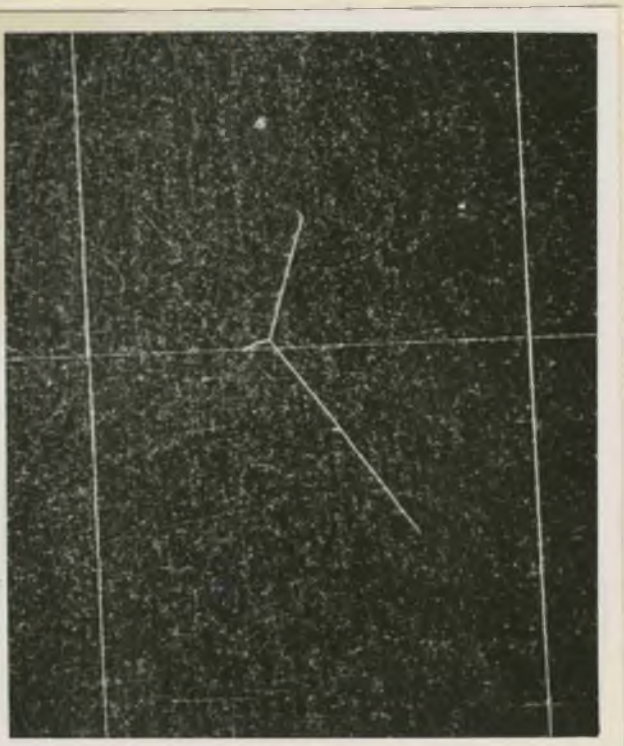

To

Came

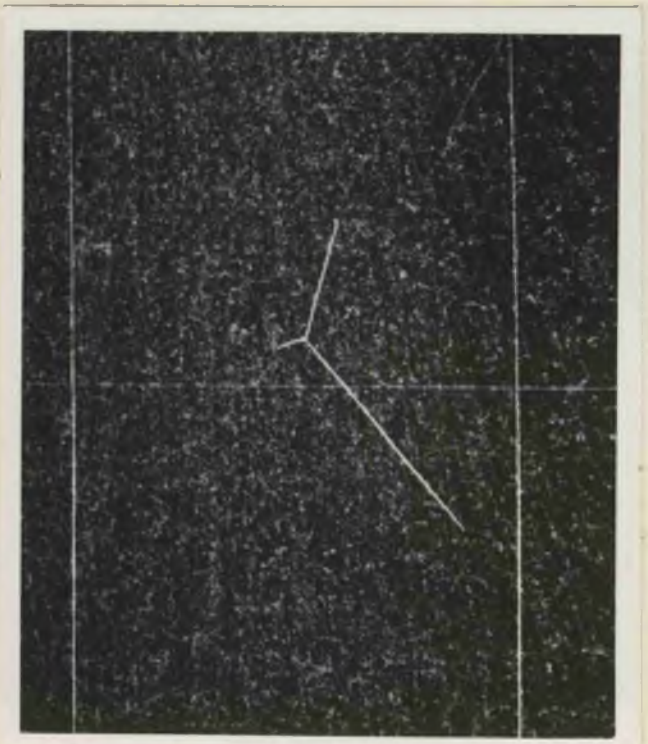

PLATE 13.

Neon Experiment.

Full chamber and stereo views of $Ne^{20}(\gamma,2\alpha)$ event. This illustrates that the neon tracks were perfectly sharp from all positions of viewing.

Expansion Chamber Conditions:- Gas filling (chamber expanded) 87 cm. Neon + 1 cm. Oxygen + water. Clearing field turned off during expansion. X-ray beam 10 cm. wide x 2.5 cm. high enters chamber through 0.090" Perspex window.

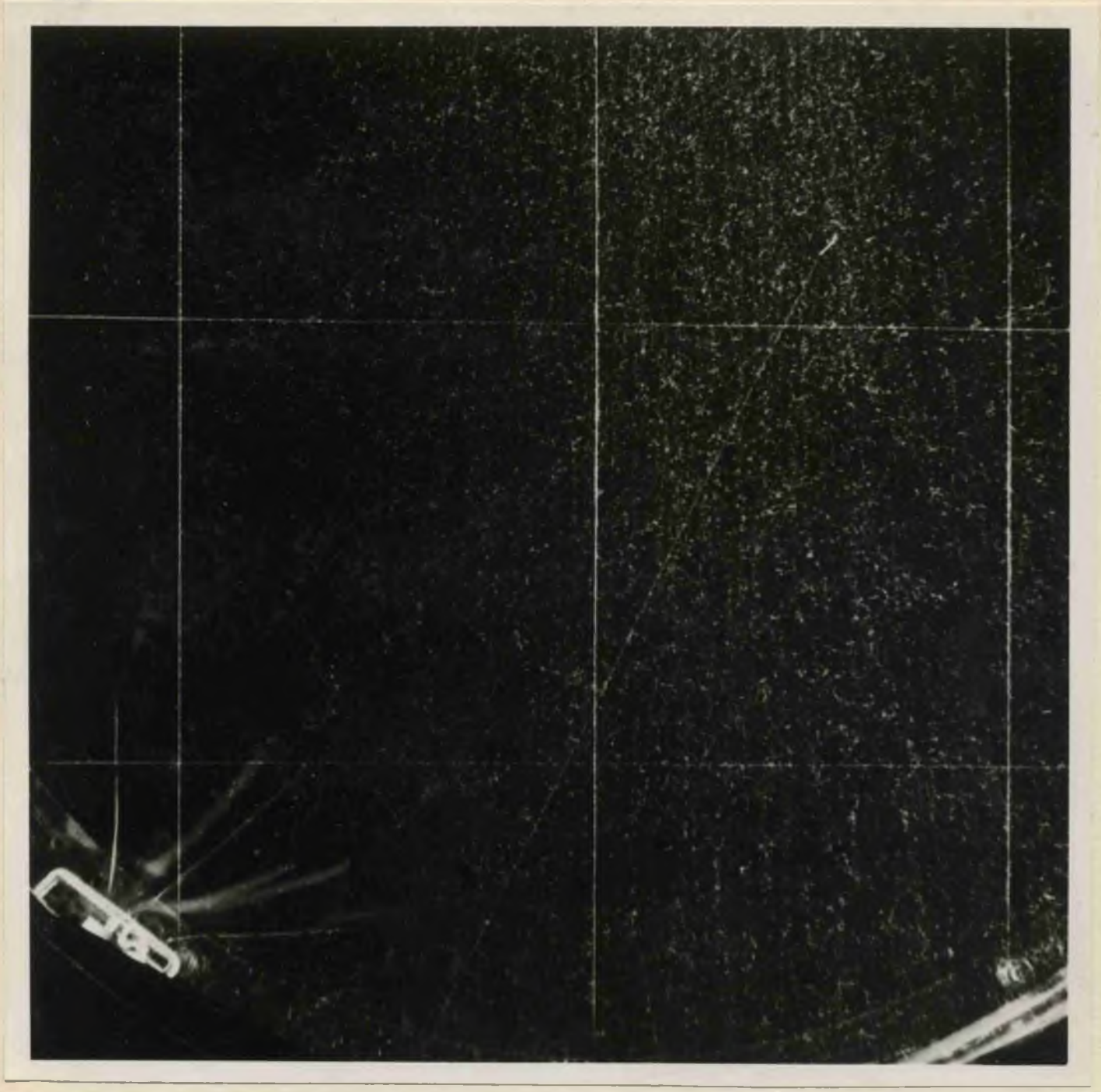

Plate 14

PLATE 14.

Neon Experiment.

Ne(γ,p) disintegration.

Expansion Chamber Conditions:- As for Plate 13.

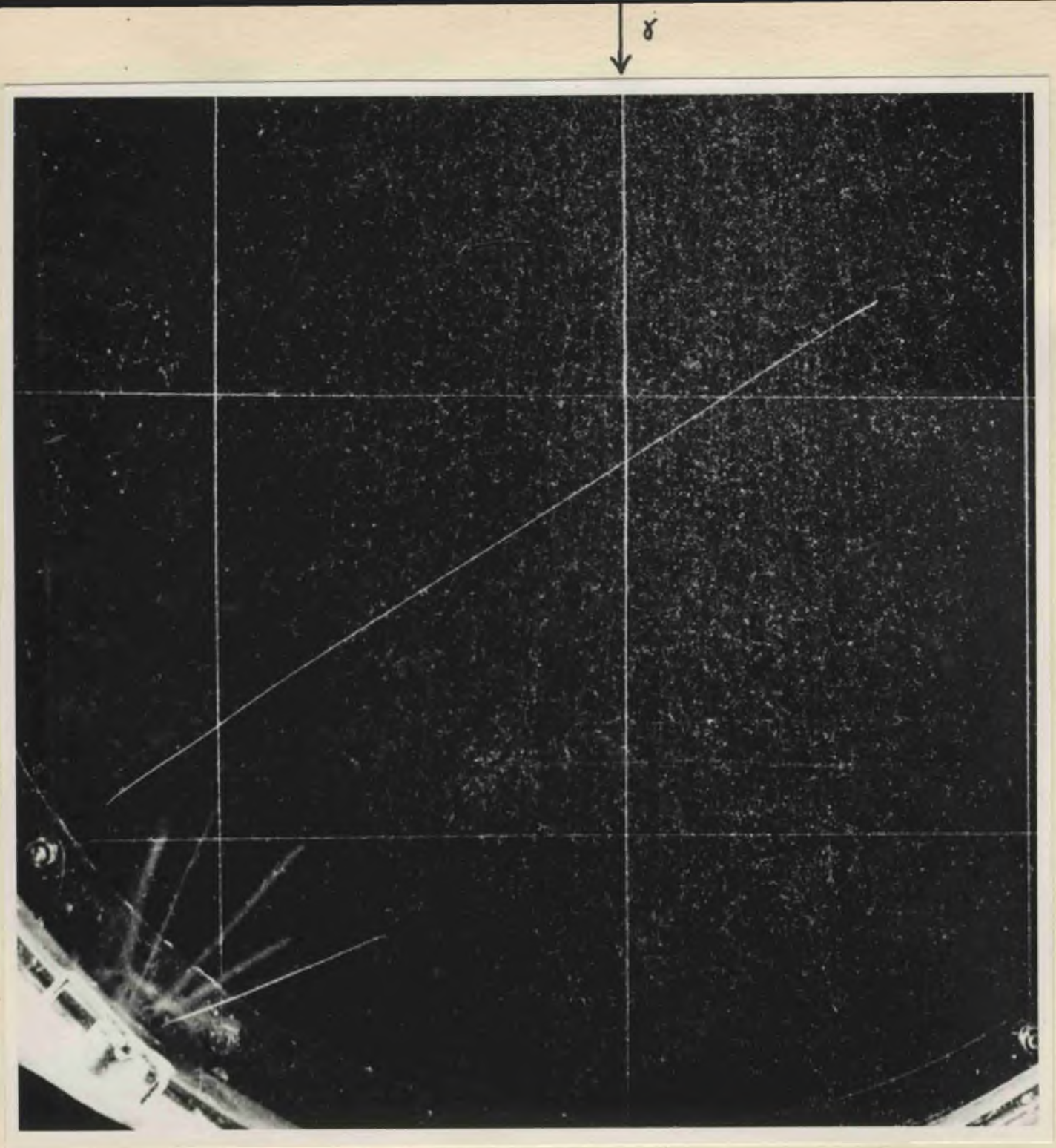

Plate 15

PLATE 15.

Neon Experiment.

$Ne^{20}(\gamma,\alpha)$ disintegration.

Expansion Chamber Conditions:- As for Plate 13.

PLATE 16.

Neon Experiment.

$Ne^{20}(\gamma, \alpha p)$ disintegration in which the proton is scattered by a nucleus in the gas before coming to rest in the chamber.

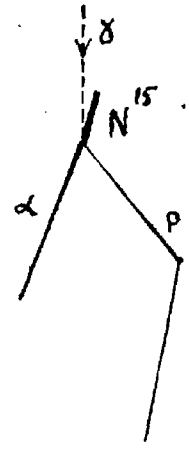

Expansion Chamber Conditions:- As for Plate 13.

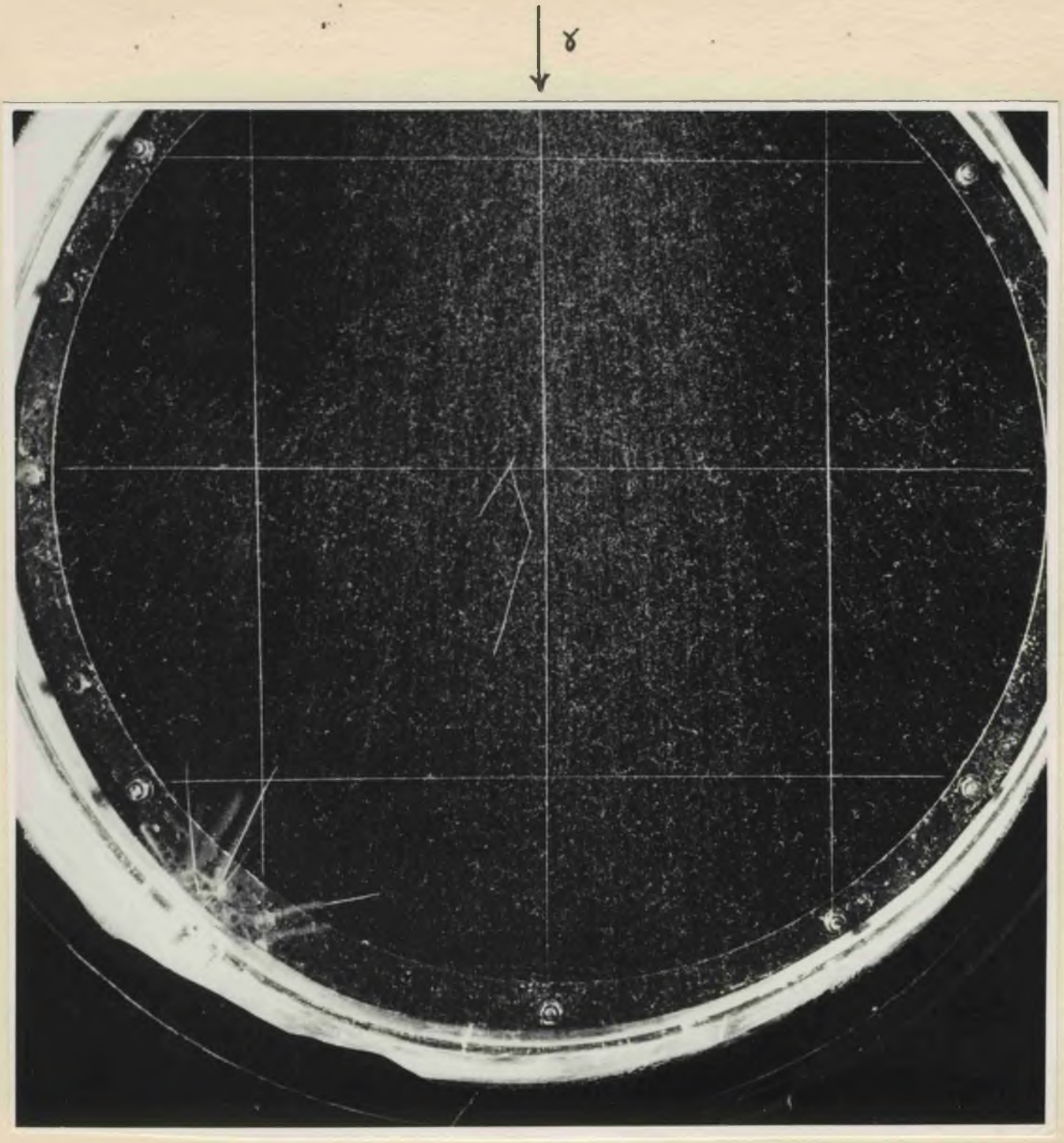

Plate 16